THE UNIVERSITY
of EDINBURGH

A Kinetic Model of a CO2 Recycling Rotary Adsorption Wheel for Gas Turbine Power Plants with Carbon Capture

Erika Palfi M.Sc.

THE UNIVERSITY
of EDINBURGH

Doctor of Philosophy

The University of Edinburgh

August 2019

Lay Summary

Reducing emissions from power generation has a key role to play to reduce the risk and mitigate the effects of climate change. In this context the capacity of large-size combined cycle gas turbines (CCGT) is expected to increase, due to their low emissions compared to other fossil fuel power plants and due to their relatively low investment costs. CCGT will fill the gap between electricity demand and renewable and nuclear output to ensure security of supply, while maintaining operational flexibility required in the electricity system.
To achieve 2050's Green House Gas targets, a large portion of new-build, as well as existing CCGTs will need to implement Carbon Capture and Storage (CCS) between 2020 and 2030.
However, flue gases from natural gas-fired power plants raise specific challenges for post-combustion CO2 capture (PCC) technologies. This is due to the low CO2 concentration, based on the nature of the combustion itself, and the large volume of exhaust gases produced, that need to be treated in the capture plant. These challenges lead to an increasing in the size of the capture plant and thus to an increase in capital and operational costs, which in turn has a major impact on the cost of electricity generation.
There are different technologies under investigation, which try to mitigate those challenges.

This study examines one very promising technology called Selective Exhaust Gas Recirculation (SEGR). SEGR increases the CO2 concentration upstream of the capture plant, by transferring CO2 selectively from the flue gas stream, back to the gas turbine. This increases the overall CO2 content in the flue gas and reduces the mass flow of flue gas treated by the capture plant, hence it leads to a reduction in equipment size and energy requirements.

Under investigation for SEGR application is here a novel system of a rotating regenerative CO2 transfer device using physical adsorption. In contrast to other proposed technologies, like selective membranes, a scale up of solid adsorbents technologies to treat the large amount of flue gases produced in a CCGT, is feasible.

For the evaluation of this system a novel kinetic model of a rotating CO2 transfer device is developed and validated against kinetic measurements of a promising material.
The kinetic model allows for a better assessment of the realistic amount of solid adsorbent needed. It also gives guidelines to material developer to tailor materials for the purpose of selective CO2 transfer. Better tailored material are key to reduce the overall solid mass requirement and therefore the cost of an emission free future.
Further it is now possible, based on the kinetic model, to advise power plant operators how to optimise the operation of such a regenerative CO2 transfer device to advance CO2 transfer and therefore reduce the total amount of CO2 emissions of the overall power plant.

This study continues by reviewing the impact of such rotating regenerative CO2 transfer devices on an integrated new-build CCGT with PCC and the possibility to retrofit such rotary regenerative CO2 transfer wheels to existing CCGTs with PCC through process simulation. The aim of such an integration for a new build CCGT with PCC is a reduction in equipment size and energy requirements. For existing CCGTs with PCC the aim is to achieve higher overall capture rates of CO2 emissions, in a future world where existing CCGTs with PCC are needed to chase CO2 emission residues. The operation of the absorber column at reduced gas velocity is, however, shown to be detrimental to retrofitting selective CO_2 recycling to existing CCGT plants with solvent-based capture.

Abstract

The selective recycling of carbon dioxide (CO_2) upstream of post-combustion capture processes can greatly reduce both the size of equipment and capital costs by process intensification. For combined cycle gas turbine (CCGT) power plants, flue gas flow rates can be lowered by two thirds and CO_2 concentration greatly increased from 4% to 14% v/v.

Selective recycling of carbon dioxide (CO_2) can be achieved in CCGT plants with a low pressure drop, regenerative rotary CO_2 transfer device using physical adsorption. A newly developed kinetic model of this CO_2 transfer device shows that, for an activated carbon material with suitable equilibrium properties, a mass requirement of circa 600 tonnes is necessary for a new build CCGT plant of 800 MW with 90% capture. This is 3.7 times higher than the mass previously reported, by means of an equilibrium model, for the best performing commercially available activated carbon material.

A rigorous design shows that the mass of 600 tonnes of activated carbon can be distributed on a honeycomb structure on two CO2 transfer wheels of 30m diameter and 2.2m height, rotating at 1rpm, with a preferential direction of leakages towards the flue gas side. The design then provides the basis for an optimisation study of CO_2 recovery rate and adsorbent mass by examining first kinetic properties of the CO2 adsorbent to inform material development and research; second, rotational speed; and, last, the partitioning of the wheel.

Further, the selective recycling of CO_2 is examined as a retrofit option for CCGTs with solvent-based post-combustion capture. The aim is to explore the possibility to increase overall capture level beyond the initial design of 90% capture using an integrated model consisting of a gas turbine combined cycle, a rotary CO2 transfer device and a post-combustion capture unit and compression train. The operation of the absorber column at reduced gas velocity is, however, shown to be detrimental to retrofitting selective CO_2 recycling to existing CCGT plants with solvent-based capture.

Finally, a comparison between a new build CCGT with PCC and fully integrated regenerative selective CO2 transfer wheel to a new build CCGT with PCC without SEGR is performed. The results show a possible reduction in absorber total packing volume of 42% and a marginal increase of net power output of 0.3% relative to a new build CCGT with PCC without SEGR.

Acknowledgment

This thesis would not have been possible without the continuous support and guidance of my supervisors Dr. Mathieu Lucquiaud and Dr. Hannah Chalmers.
A very special thanks goes out to Dr. Laura Herraiz Palomino for her guidance and advice. The time spent with discussions was very valuable and appreciated.
Further I would like to thank my friends and colleagues at the School of Engineering and the Institute of Energy Systems for the special time spend together and after work conversations. In particular I would like to thank Thomas Spitz, Laura Herraiz, Bill Buschle, Juan Riaza, Paul Tait, Vitali Avagyan, Charlotte Mitchell and Mennat Labib for making office life over the years so enjoyable and for giving technical advice whenever needed.
Outside of academia, I would like to send out my thanks to Dougal Hogg, Jim Cooper, Richard Smith, Meron Reid and Joanne Moore from the Howden Group in Glasgow, for all technical advice and extremely valuable input regarding large rotary devices. And of course for the financial support I received from the Howden Group UK in the context of my PhD funding.
Finally, I would like to thank my family and especially my partner, who was my rock and kept me going and my dog, who made my breaks so adventurous to take work off my mind.

Financial support given by the ETP Energy Industry Doctorate Program, supported by the University of Edinburgh, Howden Group UK and the Scottish Government, was gratefully received.

Declaration of Originality

The work included in this Ph.D. thesis, except when referenced, is the results of the effort of years that has been done by the author alone under the guidance of her supervisor Dr. Mathieu Lucquiaud. The author acknowledges essential contributions by others in the acknowledgment section of this thesis and in further sections of the work where required.

This Ph.D. thesis has not been submitted for any other degree or professional qualifications in the UK or elsewhere. The author recommends referencing this thesis as follows:

Palfi, E. (2019), A Kinetic Model of a CO2 Recycling Rotary Adsorption Wheel for Gas Turbine Power Plants with Carbon Capture, Ph.D. Thesis, School of Engineering, University of Edinburgh, United Kingdom of Great Britain and Northern Ireland (UK).

Erika Palfi

List of Publications

Journal Presentations

Herraiz L., Palfi E., Sanchez-Fernandez E, Lucquiaud M., 2019. Rotary Adsorption: Selective Recycling of CO2 in Combined Cycle Gas Turbine Power Plants. Frontiers in Energy Research, no. under review.

Herraiz L., Palfi E., Sanchez-Fernandez E, Lucquiaud M., 2018. Selective Exhaust Gas Recirculation in Combined Cycle Gas Turbine Power Plants with Post-Combustion CO2 Capture. International Journal of Greenhouse Gas Control 71 (June 2017): 303–21.

Oral Presentations

Palfi E., Herraiz L., Lucquiaud, M., 2018. Rotary Wheel Configuration for Selective Exhaust Gas Recirculation Application for CO2 Post Combustion Capture. *Energy Technology Partnership Annual Conference 2018*, Glasgow, UK.

Spitz T., Palfi E., Mitchell C., Reiner D., Wilkinson M., Lucquiaud M., 2018. Learnings from the world's first Massive Open Online Course on CCS. 14th International Conference on Greenhouse Gas Control Technologies, Melbourne, Australia.

Palfi E., Herraiz L., Lucquiaud, M., 2017. Activated Carbon for Selective Exhaust Gas Recirculation in Combined Cycle Gas Turbine Power Plants With Carbon Capture. *Energy Technology Partnership Annual Conference 2017*, Edinburgh, UK.

Palfi E., Herraiz L., Shahkarami S., Dalai A., Lucquiaud,M., 2017. Activated Carbon for Selective Exhaust Gas Recirculation in Combined Cycle Gas Turbine Power Plants With Carbon Capture. 9th Trondheim Carbon Capture and Storage Conference, Trondheim, Norway.

Palfi E., Herraiz L., Lucquiaud, M., 2016. Selective Exhaust Gas Recirculation in Combined Cycle Gas Turbine Power Plants With Carbon Capture Using Adsorption Technology. *Energy Technology Partnership Annual Conference 2016*, Aberdeen, UK.

Herraiz L., Sánchez Fernández E., Palfi E., Lucquiaud, M., 2016. Selective Exhaust Gas Recirculation in Combined Cycle Gas Turbine power plants with Post-combustion Carbon Capture. 3rd University of Texas Conference on Carbon Capture and Storage (UTCCS3), University of Texas, Austin, United States.

Herraiz L., Sánchez Fernández E., Palfi E., Lucquiaud, M., 2015. Selective Exhaust Gas Recirculation in Combined Cycle Gas Turbine power plants with Post-combustion Carbon Capture. 8th Trondheim Carbon Capture and Storage Conference, Trondheim, Norway.

Herraiz L., Sánchez Fernández E., Palfi E., Lucquiaud M., 2015. Selective Exhaust Gas Recirculation in Combined Cycle Gas Turbine power plants with Post-combustion Carbon Capture. 14th Annual Conference on Carbon Capture Utilization and Storage (CCUS), Pittsburgh, Pennsylvania, U.S.A.

<u>Poster Presentations</u>

Mitchell C., Herraiz L., Palfi E., Spitz T., Labib M., Lucquiaud M., 2018. The Gas Turbine Power Plants of the Future. Accelerating CCUS: A Global Conference to Progress CCUS. Edinburgh, UK.

Herraiz L., Palfi E., Lucquiaud M., 2018. A Regenerative Adsorption Wheel: Conceptual Design for CO2 Recycling in Combined Cycle Gas Turbine with CO2 Capture. 14th International Conference on Greenhouse Gas Control Technologies, Melbourne, Australia.

Palfi E., Herraiz L., Sánchez Fernández E., Gibbins J.,Lucquiaud M, 2015. Selective Exhaust Gas Recirculation in Combined Cycle Gas Turbine Power Plants with Post-combustion Carbon Capture. SCCS annual conference, Edinburgh, UK.

TABLE OF CONTENTS

List of Figures

List of Tables

Acronyms

AC	Activated Carbon
AMPGas	Adsorption Materials and Processes for Carbon Capture from Gas-Fired Power Plants - project
CCGT	Combined Cycle Gas Turbine
COT	Combustor Outlet Temperature
CP	Capture Plant
DCC	Direct Contact Cooler
EBTF	European Benchmarking Task Force
EGR	Exhaust Gas Recirculation
EOR	Enhanced Oil Recovery
EPSRC	Engineering and Physical Sciences Research Council
ETI	Energy Technology Institute
EvGT	Evaporative Gas Turbine
Gas-FACTS	Gas - Future Advanced Capture Technology Options
GC	Gas Chromatograph
GE	General Electrics
GT	Gas Turbine
HP	High Pressure
HRSG	Heat Recovery Steam Generator
IEAGHG	International Energy Agency Greenhouse Gas
IP	Intermediate Pressure
IUPAC	International Union of Pure and Applied Chemistry
LDF	Linear Driving Force
LP	Low Pressure
MEA	Monoethanolamine
MFC	Mass Flow Controller
MIT	Massachusetts Institute of Technology

MOF	Metal-Organic Framework
MTZ	Mass Transfer Zone
NETL	National Energy Technology Laboratory
PCC	Post-Combustion Capture
PDMS	Dense polydimethylsiloxane
PSA	Pressure Swing Adsorption
RWA	Rotary Wheel Adsorber
SCR	Selective Catalytic Reduction
SEGR	Selective Exhaust Gas Recirculation
SELECT	Selective Exhaust Gas Recirculation for Carbon Capture with Gas Turbines - project
SFCC	Supplementary Fired Combined Cycles
SSFCC	Sequential Supplementary Fired Combined Cycles
STIG	Steam Injection Gas Turbine
TIT	Turbine Inlet Temperature
TSA	Temperature Swing Adsorption

Symbols

Symbols

A_c	Cross sectional area
A_{hc}	Cross section area of the empty space of one honeycomb
$A_{\mathrm{hc}_{\mathrm{wall}}}$	Cross section area of one honeycomb including surrounding wall
A_s	Total surface area
A_{spec}	Specific area
A_{wheel}	Cross section area of the rotor
c_{in}	Gas phase inlet concentration
c_k	Concentration of the component k in the gas phase
c_{out}	Gas phase outlet concentration
C_s	Specific heat of the solid
c_t	Total gas phase concentrations
C_p	Specific heat at constant pressure
C_v	Specific heat at constant volume
D	Diffusion coefficient
D_{ax}	Axial dispersion
$D_{c,k}$	Crystal diffusion coefficient of component k
$D_{c,k}^{\infty}$	Temperature dependent diffusivity at high temperatures of component k
$D_{c,k\,0}$	Temperature independent pre-exponential constant of component k
D_{eff}	Effective diffusion coefficient
D_{Kn}	Knudsen diffusion coefficient

$d_{molecule}$	Diameter of the molecule
d_{pore}	Pore diameter
d_{wall}	Wall thickness
D_{wheel}	Diameter of the rotor
E_{ai}	Activation energy
f_{Area}	Fraction of the wheel available for the process
f_{Howden}	Effective cross section factor/ basket factor
$\dot{G}$	Gas/air molar flow rate
H	Height of the structured adsorbent
$h_{0\ air}$	Enthalpy of the air
$-\Delta H_{ads,k}$	Enthalpy of adsorption of component k
h_{hc}	Height of the equilateral triangle
h_{cv}	Convective heat transfer coefficient
h_g	Enthalpy of the gas
h_{steam}	Enthalpy of the steam
H_{wheel}	Height of the wheel
j	Running variable
k	Running variable
k_{eff}	Effective mass transfer coefficient
K_{L0}	Pre-exponential constant
K_L	Equilibrium constant
Kn	Knudsen number
l	Running variable
LHV	Low heating value
m	Mass
$\dot{m}$	Diffusion mass flux

M_A	Molar mass of the gas
$\dot{m}_{air}$	Mass flow rate of air
$\dot{m}_{EFG}$	Mass flow rate of exhaust flue gases
$\dot{m}_{fuel}$	Mass flow rate of fuel
m_{s}	Mass of the solid adsorbent
$\dot{m}_{steam,j}$	Mass flow rate of steam in each turbine stage j
m_{total}	Total mass
n	As exponent, relates to the heterogeneity of the adsorbent surface
$\mathrm{N_H}$	Number of stages in longitudinal
n_{hc}	Number of honeycombs
$\dot{n}_{\mathrm{k}}$	Molar flow rate of the k component
N_L	Number of stages in the longitudinal direction
N_{τ}	Number of stages in rotational direction
n_{wheel}	Number of wheels
p	Pitch
P_k^*	Partial pressure of component k
$\dot{Q}$	Heat
$\overline{q}_{\mathrm{k}}$	Average amount adsorbed of component k
q_k^*	Adsorbed phase concentration of component k in equilibrium
q_s	Saturation capacity
$q_{s,T}$	Saturation capacity of the Tóth model
r	Radius
R	Gas constant
r_c	Crystal radius
r_{p}	Mean pore radius
R_{p}	Mean particle radius

$\dot{S}$	Solid mass flow rate
S_{CO2}	Adsorption capacity
t	Time
T	Temperature
$t_{\text{adsorption}}$	Absorption time
t_b	Breakthrough time
t_c	Cycle half time
t_{cycle}	Cycling time
T_G	Temperature of the gas
$T_{g\ (\text{i,j})}$	Temperature of the gas
T_S	Temperature of the solid
$T_{s\ (\text{i,j})}$	Temperature of the solid
$t_{saturation}$	Saturation time
u_g	Superficial velocity
$\dot{V}$	Volume flow rate
V_{bed}	Volume taken up by the solid
v_g	Velocity of the gas
V_{hc}	Empty space of one honeycomb
V_T	Total volume
V_{total}	Total volume
V_{void}	Void volume
V_{wheel}	Volume available for the solid in the wheel
$\dot{W}_{aux}$	Auxiliary power consumption of all the elements of the power plant
$\dot{W}_{aux\ PCC}$	Power consumption of the post carbon capture plant
$\dot{W}_c$	Compressor work
$\dot{W}_{CCGT,net}$	Net power output of the CCGT

$\dot{W}_{CO2\ compression}$	Power consumption of the CO2 compression
$\dot{W}_{fans}$	Power consumption of the fans
$\dot{W}_{fuel\ compressor}$	Power consumption of the fuel compressor
$\dot{W}_{GT}$	Electrical power generated in the gas turbine
$\dot{W}_{GT,net}$	Net power output of the gas turbine
$\dot{W}_{reboiler\ duty}$	Work equivalent to reboiler duty
$\dot{W}_{solvent\ pumps}$	Work required to pump the solvent
$\dot{W_{ST}}$	Power generated in the steam cycle
$\dot{W}_{t}$	Power generated in the turbine section
$\dot{W}_{water\ pumps}$	Power consumption of the water pumps
x	Axial direction in which the gas is flowing
y_{k}	Molar fraction of component k

Greek Letters

α_T	Affinity constant
ε_b	Bed porosity; bed void fraction
ε_p	Particle porosity
ε_t	Total porosity
$\eta_{generator}$	Efficiency of the generator
η_{mech}	Mechanical efficiency of the compressor
η_{ST}	Efficiency of the steam turbines
η_t	Efficiency of the turbine
$\eta_{th,CCGT}$	Thermal efficiency of the CCGT
θ	Loading of the adsorbent
θ_c	Dimensionless time of cyclic processes
λ_F	Free path length of the molecule
$\mu_{P,Diff}$	Free pore tortuosity factor
$\mu_{P,Kn}$	Knudsen tortuosity factor
ρ_b	Bulk density
ρ_g	Gas density
ρ_p	Density of particle
ρ_s	Density of the solid
ρ_s	Skeletal density
τ	Time in rotational direction
ω	Rotational/ angular speed

Chapter 1 Introduction

1.1 Background

1.1.1 Climate Change and Global Status of Carbon Capture and Storage

Over the next few decades, greenhouse gas emissions (GHG), primary carbon dioxide (CO2), need to be significantly reduced to mitigate the effects of climate change. Reducing emissions from power generation has a key role to play, as one of the major sources of CO2 emissions, as illustrated in Figure 1-1. There are several possible scenarios proposed to reduce CO2 emissions, for a future sustainable, secure and competitive low-carbon energy system, meeting the global warming targets set by the Paris Agreement at COP21 (European Commission 2019; UNFCCC 2017; IPCC 2014).

There is a common acknowledgement that fossil fuel consumption needs to be reduced by increasing the amount of low carbon power generation technologies in form of renewable and nuclear power. However, fossil fuel power plants are in many scenarios needed as a cost effective way (e.g. capital costs) of stabilising the electricity grid by providing firm and flexible back-up power for times of low and/or variable renewable energy. Though, only in conjunction with CCS technologies can those fossil fuel power plants have a low enough carbon intensities to meet global warming targets.

Decarbonising the energy system alone will not bring the reductions in emissions that are necessary to reach global warming targets. A deep decarbonisation of the world economy requires to address all sources of emission. In this context CCS is currently the only available technology that can decarbonise carbon-intensive industries such as refineries, steelworks and cement plants.(IPCC 2014)

As a retrofit technology, CCS also offers to keep part of the current infrastructure by avoiding turning existing power and industrial plants into stranded assets.

Excluding CCS from the capacity mix will increase the cost of reaching our global warming targets according to the IPCC by 138% by the end of the century. Given the scale of the future changes required this number tremendous.(IPCC 2014)

It is therefore evident why CCS plays such a vital role in all of the models' mitigation scenarios (Koelbl et al. 2014; W. Huang, Chen, and Anandarajah 2017).

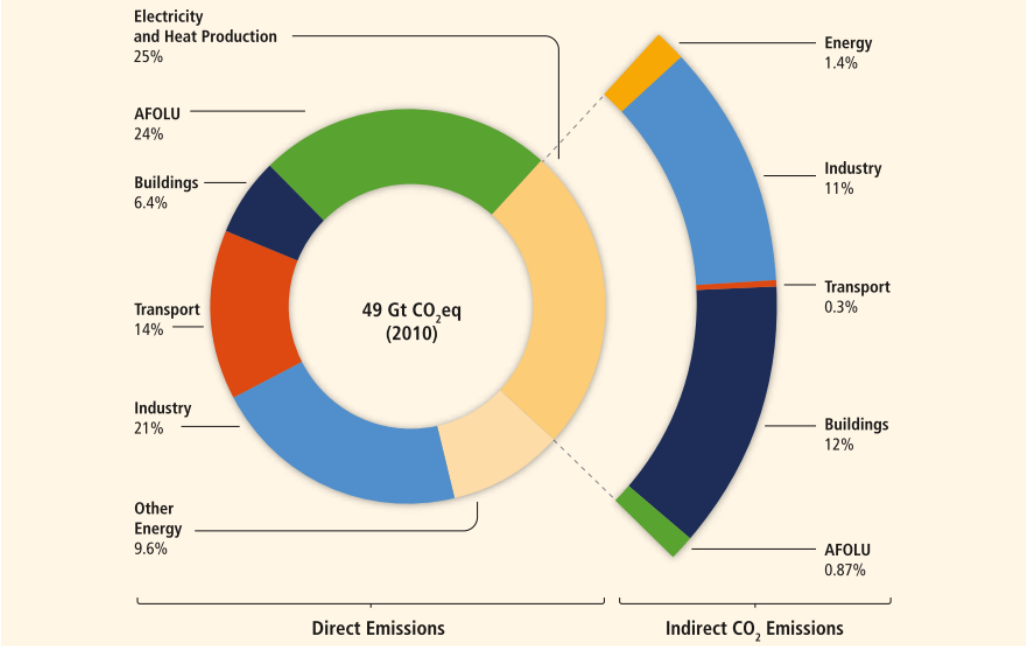

Figure 1-1: Total anthropogenic GHG emissions (GtCO2eq/year) by economic sectors. Inner circle shows direct GHG emission shares (in % of total anthropogenic GHG emissions) (IPCC 2014)

Different technologies are being developed for CO2 capture, transport, storage and utilisation, with only a few projects and technologies reaching large/ commercial-scale deployment. Each of these projects provides vital feedback for technology improvements and contributes to the required CCS capacity to meet global warming targets.

CCS technologies can be classified either by application or capture source, by capture strategy, by capture method, or by the net climate effect.

This thesis uses capture strategies as classification method. The strategies can be generally distinguished into pre-combustion, post-combustion and oxy-fuel combustion. Pre-combustion and post-combustion capture refer to the location of

the separation process, so the location where CO2 is captured from the combustion gases. Oxy-fuel combustion refers to a strategy, in which fuel is burned in a pure oxygen environment. The flue gas generated consists of predominantly CO2 and water. The CO2 subsequently only needs purification, drying and compression before it is ready for transportation and permanent storage. CCS technologies can be applied to capture CO2 from all kinds of CO2 containing gases. (Haszeldine 2009)

The first large-scale CCS project was Val Verde CO2-EOR, Texas, USA, which began operation in 1972, separating CO2 from gas processing (GCCSI 2018). The first full scale post-combustion CCS project in the power sector was Boundary Dam (SaskPower 2019), Canada in 2014, capturing CO2 1MtCO2 per year from coal-fired power plant flue gases using amine scrubbing technology. In 2016 the first commercial CCS facility in the iron and steel industry commenced operation in Abu Dhabi (Emirates Steel 2019). (GCCSI 2018)

Currently there are 23 large-scale CCS project in operation (18) or under construction (5), with most of these projects using enhanced oil recovery (EOR) as primary storage and only five projects using dedicated geological storage (Illinois Industrial, Quest, Sleipner, Snøvit, and Gorgon) Figure 1-2 (GCCSI 2018).

Most of the projects, including Century Plant (MIT 2019) with the largest capture capacity in the world of 8.4 MtCO2 per year, are located in the US. Europe has two operational projects in Norway. The Sleipner CO2 Storage Project in operation since 1996 with a capacity of 1 MtCO2 per year, and the Snøhvit CO2 Storage Project in operation since 2008 with a capacity of 0.7 MtCO2 per year (Equinor 2019). (GCCSI 2018)

At the end of 2017, over 230 cumulative million tons of CO2 have been captured and injected into deep underground geologic formations globally. The installed CO2 capture capacity is expected to reach 42 MtCO2 per year in 2019. (GCCSI 2018) However, these 42 MtCO2 per year represent only a small fraction, compared to the required CO2 capture capacity of 3800 MtCO2 per year to meet global warming target by 2040. This shows clearly the discrepancy between what needs to be

achieved in quite a short time frame, to keep to the targets set by the Paris Agreement at COP21 (European Commission 2019), and where the development and deployment is right now.

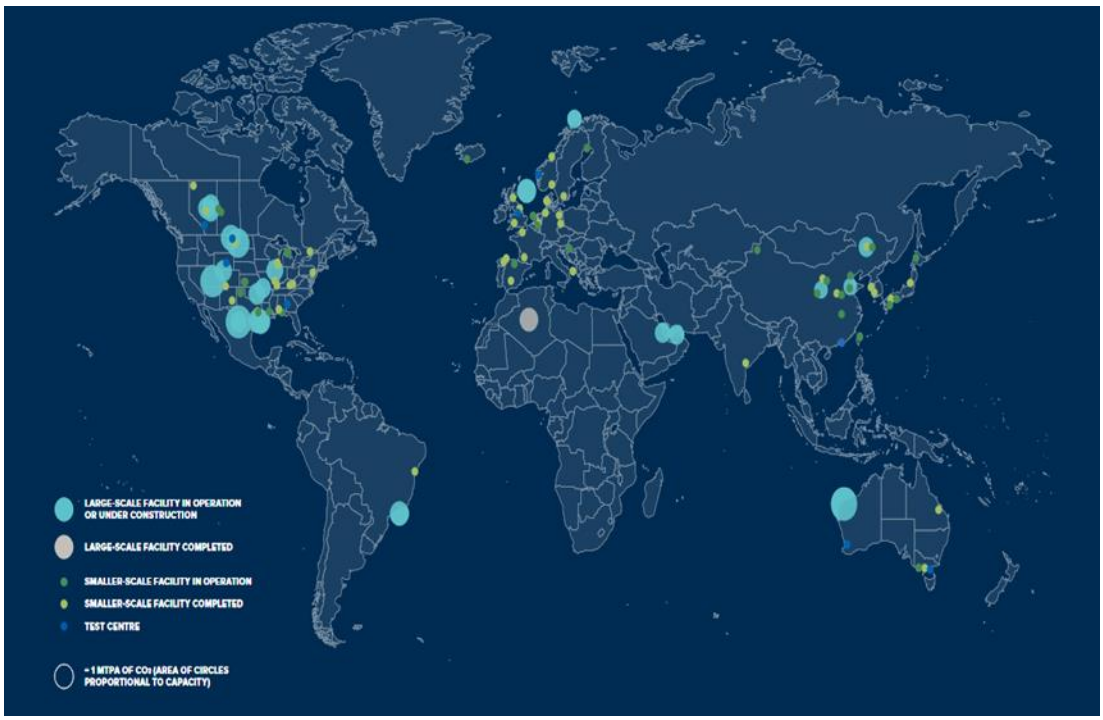

Figure 1-2: Current commercial large-scale CCS facilities and smaller-scale (pilot and demonstration) CCS facilities under construction and in completion; for colour coding see legend (GCCSI 2018)

1.1.2 The Future of Gas Power Plants

The electricity demand worldwide is increasing further, and natural gas as fuel is predicted to contribute 24% of the total share of electricity produced by 2035. (BP 2017)

Advantages of Combined Cycle Gas Turbines (CCGT), compared to other fossil fuel power plants, are relatively low investment cost, short construction time and low emissions, leading to competitive electricity prices, while ensuring security of supply. (DECC 2015)

For a deep decarbonisation of the electricity generation the Committee on Climate Change (CCC 2019) set out in their Net Zero Technical report a level of 10 gCO2/kWh. However, the average CO2 emission of gas fired power plants is around 350-400 gCO2/kWh and therefore, above required levels for a deep decarbonisation. Consequently, to meet the net-zero GHG emission targets by 2050, there is an urgent need to capture CO2 emissions from CCGT power plants. (CCC 2019; IEA 2016; IPCC 2014)

Admittedly, flue gas generated in CCGT power plants provides particular challenges for post-combustion carbon capture (PCC), that are connected to the low concentration of CO2 (3-4vol%) in the flue gas and the large volume of flue gas required to be treated by a post-combustion carbon capture system (a more detail explanation is provided in this thesis in Chapter 2). Those two factors lead to larger capture plant and auxiliary equipment size requirements and are therefore directly affecting the capital costs of the capture plants. For every 10% reduction in the capital costs of the capture plant, the electricity cost of CCGT with CCS reduces by 1.5-2 % for base load plants according to the UK Energy Technology Institute (ETI) (ETI 2016). If operated flexibly, as can be expected for CCGT power plants with any further increase in renewable energy capacity, low capital costs become a priority, since the contribution of capital costs to the electricity price increases. Hence, a reduction in capital costs for PCC becomes increasingly significant for low load factor operation (ETI 2016; Adderley et al. 2016).

1.1.3 Cost of CO2 Capture

In any realistic scenario, CO2 emissions cannot be cut fast enough to keep to the carbon budget of the atmosphere. (Koelbl et al. 2014; W. Huang, Chen, and Anandarajah 2017)

The Paris Agreement assumes net zero emissions to the atmosphere, hence, CO2 removal from the atmosphere at an industrial scale will be needed (European Commission 2019). Negative Emission Technologies appear to be crucial, unless a radical reduction in global CO2 emissions takes place.

In the context of achieving net zero emissions and the deployment of negative emission technologies, it is important to give consideration to the marginal cost of increasing capture levels on existing CCS facilities, beyond the nominal 85-90% capture level (Figure 1-3). Minimising residual emissions from existing CCS facilities is likely to make the best use of existing assets, such as the capture facility and the existing transport and storage infrastructure. This could be achieved without mobilising large amount of additional capital, although the magnitude of emission reductions is likely to be at least one order of magnitude smaller than what can be achieved by deploying negative emission technologies.

Therefore, it seems sensible to try to push for higher capture rates in capture plants fitted to large CO2 emitters like power plants, while dispatching negative emission technologies at a large scale.

Figure 1-3 also shows the reasoning behind the extensive research conducted on the field of increasing CO2 concentration in exhaust gases. Any increase in CO2 concentration directly relates to reduction in the associated minimum work required to separate CO2 from the stream source.

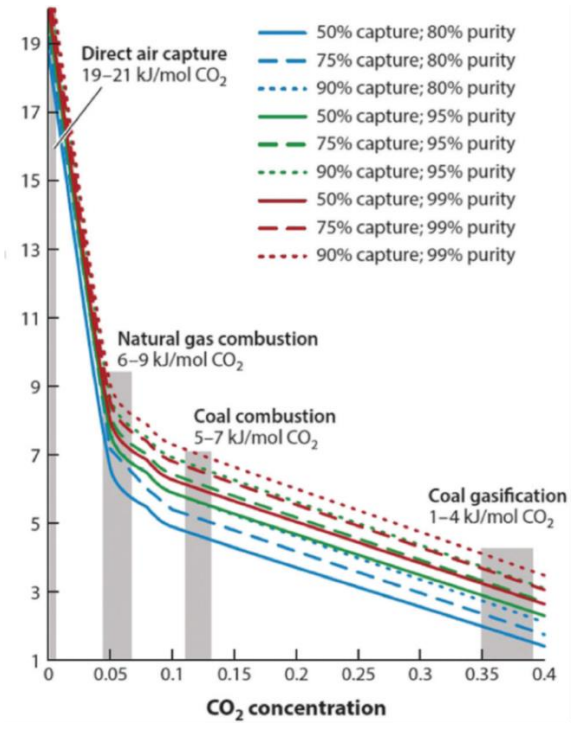

Figure 1-3: Minimum work required for CO2 capture based upon initial CO2 concentration, capture rate, and final CO2 purity (Wilcox et al. 2014)

1.2 Objectives

The main research objectives of this work in this context are:

- Understanding the technology of regenerative rotary adsorption wheels for selective CO2 transfer. Proving the concept on an adsorbent material with promising properties.
- Identifying possibilities to improve the performance of the wheel and adsorbent, leading to a reduction in adsorbent mass requirement and/ or an efficiency improvement.
- Developing guidelines for adsorbent developers for improving the performance of adsorbent materials for SEGR application.
- Identifying operational limits and possible improvements of the regenerative rotary wheel to inform operators about possibilities to push process intensification.
- Assessing the impacts of applying regenerative rotary CO2 transfer devices to new-build CCGTs with PCC and comparing the power output and efficiency to conventional new-build CCGTs with PCC.
- Understanding the effect and consequence of retrofitting regenerative rotary CO2 transfer devices to existing CCGTs with PCC. Identifying retrofit strategies and limitations in the capture plant.
- Assessing the possibilities to push capture levels above initial values and therefore lowering CO2 emissions using SEGR.

1.3 Novelty and Contribution

The following results can be considered an original contribution to advancing the body of knowledge in the field of increasing CO2 concentration in exhaust flue gas by means of selective exhaust gas recirculation to push process intensification for post-combustion CO2 capture and thereby overcoming current challenges for carbon capture and storage in gas power plants.

- For the first time in the literature a detailed kinetic model of a large-scale regenerative rotary CO2 transfer wheel, including resistance to mass and heat transfer, is provided and validated.
- Identification and optimisation study of kinetic properties and operational conditions affecting the performance of the large-scale regenerative rotary CO2 transfer wheel is performed. Providing guidelines for adsorbent development for SEGR application and operational guidelines to power plant operators.
- A rigorous design assessment of the regenerative rotary CO2 transfer device, utilizing honeycomb structured adsorbent, and considering preferential direction of leakages.
- A technical assessment of the effect of regenerative rotary CO2 transfer devices on new-build CCGTs with PCC system, using amine based scrubbing technology. Quantitative evaluation of the reduction in equipment size and energy penalty for the PCC system and of the performance of the CCGT power plant, by means of power output and net efficiencies, in comparison to conventional new-build CCGT with PCC.
- Identification of the operating framework for existing CCGT with PCC, using amine based scrubbing technology, retrofitted with regenerative rotary CO2 transfer devices. Assessment of limiting factors for retrofit deployment of SEGR in CCGTs with PCC and establishment of CO2 concentrations possible in the exhaust flue gas in achievable SEGR ratios.
- Technical assessment of pushing capture levels above original values by means of SEGR.

Table 1-1 shows the models used this thesis and the person responsible for developing these models.

Table 1-1: Summary of utilised models

Model	Developer
Equilibrium model of the Rotary Adsorption Wheel	L. Herraiz
Kinetic model of the Rotary Adsorption Wheel including heat transfer	E. Palfi
Combined Cycle Gas Turbine	L. Herraiz
Post Combustion Capture Plant	E. Palfi
CO2 Compression Train	E. Palfi
Integration of the models for process simulation	E. Palfi

1.4 Structure of the Thesis

The thesis is composed of eight Chapters. The content is summarised below.

- Chapter 2 describes the challenges associated with applying carbon capture and storage to gas power plants. It provides the background for the research conducted in the following chapters of this work, by assessing state of the art strategies to increase CO2 concentration in exhaust flue gases of CCGTs.
- Chapter 3 describes the fundamental theory of adsorption and the development of rotary devices in adsorption. It further introduces the previously conceptual equilibrium model of a rotary wheel for SEGR application and preliminary results. It continues then to present the developed kinetic model of a regenerative rotary CO2 transfer, including the experimental methodology and the developed design consideration for honeycomb structured adsorbent distributed in a regenerative rotary CO2 transfer wheel.
- Chapter 4 presents the experimental assessment of the activated carbon used to validate the system. It continues to present the validation of the kinetic model of a regenerative rotary CO2 transfer device and associated performance and operational profiles of the rotary wheel in operation. It then

further assesses and investigates, by means of sensitivity analysis, the limitation presented by the kinetic properties of the adsorbent and operational conditions of the system.

- Chapter 5 describes the fundamental principles considered in the process modelling of the combined cycle gas turbine power plant with amine solvent post-combustion carbon capture technology. It further describes the integration between the different parts of the power plant, the capture plant and compression train and the optimisation procedure followed to evaluate operating and design parameters in the CO2 capture plant.
- Chapter 6 investigates the effect of the integration of the regenerative rotary CO2 transfer device on a new-build CCGT with PCC system. It reports the technical performance of the CCGT and evaluates the reduction in equipment size and energy requirements in the PCC system in comparison to a conventional CCGT with PCC.
- Chapter 7 explores the effect of retrofitting regenerative rotary CO2 transfer to existing CCGT with PCC system. It reports the technical performance of the post-combustion carbon capture plant, using amine based scrubbing technology, and reports operational limitations. It then investigates the possibility to lower CO2 emissions by pushing capture levels above design values by means of SEGR and operational changes and compares the resulting capture levels with achievable capture levels by pushing the capture plant in a configuration without SEGR.
- Chapter 8 summarises and concludes the work performed in this thesis and discusses recommendations and improvements for future work.

Chapter 2 State of the Art on Process Intensification for Gas Power Plants with CCS

This chapter covers the literature review of current challenges encountered in capturing CO2 from flue gases produced in CCGT power plants (Section 2.1). It goes on to briefly show how higher flue gas CO2 concentrations can benefit all kind of post-combustion capture technologies (Section 2.2). Followed by strategies to increase CO2 concentration in exhaust gases and a detailed assessment of recent technology developments in selective exhaust gas recirculation (Section 2.3).
The state of the art on regenerative rotary CO2 transfer wheels is covered in Chapter 3.

2.1 Current Challenges of CCS in Gas Power Plants

Flue gas produced in gas-fired power plants, like CCGTs, provides challenges for PCC technologies. These challenges influence net thermal efficiency, and capital and operational costs of the post-combustion capture plants.

Gas turbines need to be operated with a high amount of excess air, due to gas turbine material constraints limiting the acceptable turbine inlet temperature, and to limit temperature related NOx emissions. (Horlock, Watson, and Jones 2001; Boyce 2012; Brooks 2000; Pavri and Moore 2001)
This high amount of excess air results in large flue gas flow rates and in CO2 concentrations as low as ∼3–4%vol. In comparison typical CO2 concentrations in flue gases from coal power plants are in the magnitude of around 10-15% vol. (IEAGHG 2012; EBTF 2011)
The large amount of flue gas and the low driving force, associated with the low CO2 concentration, lead to higher power output penalties, linked to the energy needed to regenerate the solvent, and large capture plant equipment sizes, linked to higher

capital costs. Higher CO2 concentrations in the flue gas have shown for amine-based post-combustion capture, as investigated in this thesis, to be connected to lower reboiler duty and capital cost savings, by reducing capture plant size requirements. (Li, Ditaranto, and Yan 2012; Merkel et al. 2013; Yingying Zhang et al. 2014; Akram et al. 2016; Diego, Bellas, and Pourkashanian 2018; Diego et al. 2017; IEAGHG 2012; Aboudheir and ElMoudir 2009; Hellat and Hoffmann J. 2016)

A last point, which needs to be considered in the context of the large amount of excess air, is the high concentration of unburned O2 in the flue gas (10-15%vol), which increases solvent oxidative degradation and hence operational costs. (Goff and Rochelle 2004; Lepaumier, Picq, and Carrette 2009; Sexton and Rochelle 2011)

2.2 Post-Combustion Carbon Capture

Post-combustion capture technologies can currently be roughly divided in five subsections, as shown in Figure 2-1.

The most advanced CO2 capture technology on the market is currently amine solvent absorption, which is the only CCS technology currently considered at a technology readiness level (TRL) of 6 - 8. A technology at TRL 6 is considered to be at a fully integrated pilot stage and tested in a relevant environment, TRL 7 is a subscale fully functional prototype of the technology and TRL8 a commercial demonstration of the technology.(IEAGHG 2014; M. Wang et al. 2011)

Hence, it can be expected that many first generation CCS projects will be fitted with solvent based PCC technology. As this technology is applied in this thesis, it will be discussed further in general, in contrast to the others.

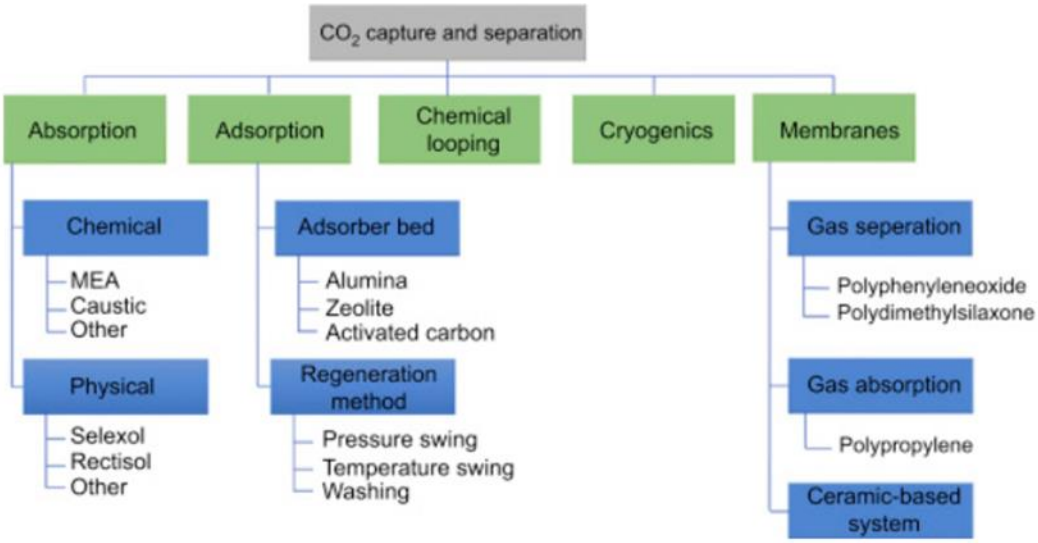

Figure 2-1: CO2 capture technology routes (Abu-Zahra, Sodiq, and Feron 2016)

Independent of the CO2 capture technology, higher CO2 concentration in flue gases lead to more CO2 bound to the solid material or liquid solvent, or higher permeation rates in membranes. Which in turn leads to a reduction in minimum energy requirement to separate CO2 from the flue gas. An illustration of minimum energy requirement based on the increase in CO2 concentration in the feed gas flow is given in Figure 2-2, showing that an increase of CO2 concentration from 5% (current ~CO2 concentration in gas fired power plants) to 15% (~CO2 concentration in coal fired power plants and reported possible CO2 concentration in flue gases of gas fired power plants with SEGR) in the feed flow would lead to a decrease of 15% in minimum CO2 separation energy required. Therefore, any kind of post-combustion technology applied to combustion power generation can consequently profit by adding SEGR.

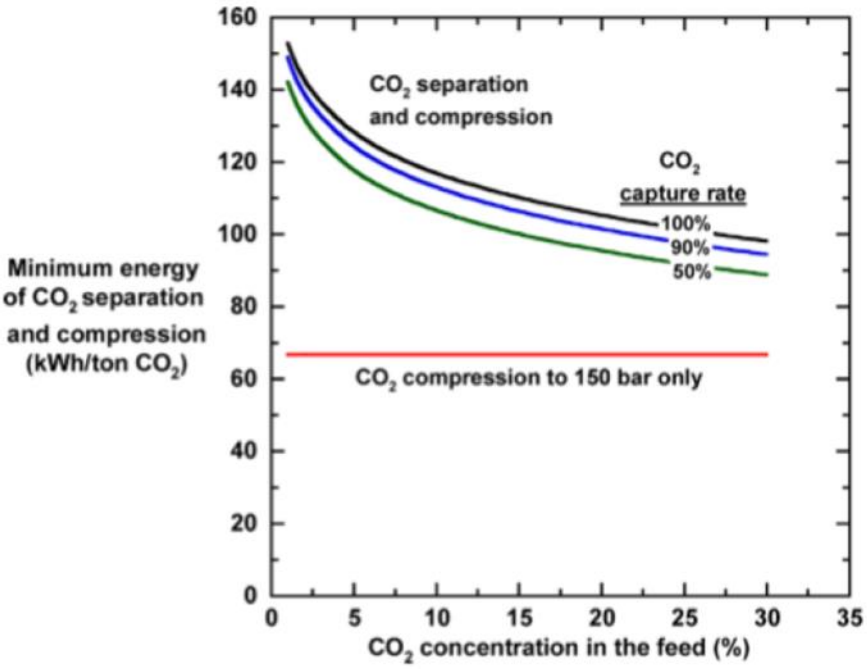

Figure 2-2: Minimum energy per ton of CO2 captured as a function of CO2 concentration in a flue gas stream (Merkel et al. 2013)

Chemical absorption is currently viewed as the most advanced post-combustion technology. It has been proven on commercial scale on two coal-fired power plants, Boundary Dam and Petra Nova. (Singh and Stéphenne 2014; MIT 2016; SaskPower 2019; NRG Energy 2019)

The energy requirement to separate CO2 from the flue gas in chemical absorption is measured in reboiler duty in [MJ/kgCO2]. It is the energy needed to regenerate the solvent per mass of CO2 recovered, as given in Equation (2.1).

$$Specific\ Reboiler\ Duty\ = \frac{Thermal\ energy\ rate}{CO2\ mass\ flow\ rate} \tag{2.1}$$

The capture rate of the capture plant, also referred to as capture efficiency, is defined as the ratio of amount of CO2 leaving the capture plant at the top of the absorber to the amount of CO2 entering the capture plant at the absorber inlet (Equation (2.2)).

$$Capture\ Rate\ = 1 - \frac{[mol\ CO2]_{absorber\ outlet}}{[mol\ CO2]_{absorber\ inlet}} \tag{2.2}$$

Aqueous monoethanolamine (MEA 30 wt%), used in the work performed in this thesis, is regarded as the benchmark amine for CO2 capture from power generation, against which new solvents and other capture technologies are measured. The typical setup of a MEA post-combustion capture plant is described under Section 5.3. Energy penalties related to regenerating 30 wt% MEA capturing 90% of the CO2 presented in flue gases with 10-15vol% CO2 are in the range of 3.5 to 4 MJ per kg CO2 captured. (Sharifzadeh and Shah 2015; Stec et al. 2016; Brigman et al. 2014)

Several new solvents are under investigation, however only few progress from bench scale to pilot scale, which is necessary to assess hydrodynamics, volatility and degradation. (Bui et al. 2018)

2.3 Strategies to Increase CO2 Concentration in the Exhaust Flue Gas and their Effects

In this section a comprehensive literature review about the possibilities to solve the challenges for CO2 post-combustion capture from flue gas produced in gas-fired power plants, given in Section 2.1, is performed.

Different process modifications are being investigated to increase the CO2 concentration in the flue gas entering the capture plant. They can be divided into five types of modifications:

- Gas Turbine Humidification
- Supplementary Firing
- Sequential Supplementary Firing
- Exhaust Gas Recirculation (EGR)
- Selective Exhaust Gas Recirculation (SEGR)

2.3.1 Gas Turbine Humidification

Gas turbine humidification technologies are used to replace part of the excess air for cooling by saturated air or steam. Part of the amount of excess O2 and N2 in the exhaust gas is replaced by H2O. H2O can be easily separated from the flue gas by condensation. Consequently, this leads to a higher CO2 concentration at the inlet of the capture plant, than in conventional systems. Heat available in the system is used to generate the water vapour or steam. Such systems show higher power outputs and increased thermal efficiencies, compared to conventional gas turbines. (Rao 2015; Jonsson and Yan 2005; Li, Ditaranto, and Berstad 2011)

Two different kind of gas turbine humidifications are differentiated (Rao 2015; Jonsson and Yan 2005; Poullikkas 2005; Li, Ditaranto, and Berstad 2011; Bianchi et al. 2010):

- Inlet air cooling - ambient air is used to evaporate water, increasing the humidity in the air to saturation concentration
- Combustion chamber injection – injecting either steam directly (steam injection gas turbine STIG), or water to evaporate, using a setup of humidification tower and water recirculation loop (evaporative gas turbine cycle EvGT)

The combustion itself in humidified gas turbines is limited by the amount of O2 and the amount of water vapour in the combustion. State-of-the-art burners in gas turbines are operated in a dry manner, known as Dry Low-NOx burners. In general, the development from dry to wet burners would need extensive investment in testing beyond the research and pilot plant testing conducted over nearly two decades by various authors. Disadvantages of such cycles include increased costs due to complexity and large consumption of water, combined with demineralization equipment to avoid issues like deposition and corrosion.(Ågren et al. 2002; Takahashi, Nakao, and Koda 2007; T. Lindquist, Thern, and Torisson 2002; Rao 2015; Li et al. 2009; Li, Ditaranto, and Berstad 2011; T. O. Lindquist, Rosen, and Torisson 2000a, 2000b).

Gas turbine humidification seems only feasible in the context of small scale applications of a few MWs, when, due to technical and cost limitations, large scale CCGTs are not an option. (Rao 2015)

Achievable CO2 concentration depend on the ratio between water and air and the flue gas temperature achievable in the flue gas conditioning system prior to entering the CO2 capture plant. CO2 concentrations up to 5 mol% in the conditioned flue gas stream have been reported for EvGT, at a water to air ratio of 15% leading to a O2 concentration in the combustor of 16.5 mol%. When EvGT is compared to EGR it represented the lowest possible electrical efficiency for the thermally integrated system with 41.6%, compared to an efficiency of 50.5% for EGR. This can be tracked back to part of the heat in the flue gas being used to generate the steam or to heat up the water for saturating the air for the gas turbine humidification step, resulting in less available heat for the steam cycle of the power plant. (Li et al. 2009; J. R. Li, Kuppler, and Zhou 2009; Li, Ditaranto, and Berstad 2011)

2.3.2 Supplementary and Sequential Supplementary Fired Combined Cycle

Supplementary and sequential supplementary firing are previously proposed options in literature to increasing the CO2 concentration in the exhaust flue gas of gas turbine systems.(H. Li, Ditaranto, and Berstad 2011; H. Li, Ditaranto, and Yan 2012; González Díaz et al. 2014; Herraiz 2016)

(González Díaz et al. 2014) show that these modifications can only be considered financially attractive under the restrictions of low gas prices and the utilisation of the CO2 for enhanced oil recovery (EOR) projects.

However, supplementary firing increases the CO2 concentration in the exhaust by burning additional fuel. Considering that in the context of reducing overall CO2 emissions and fossil fuel consumption, these kind of modification cannot be considered part of the solution for a deep decarbonisation of the electricity generation.

In supplementary fired combined cycles (SFCC), additional fuel is burned in an additional combustor, called in-duct burner, using the flue gas of the gas turbine as comburent. This results in lower O2 levels and higher CO2 concentrations in the capture plant. The flame is stabilised by the temperature of the flue gas exiting the gas turbine. The in-duct burner is located downstream of the gas turbine and upstream of the heat recovery steam generator (HRSG), as illustrated in Figure 2-3. The maximum additional combustion of fuel is limited by the metallurgical temperature constrains in the HRSG. This also limits the highest achievable CO2 concentration in the flue gas. Supplementary firing, as modification in CCGTs, are typically used as response to increased peak demands at times when high electricity prices can be achieved, or to produce more steam for other industrial facilities. They show a higher load flexibility than conventional CCGTs when energy demand increases.(González Díaz 2016; Herraiz 2016; Kehlhofer et al. 2009; Biliyok and Yeung 2013; Arrieta and Lora 2005; Li, Ditaranto, and Berstad 2011; Li, Ditaranto, and Yan 2012)

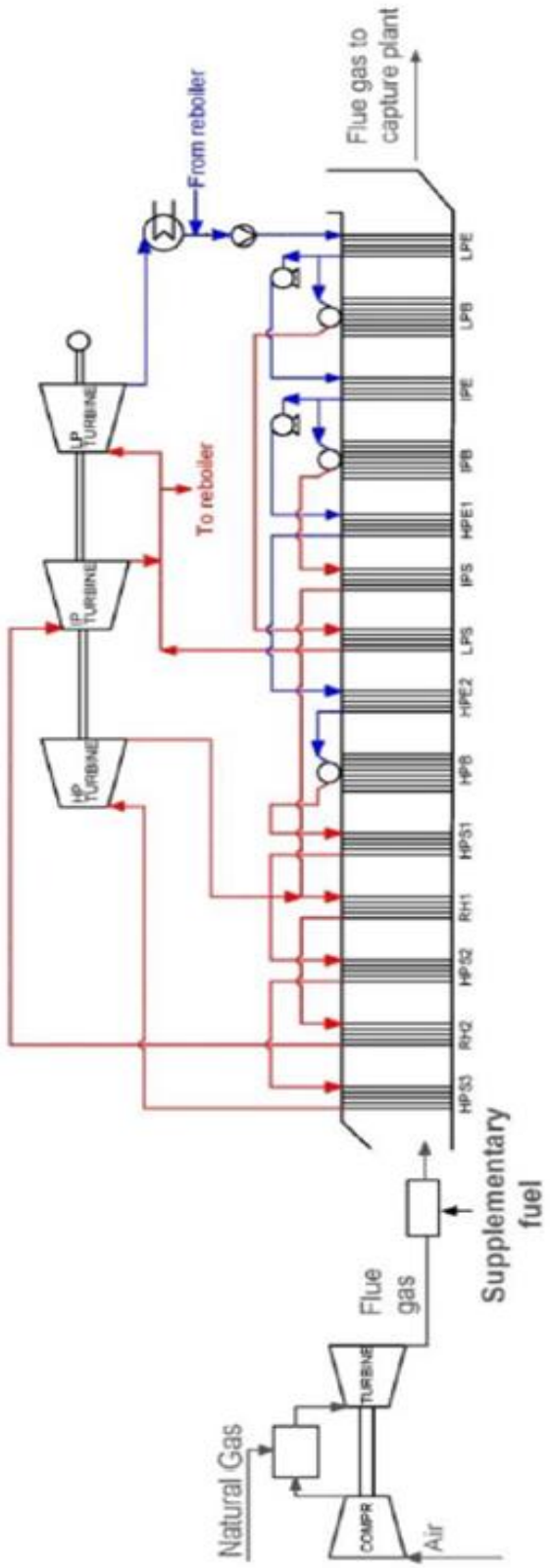

Figure 2-3: **Schematic of the natural gas combined cycle with supplementary firing** (González Díaz 2016)

In the context of a reduced carbon intensity, research is investigating the benefits of SFCC modifications with burning biomass instead of natural gas in the supplementary combustor. In combination with PCC this could be a further step towards a net negative emission power generation. (Gnanapragasam, Reddy, and Rosen 2009; Datta, Mondalz, and Gupta 2008)

For gas fired SFCCs (Li, Ditaranto, and Yan 2012) report an increase in CO2 concentration achievable of 8.4mol% from previous 3.9 mol%, thus similar to concentrations achievable with EGR, with only a marginal decrease in flue gas mass flow rate towards the capture plant and a reduction in electrical efficiency to 43.3%.

Different strategies are proposed to increase the efficiency of the overall cycle for SFCCs further. Those include an exhaust gas reheater, to extract part of the additional heat generated in the second combustor and transfer it back to the flue gas passing through a two-stage gas turbine. The flue gas, passing first through the high pressure stage of the gas turbine, would be reheated with the additional available heat from the flue gas leaving the second combustor, and then be expanded in the second low pressure stage of the gas turbine. This would increase the efficiency of the gas turbine. Another option proposed includes the use of a supercritical HRSG, which would be able to use the additional available heat to generate more steam for the steam cycle and therefore increase the power output of the steam cycle. A third option includes the use of EGR with supplementary firing to further increase the CO2 concentration and to reduce the mass flow rate towards the capture plant, and therefore reduce the penalty of the solvent regeneration in the capture plant. In this option the oxygen limitation in both combustors would need to be investigated further.(González Díaz 2016; González Díaz et al. 2014; Li, Ditaranto, and Yan 2012)
According to (Li, Ditaranto, and Yan 2012) a combination of all three options combined would be able to increase the electrical efficiency from previous 43.3% to 54.1%, and the CO2 concentration up to 11.2 mol%. However, the gain of these

additional modifications would need to justify the additional cost associated with the different options.

A further increase in the CO2 concentration in the flue gas and reduction in the mass flow rate to the capture plant is achieved by sequential supplementary firing as applied in sequential supplementary fired combined cycles (SSFCC). A schematic process flow diagram is depicted in Figure 2-4. This technology overcomes metallurgical temperature constrains in the HRSG, by burning additional fuel in several stages in between the heat transfer bank along the flow direction in the HRSG, adhering to the temperature constrains of each section. Therefore, no special alloys or changes in the HRSG configurations are necessary. The resulting smaller temperature difference in the HRSG increases the steam cycle efficiency. The limiting factor in this modification becomes the minimum excess of oxygen in the flue gas, which is the comburent in each combustion step. Reported achievable CO2 concentrations are 9.4 mol% and a flue gas mass flow reduction of approximately 50%. (González Díaz 2016; González Díaz et al. 2014)

However, a low level of O2 (1 mol%) in the last burner stage in the HRSG could limit the combustion. The stabilisation of the combustion in low O2 concentrations by the high combustion temperature, an assumption based on data presented by (Li, Ditaranto, and Berstad 2011) for SFCCs, might occur, yet due to the lower combustion temperature in SSFCCs further testing is needed.

In a supercritical CCGT plant, the power output can be maintained by operating only one GT-HRSG train of previously two trains, due to the increase in steam flow rate and corresponding output of the steam turbines. Nevertheless, this is connected to an efficiency penalty of 5.7% for supercritical and 8.2% for subcritical SSFCC. This can be explained by the fact, that the additionally burned fuel is only used in the less effective steam cycle and the higher pinch temperature difference in the HRSG.

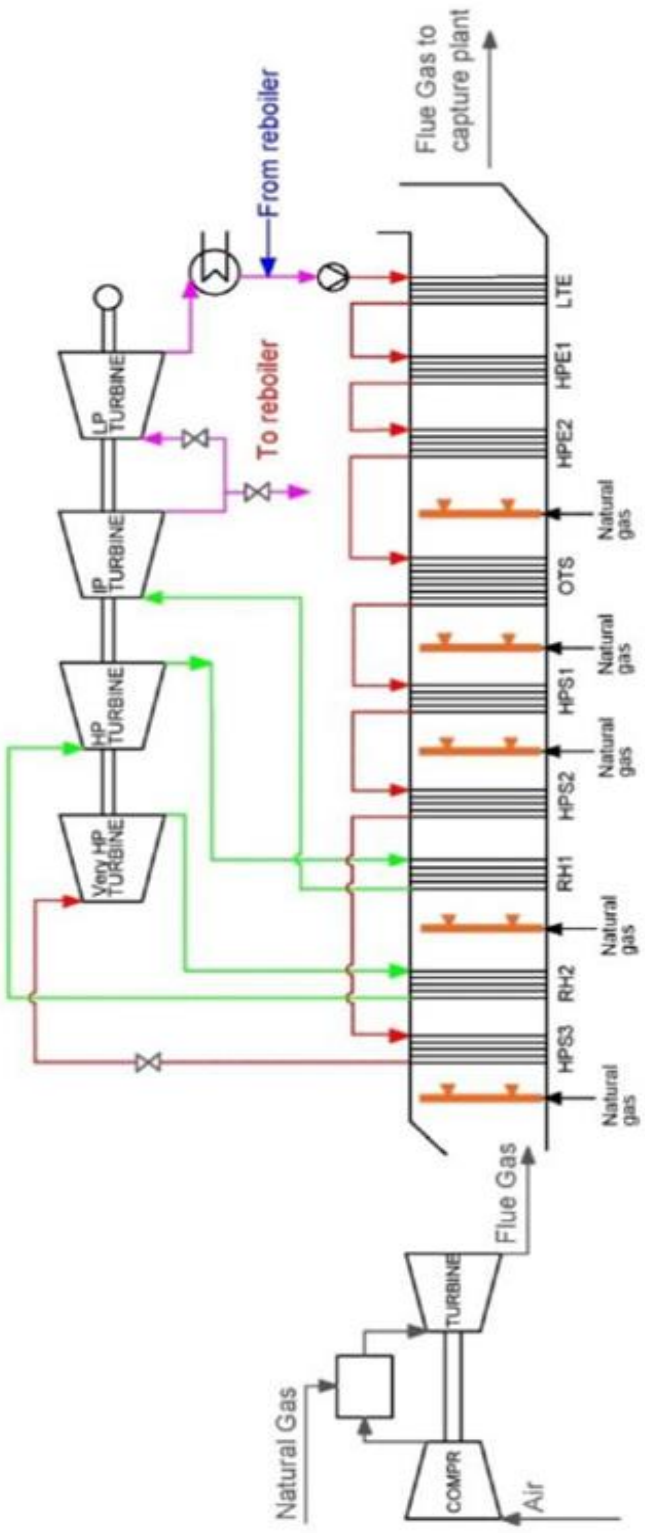

Figure 2-4: **Schematic process flow diagram of a supercritical sequential supplementary firing configuration with HRSG train combined cycle with a double reheat steam cycle** (González Díaz 2016)

2.3.3 Exhaust Gas Recirculation

In exhaust gas recirculation (EGR) a fraction of the flue gas exiting the HRSG is conditioned and recirculated back to the inlet of the compressor, replacing some of the air going to the combustor. The resulting O2 concentration in the combustor is reduced because of the lower O2 concentration in the exhaust flue gases. A schematic block flow diagram of a CCGT power plant with EGR and PCC is illustrated in Figure 2-5. Originally used as a strategy to decrease NOx emissions, current reasons for recirculating a fraction of the exhaust gas include, reducing the O2 concentration in the flue, increasing the CO2 concentration in the flue gas and reducing the flue gas mass flow rate entering the capture plant. This results in a lower regeneration penalty for the capture plant and possible reduction in capture plant size requirements. (Akram et al. 2016; González-Salazar 2015; Evulet et al. 2009; ElKady et al. 2009; Herraiz et al. 2018; Li et al. 2011; Li, Ditaranto, and Yan 2012).

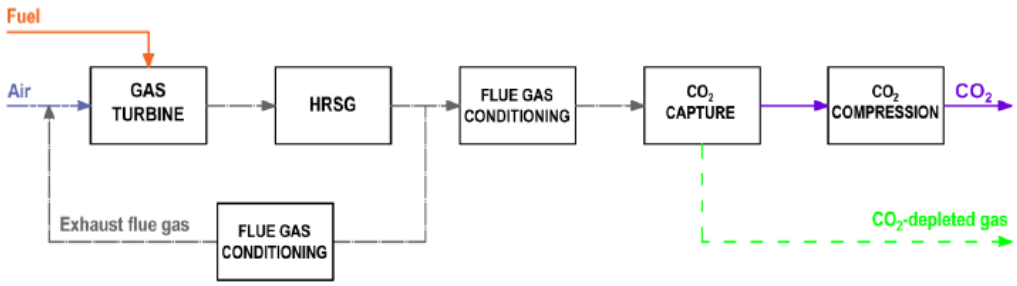

Figure 2-5: Block flow diagram of CCGT with PCC and EGR (Herraiz 2016)

An important variable is the exhaust gas recirculation ratio (EGR ratio), which is defined as the ratio of the mass flow rate of the recirculated flue gas to the total flue gas mass flow rate at the exit of the HRSG, as shown in Equation (2.3).

$$EGR\ ratio = \frac{mass\ flow\ rate\ of\ recirculated\ flue\ gas}{total\ mass\ flow\ rate\ of\ flue\ gas}\Big|_{HRSG\ outlet} \quad (2.3)$$

The recirculation ratio is limited by the O2 concentration presented in the combustor. Therefore, the O2 concentration also limits the maximum CO2 concentration achievable in the flue gas. The theoretical limit is given by the stoichiometric amount

of O2 in a complete combustion of the fuel. However, due to the dependence of the combustion on inlet temperature, velocity, turbulence, and resident time the O2 concentration needs to be chosen high enough to guarantee flame stability and complete combustion. Incomplete combustion of the fuel may lead to efficiency losses. These are the main challenges associated with EGR applications in CCGTs.(Evulet et al. 2009; ElKady et al. 2009; Herraiz et al. 2018; Li et al. 2011; ElKady et al. 2008)

Several authors studied the effect of O2 concentration on flame stability and combustion experimentally.

(Røkke and Hustad 2005) establish a blowout O2 concentration limit of 13-14 vol% for a 65kW combustor operated in pre-mixed flame mode.

(Ditaranto, Hals, and Bjørge 2009) established a blowout O2 concentration limit of 14 vol% in an atmospheric laboratory-scale setup of a 5 kW methane jet flame with the exhaust gas of a virtual 10 kWth gas turbine as comburent. However, he showed that even though the flame was stable at that O2 concentrations in the oxidiser, the levels of unburned hydrocarbons and CO were high.

(ElKady et al. 2009b; Evulet et al. 2009) establish for a bench- scale lean pre-mixed burner as applied in Dry Low-NOx combustor systems in General Electric (GE) F-class gas turbines, an O2 concentration limit of 16-17 vol% to secure a complete combustion with low levels of unburned hydrocarbons and low levels of CO. They also suggest that O2 concentration below 16 vol% would be achievable with minor modifications to existing combustion systems. The experiments were conducted at 10 bar and for temperatures up to 1630◦C. Typical operating pressures of gas turbines are however in the range of 18 bar.

In literature it is now commonly accepted, that for stable and complete combustion and reduced emissions with current combustor designs a minimum O2 concentration of 16 vol% is required. (Akram et al. 2016; González Díaz 2016; Herraiz et al. 2018; Li et al. 2011).

According to (ElKady et al. 2009b), (Li et al. 2011) and (Herraiz 2016) to maintain a minimum O2 concentration in the combustor of 16 vol%, a maximum EGR ratio of 35% can be achieved. This results in a CO2 concentration of 6 vol% in the turbine exhaust gas according to (ElKady et al. 2009b), in a CO2 concentration of 5.8 vol% at the absorber inlet according to (Li et al. 2011) and in a CO2 concentration of 6.5 vol% in the flue gases according to (Herraiz 2016).
For EGR ratios beyond 35% (Li et al. 2011) and (ElKady et al. 2009b) suggest new optimized combustor designs, by either modifying the combustion system to allow O2 inlet concentration below 16 vol%, or by injecting additional O2.

The effect of EGR on the gas turbine performance was studied by (Klas Jonshagen, Sipöcz, and Genrup 2011), by modelling a state-of-the-art CCGT power plant with GE class F turbine technology. The deviation of a set of dimensionless parameter groups is used to evaluate the performance of compressor and turbine at off-design conditions. (Klas Jonshagen, Sipöcz, and Genrup 2011) concludes that an EGR ratio up to 40% leads to a minimal deviation in the gas turbine engine.

The effect of EGR on microturbines in pilot scale have been experimentally assessed by (Akram et al. 2016) and (De Paepe et al. 2012). The engine control in microturbines will maintain the power output constant at a constant turbine inlet temperature, by changing the shaft speed and the fuel flow rate. (Akram et al. 2016)
Therefore, both performed experiments cannot be used to predict the behaviour of large scale axial flow gas turbines at constant rotational speed.
(De Paepe et al. 2012) report unsteady operation of the microturbine during EGR operation, due to continuously changing composition and temperature of the inlet air.
(Akram et al. 2016) used the exhaust gases of the microturbine and injected CO2 (up to 11 vol%) into the stream in order to simulate flue gas compositions according to EGR ratios and assessed the effect of the increased CO2 concentration on the integrated post combustion CO2 capture plant, using 30 wt% MEA. The results show

a reduction in specific reboiler duty by around 7% per unit percentage increase in CO2 concentration.

Several studies assess the effect of EGR on the energy requirement to separate CO2 from the flue gas of CCGTs and the overall effect on the power output and efficiency of the cycle.

In 2010 the National Energy Technology Laboratory (NETL) (National Energy Technology Laboratory 2010) considered CCGTs with PCC using MEA and an EGR ratio of 35% as the lowest cost option to capture CO2. In 2013 NETL (National Energy Technology Laboratory 2013) reported an efficiency increase of 0.3 % and a reduction in electricity costs by 3 %, when a CCGT with PCC is operated with EGR at a ratio of 35%, compared to a conventional CCGT with capture. Corresponding reported CO2 concentration in the exhaust gas are up to 6.7 vol%.

The techno-economical study on CO2 capture in gas fired power plants by the International Energy Agency Greenhouse Gas (IEAGHG) R&D Program (IEAGHG 2012) reports for CCGT with PCC and an EGR ratio of 50%, compared to a conventional CCGT with PCC using MEA, a reduction in electricity cost by 3.2% and the reboiler duty by 7.17%. Leading to an increase in net power efficiency from 51.04% to 51.33%. However, these results need to be re-evaluated in the context that an EGR ratio of 50 % might not be feasible in the context of flame stability and complete combustion.

(Li et al. 2011) report for an EGR ratio of 35% an electrical efficiencies of ~50.5%, corresponding to an efficiency penalty of approximately 0.3% in comparison to a conventional CCGT with PCC.

On the other hand (Herraiz 2016) reports for an EGR ratio of 35% a net thermal efficiency of ~52.3%, corresponding to an increase in net thermal efficiency of approximately 0.4% in comparison to a conventional CCGT with PCC. Furthermore, results show an approximate reduction in absorber packing volume for a CCGT with 35% EGR of 40% when compared to a conventional CCGT with PCC and a reduction in reboiler duty of 2.9%.

In conclusion, EGR is an option to increase CO2 concentration in CCGT flue gases and to reduce flue gas mass flow rates towards the capture plant, leading to a reduction in required reboiler duty. However, there is a clear limitation in achievable EGR ratios, due to limitation based on O2 levels in the combustion to guarantee flame stability and complete combustion. Moreover, demonstrating the potential of EGR at a larger scale and therefore showing the maturity of this kind of technology is still necessary to move EGR forward.

2.3.4 Selective Exhaust Gas Recirculation

In selective exhaust gas recirculation (SEGR), CO2 from the flue gas is selectively recycled back to the air inlet stream of the gas turbine compressor. Other components presented in the flue gas, like N2 and water vapour, are not recirculated. Therefore, it is possible to increase the CO2 concentration in the flue gas beyond the values reported for EGR, since less amount of excess air is replaced. Consequently, the O2 concentration in the combustor remains sufficiently above the limiting 16 vol% reported as combustion limit for EGR. Several authors report achievable CO2 concentrations in the flue gas of around 14 vol%, while simultaneously keeping the O2 concentration at 19 vol% (Merkel et al. 2013; Herraiz et al. 2018).

In the context of SEGR some important variables need to be defined, those are recovery rate and overall CO2 capture rate.

The recovery rate of the SEGR device, also referred to as SEGR capture efficiency, is defined as the ratio of amount of CO2 leaving the SEGR unit at the flue gas outlet of the transfer device to the amount of CO2 entering the SEGR unit at the flue gas inlet of the transfer device, as given in Equation (2.4). It is the amount of CO2 removed from the flue gas and transferred to the air stream.

$$Recovery\ Rate\ = 1 - \frac{[mol\ CO2]_{SEGR\ flue\ gas\ outlet}}{[mol\ CO2]_{SEGR\ flue\ gas\ inlet}} \quad (2.4)$$

Since flue gas, and therefore CO2 emissions, can leave the power plant boundaries through two streams under SEGR application, it is necessary to introduce an overall CO2 capture rate for the power plant, also referred to as overall CO2 capture efficiency, as given by Equation (2.5).

$$Overall\ CO2\ Capture\ Rate\ = \frac{[mol\ CO2]_{to\ transport\ and\ storage}}{[mol\ CO2]_{generated\ in\ natural\ gas\ combustion}} \quad (2.5)$$

To achieve selective CO2 recirculation different configurations and technologies are proposed.

Initially two common configurations implementing SEGR in CCGT power generation with PCC are proposed and patented by Merkel and co-workers. (Richard W Baker et al. 2011; Wijmans, Merkel, and Baker 2011; Merkel et al. 2013; Wijmans, Merkel, and Baker 2012a, 2012b)

According to the position of the SEGR device, they are referred to as SEGR in parallel, or SEGR in series. A block flow diagram of these two configurations is presented in Figure 2-6.

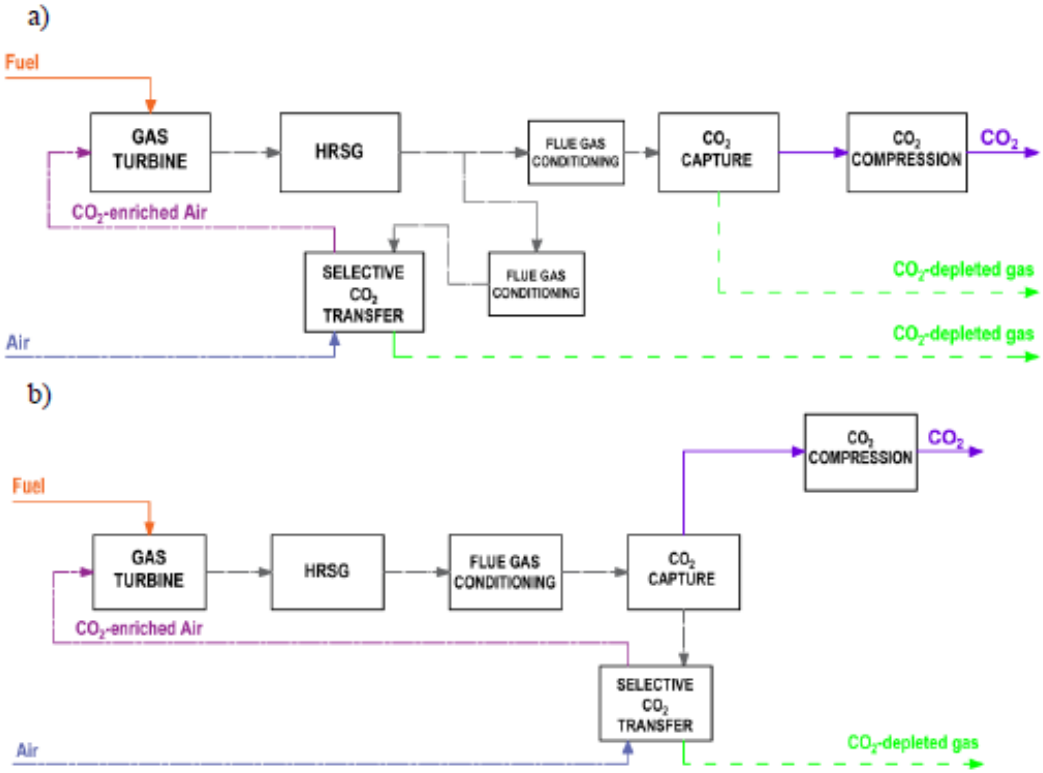

Figure 2-6: **Block flow diagrams of (a) SEGR in parallel and (b) SEGR in series** (Herraiz 2016)

In the parallel configuration, the SEGR device operates in parallel to the capture plant. Flue gas leaving the HRSG is split according to a so called SEGR ratio. One part of the split flue gas is treated by the capture plant, the other part is sent to the SEGR device, where CO2 will be transferred to the air steam used in the combustor. In this configuration the SEGR ratio becomes an important variable. The SEGR ratio is defined as the ratio of the mass flow rate of the flue gas towards the selective CO2 transfer device to the total flue gas mass flow rate at the exit of the HRSG, as shown in Equation (2.6).

$$SEGR\ ratio = \frac{mass\ flow\ rate\ of\ flue\ gas\ to\ the\ CO2\ transfer\ device}{total\ mass\ flow\ rate\ of\ flue\ gas}\Big|_{HRSG\ outlet} \qquad (2.6)$$

In the series configuration, the SEGR device operates downstream of the capture plant. The whole flue gas first passes through the capture plant, where a fraction of

the CO2 will be removed. The remaining CO2 in the flue gas then leaves the capture plant towards the SEGR device, where the rest of the CO2 is removed and transferred to the air stream used in the combustor.

There are different specific benefits and limitations associated with each configuration. In SEGR in parallel the size of the capture plant and the SEGR transfer device can be reduced, due to the reduced mass flow rates towards each of the units and the higher CO2 concentration. However, the capture rate of the capture plant and the recovery rate of the SEGR device need to achieve higher rates to keep the overall CO2 capture rate at a constant value. In SEGR in series the reduction in absorber column and SEGR device size is marginal, compared to SEGR in parallel, since the whole flue gas amount has to be treated by both units. However, the capture rate of the capture plant can in some instances be reduced by nearly 60%, since the SEGR device downstream of the capture plant will transfer the remaining CO2 into the air stream. Yet, the reduction in capture rate of the capture plant has to be balanced by an increase in recovery rate of the SEGR device, to achieve the desired overall CO2 capture rate. (Herraiz et al. 2018; Merkel et al. 2013; Maria Elena Diego, Bellas, and Pourkashanian 2017)

This thesis will concentrate on the configuration in parallel, since it shows higher potential reduction in flue gas mass flow rates and higher achievable CO2 concentrations in the flue gas, compared to the configuration in series. This is in accordance with other work performed by (Darabkhani et al. 2018; Russo et al. 2018; Ding, Freeman, and Rochelle 2017; Maria Elena Diego, Bellas, and Pourkashanian 2017).

Independent of the technology used to transfer CO2, which will be discussed later in this section, several authors (Herraiz et al. 2018; Merkel et al. 2013; Y. Huang, Merkel, and Baker 2014) indicate that a sufficient driving force for the CO2 separation and transfer is given by the use of counter-current feed air to flue gas flow and the partial pressure difference between those two flows. There is no indication of a further need for vacuum, compression, or heat. However, needed are blowers on both sides, the

flue gas and the air stream, to overcome the pressure drop across the SEGR device. (Herraiz et al. 2018) report for a parallel configuration with a recirculation ratio of 70% using an adsorbent based SEGR device an air fan consumption of 0.75 MWe, a booster fan consumption of 0.99 MWe for the SEGR device and 2.06 MWe for the booster fan upstream the capture plant, adding up to an overall consumption of 3.8MWe per train. For SEGR in series using an adsorbent based SEGR device the air fan consumption rises to 1.07MWe and the booster fan consumption upstream of capture plant, overcoming the pressure loss of both capture plant and SEGR device, rises to 7.01MWe, adding up to 8.08MWe. This needs to be in comparison with the overall fan consumption of 7.31 MWe of a CCGT with PCC without SEGR.

Challenges encountered with applying SEGR to CCGTs with PCC are similar to those encountered in CCGTs with PCC and EGR. These are flame stability, complete combustion and changes in the working fluid effecting the gas turbine performance.

Several authors (Herraiz et al. 2018; M. E. Diego, Bellas, and Pourkashanian 2018; Darabkhani et al. 2018; Merkel et al. 2013; Maria Elena Diego, Bellas, and Pourkashanian 2017) have taken as reference for SEGR a limiting oxygen level in the comburent of 16 vol%, based on the experimental work performed by (ElKady et al. 2009b) for combustion under EGR application. However, since CO2 acts as a combustion inhibitor, effectively reducing the flame temperature and burning rate in the combustion, comburent containing 8-9 vol% CO2, might lead to other flame stability and blow-off limits. Therefore, a different minimum O2 level in the comburent might need to be established.

As part of the scope of the EPSRC project “Selective Exhaust Gas Recirculation for Carbon Capture with Gas Turbines: Integration, Intensification, Scale-up and Optimisation” (SELECT 2014) the combustion process in a premixed DLE swirl burner with a CO2-enriched oxidant has been experimentally assessed. Results reported by (Marsh et al. 2016) for combustion experiments at 1.1 bar and 2.2 bar show, that for CO2 concentrations above 10 vol% in the comburent, the equivalence ratio, also

known as the fuel to air ratio, has to be adjusted to above 0.7 to maintain flame stability and ensure complete combustion. CO emissions below 100 mg/Nm^3 and NOx emissions below 50 mg/Nm^3 (dry, 15 %vol O2) are measured during those combustion tests. Further tests performed on a high-pressure generic swirl burner (HPGSB-2) at 5.5 bar and an equivalence ratio of up to 0.95, show that molar dry exhaust concentrations of CO2 up to 31% are achievable, corresponding to a CO2 inlet concentration of ~17 vol% (Giles et al. 2019). The authors however highlight, that a further increase in pressure will slightly decrease this achievable value. The authors further report, that the addition of CO_2 into the flame caused a measurable effect on the position of the balanced flame. Due to the CO2 addition the flame needed to be relocated at the lift-off point during the experiments.
Yet, in this context even experiments at 5.5 bar are still below the operational pressure of large scale gas turbines, so further experiments are necessary.

The effect of SEGR on the gas turbine performance was studied by (Herraiz et al. 2018; Herraiz 2016) adapting the methodology of (Klas Jonshagen, Sipöcz, and Genrup 2011). A state-of-the-art CCGT 800 MW power plant with GE class F turbine technology was modelled and the deviation of a set of dimensionless parameter groups used to evaluate the performance of compressor and turbine at off-design conditions. (Herraiz 2016) evaluated the performance with the new working fluid composition and operational conditions under SEGR. For SEGR in parallel the performance is evaluated at different SEGR ratios (0-80%) and for SEGR in series at different recovery rates (85% to 95%). The author concludes that for the investigated range of SEGR ratios and recovery rates only a minimal deviation in the gas turbine engine is expected.
(Herraiz et al. 2018) analysed further the effect of the changed working fluid on the gas turbine and the steam cycle. The higher concentration in CO2 leads to a higher density of the CO2-enriched air and a change in heat transfer properties, resulting in a higher gas turbine exhaust temperature, which consequently generates more additional steam in the HRSG of the steam cycle. For a CCGT with PCC and SEGR in

parallel an increase in net power output of ca. 42 MW and net thermal efficiency of roughly 0.83 %, when compared to a conventional CCGT plant with PCC, are reported. For a CCGT with PCC and SEGR in series (Herraiz et al. 2018) report an increase in net power output of 18 MW and an increase in net thermal efficiency of roughly 0.55 %, point, when compared to a conventional CCGT plant with PCC.

Several studies assess the effect of SEGR on the energy requirement to separate CO2 from the flue gas of CCGTs. Investigations of the effect of SEGR on a post-combustion capture system using membranes as capture system were performed by (Merkel et al. 2013; Turi et al. 2018; Voleno et al. 2014). The same was conducted for a post-combustion capture system using amine-based solvent absorption by (Merkel et al. 2013; Herraiz et al. 2018; Ding, Freeman, and Rochelle 2017; Yue Zhang et al. 2016; Maria Elena Diego, Bellas, and Pourkashanian 2017).

The previous under EGR presented study performed by (Akram et al. 2016) on pilot scale, evaluating the reduction in reboiler duty for an increase in CO2 concentration in the flue gas, can be referred to in the case of SEGR, based on how the tests were performed. The authors showed a reduction of around 7.1% of reboiler duty relative per unit %vol in CO2 concentration increase. The largest reduction is reported from 7.1 to 5.3 MJ/kgCO2 for a CO2 concentration increase from 5.5%vol to 9.9%vol. However, this reduction is depending on the pilot plant dimension and operational condition, which both were not optimised for the reference case.

SEGR seems to be a promising technology in the context of process intensification of post-combustion carbon capture, leading to a reduction in packing volume and reboiler duty. However, its application will eventually be dependent on a number of aspects, including economical and technical issues. Its value for the future lies with the potential reduction in cost and energy penalty associated with the CO2 capture plant.

There are currently two different technologies investigated regarding their potential as CO2 transfer device for SEGR application. In general, any technology able to

selectively transfer CO2 from a flue gas stream in an ambient air stream, solely relying on the CO2 partial pressure difference between these two streams as the driving force, can theoretically be used as a SEGR transfer device.

The majority of the work performed is focused on membranes as CO2 transfer device. Ambient air is in those setups used as sweep gas. The separation is driven by the CO2 partial pressure difference between permeate and retentate stream. To overcome the pressure drop through the membrane, additional compression or vacuum work is required. However, the power consumption and therefore the size of the compression or vacuum system is relatively small. Nevertheless, a higher partial pressure gradient across the system would improve the CO2 transfer. The optimal pressure ratio is therefore a trade-off between the SEGR efficiency and the operational cost to drive the system. For SEGR applications it is acceptable to achieve higher permeability at the expense of CO2/N2 selectivity. (Merkel et al. 2013; R.W. Baker 2004; Y. Huang, Merkel, and Baker 2014)

As membrane materials for CO2 transfer selective polymeric membranes (Darabkhani et al. 2018; Russo et al. 2018; M. E. Diego, Bellas, and Pourkashanian 2018; Merkel et al. 2013; Richard W Baker et al. 2011; Maria Elena Diego, Bellas, and Pourkashanian 2017; Wijmans, Merkel, and Baker 2012a, 2012b) and solvent supported membranes (Ding, Freeman, and Rochelle 2017; Voleno et al. 2014; Swisher and Bhown 2014; Yue Zhang et al. 2016) are studied.

(Merkel et al. 2013) report for their Polaris membranes, specifically for lower CO2 concertation developed CO2 capture, good performance for SEGR application at laboratory scale. They achieved sufficient CO2 transfer efficiencies with a pressure drop through the membrane system of around 100 mbar.

Dense polydimethylsiloxane (PDMS) membranes were recently used experimentally at pilot-scale by (Darabkhani et al. 2018) and (Russo et al. 2018). Both used their membrane system to recover and recycle CO2 from a flue gas stream of a 100 kW MP4 Nu-Way natural gas fired burner.

(Darabkhani et al. 2018) report the highest achievable separation performance for a sweep air to flue gas to membrane ratio between 5 and 9, achieving separation efficiencies of 40% to 45%.

(Russo et al. 2018) reports recovery rates below 10% for a feed pressure of 1 bar and 40% for a feed pressure of 2.4 bar. Furthermore, the authors report a loss of oxygen in the air stream through the membrane between 2.8% (at 1 bar) and 3.1% (at 2.4 bar) and point out that water vapour from the combustion would affect the CO2 separation negatively.

In general, authors agree, that further investigations and testing are needed under real flue gas conditions to develop membrane materials, capable to be deployed as SEGR transfer device (Russo et al. 2018; Maria Elena Diego, Bellas, and Pourkashanian 2017).

However, there are several further challenges related to membranes that are not addressed so far in the literature. Membranes have up to now not been demonstrated at scale for SEGR applied to a large scale CCGT and over relevant timescales. To show its potential for large scale application, or to advance development, this is a necessary step.

Furthermore, challenges related to membrane sealing in relevant scales need to be assessed.

Finally, a clear disadvantage associated with membranes is the relatively high capital cost combined with a short lifetime of 3 to 5 years. This cost needs to get in a price range, where the cost of CO2 emissions avoided, are sufficient enough to justify the investment in such membrane systems.

The challenges membranes are facing, provide opportunities for existing or new technologies to be adapted for SEGR application.

Adsorption with CO2 selective porous adsorbent materials in a regenerative rotary wheel configuration for SEGR application was first proposed by (Herraiz et al. 2019).

The results, as well as unanswered questions of the study performed by the authors, are discussed in detail in Section 3.3.

Here in this section a brief overview of the rotary wheel design, its operation and its potential and distinction to CO2 capture with adsorption will be provided.

The process of the regenerative adsorption CO2 transfer wheel can be described as a continuous adsorption/desorption cycle and the design is illustrated in Figure 2-7. CO2 is adsorbed when the flue gas enters into contact with the solid material located in a rotor operating at low rotational velocity in the adsorption section, and then gets desorbed into an ambient air stream under counter current flow condition to the flue gas stream in the desorption section. The CO2 enriched air leaves towards the gas turbine compressor, the CO2 depleted gas leaves towards the stack.

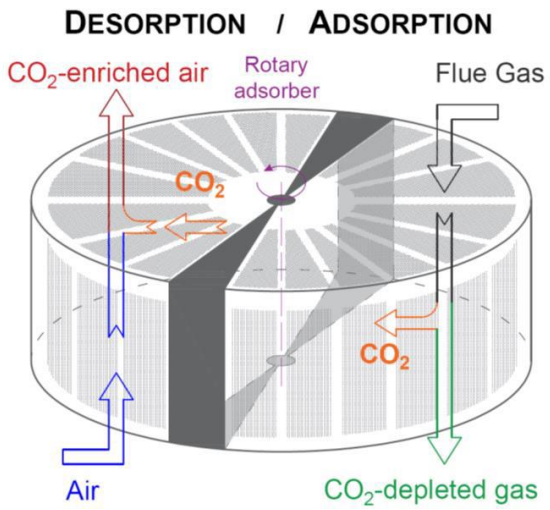

Figure 2-7: Schematic diagram of a rotary adsorbent for selective CO2 transfer (Herraiz et al. 2019)

The adsorbent is proposed to be distributed as a honeycomb-monolithic structure in basket allocated in the wheel as shown in Figure 2-8. The structure consists of a large number of parallel channels providing high contact efficiencies.

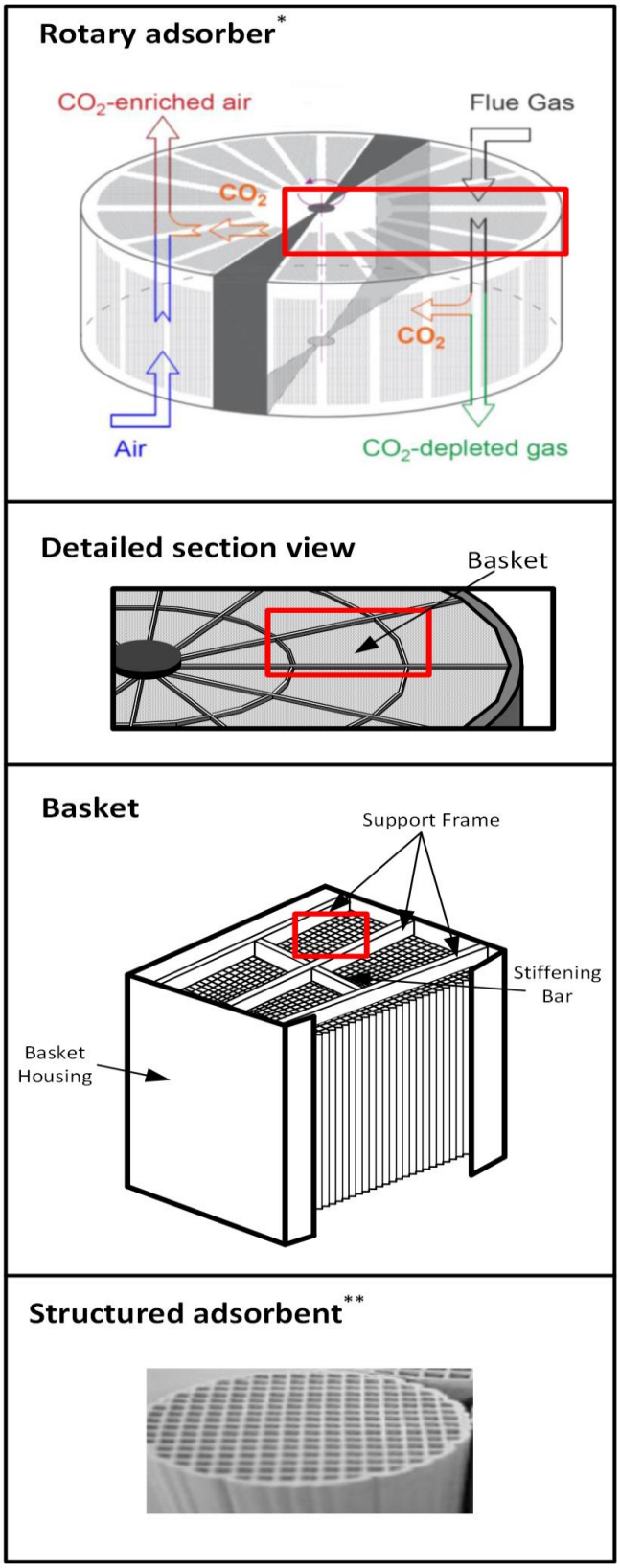

Figure 2-8: **Schematic diagram of the adsorbent distribution in the rotary transfer wheel**
(Herraiz et al. 2019) *(MUST 2020)

Advantages of SEGR with adsorption are associated with the small pressure drop in the flow streams related to the proposed monolithic structured adsorbent, when compared to conventional packed beds or membranes. Energy penalties related to overcoming those pressure losses should therefore be small. The proposed monolithic structure furthermore advances mass transfer since a high contact surface area is provided between the solid adsorbent and the flow streams passing through the adsorber. In general adsorbents can cover a wide range of temperature and pressure conditions and are therefore less affected by the process conditions in comparison to membranes. (Brandani et al. 2004; F. Rezaei and Webley 2010; Grande and Rodrigues 2008; Webley 2014)

Extensive research in adsorbent development focuses on improving solid materials by increasing surface area, improving pore structure and introducing chemical modifications on the surface to increase working capacity and CO_2 selectivity over nitrogen and oxygen. This is done to develop material capable to capture CO2 from flue gas sources with low CO2 concentrations, like gas fired power plants. (Abanades et al. 2015; Gibson et al. 2016; Mangano et al. 2013; IGSCC (2012) n.d.) Therefore, developed adsorbent materials show either strong physical or chemical interactions with CO2. Due to these strong interactions, the regeneration of these materials is associated with higher energy penalties. Regeneration is either done by decreasing the pressure, known as pressure/vacuum swing (PSA), or by increasing the temperature, known as temperature swing (TSA), or by a combination thereof. (Grande and Rodrigues 2008; Bui et al. 2018)

However, one of the most important aspect to consider for SEGR applications is balancing the affinity for CO2 with the energy requirements for regeneration. Especially in the context, that the regeneration of the adsorbent for SEGR application is performed with ambient air at near ambient temperature and pressure, relying on the partial pressure difference of CO2 in the flue gas to the air stream as driving force. (Herraiz et al. 2019; Merkel et al. 2013; Herraiz et al. 2018; Y. Huang, Merkel, and Baker 2014)

Therefore, weak physical adsorption is proposed as adsorption method for SEGR application, even though weak interaction between the adsorbent and the adsorbate will negatively affect the selectivity of CO2/ N2 (T. Dantas et al. 2011). However, as previously discussed for membranes for SEGR application, a reduced CO2/N2 selectivity can be accepted (Merkel et al. 2013; R.W. Baker 2004; Y. Huang, Merkel, and Baker 2014) for adsorbents with high recovery rates. Moreover, due to the similar partial pressure of N2 in the flue gas and in the air stream, only a very low N2 transfer rate is expected in SEGR applications. (Herraiz et al. 2019)

Other aspects to consider when choosing an adsorbent next to regenerability with air are selectivity, working capacity and stability. (Y. S. Bae and Snurr 2011)

A process related challenge the adsorbent has to face is the water content in the flue gas, which has an influence on the performance of some adsorbents.

The tendency of fluids to bond on solid surfaces as a consequence of surface energy is termed adsorption, the reverse process desorption. CO2 adsorbent material can be categorised into zeolites, metal-organic frameworks and carbonaceous materials. Extensive review work has been conducted by several authors looking at their potential for post-combustion carbon capture.(Samanta et al. 2012; Abanades et al. 2015; Ben-Mansour et al. 2016; Joss, Gazzani, and Mazzotti 2017; Lee and Park 2015; Gibson et al. 2016)

They are available in different shapes and forms such as powders, pellets, foam, sheets, fibers and monolithic structured, as depicted in Figure 2-9. Each of these solid shapes and forms have a large amount of pores, as illustrated in Figure 2-10, adding to the active surface area of adsorbents. The pores are classified according to their size into macro (>25 nm), meso (1-25 nm) and micro pores (<1 nm).

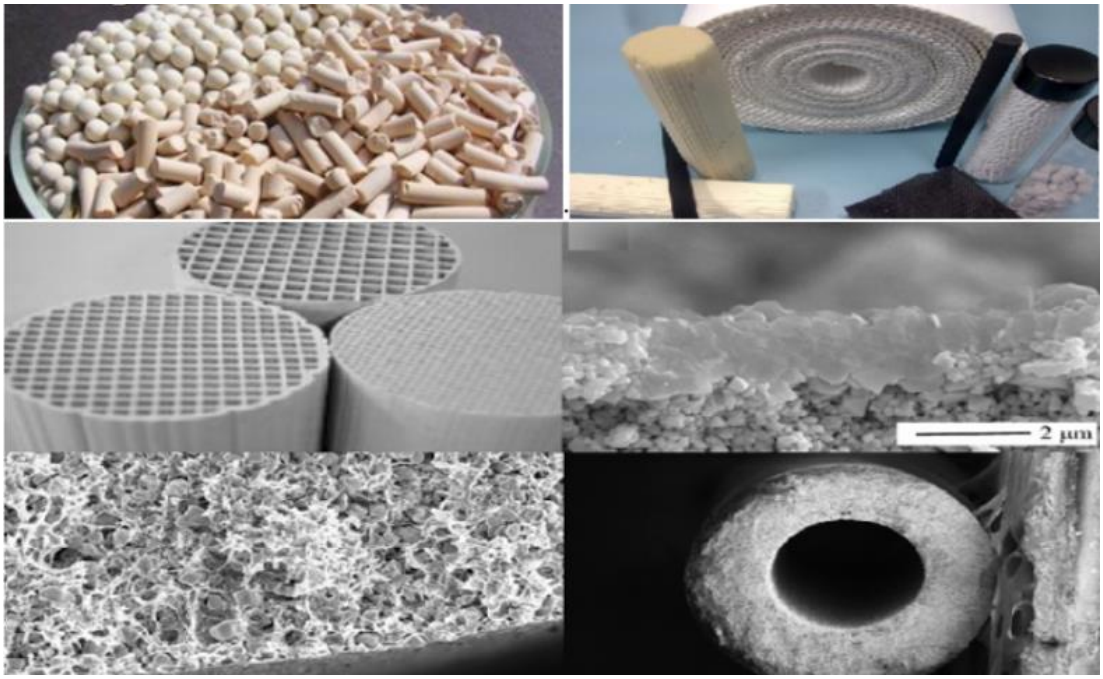

Figure 2-9: Different adsorbent structures (MUST 2020)

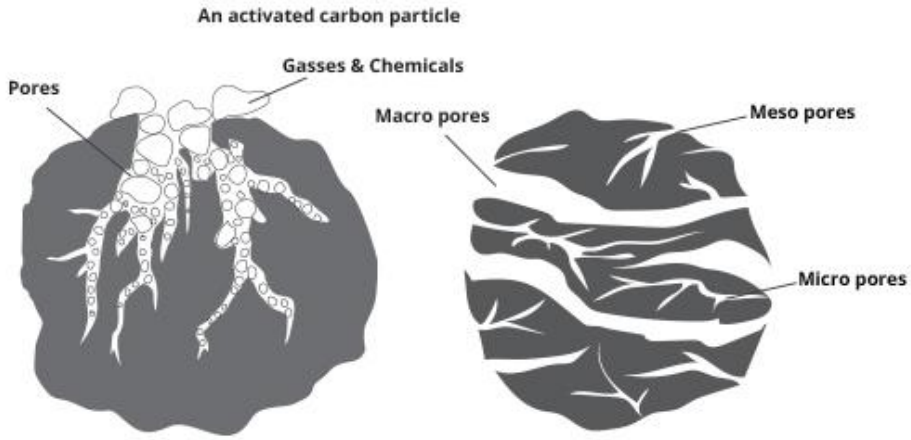

Figure 2-10: Schematic of the pores in an adsorbent particle (Aqua-Cache 2020)

Zeolites have large internal specific surface areas and porous volumes. The capacity for CO_2 adsorption is moderate. Synthetic zeolite 13X is often referred to as the benchmark of CO2 adsorbents, with CO2 adsorption capacities between 2.6 to 5.7 mmol/g at 1 atm. However, its CO2 adsorption capacity declines significantly in the presence of water vapour in flue gas streams. Water guards or flue gas dehydration

systems can be applied, though those will consequently add to capital and operational costs. (T. H. Bae et al. 2013; Xu et al. 2013; Samanta et al. 2012)

Metal-organic frameworks (MOFs) have a high surface area, due to adjustable pore size, structure and surface properties. This leads to very high adsorption capacities (3.3 to 8.0 mmol/g at 1 atm) and good diffusion properties, when compared to zeolites and carbon based materials. Their main disadvantages are their hydrophilic character with the possibility of water displacing adsorbed CO2, their low level of maturity in the context of large scale production and the very high costs of production in comparison to zeolites and carbon based materials. (Ben-Mansour et al. 2016; Samanta et al. 2012)

Carbon based materials, like activated carbon, have a low to moderate adsorption capacity for CO2 at low pressures (0.6-3.2 mmol/g at 1atm). Advantages are their widely availability at low cost, their low sensitivity to moisture, due to the hydrophobic or non-polar nature, and their thermal and chemical stability. However, although they are considered hydrophobic, water can condensate and accumulate in the pores reducing the available active surface area for adsorption. (Q. Wang et al. 2011; Abanades et al. 2015; Marx et al. 2013; Xu et al. 2013; Ben-Mansour et al. 2016; Samanta et al. 2012) (A more detail assessment of carbon based adsorbent materials as materials for SEGR application is provided in Section 3.1.1.)

In regards to SEGR application not only the adsorption capacity of an adsorbent plays an important role, but also the heat of adsorption. It determines the uptake of CO2, the needed regeneration energy and the temperature of adsorption and desorption. A high heat of adsorption would favour CO2 uptake at lower pressures, however it would also imply a larger energy demand to regenerate the solid. In the context of SEGR the only driving force for desorption is the partial pressure difference between the adsorbed amount of CO2 on the solid and the CO2 in the air stream used to desorb the CO2 from the solid. Therefore, lower heat of adsorption should be favoured at the expense of CO2 uptake. The heat of adsorption of activated carbons are between 17 to 22 kJ/mol, of zeolites in the range of 30 to 45 kJ/mol and of MOFs

in the range of 40 to 80 kJ/mol. (Mangano et al. 2013; Abanades et al. 2015; Ben-Mansour et al. 2016; Samanta et al. 2012).

Based on their availability, low costs, adsorption capacity and heat of adsorption (Herraiz et al. 2019) considered zeolites and activated carbon to investigate the concept of selective CO_2 transfer.

The work here focuses on activated carbon as adsorbent for SEGR application. More details can be found in Chapter 3.

Chapter 3 Regenerative Rotary CO_2 Transfer Wheel

This chapter covers first the choice of activated carbon as adsorbent (3.1.1) for SEGR application, followed by an introduction of relevant fundamentals of adsorption and their underlying mathematical description, including separation effects (Section 3.1.2), adsorption isotherms (Section 3.1.3), adsorption dynamics (Section 3.1.4) and mass transfer and the Linear Driving Force model (Section 3.1.5).

A brief review of the development of rotary devices in adsorption is then presented in Section 3.2.1, followed by an overview of the functional difference between adsorbents for CO2 capture and adsorbents for CO2 transfer (Section 3.2.2).

Next, the previously developed conceptual equilibrium design and model of a regenerative rotary CO2 transfer wheel by Herraiz (Herraiz 2016; Herraiz et al. 2019) is described (Section 3.3.1). The findings of a performed sensitivity analysis by (Herraiz et al. 2019) are discussed (Section 3.3.2) and limits and knowledge gaps identified (Section 3.3.3).

Under Section 3.4 the methodology surrounding the rotary adsorption CO2 transfer wheel is presented. This includes the experimental methodology used for adsorption breakthrough curve measurements (Section 3.4.1), the methodology used to develop a kinetic model of CO2 adsorption in a rotating regenerative CO2 transfer wheel for SEGR (Section 3.4.2), and the methodology applied to the design of the rotary wheel (Section 3.4.3). The experimental methodology consists of the carbon activation method, the characterization of the adsorbent and the adsorption bed, the setup of the breakthrough CO2 adsorption experiment and the experiments themselves. The methodology of the kinetic model consists of the governing mass and energy balances, their numerical solution and auxiliary conditions, the parameters and assumptions for the integration of the wheel into a reference CCGT. The design

methodology consists of structural considerations and considerations regarding leakages.

3.1 Adsorption Fundamentals

3.1.1 Activated Carbon as an Adsorbent for Post-Combustion CO2 Capture

The term activated carbon covers a wide range of processed carbon-based materials. Their production can be narrowed down to two steps, the carbonisation of the raw material to biochar and its activation with an activating agent afterwards. However, although in principle all carbon based raw materials can be transformed into activated carbon, the final product properties and therefore their function as adsorbent are strongly depending on the raw material, the carbonization process and the activation agent and method. (Bansal and Goyal 2005; Shahkarami, Azargohar, et al. 2015)

The difference between chemisorption and physisorption and why we choose a physical adsorbent for SEGR application is covered in Section 3.1.3. Yet, since activated carbon are mostly physisorbents, the pore size and pore volume are important factors in the case of physical adsorption, since they determine the surfaces area for reactions and, hence adsorption capacities. Generally activated carbons are characterised by a very high micropore volume and an extremely high inner surface area available for adsorption. Activated carbon is therefore an ideal physical adsorbent.(Dantas et al. 2011)

Activated carbons are available in different shapes and forms such as powders, pellets, foam, sheets, fibers, and monolithic structured, giving them a broad applicability and adaptability for processes where pressure losses need to be considered (Zeng et al. 2017; Ribeiro et al. 2008; Querejeta et al. 2017).

They are non-toxic and non-corrosive, making them safe to handle. The manufacture of activated carbon is very advanced, well understood and available in large-scale production, making activated carbons a low cost and readily available material. Most activated carbon have a low sensitivity to moisture in the feed stream due to their

hydrophobic nature, an important consideration for combustion gases, though some may show a decrease in their capacity in the presence of moisture due to condensation and accumulation in the pores, and need to be chosen according to the process conditions. (Bui et al. 2018; Marx et al. 2013)

The major disadvantages of activated carbons for post combustion capture are based on their mostly uniform electric potential on the surface, making them neutral in nature. It results in a lower enthalpy of adsorption for CO2 compared to other adsorbents, e.g. zeolites or MOFs, which leads to a lower uptake/ adsorption capacity and a lower selectivity of CO2 over N2. Selectivity is a key property for high purification applications such as CO2 capture. Adsorption capacity determines the maximum amount of CO2 that can be adsorbed, and therefore determines the amount of solid needed for a specific process. By creating a very narrow pore-size distribution the selectivity of activated carbon can be increased but remains mostly below the selectivity of other adsorbents. This also holds true for adsorption capacity. By increasing the surface area available for adsorption, it is possible to increase the adsorption capacity of activated carbon, but it remains low compared to zeolites or MOFs. (Pal 2017; Bui et al. 2018; Dantas et al. 2011)

In the context of SEGR the disadvantage of the lower adsorption capacity of activated carbon is important when the amount of adsorption material needs to be determined. Selectivity, as in the context of passing other parts of the flue gas, mainly nitrogen, to the air stream used for the combustion in the turbine, is less of a problem for SEGR application as the nitrogen partial pressure in both streams, the flue gas stream and the air stream, are similar. Therefore, a low transfer of nitrogen into either stream can be expected. The main disadvantage of a low adsorption capacity is out weight in the context of SEGR by the need of an adsorbent with low enthalpy of adsorption, in order to be able to be regenerated with air at ambient conditions. Hence activated carbons remain a very attractive material for SEGR application.

3.1.2 Adsorption Separation and Separation Effects

The tendency of fluids to bond on solid surfaces as a consequence of surface energy is termed adsorption, the reverse process desorption. Its technical application can be found primarily in separation processes, characterisation techniques, and heterogenic catalysis. In Carbon Capture and Storage processes it is mainly used to separate CO2 from the flue gases of the power plants. Desorption is performed by either thermal swing, pressure swing and/or purge desorption mechanisms.

Adsorptive separation of gas mixtures is based on:

- Different adsorbability, given by the selectivity and capacity of the adsorbent
- Different adsorption kinetics
- Steric effects, as nonbonding interactions resulting from overlapping electron clouds
- Easy and fast desorption, as effect on the economics of the process
- Low tendency for adsorbing water
- Low sensitivity towards components in the gas mixture, which could hinder the adsorption process

There are several effects leading to the separation of a gas mixture (J. R. Li, Kuppler, and Zhou 2009):

- Molecular sieving effect, molecular size/ shape of gas components preventing them to enter the pores.
- Kinetic effect, based on different diffusion rates.
- Thermodynamic effect, based on the interactions between the pore walls and the gas molecules.
- Quantum sieving effect, based on different diffusion rates in the narrow micropores.

Activated carbons are nonpolar adsorbents. Consequently, Van der Waals forces are dominant, with the size and polarizability of adsorbate, and pore size distribution as

the leading factors for separation. Surface chemistry is secondary for the process. (Shahkarami 2017)

This means that pore size distribution affects the selectivity of adsorbate to the adsorbent, hence high specific surface areas are desirable.

3.1.3 Adsorption Isotherms

Depending on the strength of the interactions in the adsorption complex, a distinction is made between physical adsorption (physisorption) and chemical adsorption (chemisorption).

During chemisorption strong chemical, covalent bonds are formed between adsorbate and adsorbent surface, and the heat of adsorption released during that process is in the same order of magnitude as the heat of a chemical reaction (100 kJ mol^{-1}). Such bonds are often irreversible or the required energy to break the bindings are high. If, however, the intermolecular interaction forces between adsorbent and adsorptive agent are relatively weak, in the magnitude of van-de-Waals interactions (30 kJ mol^{-1}), the phenomenon is referred to as physisorption and the adsorbate can be desorbed fully reversible. The heat of adsorption ranges in similar order of magnitude as heat of condensation.(Kolasinski 2012)

Table 3-1 shows a comparison of some of the key parameters of physisorption and chemisorption and therefore gives an insight why physisorption is to prefer over chemisorption in the context of SEGR. For the case of a regenerative rotary CO2 transfer wheel considered in this thesis, operating at near ambient air conditions, only physisorption can be considered, since the energy needed to separate a chemical bond, for the regeneration of the adsorbent, could not be provided by an air stream at near ambient condition.

Table 3-1: Comparison of parameters of physisorption and chemisorption from (Kolasinski 2012)

Parameter	Physisorption	Chemisorption
Adsorbent	All solids	Only specific solids
Adsorptive agent	All gases below their critical temperature	Some chemical reactive gases
Temperature range	Low temperatures	Generally high temperatures
Heat of adsorption	Low (condensation enthalpy)	High (heat of reaction/ dissociation energy)
Layer formation	Monolayer and multilayer possible	Monolayer
Reversibility	Fully reversible	Often reversible

After a certain time adsorption reaches an equilibrium, which depends on temperature, pressure and the amount of adsorptive agent. For practical reasons the adsorbed amount as a function of the partial pressure of the gas phase, for a given constant temperature, is regularly used. This is called the adsorption isotherm. To enable a comparison of different materials, the amount adsorbed is typical normalized by the mass of the adsorbent. According to the International Union of Pure and Applied Chemistry (IUPAC) there are six mayor types of isotherms, which are shown in Figure 3-1.

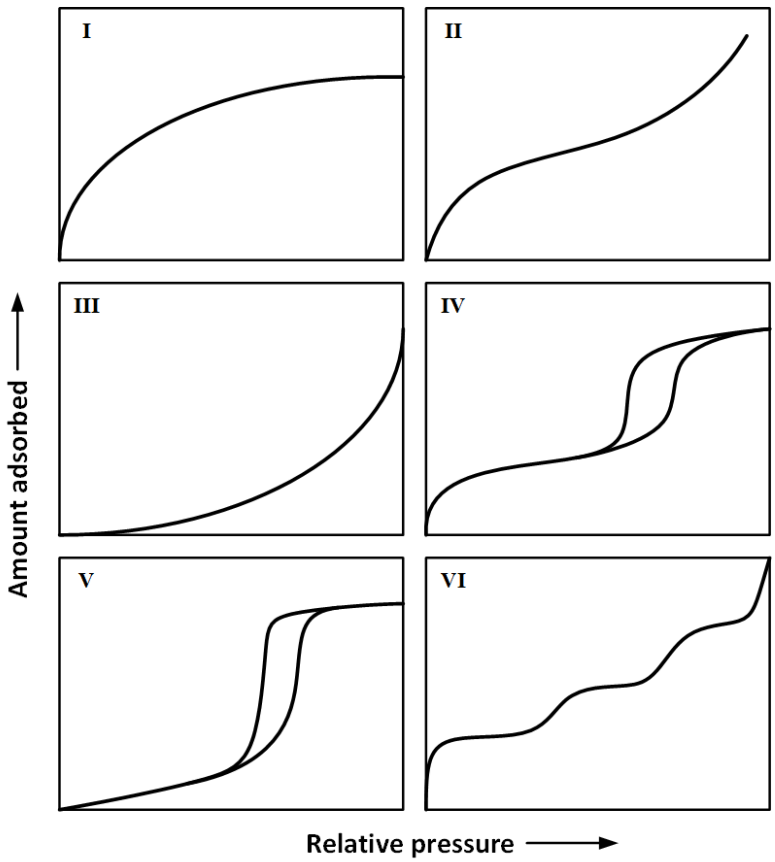

Figure 3-1: Classification of physisorption isotherms according to IUPAC classification, showing adsorption and desorption pathways (adapted from (Sing 1985)**)**

Type I is characteristic for microporous adsorbent with monolayer adsorption. Types II, III, and VI show adsorption isotherms for nonporous or macroporous adsorbent with multilayer adsorption, while type IV and V are typical for mesoporous adsorbent with multilayer adsorption and capillary condensation.(Sing 1985; Broekhoff 1979; Lowell et al. 2012)

Type I isotherm is specific for microporous solids, such as activated carbon and zeolites, with relatively small outer surface area, forming only a monolayer of adsorbate on the outer surface. After filling the micropores with increasing pressure a plateau of molecules adsorbed is reached. Increasing pressure higher than saturation vapour pressure will not lead to the formation of additional adsorbed layers on the outer surface. This isotherm can be approximated by the Langmuir model and is therefore called ‘Langmuir adsorption isotherm’. Irving Langmuir

derived the Langmuir isotherm from kinetic considerations based on the following assumptions (Joos 1999):

- Adsorption and desorption are in dynamic equilibrium.
- The adsorbate is only forming a monomolecular layer.
- The surface is homogenous and consists of energetically equivalent adsorption positions on which only one gas molecule can bind.
- There is no interaction between the adsorbed molecules. The heat of adsorption is equal for each molecule and independent from the solidity ratio.

For CO2/N2 physisorption adsorption modelling, the Langmuir isotherm/ extended Langmuir isotherm is the most frequently used isotherm type (Ben-Mansour et al. 2016). The extended Langmuir is utilised in the model proposed here, since it takes adsorption behaviour of activated carbon under multicomponent gas mixture of CO2, N2 and O2 into account.

The Langmuir isotherm can be expressed as Equation (3.1).

$$q_k^* = \frac{q_S \cdot K_{L,\,k} \cdot P_k^*}{1 + K_{L,\,k} \cdot P_k^*} \quad k = CO_2,\ N_2,\ O_2 \tag{3.1}$$

With q_k^* , the adsorbed amount of component k at a given partial pressure of P_k^* in the gas mixture, q_s , the saturation capacity relating directly to the number of active sites on the adsorbent surface, and $K_{L,k}$, the equilibrium constant of component k related to the enthalpy change of the process and the affinity of gas molecules to the adsorption sites. (Ben-Mansour et al. 2016)

Or written in form of the extended Langmuir isotherm for a multicomponent gas mixture of CO2, N2 and O2 as in Equation (3.2). (Ben-Mansour et al. 2016)

$$q_k^* = \frac{q_S \cdot K_{L,\,k} \cdot P_k^*}{1 + \sum_{j=1}^{C} K_{L,\,j} \cdot P_j^*} \quad k, j = CO_2,\ N_2,\ O_2 \tag{3.2}$$

To describe the temperature dependence of K_L the Van't Hoff equation (Equation (3.3)) is used.

$$K_{L,\,k} = K_{L0,\,k}\, exp\left(\frac{-\Delta H_{ads,k}}{RT}\right) \quad k = CO_2,\, N_2,\, O_2 \tag{3.3}$$

With $-\Delta H_{ads}$, the enthalpy of adsorption and K_{L0}, the pre-exponential constant. (Ben-Mansour et al. 2016)

Others (Vargas, Giraldo, and Moreno-Piraján 2012; Marta G. Plaza, Rubiera, and Pevida 2017) propose a modification of the Langmuir isotherm for CO2 adsorption on activated carbon honeycomb-monoliths in form of the Tóth adsorption model (Equation (3.4)), based on the model's better prediction of adsorption limits for heterogenic surfaces.

$$\frac{q_k^*}{q_{s,T}} = \frac{\alpha_T \cdot P_k^*}{\left[1+\left(\alpha_T \cdot P_k^*\right)^n\right]^{1/n}} \quad k = CO_2,\, N_2,\, O_2 \tag{3.4}$$

Where the saturation capacity of the Tóth model $q_{s,T}$ and the affinity constant α_T, are similar to the saturation capacity q_s and the equilibrium constant K_L in the Langmuir model. The exponent n relates to the heterogeneity of the adsorbent surface. (Marta G. Plaza, Rubiera, and Pevida 2017)

Although Vargas (Vargas, Giraldo, and Moreno-Piraján 2012) shows, that for the studied monolithic materials the Tóth model features a slightly higher correlation coefficient R^2 for the fitted adsorption parameters of 0.999, in comparison to the correlation coefficient R^2 for the Langmuir model of 0.996 to 0.998, for the model developed in this thesis the extended Langmuir isotherm will be applied. It is reasoned that based on the current development stage of the rotary transfer device model, no prediction about the heterogeneity of the adsorption material can be made. This simple extension of adsorption isotherm can be considered for the further development of the model, when closer attention needs to be payed to adsorption limits of honeycomb structured adsorbent for pressure values around zero and very high pressure values.

3.1.4 Adsorption Dynamics

The dynamic performance of adsorption beds is assessed by performing breakthrough curve adsorption tests. The gas enters the bed at a given concentration. While it flows through the bed CO2 gets adsorbed onto the adsorbent. The concentration of CO2 in the gas phase, as well as the adsorbed amount of CO2 on the solid, change with time and bed position in fixed-bed adsorption processes. Such concentration changes are plotted as ratio of the gas phase outlet concentration to the inlet concentration (c_{out}/c_{in}) as a function of time. Those plots, as depicted schematically in Figure 3-2(b), are called breakthrough curves and allow the evaluation of the dynamic behaviour of adsorption processes. The section in which most of the mass-transfer occurs is termed the mass-transfer zone (MTZ). The MTZ is typical defined by its limits between c_{out}/c_{in} of 0.05 to 0.95. The breakthrough time $t_{breakthrough\ point}$ or t_b is defined as the time where c_{out}/c_{in} reaches 0.05. At times before t_b , the concentration of CO2 measured at the adsorption bed outlet is either close to or equal to zero. If adsorption continues after reaching t_b , the measured concentration of CO2 at the outlet rises sharply until c_{out}/c_{in} reaches a value around 0.5. Subsequently the slope of the concentration ratio plot reduces until it reaches unity. Hence, the profile resembles S-shaped curves. The exact shape of the breakthrough curve depends on the shape of the adsorption isotherm and the mass-transfer mechanism. For an ideal adsorbent, without mass-transfer resistance and with minimal axial dispersion, the S-shape of the breakthrough curve would be a vertical line. For an adsorbent with high mass-transfer resistance the slope of the S-shaped curve is decreased. Adsorption on fixed-beds takes place layer by layer. When some time has passed, the adsorbent material at the front of the bed is nearly fully saturated and in equilibrium with the inlet CO2 concentration, with the mass-transfer taking place further away from the inlet, as shown in the sequence of adsorption beds in the upper part of Figure 3-2(a). In Figure 3-2(a) the shaded area in the adsorption beds represents the fully saturated adsorbent, followed by the mass-transfer area where the adsorbed phase concentration approximates an S-shape. This is followed by an area where no adsorption has taken place yet, since the amount of CO2 that

entered the bed is removed in the first two areas. As soon as the area in which the mass-transfer occurs is saturated, the mass-transfer area moves further along the bed, until the whole bed is saturated.(J. Wilcox 2012)

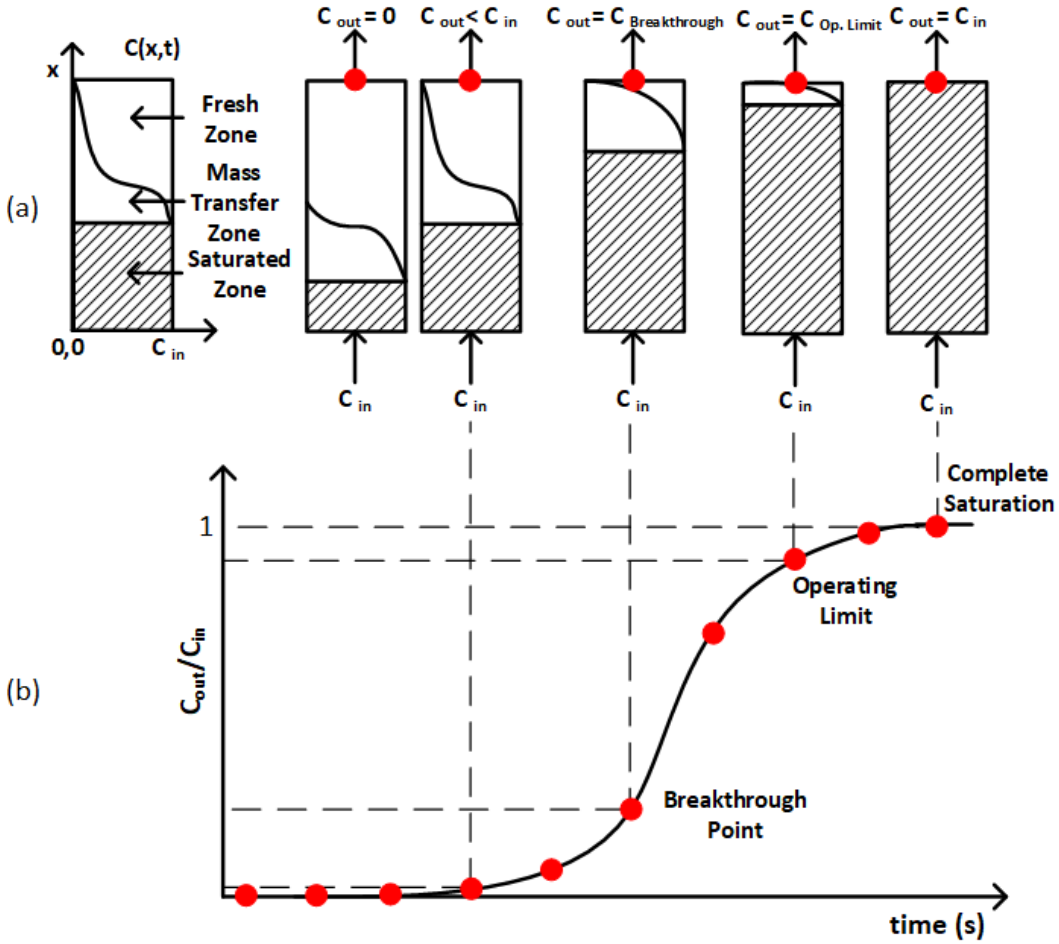

Figure 3-2: **Schematic correlation between adsorbed amount on the solid of the adsorption bed with its moving mass-transfer area 2a) and corresponding breakthrough curve 2b) (adapted from** (Shahkarami 2017)**)**

The breakthrough curve plot can be further used to graphically determine the amount of CO2 adsorbed on the solid (Equation (3.5)), and thereby the adsorption capacity S_{CO2} of the adsorbent bed (Equation (3.6)). The blue shaded area between the horizontal line at $c_{out}/c_{in} = 1$ and the S-shaped curve in Figure 3-3 is proportional to the mass adsorbed till saturation is reached at time $t_{saturation}$, assuming a constant flow throughout the bed. The total mass of CO2 passing through the adsorbent bed is proportional to the total area at $t_{saturation}$. (Shahkarami 2017)

$$m = \frac{A_{adsorption}}{A_{total}} \cdot m_{total} \tag{3.5}$$

$$S_{CO2} = \frac{m}{m_{adsorbent}} \tag{3.6}$$

With m, the mass of CO2 adsorbed at $t_{saturation}$, $A_{adsorption}$, the area above the curve at $t_{saturation}$ (blue shaded area in Figure 3-3), c , the total area at $t_{saturation}$ (red shaded area in Figure 3-3), m_{total} , the total mass of CO2 passing through the adsorbent at $t_{saturation}$, $m_{adsorbent}$ the mass of the adsorbent bed and S_{CO2}, the capacity of the adsorbent bed.

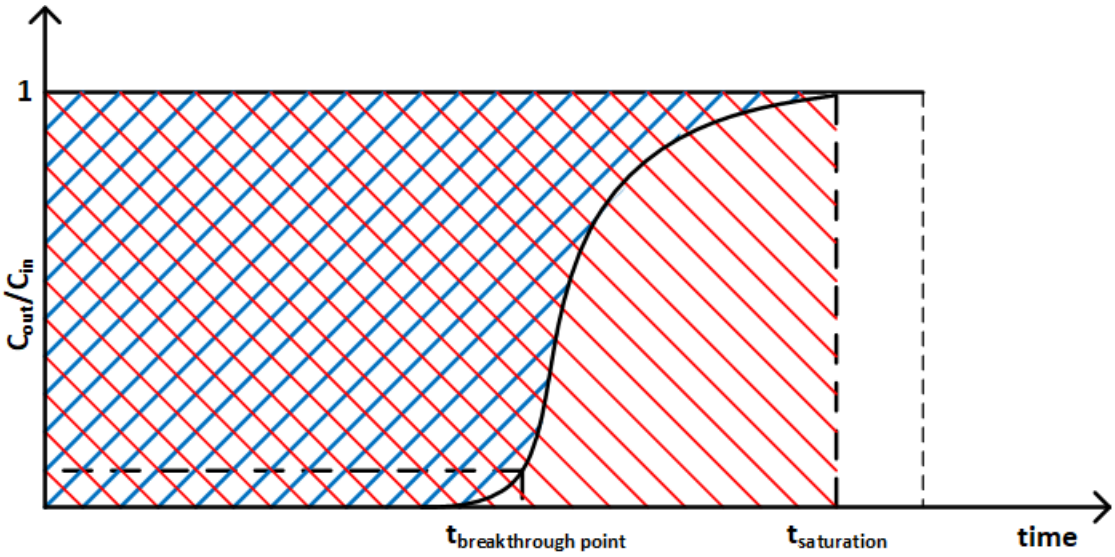

Figure 3-3: Schematic of a breakthrough curve (adapted from (M. G. Plaza et al. 2010)**)**

$A_{adsorption}$ can be determined graphically by integrating the blue shaded region above the breakthrough curve from zero to $t_{saturation}$. A_{total} can be determined by integrating the total region from zero to $t_{saturation}$, respectively.

3.1.5 Mass Transfer and the Linear Driving Force Model

Since adsorption itself takes place on the surface of the solid particle, the adsorptive agent has to be transported to the inner surface of the solid as shown in Figure 3-4. Hence, the mass transfer in a continuously operated fixed adsorption bed can be divided into different steps. Initially, the adsorptive agent molecule arrives through

convection and free diffusion to the outer surface boundary layer between fluid phase and adsorbent (step 1 - 2). From there, it is transported through the pores onto the adsorbent's inner surface (step 2 - 3). This transport mechanism can be described according to the size of the pores and molecules by different diffusion mechanisms. As the last step of the mass transfer, the actual adsorption occurs in form of energetic interaction between adsorbent and adsorptive agent (step 3 - 4). The mechanisms or steps take place consecutively. Depending on the rate of each step, the mass transfer to the outer surface boundary layer, the pore diffusion, or the adsorption itself can be the rate determining factor. If the flow conditions (low viscosity of the fluid, sufficiently high flow velocity) and adsorber dimensions are chosen appropriately, the rate determining part of the total adsorption process is the mass transport of the adsorptive agent molecule into the pore system of the adsorbent (step 2 - 3). In this case, the influence of the mass transport to the outer surface is small and the actual physisorption step is a rather fast mechanism compared to step 2 - 3. For the desorption process the adsorbate will be desorbed and transported out of the adsorbent particle back into a fluid phase. (Yang 1986; Iordanidis 2002)

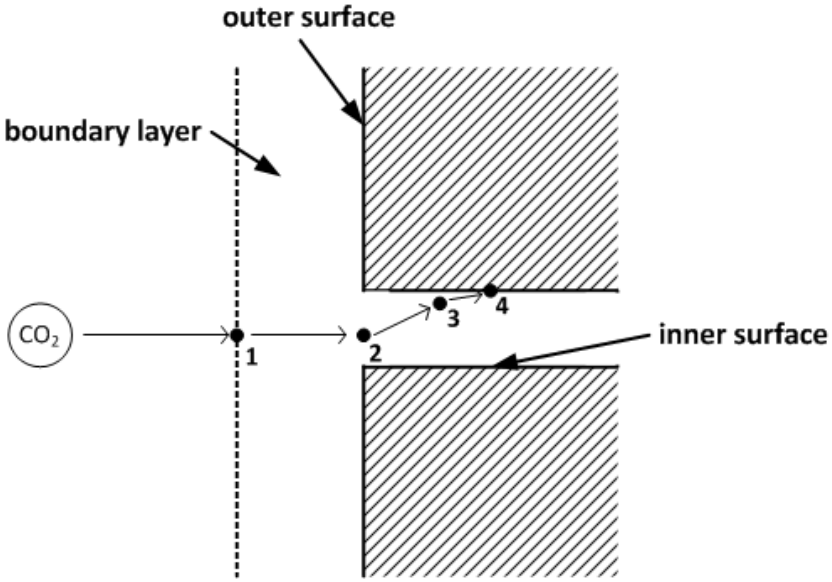

Figure 3-4: Schematic of the mass transfer of a CO2 molecule into the pore of an adsorbent, followed by its adsorption

According to Bathen (Bathen and Breitbach 2001) the mass transport into the porous solid system is depending on both the adsorbent and the adsorptive agent. Based on the gas/solid system, it is possible to differentiate between four transport mechanisms for gas phase application under low pressure, analogue to Fick's law of diffusion approach, shown in Equation (3.7).

$$\dot{m} = -D \cdot A_{spec} \cdot \frac{dY}{dx} \tag{3.7}$$

With $\dot{m}$ the diffusion mass flux, D the diffusion coefficient or diffusivity, A_{spec} the specific area and the gradient dY/dx as the driving force.

To estimate the dominant mass transfer resistance, the Knudsen number *Kn* can be used (Equation (3.8)). (Bathen and Breitbach 2001)

$$Kn = \frac{\lambda_F}{d_{pore}} \tag{3.8}$$

Thus, the following four diffusion mechanisms can be expressed (Bathen and Breitbach 2001):

- Knudsen diffusion. If the pore diameter d_{pore} is considerably smaller than the free path length λ_F of the molecule, impacts between pore wall and molecule dominate the transport.

$$d_{pore} < 0.1\lambda_F \text{ corresponding to Kn} > 10$$

- Free pore diffusion. If the pore diameter is bigger than the free path length of the molecule, impacts between molecules dominate).

$$d_{pore} > 10\lambda_F \text{ corresponding to Kn} < 0.1$$

- Surface diffusion. This type of mass transport occurs along the pore walls with the concentration gradient as driving force. It is relevant for high loads, when the molecule density in the gas phase reaches its saturation limits for the given pressure and temperature. Condensation in the pores can then be encountered.
- Intergranular/ micropore diffusion. It happens in pores with a pore diameter equal to the diameter of the molecule and is hard to distinguish from the surface diffusion.

$$d_{pore} \approx d_{molecule}$$

Depending on the predominant mechanism, a specific area and a gradient corresponding to the diffusion driving force (e.g. concentration gradient, loading gradient) can be used to describe the mass transfer.
For low operating pressures, typical for flue gas leaving the heat recovery steam generator (HRSG) of combined gas power plants as considered in this thesis, and monomolecular loading, based on the Langmuir assumption used in this thesis, Knudsen diffusion and free pore diffusion are the relevant mechanisms.

For microporous adsorbent with Kn > 10, the mass transport is dominated by the Knudsen diffusion with a high potential of impacts of molecules with the pore walls. The corresponding diffusion coefficient D_{Kn} is given by Equation (3.9). (Bathen and Breitbach 2001)

$$D_{Kn} = \frac{4}{3} \cdot \frac{d_{pore}}{\mu_{P,Kn}} \cdot \sqrt{\frac{M_A}{2\pi \cdot R \cdot T}} \tag{3.9}$$

With d_{pore} the diameter of the pore, $\mu_{P,Kn}$the Knudsen tortuosity factor, R the universal gas constant, T the temperature and M_A the molar mass of the gas.
The tortuosity factor in general is a ratio evaluating how twisted and turned a diffusion pathway in a porous solid is. It is the ratio of the real pathway length between two points extended by twist, turns and branching compared to the straight-line distance of these two points.

For adsorbent with a Knudsen number lower than 0.1, the mass transport is characterised by impacts between the adsorptive agent molecules themselves. The diffusion coefficient for free pore diffusion D_{Diff} can be estimated according Equation (3.10), with the free pore tortuosity factor $\mu_{P,Diff}$,with a relation between the two tortuosity factors given as $\mu_{P,Kn} = \mu_{P,Diff}^{1.7}$, and the diffusion coefficient of a binary gas mixture D_{12} (Bathen and Breitbach 2001).

$$D_{Diff} = \frac{D_{12} \cdot M_A}{R \cdot T \cdot \mu_{P,Diff}} \tag{3.10}$$

Depending on the porous system of the adsorbent and on the adsorptive agent a superposition of the different diffusion mechanisms can take place. The transition region between free and Knudsen diffusion, in which both diffusion effects are relevant (Treybal 1980), is given in the literature (Kajszika 1998) as

$$0.1 \leq \frac{\lambda_F}{d_{pore}} \leq 10 \tag{3.11}$$

The effective diffusion coefficient D_{eff} for the transition region between free and Knudsen diffusion can be described for equimolar diffusion with Equation (3.12) (Bathen and Breitbach 2001).

$$D_{eff} = \left(\frac{1}{D_{Kn}} + \frac{1}{D_{Diff}} \right)^{-1} \tag{3.12}$$

Due to the fact that kinetics and the prevailing mass transfer mechanism for adsorbent and adsorptive agent are often unknown and also to save computational time, it is convenient to approximate the mass transfer rate by a space independent expression. This is a common approach both in industry and academia. Such an expression is given in the Linear Driving Force (LDF) model, developed by Glueckauf and Coates (Equation (3.13)). (Bathen and Breitbach 2001; T. L. P. Dantas et al. 2011; Douglas M. Ruthven 1984; Ben-Mansour et al. 2016)

$$\frac{\partial \overline{q_k}}{\partial t} = k_{eff} \cdot (q_k^* - \overline{q_k}) \tag{3.13}$$

The underlying assumptions are (Douglas M. Ruthven 1984):

- The loading is independent from the radius of the particle.
- The mass transfer is shifted into the boundary layer.
- An effective mass transfer coefficient k_{eff} accounts for mass transport through the boundary layer, mass transport in the pores of the adsorbent due to diffusion (free pore diffusion + Knudsen diffusion) and mass transfer because of adsorption.
- The driving concentration difference of the components is given by the concentration of component k on the outer surface of the particle q_k^* (adsorption equilibrium concentration) and the average adsorbed amount of species i within the particle $\bar{q}_k$.

For the calculation of the effective mass transfer coefficient k_{eff} in gas phase processes, Glueckauf and Coates (Glueckauf and Coates 1947) propose a simplified approach. They define the effective mass transfer coefficient as the quotient of the effective diffusion coefficient divided by the second power of the particle radius *r*, multiplied with a geometrical factor equal to 15, as shown in Equation (3.14).

$$k_{eff} = \frac{15 \cdot D_{eff}}{r^2} \tag{3.14}$$

Equation (3.14) is limited to cyclic processes where the dimensionless time θ_c is bigger than 0.1. The dimensionless time is defined as Equation (3.15).

$$\theta_c = \frac{D_{eff} \cdot t_c}{r^2} \tag{3.15}$$

Where t_c is defined as the cycle half time.

The proposed effective mass transfer coefficient by Glueckauf and Coates (Glueckauf and Coates 1947) is most accurately used for packed beds. Others like Rezaei (Fateme Rezaei and Webley 2009) look into how the optimum adsorbent for gas separation processes needs to be structured, and propose for each structure a different effective mass transfer coefficient approach. They evaluate the different structures based on their pressure drop performance and their mass transfer characteristics. Generally, they conclude that monolithic structured adsorbent are very promising for gas separation processes, but the optimum structure is depending on cell density, voidage and effective diffusivity.

Although the use of a monolithic structured adsorbent is proposed for the CO2 transfer wheel and the mass of solid per wheel is calculated based on such a monolithic structure, the effective mass transfer coefficient used in the model is simplified based on the Glueckauf and Coates (Glueckauf and Coates 1947) approach, with a geometrical factor equal to 15. It is reasoned that no prediction about cell density, voidage and effective diffusivity was able to be made based on the current development stage of the rotary transfer device model. An extension of the effective mass transfer coefficient can be considered for the further development of the model. However, to analyse its effect on the needed amount of solid adsorbent mass requirement, a sensitivity analysis of the geometrical factor is performed in Section 4.2.5.

3.2 Rotary Devices in Adsorption

3.2.1 Development of Rotary Devices in Adsorption

In gas phase adsorption processes packed beds or circulating fluidised bed are commonly used. Typical problems often associated with fixed-bed reactors are discontinuity, due to dead time for regeneration of the fixed bed adsorption system, or nonlinearity control problems such as exothermic reactions (Jørgensen 1986). For circulating fluidised bed rectors, the added complexity in design, construction and operation leads to higher capital cost (Abbas Abdulkareem Mahmood 2017; Grace, J.R., Knowlton, T.M., Avidan 1997). Many of these problems can be overcome for the application of selective CO2 transfer by using a rotating fixed bed configuration, which is compact, has homogenous temperature distribution and can be operated continuously.

One of the first descriptions of a rotary adsorption configuration is the Pennington cycle mentioned in the patent of a rotary desiccant air conditioning cycle in 1955 (Pennington NA. Humidity changer for air conditioning. USA, Patent No. 2,700,537; 1955). Based on recent progress in adsorption and system configuration, more and more practical applications of rotary desiccant wheels, such as ‘‘Solar Assisted Air Conditioning of Buildings’’ in the Solar Heating & Cooling Program of the International Energy Agency (La et al. 2010; Delorme et al. 2004), have been implemented around the world. Another industrial application, where rotary adsorption systems can be found, are volatile organic compounds abatement systems (Yamauchi et al. 2007).

Those rotary adsorption systems have in common that structured adsorbents either in the form of adsorbent sheets or monoliths are used. These minimise pressure losses of the process, maximise contact between solid adsorbent and the gas stream and provide higher mass transfer coefficients, and therefore have a significant economic benefit.(D. M. Ruthven and Thaeron 1996; F. Rezaei and Webley 2010; Brandani et al. 2004)

Rotating wheel equipment have been dimensioned and operated as large-scale industrial application as regenerative rotary gas/gas heat exchangers for large

volume of flue gas typically generated in thermal power plans for decades (Howden 2019). Actual dimensions of the largest rotary heat exchanger manufactured, implemented and operated by the Howden Group are 24 m in diameter and 2 m in height (Hogg 2016). Such a regenerative rotary gas/gas heat exchangers is depicted in Figure 3-5.

An industrial application scale-up of the rotary adsorption systems technology should therefore be feasible from a mechanical and hydraulic perspective, however the complexity of handling solids at large scale, and the scare data on mass-transfer resistance and diffusion limitations, which are required to model adsorption accurately for pre-scale-up studies, make the scale up of such a technology challenging.

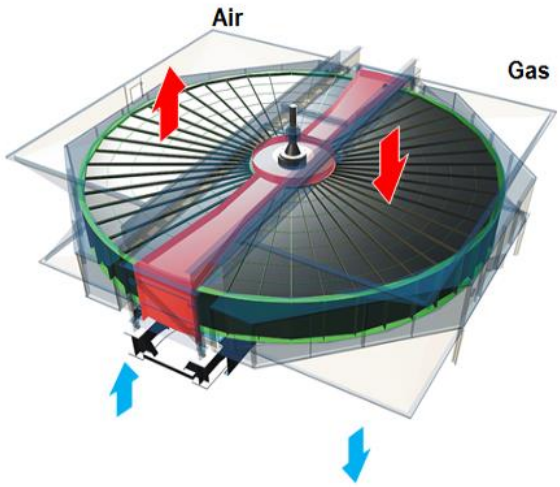

Figure 3-5: Regenerative Heat Exchanger (Howden 2019)

In the context of carbon capture, rotary adsorption wheel configurations have been studied in the Energy Technology Institute (ETI) funded collaboration 'Next Generation CCS Technology' project between InvenTys Thermal Technologies, the Howden Group and Doosan Power Systems (Green 2012). The investigated carbon capture process utilises InvenTys patented thermal swing adsorption technology VeloxoTherm™. This process, based on the design of gas/gas heat exchangers, uses structured adsorbent laminate for CO2 capture in a steam regenerated cycle, shown schematically in Figure 3-6, and as pilot plant device in Figure 3-7. To confirm the

projected benefits the technology is currently being tested on a slipstream flue gas exiting a 10 MWe coal-fired unit. (Inventys Inc. 2019)

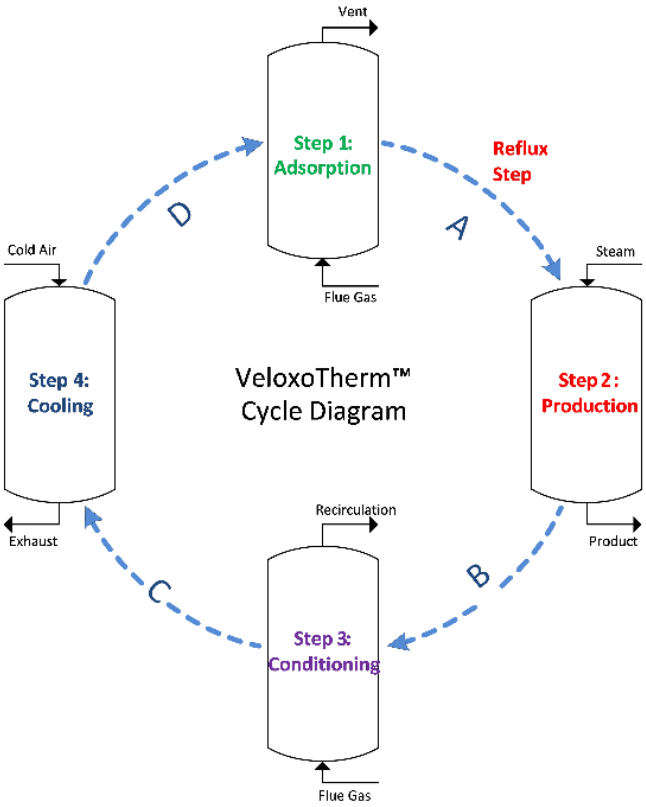

Figure 3-6: Schematic of the VeloxoTherm™ Cycle (Inventys Inc. 2019)

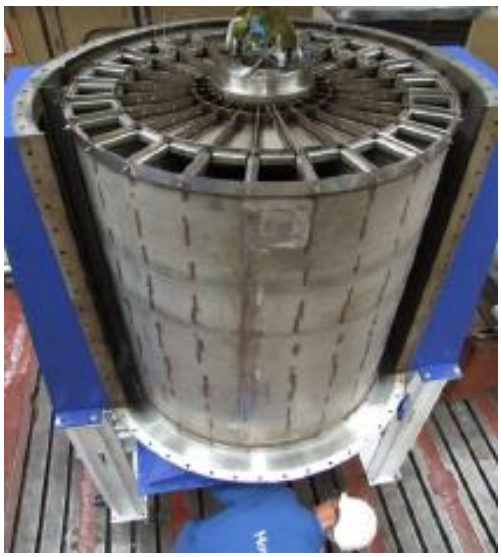

Figure 3-7: VelocoTherm™ proto type (Inventys Inc. 2019)

In the absence of global political and financial incentives to capture CO2, investments in driving CO2 capture technologies towards commercial deployment are largely missing. Funded by the Canadian Government, InvenTys built, in cooperation with Husky Energy, a CO2 capture pilot plant based on the VeloxoTherm™ technology. It is planned to be deployed at Husky Energy's Pikes Peak South heavy oil thermal project, capturing 0.01 M t of CO2/year. Commissioning was set for the end of 2018, but public information regarding completion is still outstanding at the time of writing. Academic research into rotary adsorption for CO2 capture was carried out in the context of two UK Engineering and Physical Sciences Research Council (EPSRC) funded multi-disciplinary research teams' collaborations, 'Adsorption Materials and Processes for Carbon Capture from Gas-Fired Power Plants' (AMPGas) and 'Gas - Future Advanced Capture Technology Options' (Gas-FACTS). The results of the latter are discussed in the previous Section 2.3 and again in Section 3.3. While Section 2.3 covers the strategies to increase CO2 concentration in the exhaust flue gases of power plants, Section 3.3 discusses the specifics of rotary adsorption in the form of a conceptual equilibrium model designed by (Herraiz et al. 2019). The kinetic model of the rotary transfer adsorption wheel, developed in this thesis, adds to this conceptual equilibrium model.

AMPGas was a collaboration between the University of Edinburgh, the University of St Andrews and Heriot-Watt University. The objectives of this project were to develop advanced adsorbents for carbon capture from flue gases from gas fired power plants and to develop an efficient separation processes with rapid thermal cycles using a rotary wheel adsorber setup. For this reason, a novel 12-tube bench-top lab-scale rotary wheel adsorber (RWA) has been designed and built, in which developed, strong and highly selective, palletised adsorbents have been tested in full rotary embodiment, to produce experimental data to validate adsorption models. (Gibson et al. 2016)

3.2.2 Difference between Adsorbents for CO_2 Capture and SEGR Application

The majority of research conducted to develop new adsorbents for post-combustion carbon capture is less relevant for the selection of adsorbents for SEGR applications. Both applications ideally require high-selectivity adsorbents to achieve relatively high CO2 uptake at low partial pressures.

In contrast to post-combustion capture applications, where the separation process is based on either strong physisorption or chemisorption with thermal regeneration, weak physisorption is considered here for the rotary CO2 transfer wheel. This is due to the importance of balancing the affinity for CO2 of the material to allow for the release of CO2 into ambient air, without any external source of mechanical work or thermal energy. Since ambient air is used, the regeneration of the adsorbent is achieved by the difference between the amount of CO2 adsorbed on the adsorbent and the partial pressure of CO2 in the ambient air. Breaking the strong interaction between the CO2 molecules and the adsorbent, such as a chemical bond, would need a separate energy input, either in the form of heat or mechanical work to create a vacuum. Thus, any material using strong physisorption or chemisorption for adsorption is not suitable.

Thermal energy is obviously not available at ambient air. Yet, there is a concentration gradient between flue gases and the air of two orders of magnitude, with respect to the partial pressure of carbon dioxide. Weak adsorbate-adsorbent bonds are thus suitable in this context.

Although they lead to lower achievable selectivity of CO2 over N2 compared to materials using chemisorption or strong physisorption, the small gradient of N2 partial pressure between flue gas and air limits the driving force, and a low N2 transfer rate is expected for SEGR application (Herraiz et al. 2019).

It is also important to note that selectivity is not a critical parameter, since the consequence of transferring nitrogen into combustion air are essentially a marginal dilution of the other gases.

Another important design consideration is the absence of drivers for maximum regeneration of the adsorbent in order to achieve maximum working cycle capacity, unlike common practice used in adsorption for post-combustion CO2 capture.

A certain amount of CO2 remains adsorbed on the solid during the regeneration phase, which is also the phase where CO2 is transferred to combustion air.

Therefore, sizing the system requires optimisation based on several parameters:

- The recycling ratio, i.e. the amount of CO2 that is transferred into the air stream.
- The amount of solid mass.
- The rotational speed.
- The partition of the cross-sectional area of different sectors of the wheel, between the adsorption and the desorption side.

So, in contrast to the large ongoing effort in adsorbent development for post-combustion CO2 capture, this work proposes the use of weaker physical adsorption with CO2 selective porous materials in a rotary wheel device for SEGR application, using ambient air for regeneration and achieving selective CO2 recycling. This combines the principle of a large scale rotating adsorption unit with continuously regeneration, with the advantages SEGR can provide for CCGTs with post-combustion CO2 capture.

3.3 Previous Conceptual Design

In this section, the process of the conceptual design of structured adsorbents in a regenerative adsorption wheel configuration for the application of SEGR is presented in connection with the developed mathematical equilibrium model of the rotary transfer wheel developed by Herraiz (Herraiz 2016; Herraiz et al. 2019). The sensitivity analysis of this model is discussed in Section 3.3.2, the SEGR configurations are discussed in previous Section 2.3.4. A more detailed assessment and performance

analysis of the conceptual design of structured adsorbents in a regenerative adsorption wheel configuration for SEGR application can be found in (Herraiz 2016).

3.3.1Equilibrium Model

The process of the regenerative adsorption CO2 transfer wheel can be described as a continuous adsorption/desorption cycle and the design is illustrated in Figure 3-8. CO2 is adsorbed when the flue gas enters into contact with the solid material located in a rotor operating at low rotational velocity in the adsorption section, and then gets desorbed into an ambient air stream under counter current flow condition to the flue gas stream in the desorption section. This replicates in size large scale regenerative rotary gas/gas heat exchangers used in pulverised coal boilers.

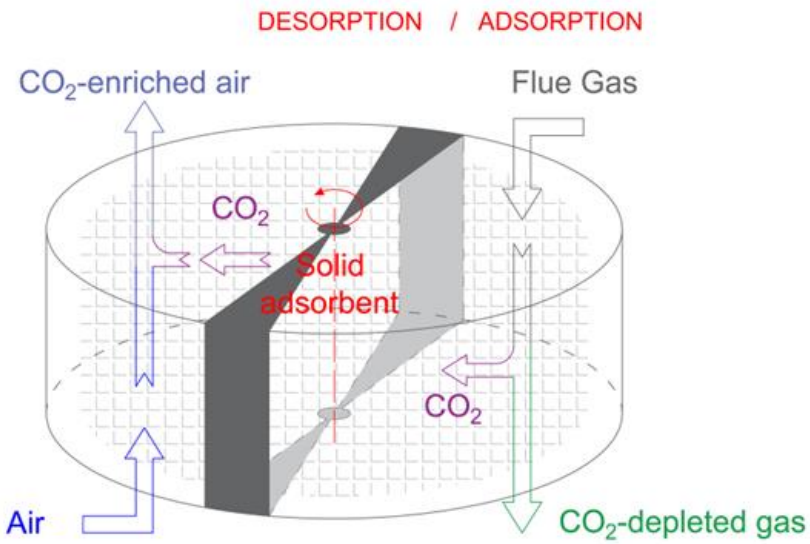

Figure 3-8: Schematic diagram of a rotary adsorbent for selective CO2 transfer (Herraiz 2016)

This design is then transferred by Herraiz (Herraiz 2016; Herraiz et al. 2019) into a process model based on mass transfer and thermal equilibrium performance, using gPROMS Model Builder (PSE Enterprise 2016b), which enables to investigate the adsorption process and solid properties. To do so, the wheel design is discretized into N_H x N_τ equilibrium stages, using finite difference method, as illustrated in Figure 3-9(a). N_τ is the number of stages in rotational direction, whereas N_H represents the

number of stages in longitudinal or height direction. For simplification of the process simulation, it is assumed that stream variables and flue gas, air and solid properties are constant along the radial direction, so that the system can be transferred into a two dimensional mathematical cell model, as depicted in Figure 3-9(b). The relative flow condition of gas and solid adsorbent in the rotor is cross-flow. (Herraiz et al. 2019)

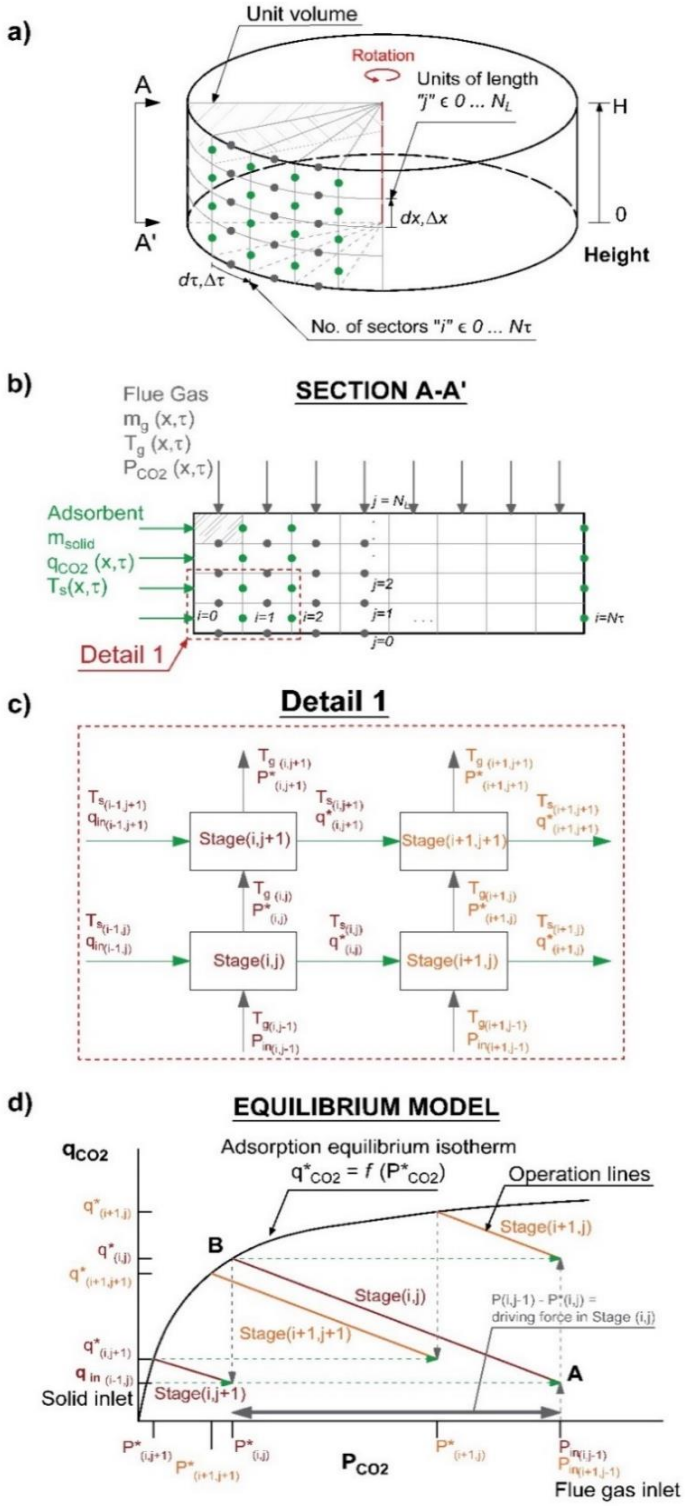

Figure 3-9: **Performance model of the rotary adsorber showing (a) the division of the equilibrium model into cells, (b) the cross-flow arrangement, (c) the equilibrium stages, and (d) the operation lines and the equilibrium curve.** (Herraiz et al. 2019)

For each cell/ stage it is assumed that thermal and mass transfer equilibrium is achieved. Consequently, the adsorption equilibrium isotherm, the Langmuir isotherm in this case, correlates the partial pressure of CO2 in the flue gas with the adsorbed amount of CO2 for each cell at its corresponding temperature. This is shown representatively in Figure 3-9(d) for the four cells depicted in Figure 3-9(c). The partial pressure of CO2 in gas phase and the adsorbed amount of CO2 in solid phase entering and leaving each equilibrium stage are connected via red and orange operation lines in Figure 3-9(d). The green and grey dashed lines connect two consecutive equilibrium stages. (Herraiz et al. 2019)

A set of partial differential equations is used to describe the mass and energy balances in the rotary adsorber. The mass balance for each component k is given by Equation (3.16) and can as well be written in terms of the molar flow rate of the component k, Equation (3.17). The energy balance is given by Equation (3.18) and again can be written in terms of the molar flow rate of the component k, Equation (3.19). Axial dispersion is neglected and steady state and equal affinity of the adsorbent to CO2 and N2 is assumed. (Herraiz et al. 2019)

$$\frac{\partial(u_g \cdot C_{\mathrm{k}})}{\partial x} = -(1-\varepsilon_b)\cdot\rho_p \cdot \frac{\partial \bar{q}_{\mathrm{k}}}{\partial \tau} \tag{3.16}$$

$$\frac{1}{A_c}\cdot\frac{\partial(\dot{n}_{\mathrm{k}})}{\partial x} = \frac{m_s}{A_c \cdot H}\cdot\frac{\partial \bar{q}_{\mathrm{k}}}{\partial \tau} \tag{3.17}$$

$$C_t \cdot \frac{\partial(u_g \cdot h_g)}{\partial x} = (1-\varepsilon_b)\cdot\rho_p \cdot C_s \cdot \frac{\partial T_s}{\partial \tau} + (1-\varepsilon_b)\cdot\rho_p \sum_{k=1}^{C}(-\Delta H_{ads\ k})\cdot\frac{\partial \bar{q}_{\mathrm{k}}}{\partial \tau} \tag{3.18}$$

$$\dot{n}_G \cdot \frac{\partial h_g}{\partial x} + \sum_{k=1}^{C}(\Delta H_{ads\ k})\cdot\frac{\partial(\dot{n}_k)}{\partial x} = \frac{m_s \cdot Cp_s}{H}\cdot\frac{\partial T_s}{\partial \tau} \tag{3.19}$$

Where:

C_{k} : concentration of the k component

u_g : superficial velocity

$\bar{q}_{\mathrm{k}}$: average amount adsorbed of the k component

ε_b : bed void fraction

ρ_p : particle density

∂x : change in longitudinal direction

$\partial \tau$: change in rotational direction

$\dot{n}_{\mathrm{k}}$: molar flow rate of the k component

m_s : total mass of solid

C_t : total gas phase concentration

h_g : molar enthalpy of the gas

C_s : solid specific heat

T_s : temperature of the solid

$(-\Delta H_{ads\ k})$: heat of adsorption of component k

A_c : cross sectional area

H : height of the structured adsorbent

Thermal and mass transfer equilibrium conditions for each cell are given by Equation (3.20) and (3.21). Gas/air and adsorbent will leave correspondent stage (i,j) at the same temperature. The adsorption equilibrium isotherm correlates the partial pressure of the adsorbate (P_{k}^{*}), with the adsorbed amount of component k on the adsorbent (q_{k}^{*}). (Herraiz et al. 2019)

$$T_{g\ (\mathrm{I,j})} = T_{s\ (\mathrm{I,j})} \tag{3.20}$$

$$q_{\mathrm{k}(\mathrm{I,j})}^{*} = f\left(P_{\mathrm{k}\ (\mathrm{I,j})}^{*}, T_{g\ (\mathrm{I,j})}\right) \tag{3.21}$$

3.3.2 Sensitivity Analysis

This section presents the sensitivity analysis conducted by Herraiz and co-workers (Herraiz et al. 2019). For more details into the assessment and the performance of the conceptual design, estimating the amount of solid material, sizing the wheel rotor and evaluating the number of rotary devices for a CCGT plant, please refer to (Herraiz 2016).

The sensitivity analysis is performed on the following properties of the solid adsorbent:

- Its saturation capacity q_s .
- Its equilibrium constant K_L .
- Its enthalpy of adsorption $(-\Delta H_{ads})$.

Air inlet temperature and flue gas inlet temperature are evaluated in a second step.

The governing equation for the solid properties in the conceptual equilibrium model is the extended Langmuir adsorption isotherm (Equation (3.2)), as described in Section 3.1.2. The dependence of the equilibrium constant K_L on the enthalpy of adsorption and the pre-exponential factor is given by the Van't Hoff equation (Equation (3.3)), repeated below for convenience.

$$K_{L,\,k} = K_{L0,\,k}\, exp\left(\frac{-\Delta H_{ads,k}}{RT}\right) \quad k = CO_2,\ N_2,\ O_2$$

To evaluate the effect of both solid properties and operating conditions, the term working cycle capacity needs to be introduced. The working cycle capacity of the adsorbent is defined as the difference between the adsorbed amount of CO_2 at the beginning (t = 0) and at the end of the adsorption cycle ($t = t_{\text{adsorption}}$), with N_L is the number of stages in the longitudinal direction of the wheel, as shown in Equation (3.22).

$$\text{Working cycle capacity} = \sum_{j=1}^{N_L} q_{CO2,t=t_{adsorption}} - \sum_{j=1}^{N_L} q_{CO2,t=0}\,;\ \text{for j} = 1 \ldots N_L \qquad (3.22)$$

It is the amount of CO2 taken up by the solid adsorbent per mass unit during one adsorption cycle of the wheel. The time $t_{\text{adsorption}}$ is depending on how the whole wheel is divided between the area for adsorption and the area for desorption and the rotational speed. It can be either divided equally, or, if either the adsorption or desorption process is time limiting, it can be optimized proportionally. Herraiz and

co-workers (Herraiz 2016; Herraiz et al. 2019) assume for the conceptual design an equal division between the adsorption and desorption part of the wheel, leading to $t_{adsorption}$ being half the total rotational time ($t_{adsorption} = t_{1/2}$).

Sensitivity analysis of solid properties

Herraiz and co-workers (Herraiz et al. 2019) showed that increasing the adsorbed saturation capacity leads to a reduction of mass of solid necessary to achieve a selective CO2 transfer efficiency of 97% for the configuration of SEGR in parallel. This is shown in Figure 3-10 for the activated carbon under consideration. Increasing the saturation capacity around 1 mol/kg leads to a reduction in adsorbent inventory of 42 tonnes. This trend continues up to an adsorbent saturation capacity of 8 mol/kg, which leads to a corresponding reduction in adsorbent mass of 40%. However, due to the asymptotic behaviour beyond 10 mol/kg, a further increase of the saturation capacity of 1 mol/kg results in a marginal reduction of adsorbent mass requirement of less than 5%.

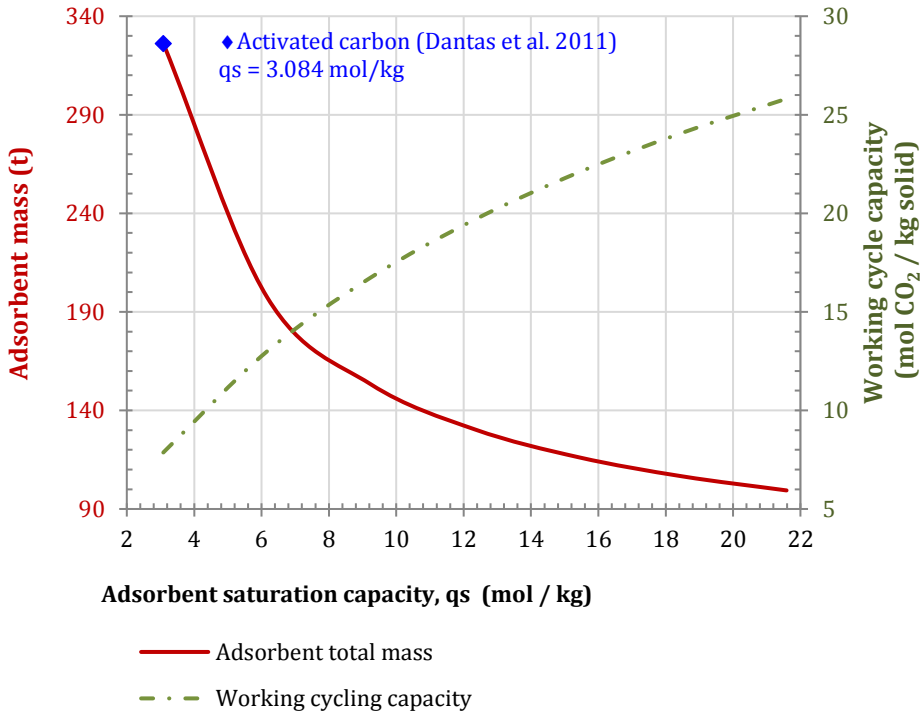

Figure 3-10: Sensitivity of adsorbent mass and working cycle capacity to the adsorbed saturation capacity. Configuration parallel SEGR at 70% recirculation ratio, 97% selective CO2 transfer efficiency and 96% post-combustion CO2 capture efficiency (Herraiz et al. 2019)

The effect of equilibrium constant on the adsorbent mass is studied by varying the enthalpy of adsorption and the pre-exponential factor across ranges typical of activated carbon materials. Herraiz and co-worker (Herraiz et al. 2019) performed this study for three adsorbed saturation capacities of 3, 6.2 and 12.3 mol/kg and the results are presented in Figure 3-11. They concluded that, for a given saturation capacity, there is a combination of enthalpy of adsorption and pre-exponential factor of the equilibrium constant resulting in a minimum mass of adsorbent. Although large pre-exponential factor and large enthalpy of adsorption indicate that CO2 adsorption is favourable, they are detrimental to desorption in ambient air. This reduces the working cycling capacity of the adsorbent and therefore increase the mass of adsorbent for a given CO2 transfer efficiency. In contrary small CO2 adsorption equilibrium constants are detrimental for the CO2 adsorption, by increasing the adsorbent mass requirement. Typical heat of adsorption values of activated carbon are currently in the range of 17 to 22 kJ/mol (Abanades et al. 2015). This analysis indicate however, that an adsorbent material with a saturation capacity of 3 mol/kg, an enthalpy of adsorption in the range of 24 to 28 kJ/mol and a pre-exponential factors in the range of 2·10-6 to 9·10-6 kPa-1, would reduce the adsorbent amount requirement to under 200 kg, and therefore nearly halve the required mass. (Herraiz et al. 2019)

Herraiz and co-workers (Herraiz 2016; Herraiz et al. 2019) only assess the effect of the adsorption parameters with respect to CO2. However, to improve the adsorption process in general it is also important to have advantageous properties with regard to N2 and O2, e.g. selectivity and non-competing adsorption to CO2.

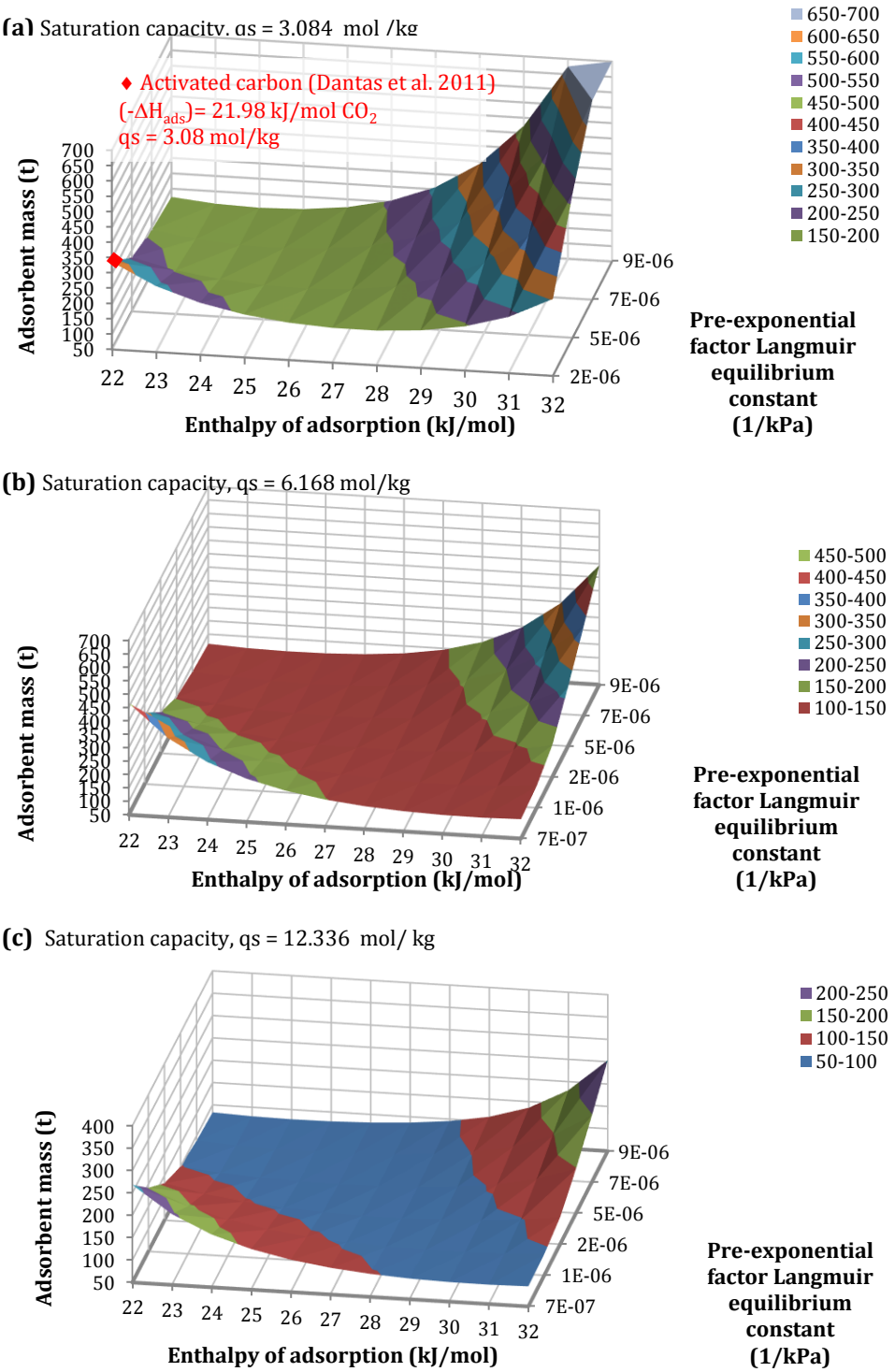

Figure 3-11: Sensitivity of adsorbent mass to the enthalpy of adsorption and the pre-exponential factor of the equilibrium constant, for a adsorbed saturated capacity of (a) qs= 3.08 mol/kg, (b) qs= 6.17 mol/kg, (c) qs= 12.34 mol/kg. Configuration: SEGR in parallel at 70% recirculation ratio, 97% selective CO2 transfer efficiency. (Herraiz et al. 2019)

Sensitivity analysis of operating conditions

It is possible to increase the temperature of the air inlet stream used for desorption by using available sensible heat from the HRSG. Herraiz and co-workers (Herraiz et al. 2019) predict that a 10 ºC increase in the air temperature results in an marginal increase of adsorbent mass of approximately 5.5 tonnes, as shown in Figure 3-12(a). Although a higher temperature is favourable for the desorption process, the cooling capacity of the air stream decreases, and therefore the adsorbent enters the adsorption section at a higher temperature resulting in a lower CO2 adsorption, as shown in Figure 3-12(b). That results in a lower working cycle capacity of the adsorbent. However, the tendency towards higher adsorbent mass requirements are marginal when put into the context of total mass requirement and amount to 1.5% adsorbent mass increase.

In addition (Herraiz et al. 2019) points out that the higher air inlet temperature increases the CO2-enriched air outlet temperature over the investigated range by 2 ºC, derating the gas turbine by 2 MW. However, this corresponds to a 0.25% change of absolute change in power output to the relative net power output.

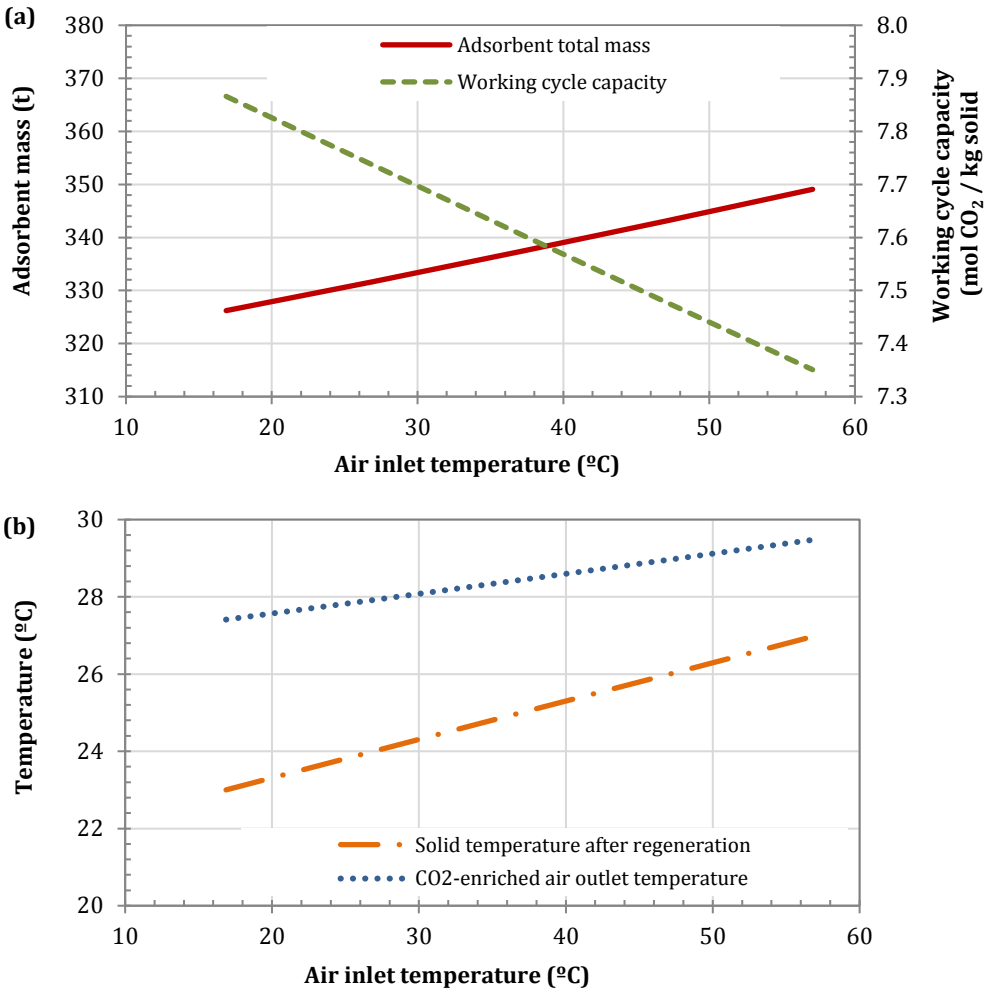

Figure 3-12: Effect of the air inlet temperature on (a) the adsorbent mass and the working cycle capacity and (b) on the CO2-enriched air and the solid temperatures. Configuration: SEGR in parallel at 70% recirculation ratio (Herraiz et al. 2019)

The flue gas inlet temperature can be controlled by a cooling system, since low temperatures are thermodynamically favourable to increase CO2 adsorption. Yet, the lowest achievable temperature is, in practice, limited by the type of cooling system and the temperature of cooling water or air available.

However, the main impact is not on the reduction of amount of adsorbent, which is rather marginal, as illustrated in Figure 3-13, but on maintaining the lowest temperature possible for the CO2-enriched air entering the gas turbine compressor. It depends on achieving a as low as possible CO2-enriched air outlet temperature of the rotary wheel. This is necessary since the inlet air temperature has an impact on the density of the working fluid. With increasing temperature, the density of the air

increases and more work is required to compress the warmer inlet air. (Herraiz et al. 2019)

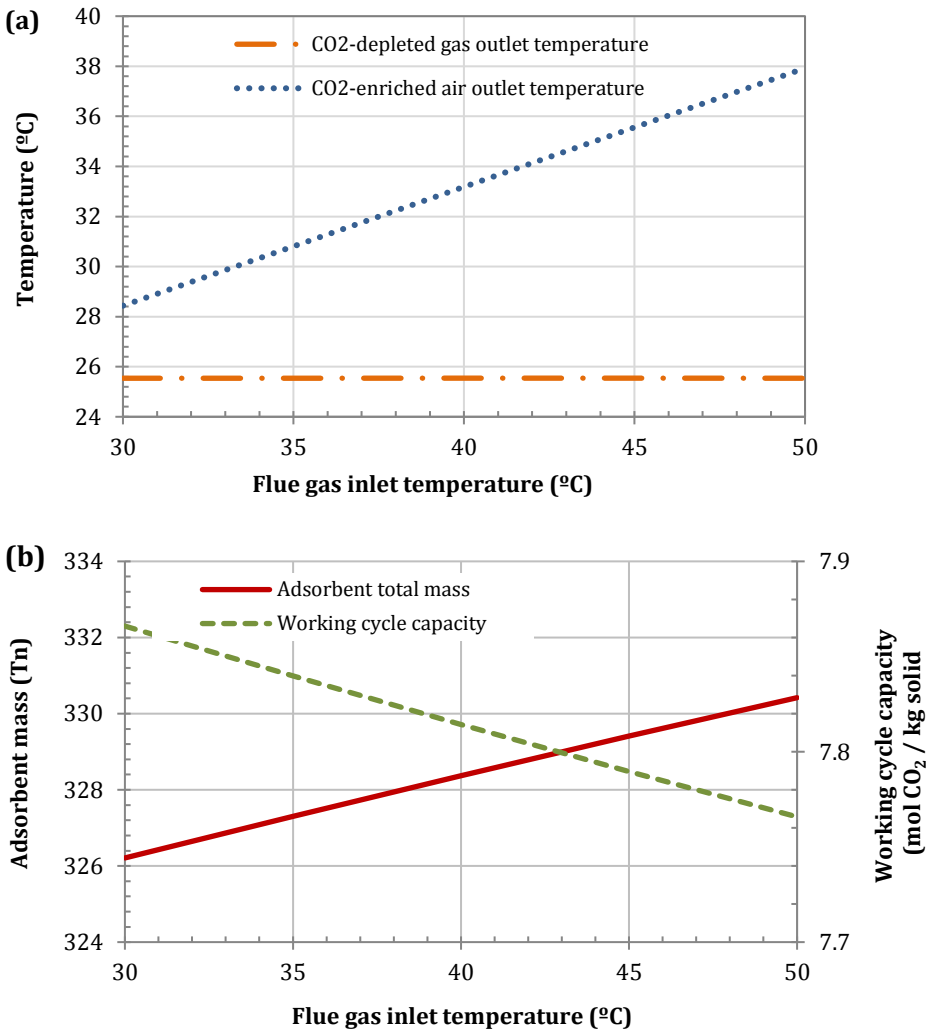

Figure 3-13: Effect of the flue gas inlet temperature on (a) the air and flue gas outlet temperatures and (b) the adsorbent mass and the working cycle capacity. Configuration: parallel SEGR at 70% recirculation ratio (Herraiz et al. 2019)

3.3.3 Knowledge Gaps

The conceptual design assessment done by Herraiz and co-worker (Herraiz et al. 2019) shows that the use of structured adsorbents in a rotary adsorber is technically feasible for selectively transferring CO2 from a flue gas stream into an ambient air

stream fed to the gas turbine compressor. Nevertheless, the sensitivity analysis of key adsorbent properties indicates that a development of new materials is required to minimise the amount of solid required and, ultimately, the size and number of rotary wheels within practical limits. (Herraiz et al. 2019)

Some important questions remain unanswered.

The effect of water:

- How does a water concentration in the flue gas for a range of up to 10 vol% affect the adsorption on activated carbons?

The effect of flue gas conditions on the adsorbent:

- How do adsorbents behave under expected flue gas conditions for SEGR? Do other flue gas components such as N2 or O2 change the adsorption behaviour, and if so how?

Regeneration with air:

- Is the assumption of regeneration with ambient air possible? Is the partial pressure difference of CO2 on the adsorbent and in ambient air enough as a driving force to regenerate the adsorbent?

The effect of mass transfer resistance:

- Will the kinetics of the adsorption process be a dominant resistance for the system? Which process variables could be limiting mass transfer?

The effect of heat resistance:

- Which is the influence of heat transfer in contrast to the thermal equilibrium assumption in the conceptual design?

Verification:

- Can data from isothermal fixed-bed tubular reactor tests – an experimental method of characterising adsorbents - be used to verify the rotary CO2 transfer wheel model?

Process optimisation:

- How do equilibrium and kinetic parameters, and other properties, feed back into process simulations of large scale selective CO2 transfer rotary adsorption systems?

The systematic approach to answer these questions is listed in Table 3-2.

Table 3-2: Remaining knowledge gaps in the development of regenerative rotary wheel devices for SEGR application

Knowledge gap	Method
Effect of water content on the adsorption	Experimental observation; testing how water changes mass transfer characteristics
Desorption with ambient air	Experimental observation; testing how desorption with air changes the mass transfer characteristics of following adsorption processes
Effect of the kinetics of adsorption	Experimental observation and expansion of the conceptual equilibrium model with mass transfer resistance
Effect of heat transfer resistance	Expansion of the conceptual equilibrium model with heat transfer resistance
Identifying limiting parameters	Expansion of the conceptual equilibrium model to include kinetics, rotational speed, partition of the cross sectional area of the wheel, height to diameter dependency of the adsorption
Verification	Experimental observation; using those experiments to verify the extended model simulations
Feedback loop	Process model of the integrated system for a new build CCGT; process model of the integrated system for a retrofitted CCGT

3.4 Methodology

3.4.1 Experimental Methodology

The methodology relies on experiments conducted by the author, using the facilities of the University of Saskatchewan, Canada, research group Bioenergy and Environmentally Friendly Chemical Processing of Prof. Ajay Dalai. It uses an activated carbon developed by Shahkarami in 2015 (Shahkarami 2017; Shahkarami, Dalai, et al. 2015; Shahkarami, Azargohar, et al. 2015) at the University of Saskatchewan.

The material chosen in this work is used to prove the concept of the regenerative rotary wheel. However, in general any ideal adsorbent materials should present: a large capacity for CO2 adsorption for a CO2 partial pressure ranging from 0.04 to 0.2 bar, and good selectivity of CO2 over nitrogen and oxygen, but moderate affinity for CO2, allowing CO2 desorption into air, low sensitivity to moisture for water concentrations up to 10 vol%, and large availability at relatively low cost.

The activated carbon is chosen based on two points. First, as an activated carbon it presented a less likelihood, in contrast to MOFs and zeolites, to be affected by the water vapour content in the feed gas, simulating the flue gas conditions expected in CCGTs with SEGR. And second, the reported equilibrium properties (Shahkarami 2017) match a predicted reduction in needed adsorbent mass provided by the sensitivity analysis of Herraiz equilibrium model (Herraiz et al. 2019) presented in Section 3.3.2 Figure 3-11 (c). Its equilibrium properties are presented in Table 3-6 next to its kinetic parameters. With a saturation capacity of 10.82 mol/kg, a pre-exponential equilibrium constant of 7.30E-06 1/kPA and an enthalpy of adsorption of 17.44 kJ/mol the equilibrium model predicts a reduction of adsorbent mass requirement of nearly 50% for all by (Herraiz et al. 2019) studied SEGR configurations in comparison with the previous studied commercially available activated carbon (Dantas et al. 2011). The comparison for the adsorbent mass requirement of the equilibrium model for both activated carbons (AC), the commercially available AC and the novel AC, later referred to as KOH activated

carbon, for different SEGR configuration studied by (Herraiz et al. 2019) is presented in Table 3-3.

Table 3-3: Comparison of the adsorbent mass requirement of the equilibrium model for two activated carbons for the SEGR configurations proposed by (Herraiz et al. 2019)

Configuration	**S-EGR Parallel 97/96**		**S-EGR Series 95/31**		**S-EGR Series 90/48**	
SEGR ratio [%]	70		N/A		N/A	
Selective CO2 transfer efficiency/ recovery rate [%]	97		95		90	
PCC efficiency/ capture rate [%]	96		31		48	
Solid	**Commercial AC**	**Novel AC**	**Commercial AC**	**Novel AC**	**Commercial AC**	**Novel AC**
Mass x 1000 [kg]	326	161	959	461	388	194
Volume [m^3]	287	170	843	484	341	204

Carbon activation method

The activated carbon is generated out of whitewood carbonized through fast pyrolysis and activated with the activating agent potassium hydroxide KOH. The carbonization eliminates most non-carbon elements and is carried out at high temperature and inert atmosphere. The resulting product is a char with porous structure and therefore a large internal surface area. (Shahkarami 2017)

The detailed steps of the activation of the char used as activated carbon in the breakthrough adsorption experiments can be seen in Table 3-4.

Table 3-4: Activation of the biochar by Shahkarami (Shahkarami 2017)

Step	Procedure
1	Sieving of biochar (150-355 µm).
2	Impregnation with KOH in 100 ml of water with biochar to KOH mass ratio of 0.81 on a dry basis and mixing at room temperature for 15 h.
3	Drying of the mixture in an oven at 110 °C for 15 h.
4	Loading sample into a tubular reactor under a nitrogen flow of 240 SmL/min and heated to 300 °C, hold temperature for 1 h.
5	Increasing temperature of the reactor to 775 °C with a heating rate of 3 °C/min and hold this temperature for 2 h.
6	Cooling sample down to room temperature.
7	Washing sample with hot water, followed by 0.1M HCl, and distilled water.
8	Drying sample in an oven overnight at 110 °C.
9	Sieving activated carbon (150-355 µm).

Characterization of the adsorbent and the adsorption bed

Table 3-5 provides the characteristic physical properties of the activated carbon obtained experimentally and the properties of the fixed-bed.

Table 3-6 shows the parameters of the adsorption equilibrium, obtained through fitting, and the kinetic parameters for adsorption on activated carbon. The equilibrium data are taken from Shahkarami (Shahkarami 2017) for 15 mol% CO2 in N2 adsorption on the activated carbon and are measured at different temperatures at atmospheric pressure in the fixed bed reactor system. (Shahkarami 2017)

Table 3-5: Properties of the used activated carbon sample and the adsorption bed (Shahkarami 2017)

Specific surface area	m^2/g	1461
Pore volume	m^3	5.80E-04
Bed length	m	0.030
Bed diameter	m	0.022
Total flowrate	ml/min	50
Skeletal density	kg/m^3	2111
Particle density	kg/m^3	952
Bulk density	kg/m^3	435
Bed porosity	[-]	0.543
Particle porosity	[-]	0.549
Total porosity	[-]	0.794
Mean particle radius	m	1.10E-04
Mean pore radius	m	6.54E-09

Table 3-6: Adsorption equilibrium and kinetic parameters for adsorption on activated carbon (Shahkarami 2017)

Saturation capacity (q_s)	mol/kg	10.82
Equilibrium constant (K_L)	1/kPa	7.30E-06
Enthalpy of adsorption ($-\Delta H_{ads}$)	kJ/mol	17.44
Temperature independent pre-exponential constant (D_{ci0}/r_c^2)	s^{-1}	12.995
Diffusion activation energy (Ea_i)	kJ/mol	18.05

Breakthrough CO2 adsorption setup

The breakthrough curve experiments are conducted by passing the gas mixtures through a 25 mm fixed-bed Inconel tubular reactor, the adsorber column. A dual channel micro-gas chromatograph (490 micro-GC, Agilent Technologies Inc., USA) equipped with a micro-thermal conductivity detector is used for chemical analysis. As carrier gases argon and helium are used. During the breakthrough adsorption experiments inlet and outlet flow rates are controlled using mass flow controllers (MFC) (5850E A/B, Brooks Instrument, USA). The water amount is controlled and

injected by a syringe pump, injecting water in liquid form into the dry N2 flow stream. It is made sure that all the water is evaporated before the combined stream of N2 and H20 reaches the adsorber column. The temperature is monitored by K-type thermocouples inside the column and controlled by heating tape around the tubular reactor connected to a Eurotherm temperature controller (2416, Eurotherm, USA). All the breakthrough experiments are repeated twice, and the average values are reported. The schematics of the experimental set-up is shown in Figure 3-14. The GC is calibrated using mixtures of known composition. The calibration curves of the MFCs are provided in Appendix A, the measurement accuracies and the uncertainty methodology are provided in Appendix B.

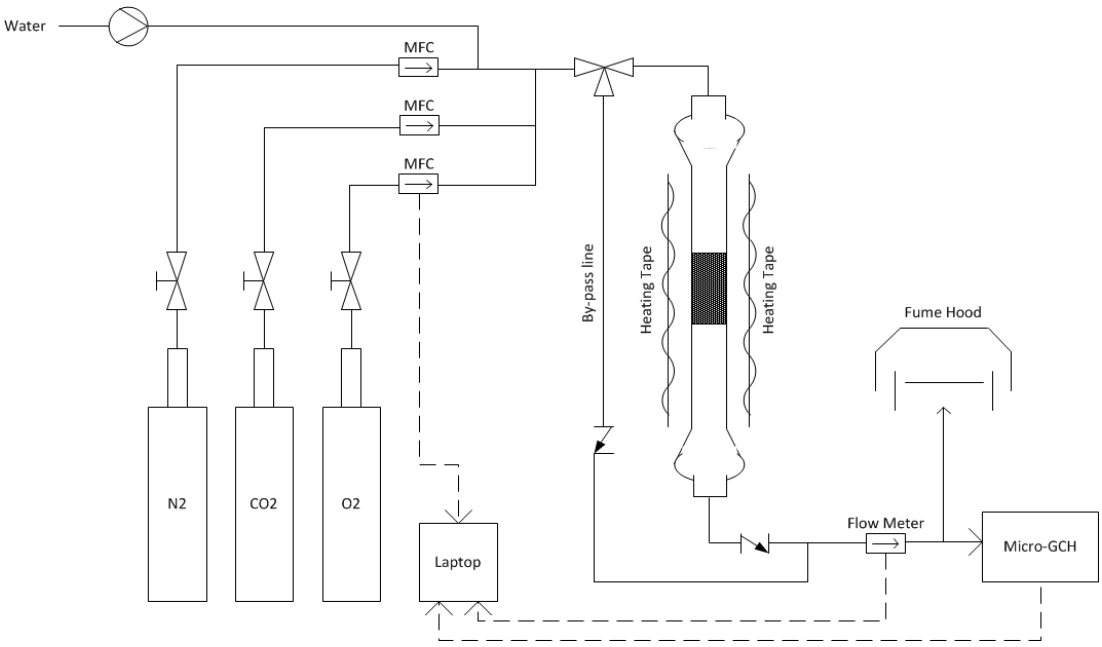

Figure 3-14: Schematic of the measurement set-up for dynamic adsorption measurement

An activated carbon amount of 5.0 g is loaded into the adsorber and pre-heated at 160 °C for 2 h under N2 prior to the adsorption experiments to desorb any previous adsorbed gases. Then, the system is cooled down to 30 °C, before the experimental feed gas composition is switched on and passed through the reactor. The total feed flow rate is kept constant at 50 mL/min and passed through the fixed-bed until saturation is achieved, shown by the outlet concentration of CO2 reaching the inlet concentration of CO2. Afterwards the saturated adsorbent is regenerated by

switching from the experimental feed gas composition to pure N2 flow and the temperature is raised again to 160 °C for 2 h. Only for the desorption test with air this regeneration step between the adsorption breakthrough experiments is skipped and replaced by regeneration with air under ambient condition.

Description of conducted measurements

In this section the adsorption curve measurements for different flow conditions are reported. The feed flow compositions are listed in Table 3-7. Parallel SEGR (97/96) (70%RR) refers to a CCGT flow composition of a SEGR in parallel configuration with a selective CO2 transfer efficiency of 97%, a PCC efficiency of 96% and a recirculation ratio of 70%. Series SEGR (95/31) refers to CCGT flow composition of a SEGR in series configuration with a selective CO2 transfer efficiency of 95% and a PCC efficiency of 31%, respectively. The molar amount of Ar [mol%] of both configurations is added proportionally to the molar amount of N2, since, due to Ar being one of the carrier gases in the dual channel micro-GC, the adsorption behaviour of Ar would not be able to be detected. For the flow compositions CO2/N2 and CO2/N2/O2, the CO2 and O2 concentration are chosen to be the same as in the case Parallel SEGR (97/96) (70%RR). These compositions are chosen so that a conclusion on their competing adsorption behaviour on the tested activated carbon can be drawn. For each of these compositions two repeated breakthrough adsorption tests were carried out at different temperatures. The tested temperatures were chosen in a range of possible occurring temperatures of CCGT flue gases. The different temperatures which were tested are listed in Table 3-8.

Table 3-7: Feed flow compositions for the conducted breakthrough adsorption tests

	CO2 [%mol]	**N2 [%mol]**	**O2 [%mol]**	**H2O [%mol]**
CO2 / N2	14.12	85.88	-	-
CO2 / N2 / O2	14.12	76.87	9.01	-
Parallel SEGR (97/96) (70%RR)	14.12	67.36	9.01	9.51
Series SEGR (95/31)	12.83	68.36	9.64	9.17

Table 3-8: Temperatures for the conducted breakthrough adsorption tests.

	Temperature [◦C]		
CO2 / N2	30	-	-
CO2 / N2 / O2	30	-	50
Parallel SEGR (97/96) (70%RR)	30	40	50
Series SEGR (95/31)	30	-	50

To understand the feasibility of regeneration of the adsorbent with air at ambient conditions multi-cycles adsorption/desorption are carried out to then examine the adsorption behaviour after desorption with air. Therefore, after the adsorbent is saturated under Parallel SEGR (97/96) (70%RR) feed flow composition conditions, the gas flow is switched from feed gas to air flow. The ratio of desorption air to flue gas mass flow is 1.12, identical to the values reported by Herraiz (Herraiz 2016) for SEGR (97/96) (70%RR). Corresponding desorption conditions, air mass flow and desorption time are listed in Table 3-9. The adsorbent is subjected to three continuous adsorption–desorption cycles and the performance for each cycle is compared.

Table 3-9: Desorption test conditions for parallel SEGR (97/96) (70%RR)

Temperature [◦C]	18
Desorption time [h]	1
Air mass flow [mL/min]	43.29

3.4.2 Mathematical Kinetic Model

This section contains the development of a kinetic mass transfer model for CO2 adsorption of a rotating regenerative CO2 transfer wheel under real possible CCGT flow composition of SEGR, as well as the convective heat transfer model and their numerical solution. Figure 3-15 illustrates the process flow diagram of the rotating regenerative CO2 transfer wheel.

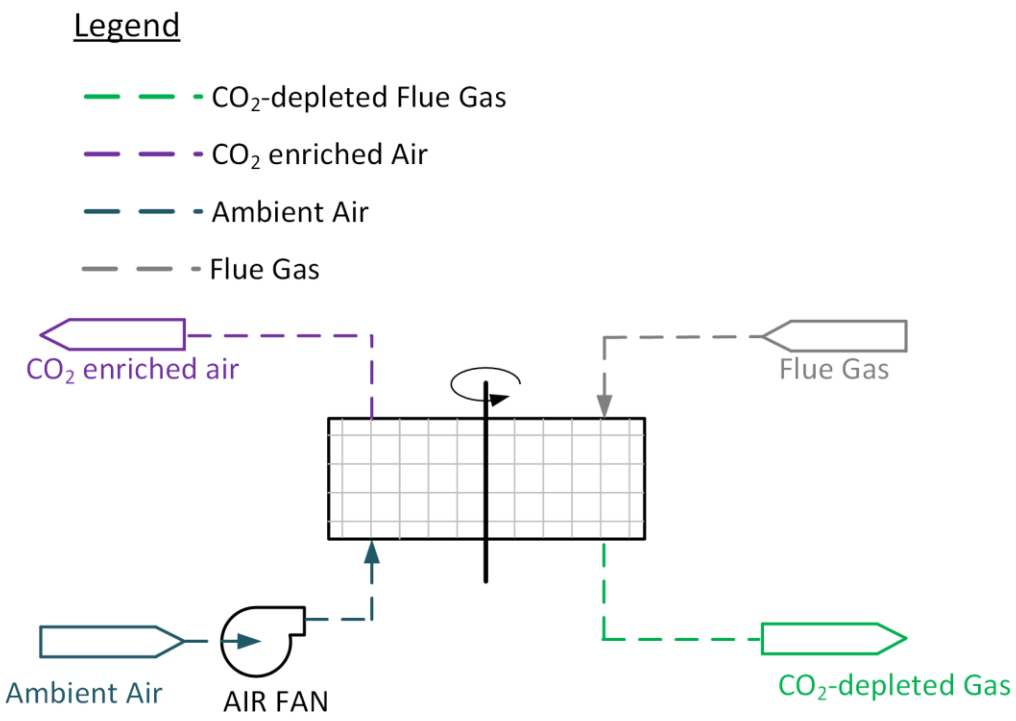

Figure 3-15: Process flow diagram of the rotating regenerative CO2 transfer wheel

The kinetic model of the adsorption and the desorption processes is developed using the model builder function of gCCS (PSE Enterprise 2016a). To design the CO2 separation process, the development of a mass transfer model to describe the transport of CO2 from a gas mixture to the adsorption sites of the activated carbon and the adsorption process onto the solid in the rotary wheel is essential. The model can be used to understand the dynamic process, predict breakthrough curves, assess process variables, investigate the solid kinetic properties and can be used to explore a more detailed design, without extensive experimental work.

The system domain is discretized into N_H x N_τ equilibrium stages using a finite difference method, as shown in previous Section 3.3.1, with N_τ the number of stages in rotational direction and N_H the number of stages in longitudinal or height direction (Figure 3-16(a)). The radial gradient of stream variables and flue gas, air and solid properties are assumed to be constant, transferring the 3-dimensional system into a 2-dimensional mathematical cell model (Figure 3-16(b)). The relative flow condition of gas and solid adsorbent in the rotor is assumed to be cross-flow. In each stage

steady state thermal transfer and mass transfer is achieved. The adsorption behaviours are described by the extended Langmuir isotherm model. The mathematical kinetic mass transfer model is based on the linear driving force model, by which the adsorption rate is calculated. To calculate the effective mass transfer coefficient the simplified approach by Glueckauf and Coates (Glueckauf and Coates 1947) is used, as discussed in Section 3.1.5.

The assumptions on which the kinetic model is build are summarized in Table 3-10. Using these assumptions and simplification, the complexity of the governing equations can be reduced to find a solution for the system of partial differential equations describing the mass and energy balances in the rotary adsorber.

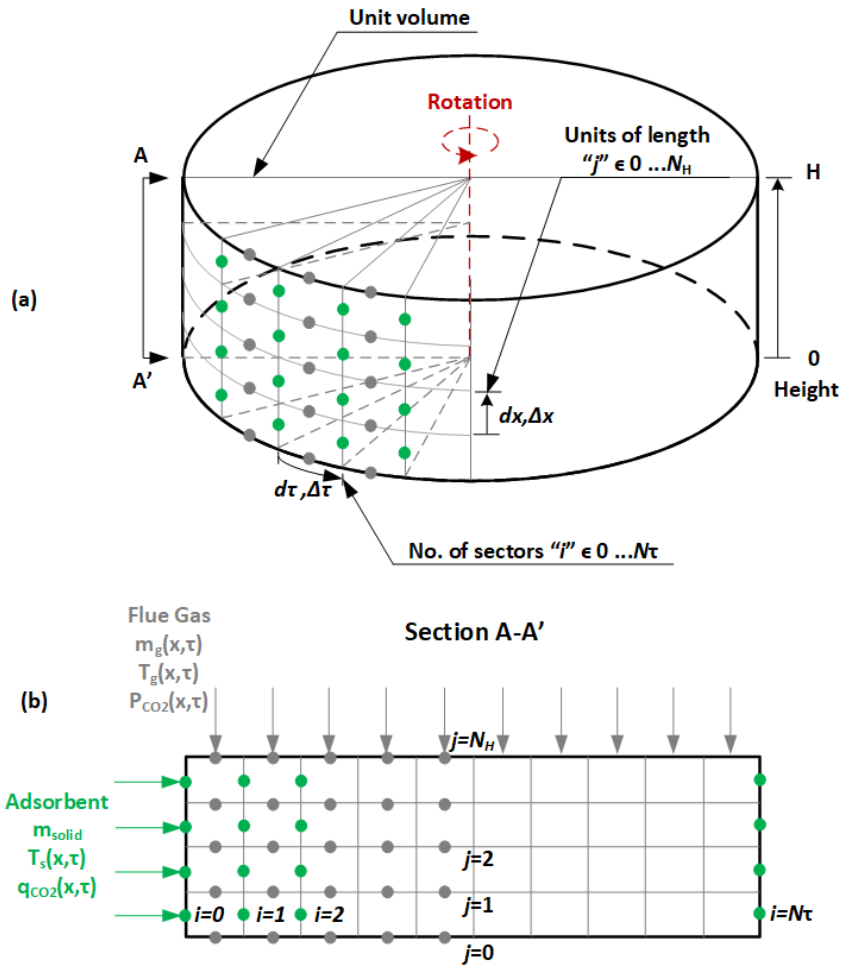

Figure 3-16: Performance model of the rotary adsorber showing (a) the division of the model into cells and (b) the cross-flow arrangement. (adapted from (Herraiz 2016)**)**

Table 3-10: Summary of model assumptions

Assumption/ Simplification	Rational
Radial gradient of the variables and properties are constant	Simplification based on assumption of no interaction with the wall
2 D model	Based on neglecting the radial component
Uniform bed	Based on equally and ideally constructed monolithic structure
Axial dispersion is neglected	Based on ideal plug flow, low viscosity, and research on dispersion in monoliths pointing towards a control by mass transfer resistance
No pressure drop implemented	Simplification at the development stage of the model; energy penalty of the booster fan is calculated on constant pressure drop assumption
Co-adsorption of N2, O2 and H2O is neglected	No equilibrium or kinetic parameters are available for the components other than CO2
Dominant mass transfer resistance is the micropore resistance	Based on the findings of (Shahkarami 2017) for the AC used to verify the model
Constant velocity	Approximation based on high velocity, no friction and steady state assumption

Mass and energy balance

Large regenerative rotary gas/gas heat exchangers, as those designed by Howden, are usually installed with thermal insulation and leakage sealing (see leakage consideration under Section 3.4.3). As such the energy and mass exchange between the wheel and environment can be assumed neglectable in most cases. This will be also assumed for the case of large regenerative rotary CO2 transfer wheels.

The overall mass balance for each component is given by Equation (3.23), where ε_b is the bed void fraction, C_{k} is the gas phase concentration of the component k, t is the time, ρ_p is the particle density, $\bar{q}_{\mathrm{k}}$ is the average amount adsorbed of the component k, u_g is the superficial velocity, x is the axial direction in which the gas is flowing and D_{ax} axial dispersion.

$$\varepsilon_b \frac{\partial c_k}{\partial t} + (1-\varepsilon_b)\rho_p \frac{\partial \bar{q}_k}{\partial \tau} = \frac{\partial u_g c_k}{\partial x} + \varepsilon_b \frac{\partial}{\partial x}\left(D_{ax} \frac{\partial c_k}{\partial x}\right) \tag{3.23}$$

The first term describes the change of concentration of component k with time, the second term the change of average adsorbent amount of component k with the rotational time, the third term the change of concentration of component k in axial direction and the forth term the change of concentration of component k in axial direction because of axial dispersion.

Assuming steady state is reached in the wheel and ideal plug flow, the first term as well as the axial dispersion term can be neglected (Douglas M. Ruthven 1984), which simplifies Equation (3.23) to Equation (3.24).

$$\frac{\partial u_g c_k}{\partial x} = (1-\varepsilon_b)\rho_p \frac{\partial \bar{q}_k}{\partial \tau} \tag{3.24}$$

The term $(1-\varepsilon_b)\rho_p$ relates to the mass of the adsorbent and can be written as the ratio between the solid mass m_s and total volume of the bed V_T , which in turn can be written as the product of the cross sectional area A_c and the height of the structured adsorbent H (Equation (3.25)).

$$(1-\varepsilon_b)\rho_p = \frac{m_s}{V_T} = \frac{m_s}{A_C \cdot H} \tag{3.25}$$

The concentration of the component k can be expressed in terms of the molar flow rate $\dot{n}_k$ of component k, with $\dot{V}$ being the volume flow, given by the product of cross sectional area and superficial velocity (Equation (3.26)).

$$c_k = \frac{\dot{n}_k}{\dot{V}} = \frac{\dot{n}_k}{A_c \cdot u_g} \tag{3.26}$$

With substituting Equation (3.25) and (3.26) in Equation (3.24) we get an expression for the molar flow rate of the component k based on the total mass of solid material and the change in average adsorbed amount of component k, as indicated in Equation (3.27).

$$\frac{\partial \dot{n}_k}{A_c \cdot \partial x} = \frac{m_s}{A_c \cdot H} \frac{\partial \bar{q}_k}{\partial \tau} \tag{3.27}$$

With the Linear Driving Force model introduced in Section 3.1.5 in form of Equation (3.28), where q_k^* is the adsorbed phase concentration in equilibrium, calculated based on the extended Langmuir isotherm (Equation (3.2)-(3.3)), the mass transfer system can be solved.

$$\frac{\partial \bar{q}_k}{\partial \tau} = \frac{15 D_{c,k}}{r_c^2} \cdot (q_k^* - \bar{q}_k) \tag{3.28}$$

For the effective diffusion coefficient D_{eff}, the crystal diffusivity/ crystal diffusion coefficient of component k $D_{c,k}$ and the crystal radius r_c is used, based on (Rodrigues and A. 2005) approach on the Darken-type model.

Here the crystal diffusivity at any loading is a function of surface diffusion at zero loading multiplied by the thermodynamic correction factor" (Shahkarami 2017), which is shown in Equation (3.29).

$$D_{c,k} = D_{c,k}^{\infty} \cdot \frac{dln(p_k)}{dln(q_k)}\Big|_T \tag{3.29}$$

With $D_{c,k}^{\infty}$ the temperature dependent diffusivity at high temperatures of component k. It can be understood as an activation energy for the adsorbed molecules in the pores to reach an energetic state high enough to overcome the adsorption energy barrier. The latter is typically expressed in the form of Equation (3.30), where $D_{c,k\,0}$ is the temperature independent pre-exponential constant of component k, E_{ai} is the activation energy, R is the universal gas constant and T_G is the gas temperature. (Grande, Gigola, and Rodrigues 2003; Rodrigues and A. 2005; Khalighi, Farooq, and Karimi 2012; Shahkarami 2017)

$$D_{c,k}^{\infty} = D_{c,k\,0} \exp\left(\frac{-E_{ai}}{R \cdot T_G}\right) \tag{3.30}$$

The factor $\frac{\partial ln(p_k)}{\partial ln(q_k)}$ can be determined for a Langmuir isotherm according Equation (3.31), where θ is the loading of the adsorbent. θ can be expressed as a quotient of q_k^* , the amount of component k adsorbed in equilibrium at a given partial pressure and q_s, the saturation capacity. (Do and Do 2001; Khalighi, Farooq, and Karimi 2012)

$$\left.\frac{dln(p_k)}{dln(q_k)}\right|_T = \frac{1}{1-\theta} = \frac{1}{1-{}^{q_k^*}/_{q_s}} \tag{3.31}$$

The heat and mass transfer within the adsorbent are coupled and should be therefore considered simultaneously when developing an adsorption model.

The energy balance without heat transfer resistance can be written as a change of the molar enthalpy of the gas h_g in the axial direction x equalling the change in the molar enthalpy due axial dispersion λ_{ax} (axial dispersion coefficient), plus the change of the temperature of the solid T_s in rotational direction τ, plus the released heat of adsorption $(-\Delta H_{ads\ k})$ of the components adsorbed by the adsorbent, as shown in by Equation (3.32).

$$C_t \cdot \frac{\partial(u_g \cdot h_g)}{\partial x} = \varepsilon_b \cdot \lambda_{ax} \cdot \frac{\partial(h_g)}{\partial x} + (1-\varepsilon_b) \cdot \rho_p \cdot Cp_s \cdot \frac{\partial T_s}{\partial \tau} + (1-\varepsilon_b) \cdot \rho_p \sum_{k=1}^{C} (-\Delta H_{ads\ k}) \cdot \frac{\partial \bar{q}_k}{\partial \tau} \tag{3.32}$$

With the total gas phase concentrations C_t and the solid specific heat Cp_s.

As before, neglecting the change due to axial dispersion Equation (3.32) simplifies to Equation (3.33).

$$C_t \cdot \frac{\partial(u_g \cdot h_g)}{\partial x} = (1-\varepsilon_b) \cdot \rho_p \cdot Cp_s \cdot \frac{\partial T_s}{\partial \tau} + (1-\varepsilon_b) \cdot \rho_p \sum_{k=1}^{C} (-\Delta H_{ads\ k}) \cdot \frac{\partial \bar{q}_k}{\partial \tau} \tag{3.33}$$

The energy balance can be written in form of molar flow rate, leading to Equation (3.34), by substituting the total gas phase concentrations C_t by the molar flow of the total gas $\dot{n}_G$, similar to Equation (3.26), implementing Equation (3.25) and (3.27) and rearranging the equation to describe the heat transfer on the gas side as equal to the heat transfer on the solid side, resulting in $T_G = T_s$.

$$\dot{n}_G \cdot \frac{\partial h_g}{\partial x} + \sum_{k=1}^{C} (\Delta H_{ads\ k}) \cdot \frac{\partial (\dot{n}_k)}{\partial x} = \frac{m_s \cdot Cp_s}{H} \cdot \frac{\partial T_s}{\partial \tau} \tag{3.34}$$

This equation is only utilised for the equilibrium model used in Section 4.2.3.
In case of a convective heat transfer resistance between the gas and solid side, the heat transfer for the gas side is given by Equation (3.35), and for the solid side by Equation (3.36) respectively, where h_{cv} is the convective heat transfer coefficient, A_s is the total surface heating area and ΔT the temperature difference between the gas temperature T_G and the solid temperature T_S (Equation (3.37)).

$$\dot{n}_G \cdot \frac{\partial h_g}{\partial x} + \sum_{k=1}^{C} (\Delta H_{ads\ k}) \cdot \frac{\partial (\dot{n}_k)}{\partial x} = h_{cv} \cdot A_s \cdot \Delta T \tag{3.35}$$

$$\frac{m_s \cdot Cp_s}{H} \cdot \frac{\partial T_s}{\partial \tau} = h_{cv} \cdot A_s \cdot \Delta T \tag{3.36}$$

$$\Delta T = T_G - T_s \tag{3.37}$$

Numerical solution

The numerical solution for this system of equation is based on discretising the system into N_H x N_τ stages (number of stages in axial direction x number of stages in rotational direction), where Δx represents the incremental step in axial direction (Equation (3.38)), and $\Delta \tau$ the incremental step in rotational direction (Equation (3.39)), respectively, where f_{Area} is the fraction of the wheel available for the process and ω is the rotational/ angular speed.

$$\Delta x = \frac{H}{N_H} \tag{3.38}$$

$$\Delta \tau = \frac{{}^{60}/_{\omega} \cdot f_{Area}}{N_\tau} \tag{3.39}$$

The number of N_H as well as N_τ stages needs to be chosen high enough, to establish a numerical independence of the discretisation. For the results in the thesis, the number of stages in axial direction was chosen to be 20 and in rotational direction 40. The negligible impact of the chosen number of stages is shown exemplary in Figure 3-17 for N_τ in rotational direction. It can be seen that an increase in stages in rotational directional above 24 changes the recovery rate of the wheel by less than 0.02%. For 40 stages the change in recovery rate of the wheel is less than 0.01%. Therefore, the choice of 40 stages in rotational direction seems sufficient enough to evaluate the impact as negligible. The same holds true for the number of stages in axial direction, where an increase in number of stages above 20 effects the results of the wheel by less than 0.01%.

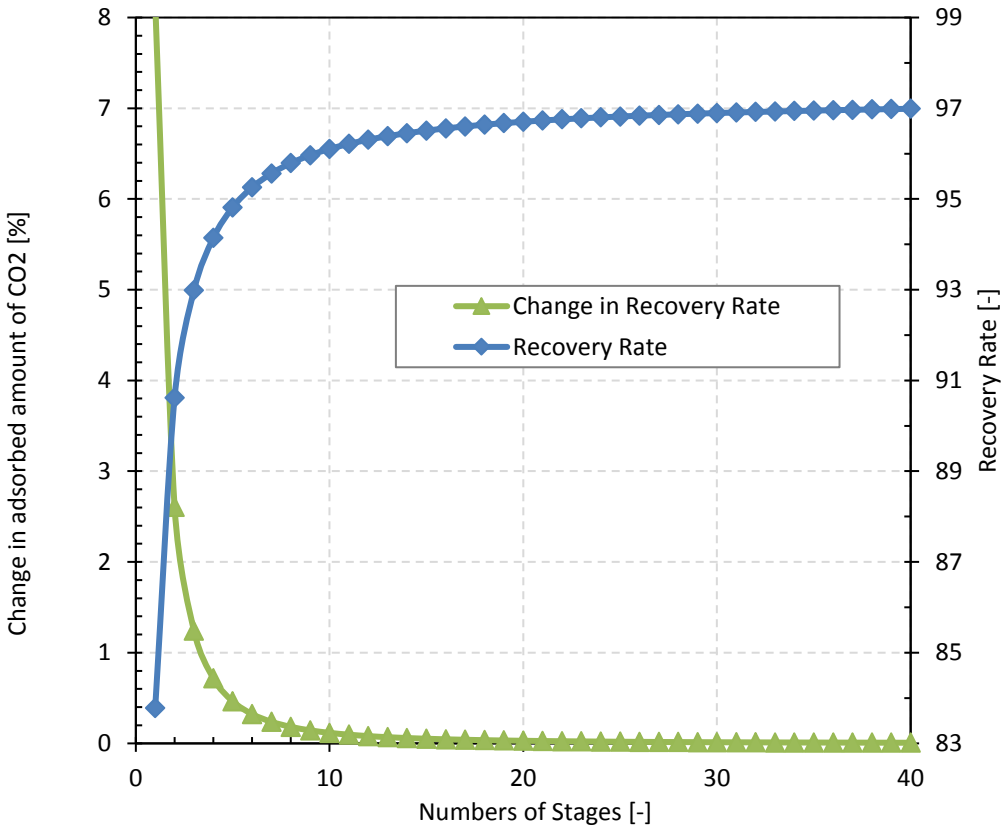

Figure 3-17: Analysis of the numerical independence of the model discretisation from the number of stages in rotational direction

The gas/air molar flow rate $\dot{G}$ in each time increment/ rotational section can be described by Equation (3.40) and the rate of solid adsorbent $\dot{S}$ in each longitudinal section by Equation (3.41). The cycling time of the process t_{cycle} is dependent on the rotational speed and the cross sectional area of the partition of the wheel available, as shown in Equation (3.42).

$$\dot{G} = \frac{\dot{n}_G}{N_\tau} \tag{3.40}$$

$$\dot{S} = \frac{m_s \cdot f_{Area}}{N_H} \cdot \frac{1}{t_{cycle}} \tag{3.41}$$

$$t_{\mathrm{cycle}} = \frac{60}{\omega} \cdot f_{Area} \tag{3.42}$$

Based on Equation (3.38)-(3.42), the mass balance on the gas side of each component k at each stage (i,j) is solved according to Equation (3.43). The mass balance on the solid side is solved according to Equation (3.44).

$$\frac{\partial n_k}{A_c \cdot \partial x} = \frac{\dot{n}_{k(\mathrm{i,j-1})} - \dot{n}_{k(\mathrm{i,j})}}{A_c \cdot \Delta x} = \frac{\left[\dot{n}_{G(\mathrm{i,j-1})} \cdot y_{\mathrm{k(i,j-1)}} - \dot{n}_{G(\mathrm{i,j})} \cdot y_{\mathrm{k(i,j)}}\right] * N_\tau}{A_c * {}^{H}/_{N_H}} = \frac{\left[\dot{G}_{(\mathrm{i,j-1})} \cdot y_{\mathrm{k(i,j-1)}} - \dot{G}_{(\mathrm{i,j})} \cdot y_{k(i,j)}\right]}{A_c \cdot H} \cdot N_\tau \cdot N_H \tag{3.43}$$

$$\frac{m_s}{A_c \cdot H} \cdot \frac{\partial \bar{q}_k}{\partial \tau} = \frac{m_s}{A_c \cdot H} \cdot \frac{\left[q_{k(i,j)} - q_{k(i-1,j)}\right]}{\frac{60}{\omega} \cdot f_{Area}} \cdot \frac{N_H}{N_H} = \frac{\dot{S}}{f_{Area}} \cdot \frac{\left[q_{k(i,j)} - q_{k(i-1,j)}\right]}{A_c \cdot H} \cdot N_\tau \cdot N_H \tag{3.44}$$

With:

$\mathrm{k} = 1 \ldots \mathrm{C}$ (no. of components);

$\mathrm{j} = 1 \ldots N_H$ (no. of stages in axial direction);

$\mathrm{i} = 1 \ldots N_\tau$ (no. of stages in rotational time direction);

y_{k}: molar fraction of component k

Combining Equation (3.43) and (3.44) into an overall mass balance leads to the expression of $\dot{n}_{\mathrm{k\ adsorbed}}$ as the molar flow rate of adsorbed amount of component k. It is expressed as the transfer of mass from the gas side onto the solid for each cell

of the adsorption process, and as a transfer of mass from the solid into the air stream for the desorption process (Equation (3.45)).

$$\dot{G}_{(\mathrm{i,j-1})} \cdot y_{\mathrm{k}(\mathrm{i,j-1})} - \dot{G}_{(\mathrm{i,j})} \cdot y_{\mathrm{k}(\mathrm{i,j})} = \frac{\dot{S}}{f_{Area}} \cdot (q_{\mathrm{k}(\mathrm{i,j})} - q_{\mathrm{k}(\mathrm{i-1,\,j})}) = \dot{n}_{\mathrm{k\ adsorbed(i,j)}} \quad (3.45)$$

Applying the same discretisation into the N_H x N_τ stages to the Linear Driving Force model Equations (3.28) – (3.30) leads to Equations (3.46) – (3.48), which are the last equations needed to solve the set of equations for the mass balance.

$$\frac{\partial \bar{q}_k}{\partial \tau} = \frac{[q_{k(i,j)} - q_{k(i-1,j)}]}{\frac{60/\omega^* \, f_{Area}}{N_\tau}} = \frac{15 D_{c,k(i,j)}}{r_c^2} \cdot \left(q^*_{k(i,j)} - \bar{q}_{k(i,j)}\right) \quad (3.46)$$

$$D_{c,k(i,j)} = D^{\infty}_{c,k(i,j)} \cdot \frac{1}{1 - q^*_{k(i,j)} / q_s} \quad (3.47)$$

$$D^{\infty}_{c,k(i,j)} = D_{c,k\,0} \exp\left(\frac{-E_{ai}}{R \cdot T_{G(i,j)}}\right) \quad (3.48)$$

Applying the same principle to the energy balance leads to Equation (3.49) for the case of no heat transfer resistance.

$$\dot{G}_{(\mathrm{i,j-1})} \cdot\ h_g(T_{(\mathrm{i,j-1})}) - \dot{G}_{(\mathrm{i,j})} \cdot h_g(T_{(\mathrm{i,j})}) + \sum_{k=1}^{C} \Delta H_{ads\ \mathrm{k}} \cdot \dot{n}_{\mathrm{k\ adsorbed(i,j)}} = \dot{S} \cdot Cp_s \ \cdot (T_{s(\mathrm{i,j})} - T_{s(\mathrm{i-1,j})}) \quad (3.49)$$

In the case of convective heat transfer, the resistance to heat transfer of Equation (3.35) and (3.36) can be expressed in form of Equation (3.50) and (3.51).

$$\dot{G}_{(\mathrm{i,j-1})} \cdot\ h_g(T_{(\mathrm{i,j-1})}) - \dot{G}_{(\mathrm{i,j})} \cdot h_g(T_{(\mathrm{i,j})}) + \sum_{k=1}^{C} \Delta H_{ads\ \mathrm{k}} \cdot \dot{n}_{\mathrm{k\ adsorbed(i,j)}} = h_{cv(i,j)} \frac{A_s}{\mathrm{N}_H \ \cdot\ \mathrm{N}\tau} \cdot \Delta T_{(i,j)} \quad (3.50)$$

$$\dot{S} \cdot Cp_s \ \cdot (T_{s\ (\mathrm{I,j})} - T_{s\ (\mathrm{i-1,j})}) = h_{cv(i,j)} \frac{A_s}{\mathrm{N}_H \cdot \mathrm{N}\tau} \cdot \Delta T_{(i,j)} \quad (3.51)$$

Boundary and Auxiliary conditions

In order to close the partial difference equations boundary conditions, inlet conditions and adsorption equilibrium correlations are necessary.

Thermal and mass transfer equilibrium conditions:

For a system without resistance to heat transfer Equation (3.52) is applied to each cell. Gas/air and adsorbent solid leave correspondent stage (i,j) at the same temperature. If the system shows a resistance to heat transfer Equation (3.53) needs to be applied instead.

Equation (3.54) is the adsorption equilibrium isotherm and correlates the partial pressure of the adsorbate (P_{k}^{*}), with the adsorbed amount of component k on the adsorbent (q_{k}^{*}).

$$T_{g\ (\mathrm{I,j})} = T_{s\ (\mathrm{I,j})} \tag{3.52}$$

$$\Delta T_{(i,j)} = T_{g(i,j)} - T_{s(i,j)} \tag{3.53}$$

$$q^{*}_{\mathrm{k(i,j)}} = f\left(P^{*}_{\mathrm{k\ (i,j)}} T_{g\ (\mathrm{i,j})}\right) \tag{3.54}$$

Inlet conditions:

Considering the counter-current flow arrangement of the inlet streams flue gas and air, the inlet mass flow rate, composition, temperature and pressure for the flue gas are defined at the top of the wheel ($j = N_H$) and for the air at the bottom of the wheel ($j = 0$), as shown in Equations, (3.55) - (3.57).

Gas (adsorption)	Air (desorption)	
$\dot{G}_{(\mathrm{i},N_L)} = \dot{G}_{\mathrm{IN}}/S$	$\dot{G}_{(\mathrm{i},0)} = \dot{A}_{\mathrm{IN}}/S$	(3.55)
$y_{\mathrm{k\ (i},N_L)} = y_{\mathrm{k\ flue\ gas,\ IN}}$	$y_{\mathrm{k\ (i},0)} = y_{\mathrm{k\ air,\ IN}}$	(3.56)
$T_{\mathrm{g,\ (i},N_L)} = T_{\mathrm{flue\ gas,\ IN}}$	$T_{\mathrm{g,\ (i},0)} = T_{\mathrm{air,\ IN}}$	(3.57)

Boundary conditions:

Due to the continuity of the closed cycle between adsorption and desorption, the adsorbed amount of CO2 and the solid temperature is given at the boundaries between those two processes, i.e. $\mathrm{i} = 0$ and $\mathrm{i} = N_\tau$, by Equations (3.58) - (3.61).

$$\left[q_{\mathrm{k}\,(0,\mathrm{j})}\right]_{\mathrm{Adsorption}} = \left[q_{\mathrm{k}\,(N_\tau,\ N_L-\mathrm{j})}\right]_{\mathrm{Desorption}} \tag{3.58}$$

$$\left[T_{S\,(0,\mathrm{j})}\right]_{\mathrm{Adsorption}} = \left[T_{S\,(N_\tau,\ N_L-\mathrm{j})}\right]_{\mathrm{Desorption}} \tag{3.59}$$

$$\left[q_{\mathrm{k}\,(0,\ N_L-\mathrm{j})}\right]_{\mathrm{Desorption}} = \left[q_{\mathrm{k}\,(N_\tau,\mathrm{j})}\right]_{\mathrm{Adsorption}} \tag{3.60}$$

$$\left[T_{S\,(0,\ N_L-\mathrm{j})}\right]_{\mathrm{Desorption}} = \left[T_{S\,(N_\tau,\mathrm{j})}\right]_{\mathrm{Adsorption}} \tag{3.61}$$

3.4.3 Design Consideration of the Rotary Wheel

Structural considerations

To determine the number of wheels (n_{wheel}), the exact distribution of the solid needs to be considered, once material properties are considered.

Two different structures need to be taken into account: The rotary wheel structure, including its internal supporting structure and the structure of the adsorbent in the wheel.

By knowing V_{wheel} , the volume available for the solid in the wheel, and V_{bed}, the volume taken up by the solid, the numbers of wheels can the calculated according to Equation (3.62).

$$n_{\mathrm{wheel}} = V_{\mathrm{bed}}/V_{\mathrm{wheel}} \tag{3.62}$$

The volume of the bed can be determined using the volume of the solid V_{s}, and the bulk void fraction $\varepsilon_{\mathrm{bulk}}$ of the structured adsorbent (Equation (3.63) - (3.65)), where

m_s is the mass of the solid adsorbent, ρ_s is the density of the solid, ε_p is the porosity of the particle and ρ_p is the density of particle. The bulk void fraction is a ration of the void volume V_{void}, which is the empty space in the rotor, and the total volume V_{total}, which equals in the case of the rotary adsorbent the volume available for the solid in the wheel.

$$V_{bed} = \frac{V_s}{(1-\varepsilon_{bulk})} \tag{3.63}$$

$$V_s = \frac{m_s}{\rho_s (1-\varepsilon_p)} = \frac{m_s}{\rho_p} \tag{3.64}$$

$$\varepsilon_{bulk} = \frac{V_{void}}{V_{total}} = \frac{V_{void}}{V_{wheel}} \tag{3.65}$$

The void volume is evaluated by taking the structure of the adsorbent into account. A honeycomb-monolithic structured adsorbent is proposed to reduce pressure drop (Fateme Rezaei and Webley 2009). It consists of a large number of parallel channels providing high contact efficiencies and is characterised by a high void fraction. Parameters defining the structure are the wall thickness d_{wall} and the pitch p, which is defined as the length from the centre of the honeycomb to the wall of the honeycomb including the wall thickness, as shown in the plan view of a honeycomb structure in Figure 3-18.

Honeycomb structures are used in Selective Catalytic Reduction (SCR) systems. In these systems nitrogen oxides present in atmospheric pressure combustion gases are removed. In such NOx reduction systems, the gases containing NOx are pushed through a monolithic structured catalyst to reduce NOx to N2 and H2O. The difference between monoliths for adsorption and catalytic reaction is based on the need for high adsorption capacity for adsorption technologies. Therefore, the monolithic structure for adsorption processes is mainly based on entirely adsorbent material, while monoliths for SCR processes normally consist of a coating of the active catalyst on a monolithic matrix. For both technologies the optimal value of wall thickness and pitch length are generally a trade-off between maximising surface area and minimising pressure drop and avoiding obstruction by particular matter

presented in the treated flue gas. For optimal mass transfer in monolithic adsorbents, the pitch and the wall thickness should be as small as possible. This leads to higher cell densities, higher surface areas and hence solid loading. However, small pitch and wall thickness have been reported to lead to higher manufacturing costs due to its complexity. (F. Rezaei and Webley 2010)

Typical values reported for wall thickness and pitch length in monolithic structures for SCR technologies are between 1-3 mm and 3-5 mm, respectively (United States Environmental Protection Agency 2002). Similar values are used in this thesis to evaluate the void volume of structured adsorbent in the rotary wheel.

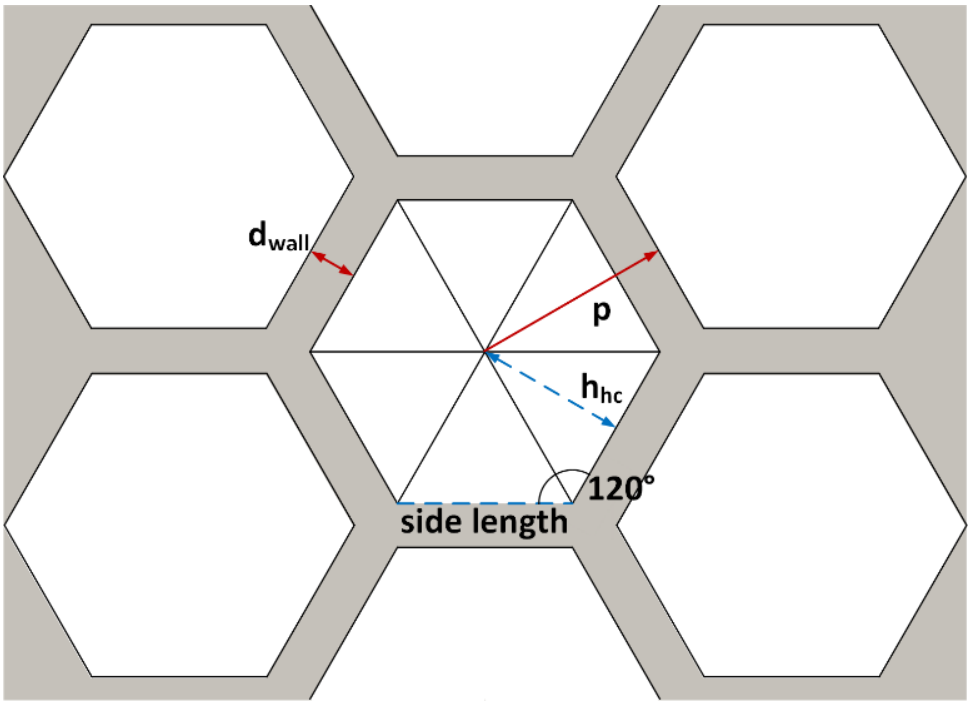

Figure 3-18: Plan view of a honeycomb structure

The void volume consists of the free space of the whole honeycomb structure and is therefore the volume of the empty space of one honeycomb V_{hc} multiplied by the amount of honeycombs n_{hc} that fit in the given rotor area (Equation (3.66) - (3.68)).

$$V_{\mathrm{void}} = V_{\mathrm{hc}} \cdot n_{\mathrm{hc}} \tag{3.66}$$

$$V_{\mathrm{hc}} = A_{\mathrm{hc}} \cdot H_{\mathrm{wheel}} \tag{3.67}$$

$$n_{hc} = A_{wheel} / A_{\mathrm{hc_{wall}}} \tag{3.68}$$

With H_{wheel} the height of the wheel, A_{hc} the cross section area of the empty space of one honeycomb, $A_{\mathrm{hc_{wall}}}$ the cross section area of one honeycomb including half of the surrounding wall and A_{wheel}, as given in Equation (3.72), the cross section area of the rotor. The surface of the empty space of one honeycomb can be calculated based on the geometry of the honeycomb structure, which consists of the surface of six equilateral triangles and leads to Equation (3.69).

$$A_{\mathrm{hc}} = 3 \cdot {}^{2}/_{\sqrt{3}} \cdot {h_{\mathrm{hc}}}^{2} \tag{3.69}$$

With the height of the equilateral triangle h_{hc} being the difference between pitch and wall thickness. $A_{\mathrm{hc_{wall}}}$ can be calculated accordingly (Equation (3.70)).

$$A_{\mathrm{hc_{wall}}} = 3 \cdot \frac{2}{\sqrt{3}} \cdot \left(h_{\mathrm{hc}} + \frac{d_{wall}}{2}\right)^{2} \tag{3.70}$$

The volume in the wheel available for the solid is defined by Equation (3.71), where D_{wheel} is the diameter of the rotor, H_{wheel} is the height of the rotor, and f_{Howden} is an effective cross section factor. A value of 0.89 is used, based on the available space for heat exchanger plates in Howden's commercially available large rotary gas/gas heat exchangers. (Hogg 2016)

$$V_{\mathrm{wheel}} = \frac{\pi}{4} \cdot {D_{\mathrm{wheel}}}^{2} \cdot H_{\mathrm{wheel}} \cdot f_{Howden} \tag{3.71}$$

$$A_{\mathrm{wheel}} = \frac{\pi}{4} \cdot {D_{\mathrm{wheel}}}^{2} \cdot f_{Howden} \tag{3.72}$$

The largest heater size within the standard range designed by Howden is 24 m diameter and about 2 m height, with a rotating weight of 1,360 tonnes.

Taking into account that the largest standard bearing can support around 2,000 tonnes rotating weight, and taking into account the lower density of CO2 adsorbent material (~1000-1200 kg/m3) compared to steel (~8000 kg/m3) typically used for

heat transfer applications, leaves potentially scope to supply larger heater diameters in the future. Limitation would be unlikely caused by the bearing, but would be given by balancing the gas mass flow and gas velocity against the pressure differentials through the rotor and the resulting pressure loss over the rotor. From a practical point of view, a rotor larger than 30 m diameter would not be reasonable. (Hogg 2018)

One important consideration in the manufacturing of the monolithic structured adsorbent is their structural integrity, and the practicality and feasibility to manufacture such monolithic structures.

Designing the monolithic adsorbent as one large unit is not practical or feasible. However, it would be possible to replicate the design of rotary gas/gas heat where series of baskets, with a maximum weight of approximately 1000 kg, containing the metal heating elements are used. These baskets would additionally provide protection to the adsorbent structure.

There are different ways to manufacture such monoliths. It is common practice to create a monolith consisting entirely of active adsorbent by extruding, which directly delivers the desired geometry. This is done for several carbon monoliths. (Lim et al. 2010; Moreno-Castilla and Pérez-Cadenas 2010; Betancur Arroyave et al. 2013; F. Rezaei and Webley 2010)

If a supporting structure is necessary, an active film can be grown onto a support structure or matrix by either dip-coating, wash-coating, or slip-coating it onto the support structure. (F. Rezaei and Webley 2010)

3D printing is a method to provide great flexibility to manufacture monoliths with exact and flexible geometric parameters. It has been recently demonstrated by Thakkar (Thakkar et al. 2016) for zeolites, that this technology can be used to create monolithic structures with a active adsorbent content of around 90wt% compared to the supporting material.

Yet, both the added cost of manufacturing high cell density monoliths, with large active adsorbent loading, and not yet available commercial quantities need to be accounted for. (F. Rezaei and Webley 2010)

Leakage considerations

The unwanted flow from one partition to another is called leakage. Since leakages lead to higher fan power consumption, they needs to be accounted for in the proposed rotational regenerative CO2 transfer systems.

Two types of leakages are typically encountered in gas/gas heaters: Direct leakage and entrained leakage. (Kitto and Stultz 2005)

- Direct or gap leakages occur between stationary and rotating unit, from higher pressure side to the lower pressure side through gaps between the seal and the solid surface. For the rotary regenerative wheel those gap leakages can be subdivided in radial, axial and circumferential leakages between the rotating and stationary parts as shown in Figure 3-19. They depend on pressure difference, air density, rotor size and geometry and perimeter of sealing and gaps. (Kitto and Stultz 2005)

  In practice, they can be minimised by operating both gas streams the smallest pressure difference practically achievable.

- Entrained or carryover leakages occur due to the gas trapped in the rotor sectors being carried through from the adsorption side to the desorption side, and vice versa, during operational rotation. It is directly proportional to the void volume of the monolithic adsorbent/rotor and the rotational speed. (Kitto and Stultz 2005)

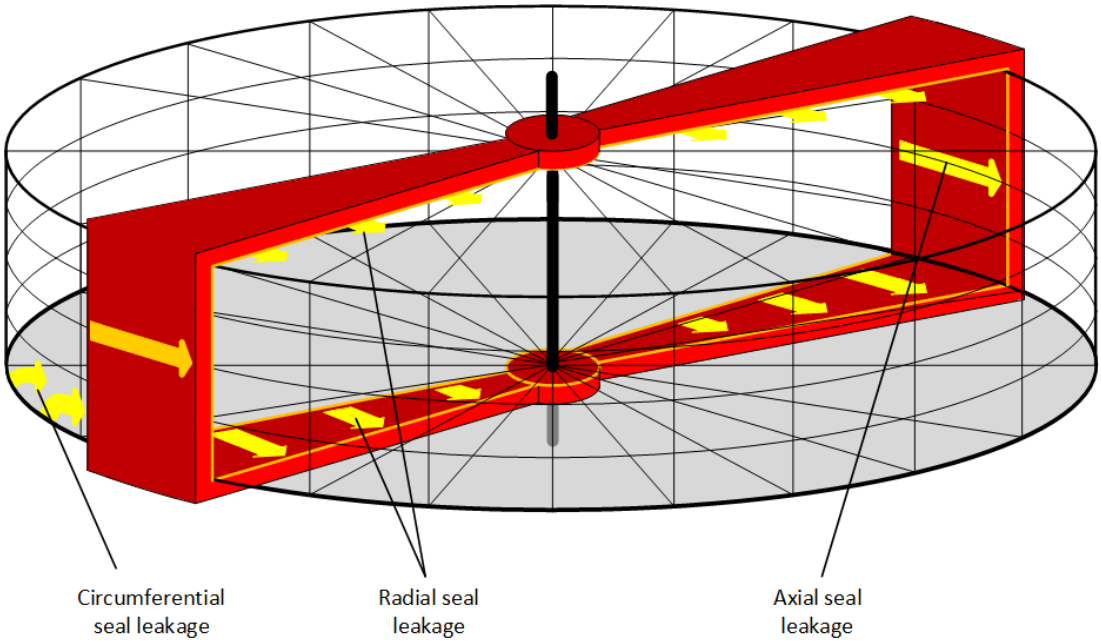

Figure 3-19: Schematic of direct leakages in the wheel design

During operation, the rotary wheel faces a temperature difference between the desorption and adsorption side, due to a fraction of the heat of adsorption being released to the flue gas, and a fraction of the heart of desorption being taken from ambient air. This leads to a certain expansion and distortion of the rotor, which in turn leads to opening gaps between the rotor and stationary parts and therefore to increased direct leakage. Automatic sealing system adapting to such changes can nearly eliminate leakage rises, by monitoring and adjusting rotating and stationary seals during operation as shown exemplary in the cross section view through an air heater rotor in Figure 3-20. (Kitto and Stultz 2005)

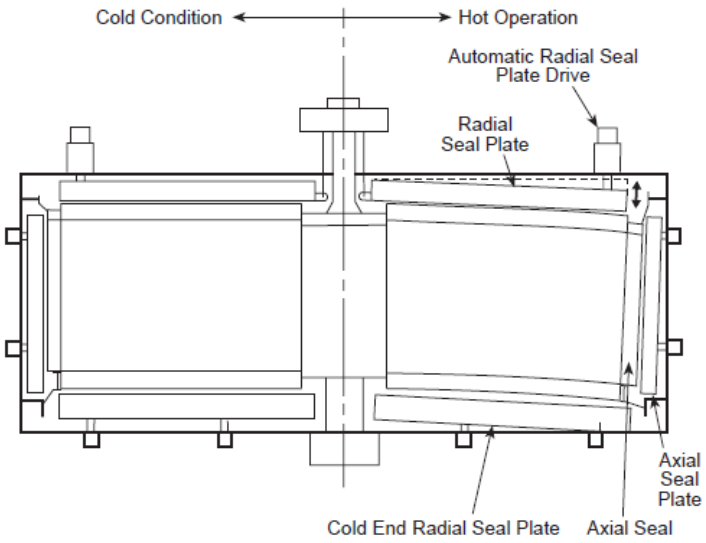

Figure 3-20: Cross section through air heater rotor and seal plates. (Kitto and Stultz 2005)

To reduce entrained leakages a purge gas can be used to push and trap off the in the sectors remaining trapped gas, similar to the concept shown by Cooper (Cooper 1991) in Figure 3-21.

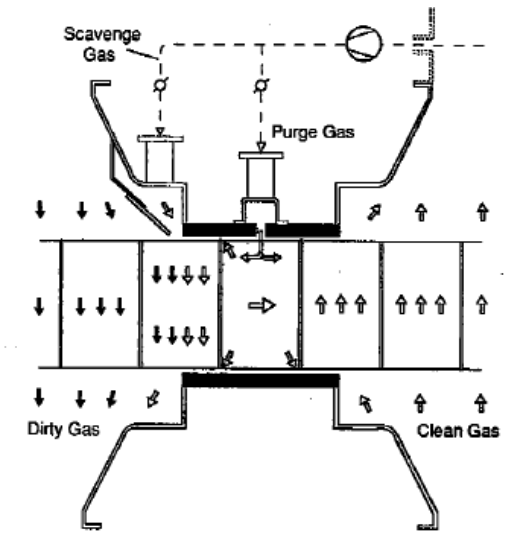

Figure 3-21: Leakage reduction by using purge and scavenge gas (Cooper 1991)

Due to seal wear and tear, leakage level will increase over time and should be therefore monitored. This can be either done by measuring the inlet and outlet flows based on velocity measurements, which is challenging for large duct cross sections,

or by calculating oxygen gas weights based on gas analysis of the inlet and outlet flows of the flue gas section. (Kitto and Stultz 2005)

For rotary regenerative CO2 transfer wheels, multiple sealing (double up to sextuple) axial and radial on the fixed sector plates/ baskets and cold end sensor controlled sealing could be implemented to minimise leakage. For rotating air heaters these combinations have demonstrated leakage levels lower than 1%. (Cooper 2013)
Further advanced concepts like the extension of Howden's purge and scavenge principles are under development and are promising applications for carbon capture, where even low leakage levels can lead to lower CO2 purity downstream. The benefits of the different concepts can be used additively and make a Near-Zero Leakage Concept feasible, and can be directly transferred from rotary heaters to regenerative rotary CO2 transfer wheels as leakage prevention. (Cooper 2013)

As it is unlikely that all leakages between the flow streams can be eliminated, an important aspect to be considered is the preferential direction of leakage. To reduce leakage levels, the pressure differential between the flue gas and the air streams should be as low as possible. However, to direct the leakage a slight pressure difference between the two sides is favourable, to generate a flow from the higher pressure to the lower pressure side.
On the on hand, leaks from the flue gas to the air stream lead to a slightly higher air flow rate and might lower the oxygen level in the combustor, since the remaining flue gas mixture has a lower oxygen concentration than ambient air. The oxygen level needs to be high enough to ensure ignition, flame stability and complete combustion. Therefore, oxygen levels in the combustor below acceptable minimum limits of 16 vol%, reported in literature for combustion tests performed on a bench-scale lean pre-mixed burner used in Dry Low-NOx combustor systems, employed in General Electric F-class gas turbine technology (ElKady et al. 2009a; Evulet et al. 2009), need to be avoided.

Leaks from the air stream to the CO2-depleted flue gas stream going to the stack on the other hand are acceptable.

Chapter 4 Results and Discussion of the Wheel Design

In this chapter an activated carbon material, with suitable equilibrium properties, is experimentally assessed on its adsorption behaviour under flue gas conditions, expected in CCGT with SEGR application. The so generated kinetic data are used to validate the kinetic model of a regenerative rotary CO2 transfer wheel and provide experimental data for further scale up of this kind of technology. This is then followed by a sensitivity analysis of kinetic adsorbent properties and operating conditions, to identify optimal ranges. Finally, the preferred direction for leakages is assessed and recommendation for the location of booster fans are provided.

4.1 Experimental Results of a Promising Material

The results of breakthrough adsorption measurements of the activated carbon introduced in Section 3.4.1 are presented in this section.

First the adsorption behaviour of different gases on the activated carbon will be assessed in Section 4.1.1, followed by the assessment of desorbing the activated carbon with air at ambient conditions in Section 4.1.2. The results of these experiments will be discussed in Section 4.1.3.

4.1.1 Adsorption of CO2 from Different Gas Compositions

In this section the adsorption behaviour of different feed gas compositions will be evaluated.

There is a discrepancy between the aimed CO2 concentrations specified in the experimental methodology (see Table 3-7) and the achieved CO2 concentration in the experiments results, as reported in Table 4-1 to Table 4-3. This difference is due

to uncertainty associated with the experimental apparatus, most probably the uncertainty of the MFCs, which ranges in the magnitude of 2% Table 4-2.

Adsorption of the gas components starts at the inlet to the adsorbent bed. After the material at the inlet is saturated, the mass-transfer zone moves through the bed steadily and leaves behind fully saturated adsorbent material. With increasing time the CO2 concentration in the outlet increases gradually until it reaches the inlet concentration. At the point where the ratio of the outlet CO2 concentration to the inlet concentration C_{out}/C_{in} is equal to one, the whole bed is saturated and no more adsorption can take place.

Figure 4-1 shows the effect of different gas compositions on the breakthrough curve and breakthrough time t_b at 30◦ for the KOH activated carbon presented in Chapter 3. The different gas compositions are chosen according to the flue gas composition for the SEGR configuration in parallel (97/96), adding for each breakthrough curve measurement another gas component, substituting N2.

For the investigated conditions, the breakthrough curves coincide. Adding O2 and H2O does not seem to affect the breakthrough curve shape or the breakthrough time greatly. The breakthrough time for CO2/N2 is 10 min and 28 sec, for CO2/O2/N2 10 min and 31 sec and for CO2/O2/H20/N2 10 min and 30 sec. Saturation is reached at 37 min and 42 sec for the CO2/N2 composition, at 37 min and 36 sec for the CO2/O2/N2 composition and at 37 min and 36 sec for the CO2/O2/H2O/N2 composition. That leads to a time difference for the breakthrough time of 0.3% and for the saturation for 0.2%. Corresponding calculated adsorption capacities, using the methodology detailed in Section 3.1.4, are presented in Table 4-1.

Although, it seems reasonable to assume the difference in CO2 adsorption capacity is caused by the varying CO2 inlet concentration, rather than the influence of the other gas components, it cannot be coherently concluded that O2 and H2O have no influence on the adsorption of CO2 onto the KOH activated carbon, since the CO2 inlet concentration was not constant over the set of measurements.

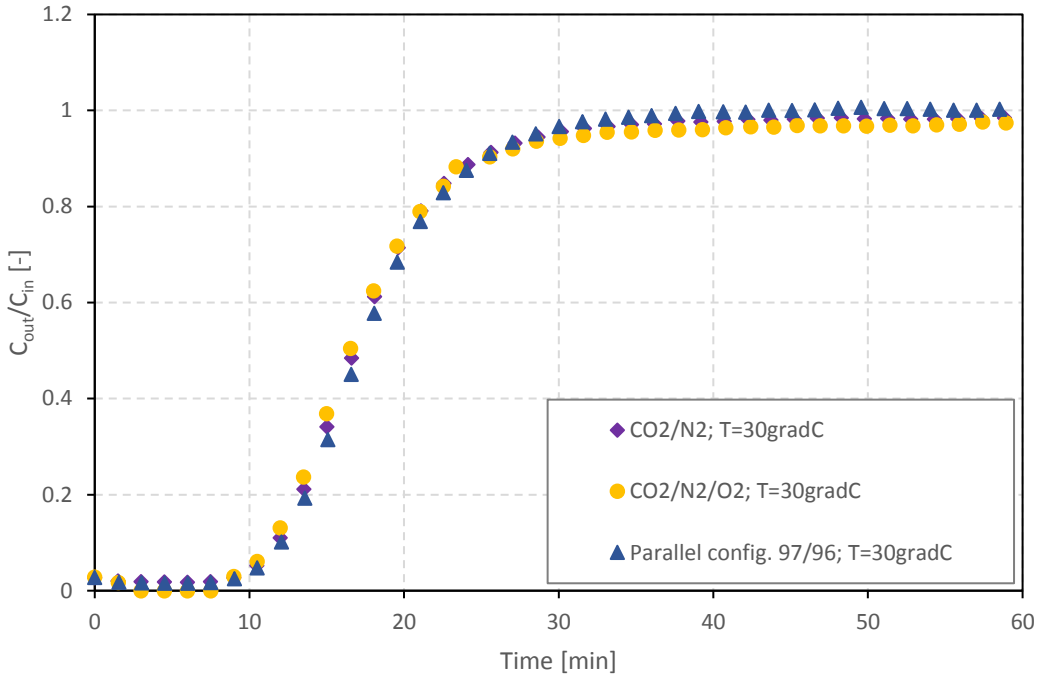

Figure 4-1: **Breakthrough curves of the KOH activated carbon performed at 30◦C in 14.12%mol CO2 in N2, at 30◦C in 14.12 %mol CO2 and 9.01%mol O2 in N2 and, as parallel SEGR configuration (97/96) case, at 30◦C in 14.12%mol CO2, 9.01%mol O2 and 9.51%mol H20 in N2**

Table 4-1: Calculated adsorption capacity based on the breakthrough curve measurements

Configuration	T [°C]	CO2 in the feed gas [%mol]	Adsorption capacity [$mg_{CO2}/g_{adsorbent}$]
S-EGR Parallel (97/96)	30	14.14	42.67 ± 2.41
CO2/O2/N2	30	13.8	42.21 ± 2.40
CO2/N2	30	13.1	38.42 ± 2.41

Figure 4-2 shows the effect of different gas temperatures on the breakthrough curve and breakthrough time t_b for the KOH activated carbon under SEGR parallel configuration (97/96) flue gas compositions at 30◦C, 40◦C and 50◦C. The temperature affects the shape and breakthrough time of the adsorbent. Keeping the concentration of the gas components constant (within the experimental uncertainty), shows that the higher the temperature, the shorter breakthrough time and the narrower the mass transfer zone, by increasing the slope of the breakthrough curve. The effect on the slope of the breakthrough curve is marginal in the studied temperature range.

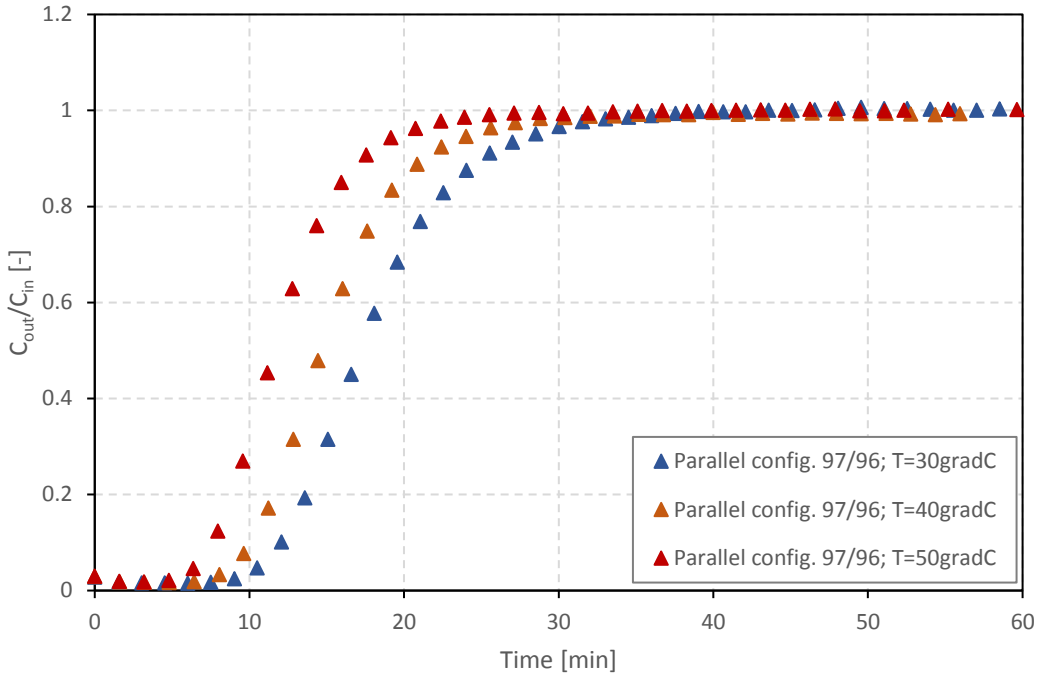

Figure 4-2: Breakthrough curves of the KOH activated carbon performed for the SEGR parallel configuration (97/96) in 14.12%mol CO2, 9.01%mol O2 and 9.51%mol H20 in N2 at 30◦C, 40◦C and 50◦C

The breakthrough behaviour of the KOH activated carbon for a gas compositions of the SEGR parallel configuration (97/96) at 30◦C and 50◦C, for a gas compositions of the SEGR series configuration (95/31) at 30◦C and 50◦C, and for a gas composition of CO2/O2/N2 (14.12 %mol CO2 and 9.01%mol O2 in N2) at 30◦C and 50◦C, are presented in Figure 4-3. Temperature and CO2 concentration affect the shape and breakthrough time of the adsorbent. Yet, the CO2 concentration difference between the two SEGR configurations is only 1.3 %mol.

As previous shown in Figure 4-2, the higher the temperature, the shorter the breakthrough time and the higher the slope of the breakthrough curve. A higher CO2 concentration does not affect the breakthrough time, but it increases the slope of the breakthrough curve. However, this is less significant as the effect of the temperature on the slope.

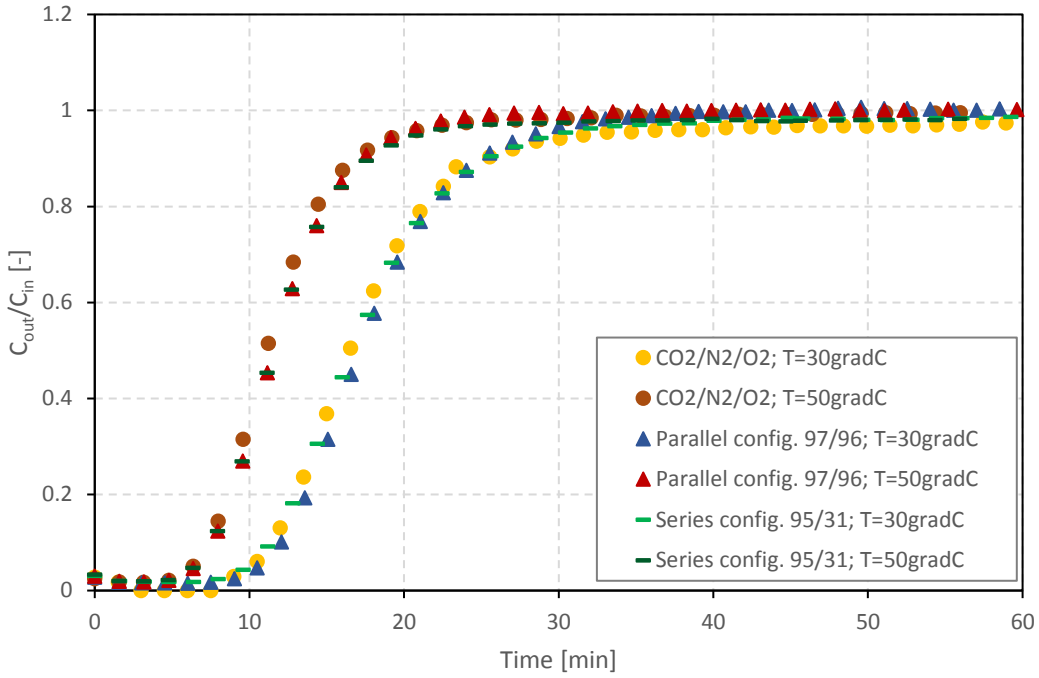

Figure 4-3: Breakthrough curves of the KOH activated carbon performed for the CO2/N2/O2 case in 14.12 %mol CO2 and 9.01%mol O2 in N2 and performed for the SEGR parallel configuration (97/96) in 14.12%mol CO2, 9.01%mol O2 and 9.51%mol H20 in N2 and for the SEGR series configuration (95/31) in 12.83%mol CO2, 9.64%mol O2 and 9.17%mol H20 in N2, at 30◦C and 50◦C

Following the methodology detailed in Section 3.1.4., the calculated adsorption capacity of the breakthrough curve experiments for both SEGR configurations at different temperatures are presented in Table 4-2. As expected, the capacity of the KOH activated carbon decreases with increasing temperature. This is due to the adsorption process being exothermic and having lower adsorption capacities at higher temperatures. An increase in CO2 concentration increases the CO2 adsorption capacity. The highest adsorption capacity is achieved at 30◦C for the SEGR configuration in parallel (97/96) where the CO2 concentration is 14.25 %mol, the lowest adsorption capacities is achieved at 50◦C for the SEGR configuration in series (95/31) where the CO2 concentration is 12.84 %mol, respectively.

Table 4-2: Calculated adsorption capacity based on the breakthrough curve measurements for the SEGR configurations parallel (97/96) and series (95/31)

Configuration	Temperature [°C]	CO2 in the feed gas [%mol]	Adsorption capacity [$mg_{CO2}/g_{adsorbent}$]
S-EGR Parallel (97/96)	30	14.14	42.67 ± 2.41
	30	14.25	45.49 ± 2.74
	40	14.21	32.97 ± 2.35
	40	14.19	32.77 ± 2.31
	50	14.33	28.99 ± 2.71
	50	14.12	27.98 ± 1.58
S-EGR Series (95/31)	30	12.81	37.85 ± 2.26
	30	12.82	37.10 ± 2.10
	50	12.84	24.89 ± 1.69
	50	12.96	26.14 ± 1.98

4.1.2 CO2 Desorption with Air

In this section, the feasibility of regenerating the adsorbent with air at ambient conditions is assessed. The aim is to proof the concept that to a certain degree regeneration is possible. It is not scope of this thesis to provide data for the simulation of desorption with air.

The KOH activated carbon is cycled multiple times to examine the adsorption behaviour after desorption with air. The adsorbent is saturated under SEGR in parallel (97/96) feed flow composition conditions before the gas flow is switched from feed gas to air flow desorption gas. The ratio of desorption air to flue gas mass flow is 1.12, according to the values reported by Herraiz (Herraiz 2016) for SEGR (97/96). The time for desorption was chosen to be 1 h based on the run time for adsorption.

Figure 4-4 shows the effect of a desorption with air, at 18◦C for 1 h with a corresponding air volumetric flow rate of 43.29 mL/min, on the breakthrough curve and breakthrough time t_b for the KOH activated carbon. The breakthrough curves generated are compared to the breakthrough curve of the KOH activated carbon after regeneration with N2 at 160◦C for 2 h, which corresponds to a fully regenerated adsorbent.

The breakthrough curve measured after desorption with N2 reaches the breakthrough time at 10 min and 25 sec and saturation at 35 min and 54 sec. The breakthrough curve measured after the first desorption run with air reaches breakthrough time at 9 min and 6 seconds and saturation at 31 min and 54 sec. The breakthrough curve measured after the third desorption run with air reaches breakthrough time at 7 min and 40 sec and saturation at 27 min and 18 sec.

The shape and slope of the breakthrough curves are only marginal affected by desorption with air for 1 h. However, the breakthrough time is shortened and saturation of the KOH activated carbon is reached earlier. Furthermore, the breakthrough curve after regeneration with air is moving progressively up, indicating a non-complete regeneration. It could mean that the cyclic steady state for a regeneration with air is not yet reached. However, the breakthrough curve of the 2nd and the 3rd cycle are starting to coincide and might therefore indicate that steady state is approaching.

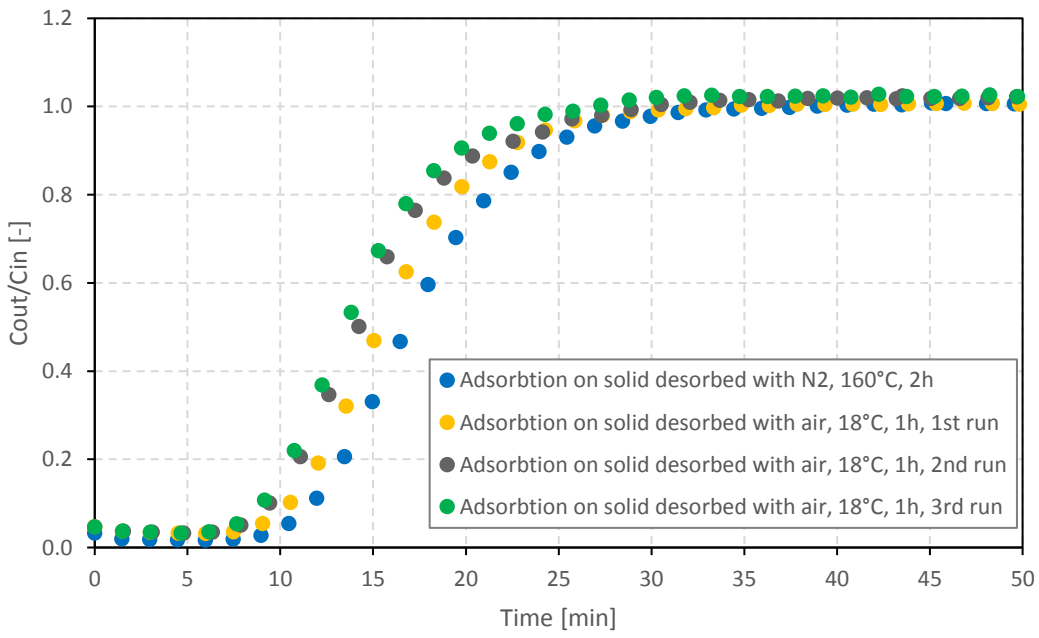

Figure 4-4: Breakthrough curves of the KOH activated carbon performed for the SEGR parallel configuration (97/96) in 14.12%mol CO2, 9.01%mol O2 and 9.51%mol H20 in N2 at 30◦C; desorption condition N2/160 ◦C/2h in blue, and air/18◦C/1h in yellow (1st run), brown (2nd run) and green (3rd run)

Table 4-3: Calculated adsorption capacity based on the breakthrough curve measurements for the adsorbent regenerated with air

Configuration	T [°C]	CO2 in the feed gas [%mol]	Adsorption capacity [$mg_{CO2}/g_{adsorbent}$]
S-EGR Parallel (97/96) conventional regenerated	30	14.10	41.31 ± 2.47
S-EGR Parallel (97/96) air 1st run	30	13.92	35.72 ± 2.12
S-EGR Parallel (97/96) air 2nd run	30	13.80	31.86 ± 1.96
S-EGR Parallel (97/96) air 3rd run	30	13.78	31.51 ± 1.92

4.1.3 Discussion

The CO2 adsorption performances of KOH activated carbon is tested under different temperatures and gas composition. Both, H2O and O2 are important in the context of SEGR application. Flue gas enters the transfer device for SEGR application with a water content at saturation at 30◦C. Consequently, a sensitive to water would negatively impact the performance of the adsorbent. Many adsorbent materials like Zeolites and MOFs are very sensitive. Therefore, the use of an activated carbon is proposed. Furthermore, a transfer of O2 from the air stream, used for desorption, needs to be avoided in the context of SEGR, since this would reduce the amount of O2 available in the comburent for combustion downstream of the SEGR device. The KOH activated carbon presents, in the range of tested parameters, the same adsorption behaviour for a constant CO2 concentration seemingly independent of the other gas components. The highest adsorption capacity is achieved at 30◦C for the SEGR configuration in parallel (97/96). The presence of O2 and H2O seem not to change the CO2 adsorption behaviour significantly. For the measured flue gas, this might indicate that the presence of O2 and H2O are not significant factors on the performance of the KOH activated carbon under selective CO2 transfer conditions. However, it cannot be coherently concluded that O2 and H2O have no influence on the adsorption of CO2 onto the KOH activated carbon, since the CO2 inlet concentration was not constant over the set of measurements. The measured CO2

concentration variation lie in the boundaries of the uncertainty of the MFCs. Even if H2O did not interfere with the adsorption of CO2, there is still the possibility that it accumulates and interferes with the performance of the adsorbent, especially for a continuous process.

For a desorption with air, 18°C for 1 h with a corresponding air mass flow of 43.29 mL/min, the shape and slope of the adsorption breakthrough curves measured afterwards are not significantly affected, in contrast to the breakthrough time. The breakthrough time in the 3rd cycle with air is reduced by 26% in comparison with the breakthrough time of the adsorbent regenerated with heat. In addition, the breakthrough curve is moving progressively upwards, indicating a non-complete regeneration. The adsorption capacity reduces by 24%. This indicates further, that some CO2 is remaining on the activated carbon, so a full regeneration is not achieved. However, due to a starting overlap of the breakthrough curves of the 2nd and the 3rd cycle it seems that the cycle is reaching a steady state for a regeneration with air
It can therefore be concluded that a full regeneration of the KOH activated carbon is not achieved with the limitation of a ratio of desorption air to flue gas mass flow of 1.12. However, a full regeneration of the adsorbent is not necessary for the regenerative rotary CO2 transfer wheel. The case study with air for desorption, at 18°C for 1 h shows in general, that a regeneration with air for SEGR might be possible, but the capacity will be lower. This is acceptable for the regenerative rotary CO2 transfer wheel as the reduced adsorption capacity can be overcome with a higher mass of solid adsorbent.

4.2 Modelling Results

In this section the kinetic model of the regenerative rotary CO2 transfer wheel is validated (Section 4.2.2) and a comparison with the equilibrium model prediction is performed (Section 4.2.3). Performance and operating profiles for a chosen solid adsorbent are generated to understand the processes in the wheel better (Section

4.2.4). This is followed by a sensitivity analysis of kinetic adsorbent properties (Section 4.2.5) and operating conditions (Section 4.2.6), to identify optimal ranges.

4.2.1 System Boundaries

Based on the results of the leakage considerations (Section 4.3) the following boundaries are given:

- Air: The regenerative air, used downstream in the gas turbine as combustion air, is supplied to the regenerative rotary CO2 transfer wheel by a fan located upstream the desorption part of the rotary wheel. The maximum amount of air mass flow is given by the fixed geometry of the compressor. A fan is used to overcome the pressure drop caused by the wheel and the ducts towards the gas turbine compressor. The temperature of the air will therefore rise above ISO conditions (15◦C).
- Flue gas: Flue gas temperature and vapour content are depending on the operation of the direct contact cooler upstream of the regenerative rotary wheel device. Low flue gas temperature favours the adsorption process thermodynamically. This will also limit a possible transfer of sensible heat from the adsorbent baskets into the CO2-enriched air stream. The temperature of the flue gas going into the regenerative CO2 transfer wheel is therefore set at 30◦C.

4.2.2 Validation

In this section the breakthrough curves of the KOH activated carbon obtained for a feed gas composition similar to the flue gas composition of SEGR in parallel (97/96) at 30◦C, are used to validate the kinetic model of a regenerative rotary CO2 transfer wheel.

To allow the results obtained by breakthrough measurements of an adsorbent in an isothermal fixed bed tubular reactor to be used to validate and verify the mass

transfer model of the rotary regenerative CO2 transfer wheel, the time dimensions of the two systems need to be aligned. Since the wheel, as a rotating system, has two dimension connected to time - one is connected to the rotation of the wheel and the other to the adsorption kinetics - the rotary wheel needs to be forced to behave like a fixed bed adsorber by slowing the rotation of the wheel down. When this happens, the simulated outlet concentration divided by the inlet concentration C_{out}/c_{in} for the cells on the top of the rotary wheel will replicate a full breakthrough curve. This is shown in Figure 4-5. Each top cell of the wheel represents hereby a time step of the fixed bed adsorber outlet for a suitably chosen rotational speed of the wheel. Connecting those data points will replicate the kinetic behaviour of the adsorbent tested in the fixed bed adsorber. To translate the rotational time of the rotary wheel for each cell Equation (4.1) can be used.

$$time = {}^{60}/_{\omega} \cdot f_{Area} \cdot \frac{i}{N_\tau} \tag{4.1}$$

With N_τ being the maximum cells in rotational direction and i the cell count of the cells in rotational direction.

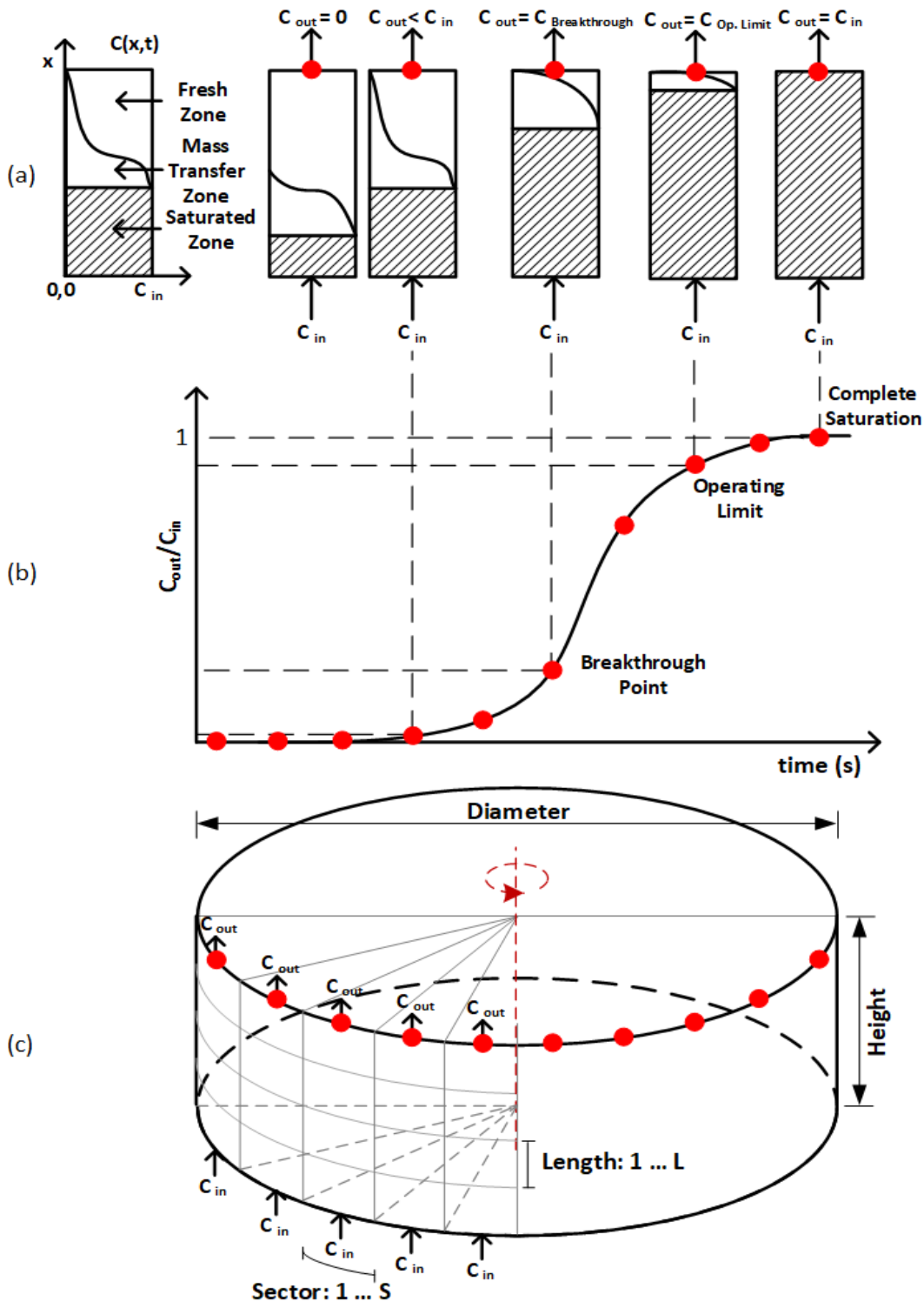

Figure 4-5: **Illustration of the correlation of fixed bed adsorption (a), breakthrough curve measurements (b) and the simulations data of the regenerative rotary CO2 transfer wheel (c)**

For validation of the model, simulation results, corresponding to a flue gas composition of SEGR in parallel configuration (97/96), are compared with breakthrough CO2 adsorption experiments on KOH activated carbon with a feed composition of 14.12%mol CO2, 9.01%mol O2 and 9.51%mol H20 in N2 at 30°C and at 40◦C. The ratio of the adsorbent mass to feed flow is kept in both cases.

Since the wheel model consists of the combination of the adsorption part and the desorption part of the wheel, the cyclic simulation results are not a representation of an isothermal process. The resulting temperature in the wheel will be a steady state temperature distribution between the exothermic adsorption and the endothermic desorption part of the rotary wheel, ranging from 30°C to 40◦C. Furthermore, based on the simulation results being at a steady state between adsorption and desorption process, the adsorbent entering the adsorption section of the wheel will have an initial loading, since it is not fully regenerated in the desorption part of the wheel.
Hence, to test for reproducibility of the experimental results, the desorption and adsorption sides in the model need to be disconnected. The resulting breakthrough CO2 adsorption curves of the disconnected simulations for a rotational speed of 0.01 rpm (solid dotted line) at 30°C and at 40◦C are compared to the CO2 breakthrough adsorption measurement for a feed composition corresponding to SEGR in parallel (97/96) at 30°C and at 40◦C in Figure 4-6. The results show a reproducibility of the experimental results with the simulation results for a rotational speed of 0.01 rpm and therefore confirming the assumptions in this model under the operational conditions.

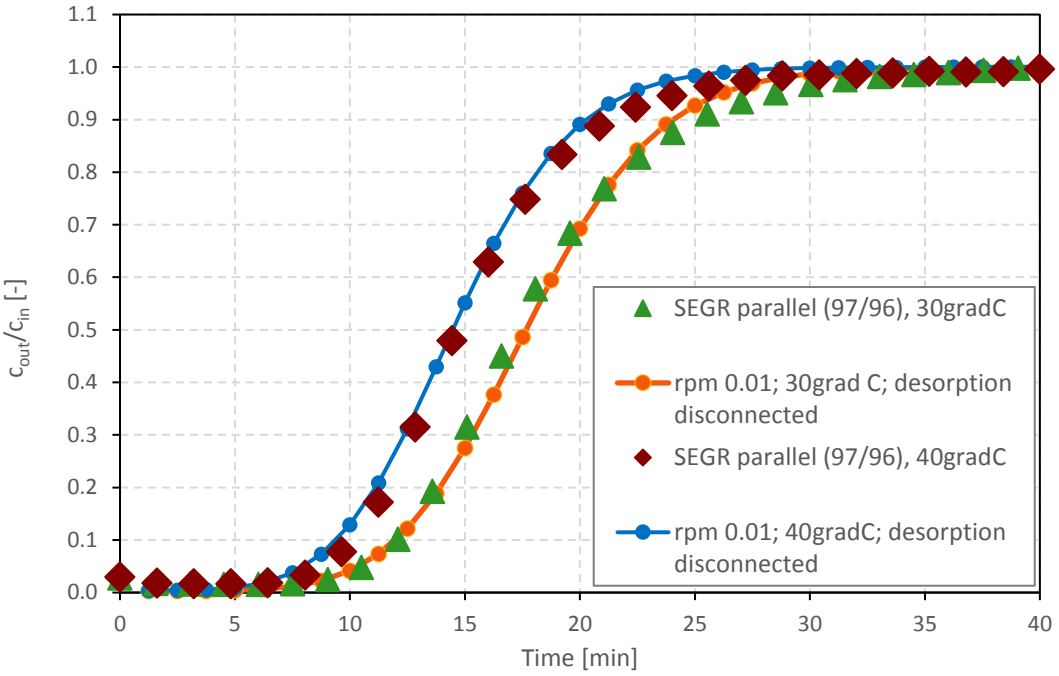

Figure 4-6: **Comparison of model predictions with disconnected desorption (solid dotted line) with experimentally measured breakthrough curves of CO2 adsorption on KOH activated carbon performed for the SEGR parallel configuration (97/96) in 14.12%mol CO2, 9.01%mol O2 and 9.51%mol H20 in N2**

4.2.3 Comparison of the Prediction of the Kinetic Model to the Equilibrium Model

The equilibrium model and the kinetic model are compared to understand the impact kinetics have on the adsorbent mass requirement on the basis of an SEGR configuration in parallel (97/96), using the adsorption equilibrium and kinetic parameters of the KOH activated carbon (Table 3-6). The results are presented in Table 4-2.

For a recovery ratio of 97% the prediction of adsorbent mass requirement of the kinetic model is higher by the factor 3.7 than the predicted adsorbent mass requirement of the equilibrium model. An explanation for this significant increase can be seen in Figure 4-7.

The kinetic model predicts already for a recovery ratio of 80% an adsorbent mass requirement double as high than the equilibrium model. That is due to the higher initial CO2 loading of the adsorbent entering the adsorption section of the wheel after

regeneration. In general the desorption predicted in the kinetic model seems to regenerate the adsorbent less than predicted by the equilibrium model. That could be due to the distribution of the heat of adsorption and on a larger mass of adsorbent, leading to a cooler adsorbent in the kinetic model. The cooler adsorbent will consequently be less regenerated.

Starting from a recovery ratio of 80%, the equilibrium model predicts a steady increase in adsorbent requirement up to a recovery ratio of 99.6 % and then transitions into a sudden exponential increase in adsorbent requirement. The kinetic model on the other hand predicts a steady increase up to 95 % of recovery ratio and transitions then slowly into an exponential increase of adsorbent mass requirement. That explains the large difference in adsorbent requirement predicted by the kinetic model for a 97% recovery rate, which is already in the transition area to the exponential adsorbent requirement prediction. This effect could be explained again by the difference in solid temperature affecting the loading of the adsorbent. In some of the cells the difference in solid temperature between the kinetic model and equilibrium model is as high as 14◦C, with the equilibrium model being warmer. Furthermore, this also affects the flue gas temperature in the rotary wheel, and the flue gas temperature has an effect on the diffusion coefficient in the kinetics, as shown in Equation (3.28) to (3.30). The lower the gas temperature the lower the diffusion coefficient and subsequently the higher the resistance to mass transfer. Consequently, increasing the required amount of adsorbent further. The effect of the diffusion coefficient on the solid mass requirement is later in the thesis assessed in form of a sensitivity analysis (see Figure 4-14).

Therefore, it might seem intuitively to avoid such high recovery ratios as 97% for the SEGR device, however, these high recovery ratio need to be achieved to achieve an overall capture rate of 90%, as defined by Equation (2.5) in Section 2.3.4., since flue gas, and therefore CO2 emissions, can leave the power plant boundaries through two streams under SEGR application.

The number of needed wheel devices are calculated based on a honeycomb wall thickness of 1 mm and a pitch of 4.5 mm, leading to a bulk void fraction of 0.77 for both models. Two different approaches are used to predict the number of wheel devices needed. The classic approach uses the standard maximum diameter (24m) of rotary heat exchangers supplied by Howden and adapts the height of the rotor to fit in the bulk volume. That leads for the adsorbent mass predicted by the equilibrium model to one wheel device of 24 m in diameter and 1.85 m in height. For the predicted adsorbent mass of the kinetic model the same approach leads to three wheel devices of 24m in diameter and 2.26 m in height needed. Since a height increase comes with an energy penalty for a higher pressure drop, a second approach is used adapting the diameter of the wheel to the maximum diameter from a practical point of view, as discussed in Section 3.4.3. That leads for the predicted mass of adsorbent of the kinetic model to two wheel devices of 30m in diameter and 2.17 m in height.

Table 4-4: Adsorbent requirement for SEGR configuration in parallel (97/96) based on different models applied

Configuration		**S-EGR Parallel 97/96**			
Recirculation ratio	%	70			
Recovery rate	%	97			
PCC efficiency	%	96			
Prediction method		**Equilibrium model**		**Kinetic model**	
Mass x 1000	kg	161		598	
Mean loading at the adsorption inlet	mol CO2/kg solid	0.096		0.315	
Mean loading at the adsorption outlet	mol CO2/kg solid	1.026		0.525	
Particle and Bulk					
Particle density	kg / m^3	952		952	
Particle Volume	m^3	170		628	
Bulk void fraction	-	0.77		0.77	
Bulk volume	m^3	737		2727	
Rotary wheel		**classic**	**adapted diameter**	**classic**	**adapted diameter**
External diameter	m	24	-	24	30
Height	m	1.85	-	2.26	2.17
Basket Factor (Hogg 2016)	-	0.89	-	0.89	0.89
Rotor volume	m^3	746	-	911	1367
No. of devices		1	-	3	2

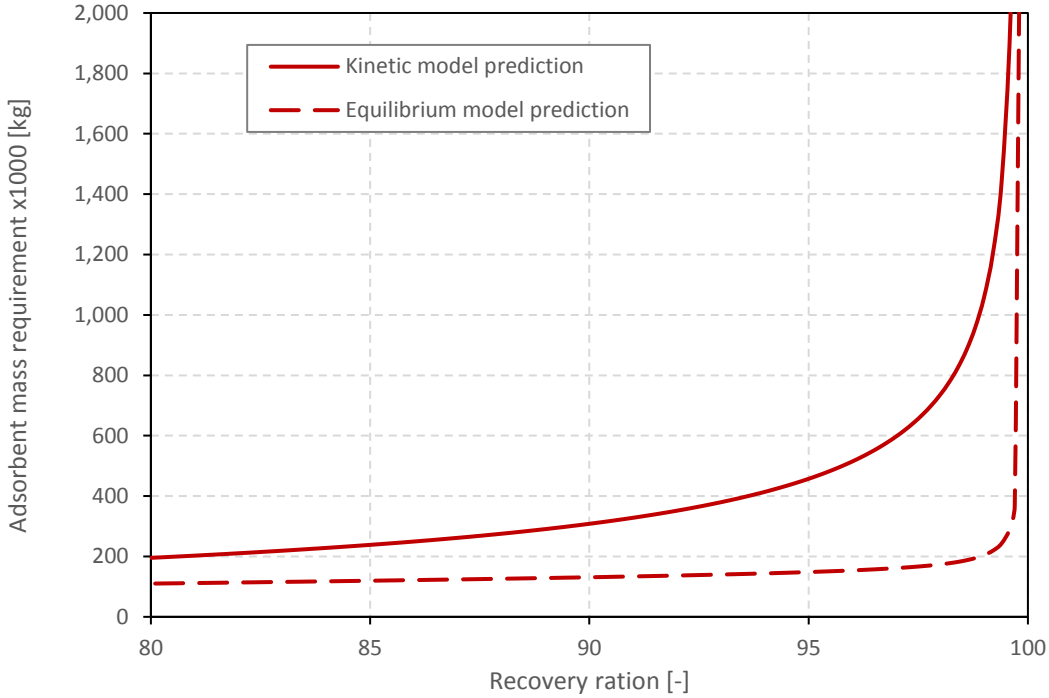

Figure 4-7: Comparison of the predicted adsorbent mass requirement of the different models used depending on the recovery rate

4.2.4 Performance and Operating Profiles

To get a better understanding of the adsorption and desorption processes in the regenerative rotary CO2 transfer wheel, performance and operating profiles are plotted for adsorption on the KOH activated carbon, for a SEGR configuration in parallel (97/96) with a rotational speed of 1 rpm.

The profile lines represent the vertical and horizontal sections of the wheel model as illustrated in Figure 4-8. The vertical sections represent the flue gas and air properties, the horizontal sections the solid adsorbent properties.

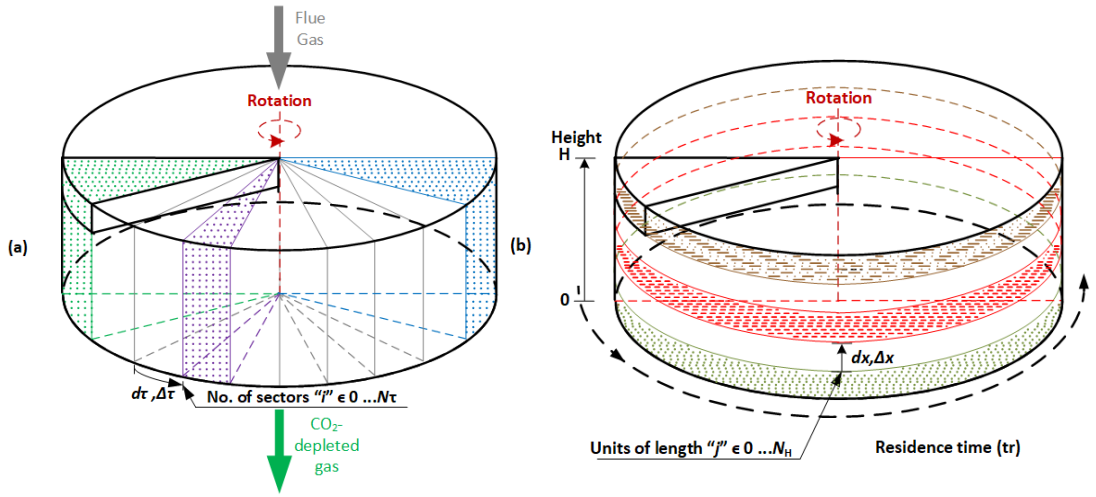

Figure 4-8: **Vertical slices represent flue gas and air profiles and horizontal slices represent the profile of the solid in the wheel (adapted from** (Herraiz et al. 2019)**)**

Profiles of gas streams

The adsorption rate is a function of the difference in partial pressure of CO2 in the gas phase and of CO2 adsorbed onto the adsorbent. High adsorption rates are correlated to high differences.

The partial pressure gradient is a function of the change in partial pressure of the gas phase over the adsorbent height increment Δx as given by Equation (4.2). High gradients are represented by horizontal lines in the vertical profiles.

$$-\frac{\partial P_{CO2}}{\partial x} = \frac{P_{CO2\,i,j=+1} - P_{CO2\,i,j}}{\Delta x} \qquad j = 0 \ldots N_H \tag{4.2}$$

Figure 4-9 shows the vertical CO2 partial pressure profiles of the flue gas in the adsorption section of the wheel (Figure 4-9 (a)) and of the air stream in the desorption section of the wheel (Figure 4-9 (b)). The highest CO2 adsorption rate correspond to the largest CO2 partial pressure gradient in the profiles. Since, the ratio of marginal change of partial pressure of CO2 for a given change of adsorbent height (Δx) corresponds to the partial pressure gradient, nearly horizontal sections represent the largest change and therefore the highest partial pressure gradient. These horizontal visualisation might seem counter intuitive. For example in Figure 4-9

(a), when the flue gas enters at the top of the wheel and gets into contact with the fresh solid, there is a steep partial pressure gradient (green line), reducing the partial pressure from 15 kPa to 10 kPa in the top part of the wheel from a height of 2 m to 1.8 m, as the flue gas flows from top to bottom. When the flue gas enters the adsorption wheel at the top, it gets in contact with regenerated/ fresh adsorbent, entering from the desorption part of the wheel. Due to the high difference in partial pressure a high amount of CO2 gets adsorbed. Therefore, the CO2 partial pressure decreases rapidly (i = 1) as the flue gas travels along the unit cells of the wheel towards the outlet at the bottom. The cell closest to the inlet of the flue gas, i.e. near the top, get rapidly loaded and the mass transfer zone moves horizontal with the rotation of the wheel, while the highest partial pressure difference in the gas phase moves towards the flue gas outlet, the bottom of the wheel (i = N_τ).

The partial pressure of CO2 in the air increases when air gets in first contact with the adsorbent loaded with CO2, as shown in Figure 4-9 (b) by the green line for i = 1. It becomes gradually steeper (lower partial pressure difference) as it moves towards the outlet of the air, before it again slows down reaching the outlet of the air. While the adsorbent rotates, the bigger gradient moves towards the inlet of the air, as indicated by the blue line i = N_τ.

For comparison the resulting partial pressure profiles of the gases produced by the equilibrium model are plotted in the Appendix C, Figure C-1.

The temperature of the flue gas and air stream are given by Figure 4-10.

When the flue gas enters into contact with the regenerated and cooled down adsorbent the temperature drops rapidly (green line) (Figure 4-10 (a)). For the first slide (s = 1), green line) the temperature of the flue gas drops for the first 0.2 m of the wheel height by 8◦C, while over the remaining 1.8m the temperature only drops by 6◦C. In these sections the released heat of the adsorption process is transferred to the solid. This temperature drop is then reduced and stopped as the heat storage capacity of the solid is reached. In contrast to the flue gas temperature in the first slide (s = 1), the flue gas temperature in the last slide of cells (s = S), represented by

the blue line, does not change significantly for the first 0.1m of the wheel height from the top. From there a reduction by 8◦C is achieved over a height difference 0.7m of the adsorbent wheel (from 1.9m to 1.2m).

Air enters at slightly higher temperature than 15°C, as the temperature of the air is increased by the fan to overcome the pressure drop of the wheel (Figure 4-10 (b)). Initially the temperature increases slowly, due to the endothermic effect of CO2 desorption. After most of the CO2 desorption took place, the air takes the heat stored from the flue gas in the solid adsorbent. This leads to an increase of the air outlet temperature.

For comparison the resulting temperature profiles of the gases produced by the equilibrium model are plotted in the Appendix C, Figure C-2.

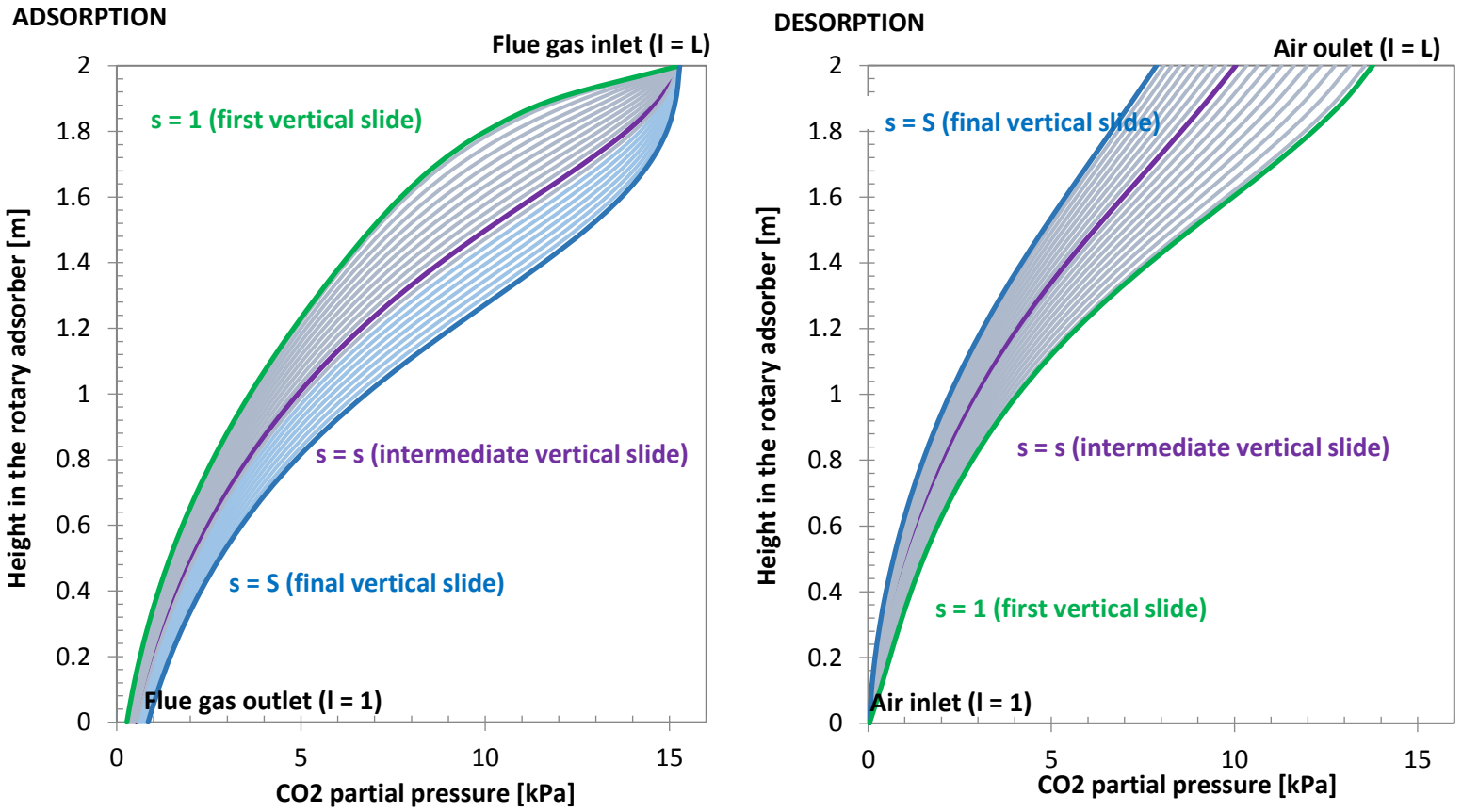

Figure 4-9: **CO2 partial pressure profiles of (a) the flue gas (adsorption) and (b) the air (desorption) in height direction for each vertical section. Rotation speed of 1 rpm, SEGR parallel configuration (97/96), Adsorbent: KOH activated carbon**

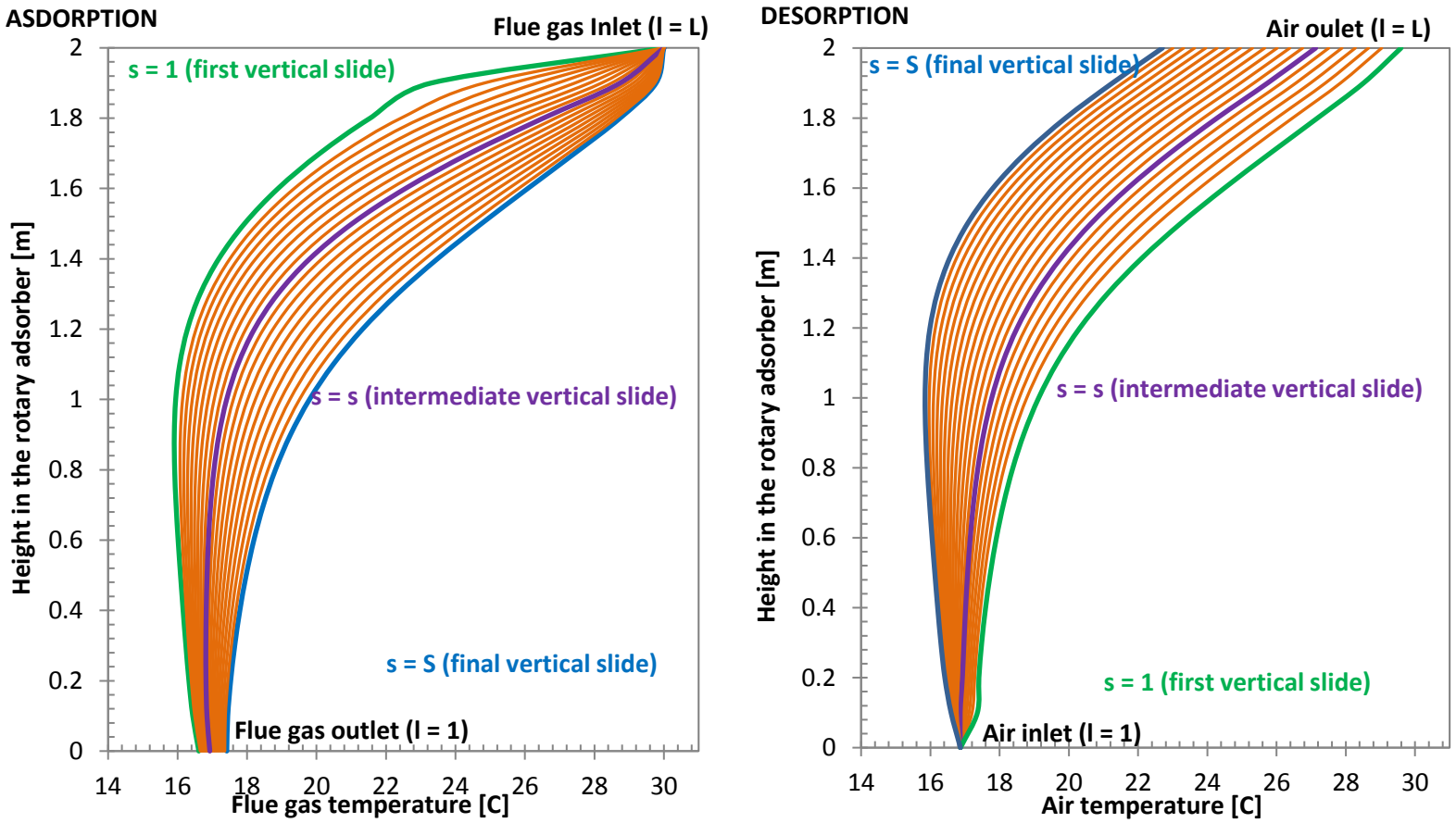

Figure 4-10: **Temperature profiles of (a) the flue gas (adsorption) and (b) the air (desorption) in height direction for each vertical section. Rotation speed of 1 rpm, SEGR parallel configuration (97/96), Adsorbent: KOH activated carbon**

Profiles of the adsorbent

The CO2 adsorption rate is a function of the change in the amount of adsorbed CO2 over the incremental change $\Delta\tau$ in rotational direction, as given by Equation (4.3).

$$\frac{\partial q_{CO2}}{\partial \tau} = \frac{q_{CO2\ i+1,j} - q_{CO2\ i,j}}{\Delta\tau} \qquad i = 0 \dots N_\tau \tag{4.3}$$

Figure 4-11 illustrates the horizontal CO2 adsorption profiles of the solid adsorbent in the adsorption section of the wheel (Figure 4-11 (a)) and in the desorption section of the wheel (Figure 4-11 (b)). The amount of CO2 adsorbed by the solid increases as the wheel rotates and gets in contact with the flue gas high in CO2 partial pressure (Figure 4-11 (a)). The solid volume close to the flue gas inlet (l=L) gets fully loaded, due to the larger driving force for the CO2 mass transfer, while the adsorbent located in the volumes closer to the flue gas outlet (l=1) gets partially loaded at the end of the adsorption cycle. Loading varies from 0.08 mol/kg to 1.08 mol/kg across the wheel. For the top slice, it changes from 0.78 to 1.08, leading to a working capacity of 0.3. For the bottom slice, it changes from 0.04 to 0.08, leading to a working capacity of 0.04.

When the adsorbent enters the regeneration part of the wheel (Figure 4-11 (b)), CO2 desorbs into the air. Due to the driving force (low partial pressure of CO2 in the fresh air and high loading of CO2 on the solid) CO2 desorbs faster at the inlet of the air (l=1). As the driving force decreases, the desorption rate decreases. Since the adsorbent is not fully regenerated at end of the cycle, it re-enters the adsorption section partially loaded.

For comparison the resulting CO2 adsorption profiles of the solid adsorbent produced by the equilibrium model are plotted in the Appendix C, Figure C-3.

The temperature profiles of the solid are shown in Figure 4-12. In the adsorption section the temperature of the solid increases (Figure 4-12 (a)). This is due to two mechanism. The release of heat of adsorption during adsorption, and the transfer of sensible heat from the flue gas to the adsorbent. The highest temperature increase

is located at the same area as the highest rate of CO2 adsorption, represented by the brown line in the first 5 seconds.

In the regeneration section (Figure 4-12 (b)), the endothermic desorption of CO2 decreases the solid temperature and sensible heat is transferred from the solid to the air stream, therefore the temperature of the solid drops. For the top cross section (brown line), the solid with the highest amount of CO2 adsorbed, the temperature drops by 10◦C.

For comparison the resulting temperature profiles of the solid adsorbent produced by the equilibrium model are plotted in the Appendix C, Figure C-4.

The difference between the amount of CO2 adsorbed at the beginning of the adsorption process (t=0) and the end of the adsorption process ($t=t_{adsorption}$) is called working cycle capacity of the solid adsorbent. It is given by Equation (3.22) and repeated below for convenience.

$$\text{Working cycle capacity} = \sum_{j=1}^{N_L} q_{CO2,t=t_{adsorption}} - \sum_{j=1}^{N_L} q_{CO2,t=0}\,; \quad \text{for } j = 1 \dots N_L$$

The adsorption time is given by half of the rotational speed $t_{adsorption} = t_{1/2}$. The amount of CO2 adsorbed accumulates along rotational direction and therefore the cumulative working cycle capacity is shown for the horizontal sections in rotational direction in Figure 4-13. The solid adsorbent in the first half of the full height of the rotary wheel, so 50% of the solid adsorbent, presents a working cycle capacity higher than 0.2 mol/kg. The working cycle capacity of the second half of the solid adsorbent is less than 0.2 mol/kg. The reduction in working cycle capacity at the flue gas outlet is due to the already reduced partial pressure of CO2 in the flue gas passing through the rotary regenerative CO2 transfer wheel.

For comparison the resulting working cycle capacity of the adsorbent produced by the equilibrium model are plotted in the Appendix C, Figure C-5.

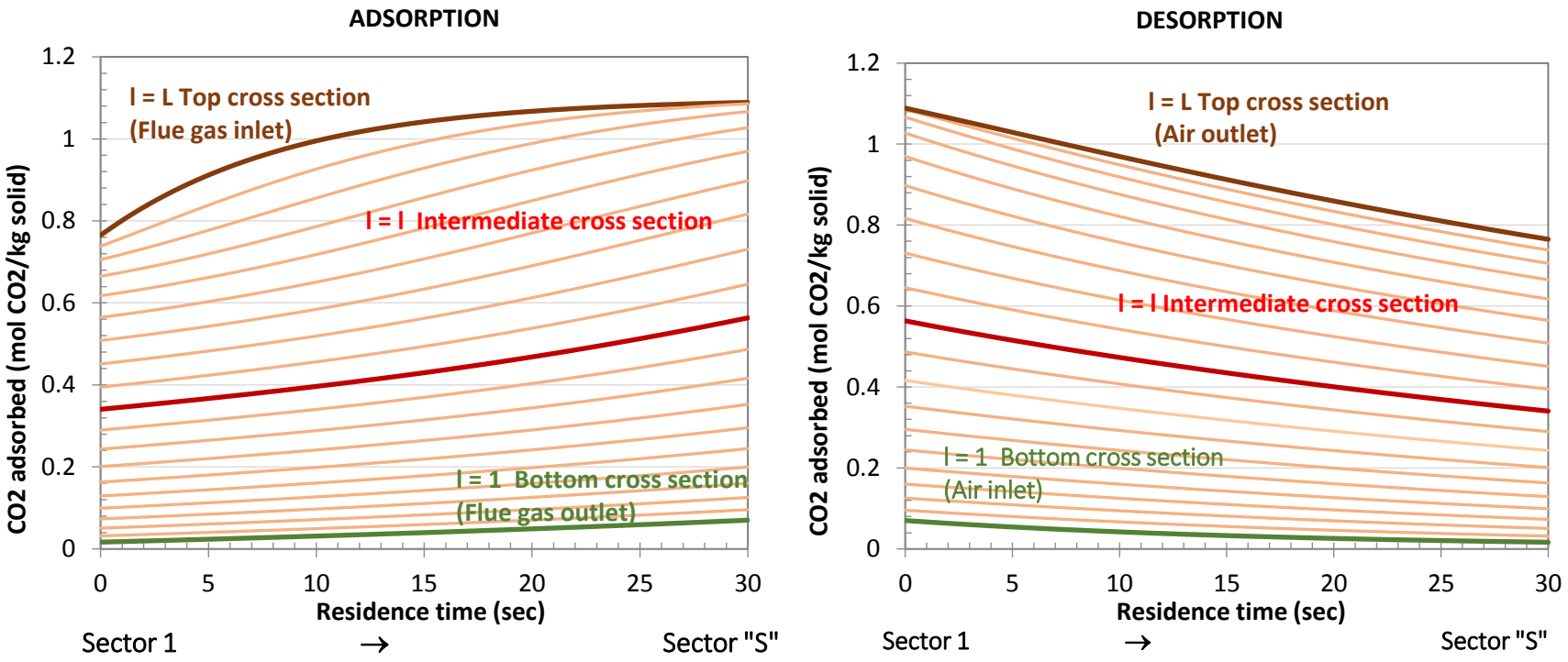

Figure 4-11: CO2 adsorption profile for adsorption (a) and desorption (b) in rotational direction for each horizontal section. Rotation speed of 1 rpm, SEGR parallel configuration (97/96), Adsorbent: KOH activated carbon

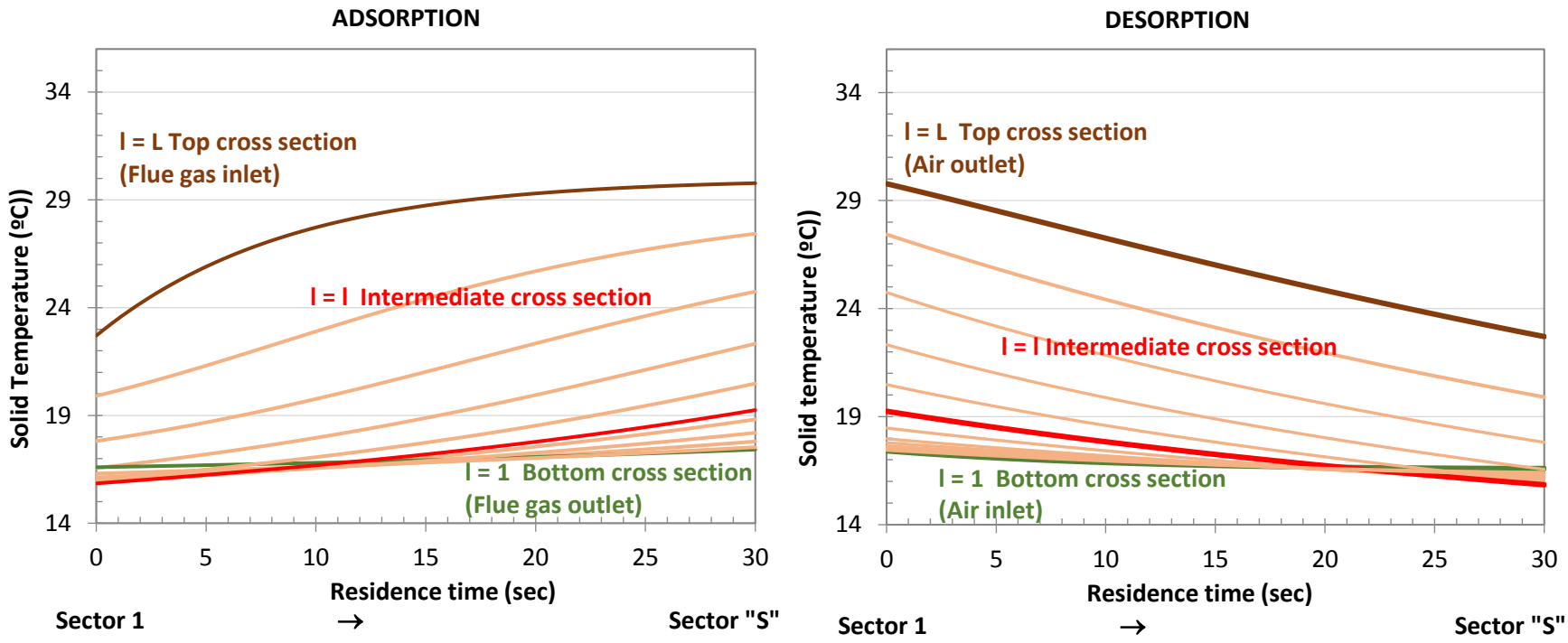

Figure 4-12: **Temperature profiles of the solid (a) in the adsorption section and (b) in the desorption section in rotational direction for each horizontal section. Rotation speed of 1 rpm, SEGR parallel configuration (97/96), Adsorbent: KOH activated carbon**

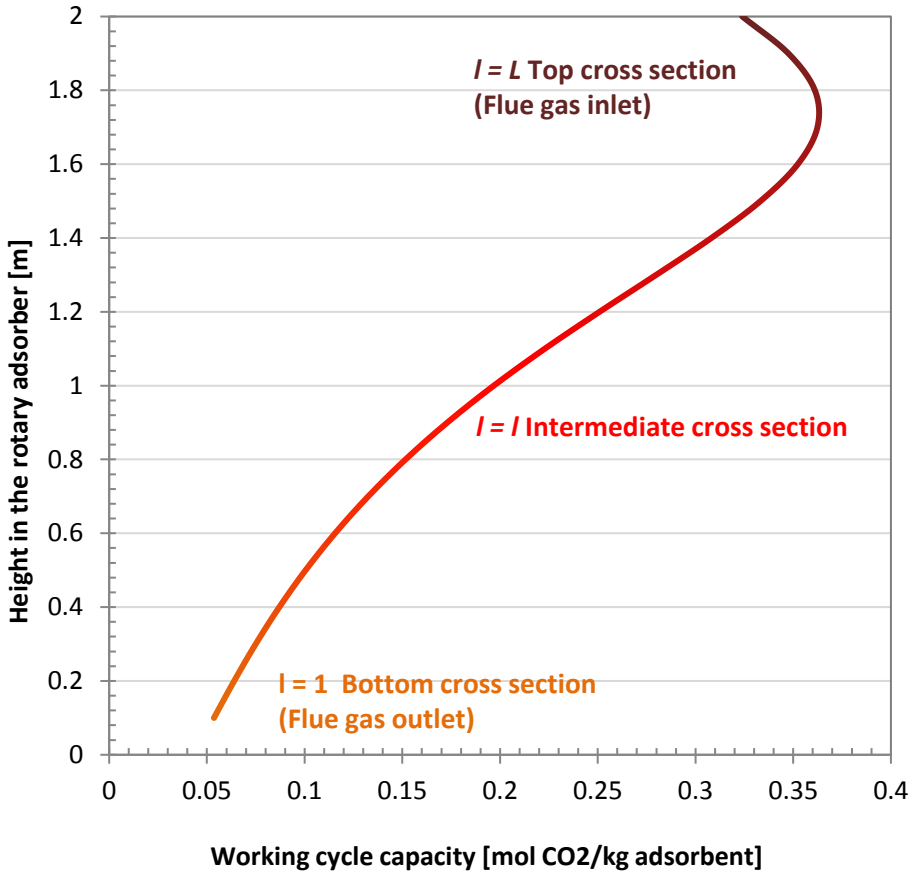

Figure 4-13: Working cycle capacity of the adsorbent along the height of the rotary wheel in height direction. Rotation speed of 1 rpm, SEGR parallel configuration (97/96), Adsorbent: KOH activated carbon

4.2.5 Sensitivity Analysis of Adsorbent Properties

The objective of this section is to assess adsorbent properties contributing to the kinetic of adsorbent and to identify, via a top down approach, the optimal range of those properties for the regenerative rotary CO2 transfer device.

This has two mutually exclusive objectives:

- Minimise the adsorbent mass requirement.
- Increase the recovery rate of the rotary transfer wheel, to push the limits of process intensification.

For the parameters of the Langmuir isotherm the properties of the KOH activated carbon are used in the simulation. Adsorbent properties related to the Langmuir isotherm are not further investigated here, as this was previously done by (Herraiz et al. 2019) and is presented under Section 3.3.2.

Diffusion coefficient

The mass transfer in the kinetic model is given by the Linear Driving Force model (Equation (3.28)), repeated here for convenience.

$$\frac{\partial \bar{q}_k}{\partial \tau} = \frac{15 D_{c,k}}{r_c^2} \cdot (q_k^* - \bar{q}_k)$$

Two parameters determine the rate of mass transfer: the concentration gradient of the component $(q_k^* - \bar{q}_k)$ and the diffusion coefficient $D_{c,k}$, which is an adsorbent dependent property. As shown through Equation (3.29) - (3.31), the diffusion coefficient depends on the loading of the adsorbent, temperature of the gas, an activation energy and on the temperature independent pre-exponential diffusion constant $D_{c,k\,0}$. Changes in $D_{c,k\,0}$ directly affect the diffusion coefficient and therefore the mass transfer in the regenerative rotary wheel.

(Shahkarami 2017) reports for the KOH activated carbon, used in this thesis, the temperature independent pre-exponential constant $D_{c,k\,0}$ in form of $D_{c,k\,0}/r_c^2$. Therefore, the crystal radius in not assessed separately in this thesis, but through the change of $D_{c,k\,0}$.

The effect of increasing the temperature independent pre-exponential diffusion constant on the adsorbent mass requirement of the regenerative rotary wheel, is shown in Figure 4-14 for different temperature independent pre-exponential diffusion constants. The green line represents the mass requirement in equilibrium for different recovery rates. The other lines represent different temperature independent pre-exponential diffusion constant values, starting from the value of 12.99 m^2/s reported by (Shahkarami 2017) for the KOH activated carbon used in this

thesis. Each increase in $D_{c,k\,0}$ leads to a significant decrease in adsorbent mass requirement. By increasing $D_{c,k\,0}$ from originally 12.99 m²/s to 20 m²/s the adsorbent mass requirement for a recovery ratio of 97% could be reduced by nearly 30%.

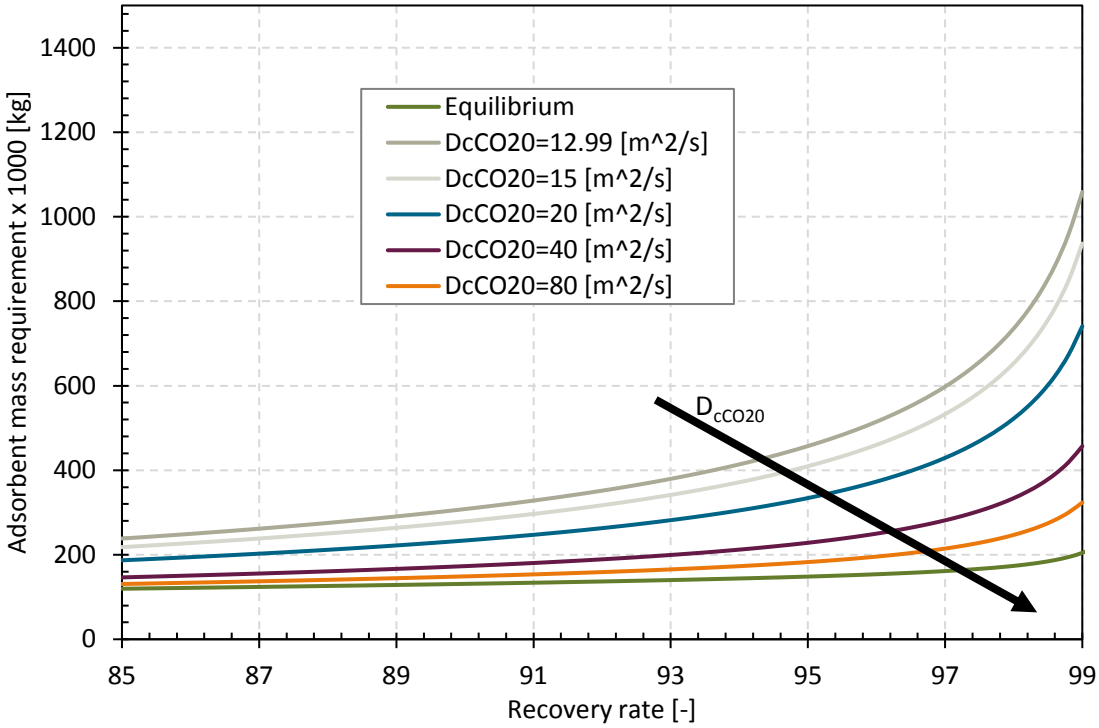

Figure 4-14: Sensitivity of adsorbent mass requirement to temperature independent pre-exponential constant DcCO2 0; flue gas composition for SEGR configuration in parallel

The effect of increasing the temperature independent pre-exponential diffusion constant on the recovery rate for CO2 of the regenerative rotary wheel and the working cycle capacity, is shown in Figure 4-15 for a constant mass of adsorbent. An increase in $D_{c,k\,0}$ leads to an increase in recovery rate. Especially in the range of 5 to 30 m²/s the corresponding increase in recovery rate is 18% point. Above a value of $D_{c,k\,0}$=40 m²/s, the recovery rate plateaus 99%. An increase from 40 up to 100 m²/s leads to a marginal increase of 0.4% point of the recovery rate.

The working cycle capacity follows a similar trend. For a range of 5 to 20 m²/s of the pre-exponential diffusion constant $D_{c,k\,0}$, the working cycle capacity increases rapidly from 3.5 to 4.36 but plateaus at 4.4 for any further increase. The asymptotic behaviour of the recovery rate and the working cycle capacity are due to the fact,

that the rate of mass transfer is not any longer limited by the value of the diffusion coefficient, but by the low driving force in form of the concentration gradient. The model starts to operate close to equilibrium and the limit is therefore a thermodynamic limit.

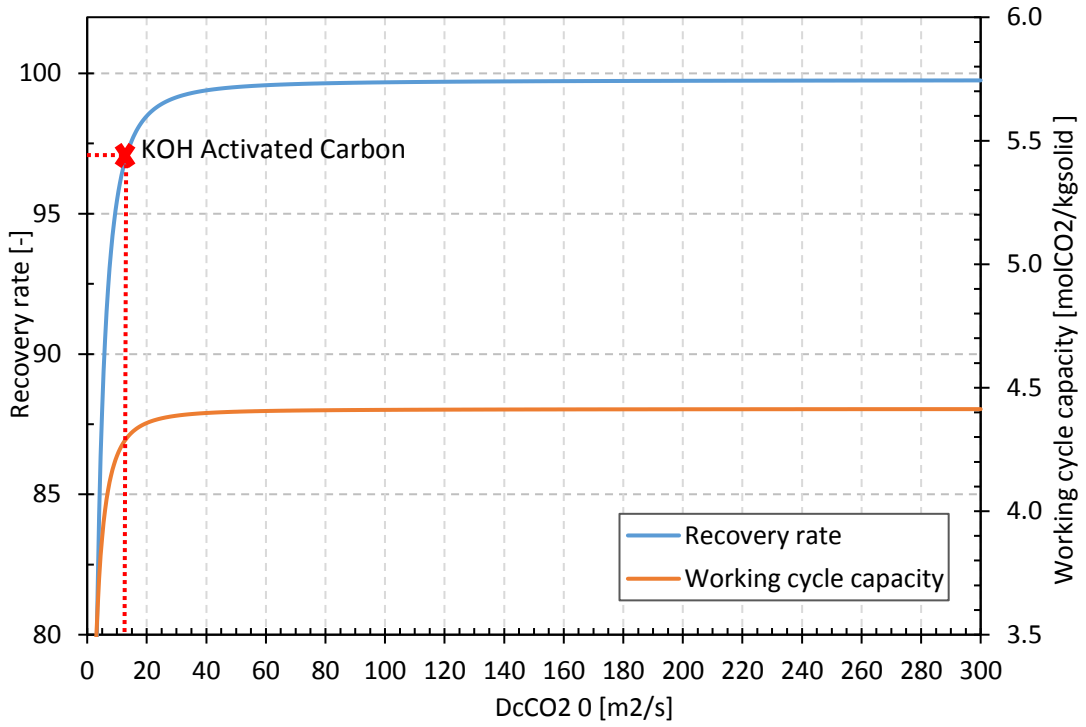

Figure 4-15: Sensitivity of recovery ratio and working cycle capacity to temperature independent pre-exponential constant $D_{cCO2\,0}$; flue gas composition for SEGR configuration in parallel; adsorbent mass = 598t

Figure 4-16 shows the effect of increasing the temperature independent pre-exponential diffusion constant on the adsorbent mass requirement and the working cycle capacity, while keeping the recovery rate constant at 97% (SEGR in parallel (97/96)). An increase in $D_{c,k\,0}$ leads to a decrease in adsorbent mass needed to achieve a recovery rate of 97%. An increase of $D_{c,k\,0}$ up to 30 m^2/s leads to a decrease in adsorbent mass required of over 85%. Above a value of $D_{c,k\,0}$=30 m^2/s an increase leads to further reduction in mass, but those are marginal compared to the initial reduction. The working cycle capacity increases as before with increasing $D_{c,k\,0}$. In the range of 5 to 80 m^2/s it increases rapidly from 1.1 to 11.9. For higher $D_{c,k\,0}$values the increase in working cycle capacity slows down until it approaches an asymptotic

behaviour reaching nearly the mol% of CO2 in the flue gas and therefore full working cycle capacity.

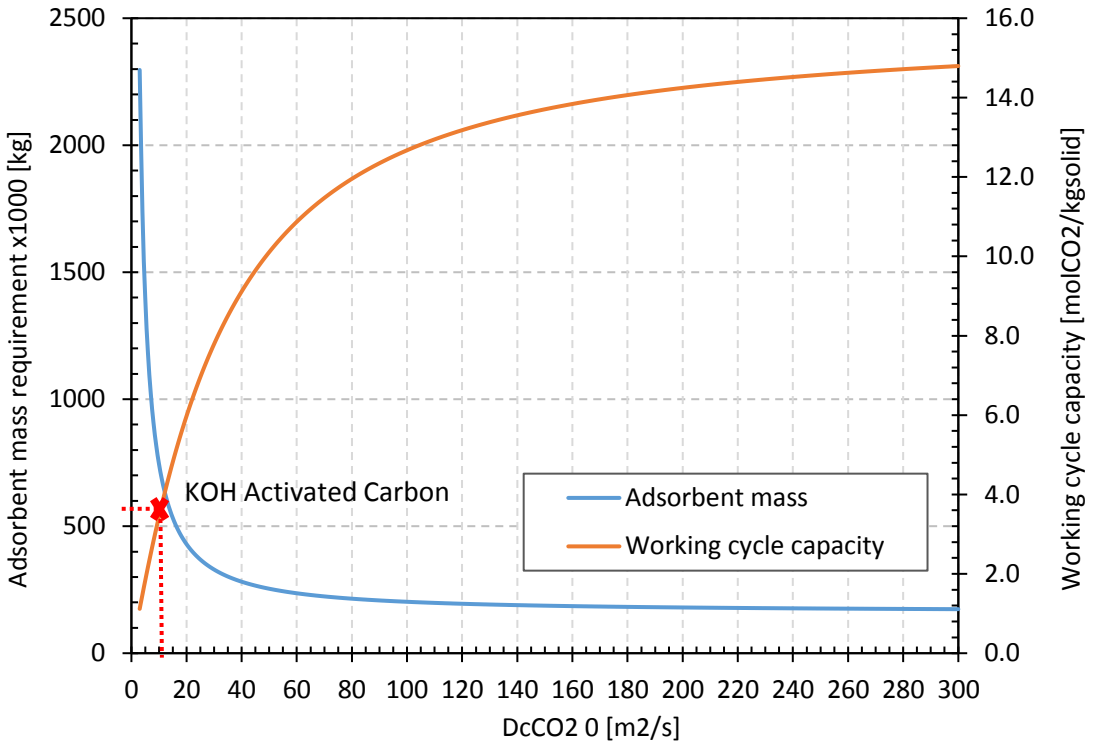

Figure 4-16: Sensitivity of adsorbent mass and working cycle capacity to temperature independent pre-exponential constant $D_{cCO2\,0}$; flue gas composition for SEGR configuration in parallel; recovery rate 97%

Geometrical factor

As stated in the section before, the mass transfer in the kinetic model is given by the Linear Driving Force model (Equation (3.28)), repeated here for convenience.

$$\frac{\partial \bar{q}_k}{\partial \tau} = \frac{15 D_{c,k}}{r_c^2} \cdot (q_k^* - \bar{q}_k)$$

In this form of the equation the geometrical factor at a value of 15 was used to be able to use the isothermal packed bed experimental results to verify the rotary wheel model.

The geometrical factor is different for different characteristic sizes of the monolith (i.e. cell density and pore volume). That implies that the size should be optimized for each application. Based on the current development stage of the rotary transfer device model, no reasonable prediction about the heterogeneity of the adsorption material, nor the expected pore volume could be made. However, to evaluate the effect of the geometrical factor on recovery ratio and on solid mass requirement a sensitivity analysis is performed in the range of reported geometrical factors reported in literature (Rezaei 2011)

Illustrated in Figure 4-17 (for a constant mass of adsorbent) is the effect of increasing the geometrical factor on the recovery rate of CO2 and the working cycle capacity of the regenerative rotary wheel. An increase in geometrical factor leads to an increase in recovery rate and cycle capacity. An increase in the geometrical factor from 15 to 20 corresponds to an increase in recovery rate of 1.2% point and an increase in working cycle capacity of 1.1%. A further increase of 5 points to a geometrical factor of 25 leads only to an increase in recovery rate of less than 0.56% points and 0.55% in working cycle capacity respectively. An increase of the geometrical factor in increments of 5 points beyond 25 has only a marginal effect on the recovery rate, as well as on the cycle capacity. Hence, the sensitivity of both recovery rate and cycle capacity seems for a constant adsorbent mass minimal, especially in the range of a geometrical factor beyond 35, where the increase in both amounts to less than 0.1%points/1%.

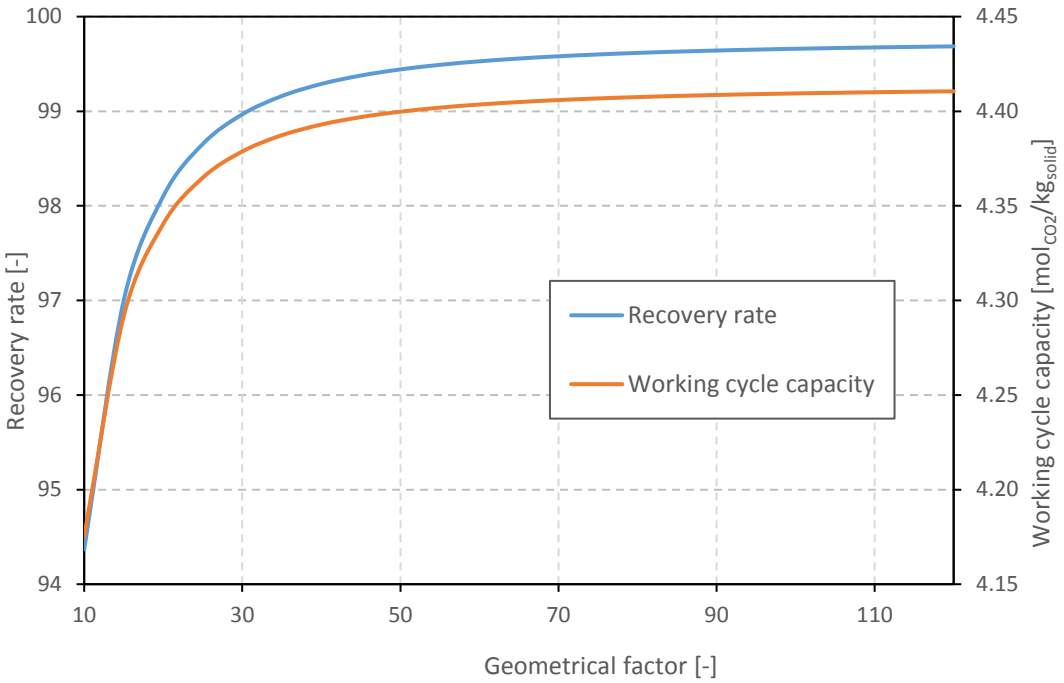

Figure 4-17: Sensitivity of recovery ratio and working cycle capacity to the geometrical factor of the adsorbent structure; flue gas composition for SEGR configuration in parallel; adsorbent mass = 598t

The effect of increasing the geometrical factor of the adsorbent structure on the adsorbent mass requirement and the working cycle capacity, while keeping the recovery rate constant at 97% (SEGR in parallel (97/96)), is shown in Figure 4-18. An increase in geometrical factor from 15 to 20 leads to a large decrease of 20.2% in adsorbent mass requirement to achieve a recovery rate of 97%. An increase of the geometrical factor from 15 up to a value of 70 leads to a significant decrease in adsorbent mass by 60.7%. For each increase in geometrical factor in increments of 5 beyond 70 the gain in reduction reduces to less than 2%. The working cycle capacity increases, for a constant recovery rate, with increasing geometrical factor. For an increase from 15 to 70 the increase in cycle capacity amounts to 60.7%, as previous the reduction in adsorbent amount. An increase further than 70 leads only to a marginal increase in cycle capacity.

From the sensitivity analysis of the effect of the geometrical factor it can be concluded that it has a much larger effect on the adsorbent mass reduction, than it

has on the recovery ratio. In the context of an improvement of adsorbent mass requirement for SEGR application a focus has definitely to be on the development of the optimal structured adsorbent for this kind of application.

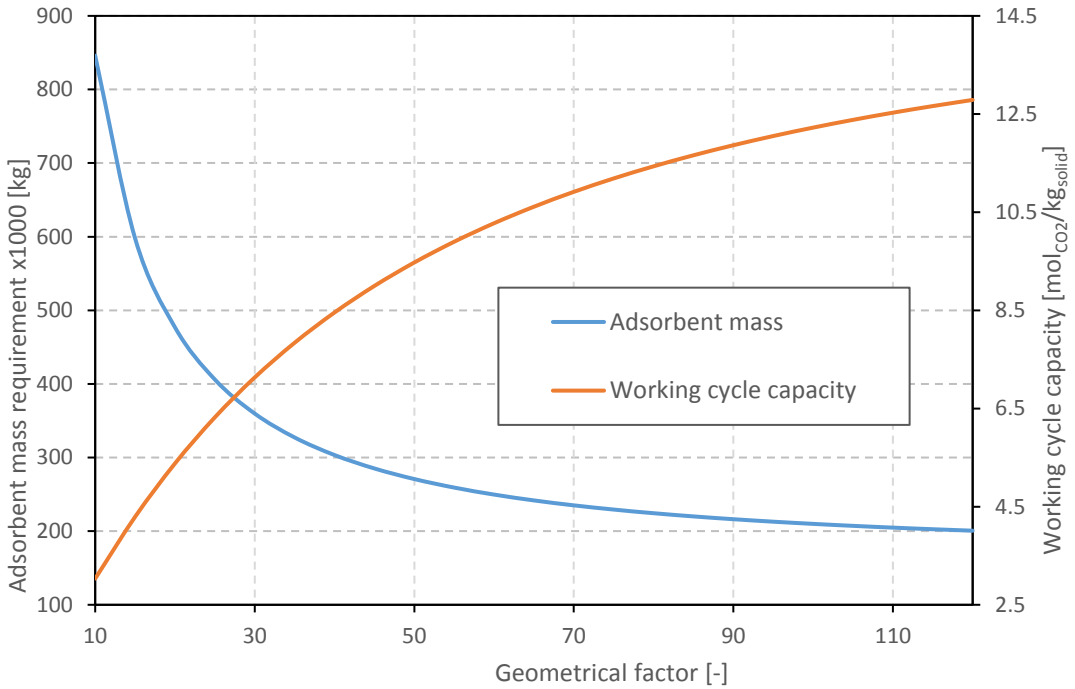

Figure 4-18: Sensitivity of adsorbent mass and working cycle capacity to the geometrical factor of the adsorbent structure; flue gas composition for SEGR configuration in parallel; recovery rate 97%

Specific heat capacity

The heat transfer on the solid side in the kinetic model is given by Equation (4.4), as previously described in Equation (3.36).

$$Q_s = m_s \cdot Cp_s \cdot \Delta T_s \tag{4.4}$$

With, the mass of the solid m_s, the specific heat capacity Cp_s and the temperature difference in the solid ΔT_s.

In all the simulation results reported in this thesis, the specific heat capacity was assumed to be constant. The specific heat capacity is a property of the adsorbent. Since the Cp_s value for the utilised KOH activated carbon was not reported by

(Shahkarami 2017), it was chosen based on in the literature reported specific heat capacity values for various activated carbons to be 1000 J/kg K (Chua, Chakraborty, and Wang 2004; Mohn 2012).

The effect of varying the specific heat capacity on the recovery rate for CO2 of the regenerative rotary wheel and the working cycle capacity, is shown in Figure 4-19 for a constant mass of adsorbent. An increase in Cp_s leads to an increase in recovery rate. However, in the range of 400 to 800 J/kg·K the corresponding increase in recovery rate is less than 0.4% point. An increase from 800 up to 1400 J/kg·K leads to a marginal increase of 0.14% point of the recovery rate.

The working cycle capacity follows a similar trend of a marginal increase of 0.5% over the whole investigated specific heat capacity range of 400 to 1400 J/kg·K.

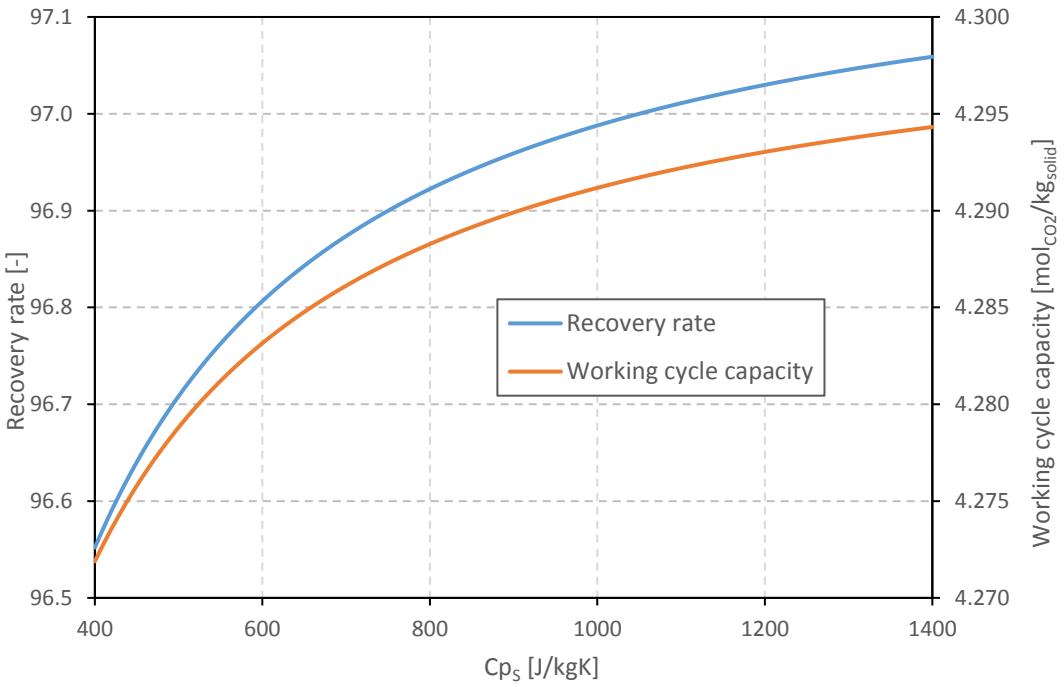

Figure 4-19: Sensitivity of recovery ratio and working cycle capacity to specific heat capacity Cp_s; flue gas composition for SEGR configuration in parallel; adsorbent mass = 598t

Figure 4-20 shows the effect of increasing the specific heat capacity of the adsorbent on the adsorbent mass requirement and the working cycle capacity, while keeping the recovery rate constant at 97% (SEGR in parallel (97/96)). An increase in Cp_s leads to a decrease in adsorbent mass needed to achieve a recovery rate of 97%. An increase of Cp_s from 400 up to 700 J/kg·K leads to a decrease in adsorbent mass required of 4.9%. From a value of 700 up to 1400 J/kg·K an increase in Cp_s leads to further reduction in mass of 3.2%. The working cycle capacity increases with increasing specific heat capacity. Over the whole investigated range the increase in Cp_s from 400-1400 J/kg·K results in an increase of the working cycle capacity of 8.2% points.

In comparison of the results of the sensitivity analysis of Figure 4-19 and Figure 4-20 it can be concluded that the specific heat capacity has a larger influence on the solid mass requirement than on the recovery ratio. However, the effect is in comparison to other adsorbent properties less significant.

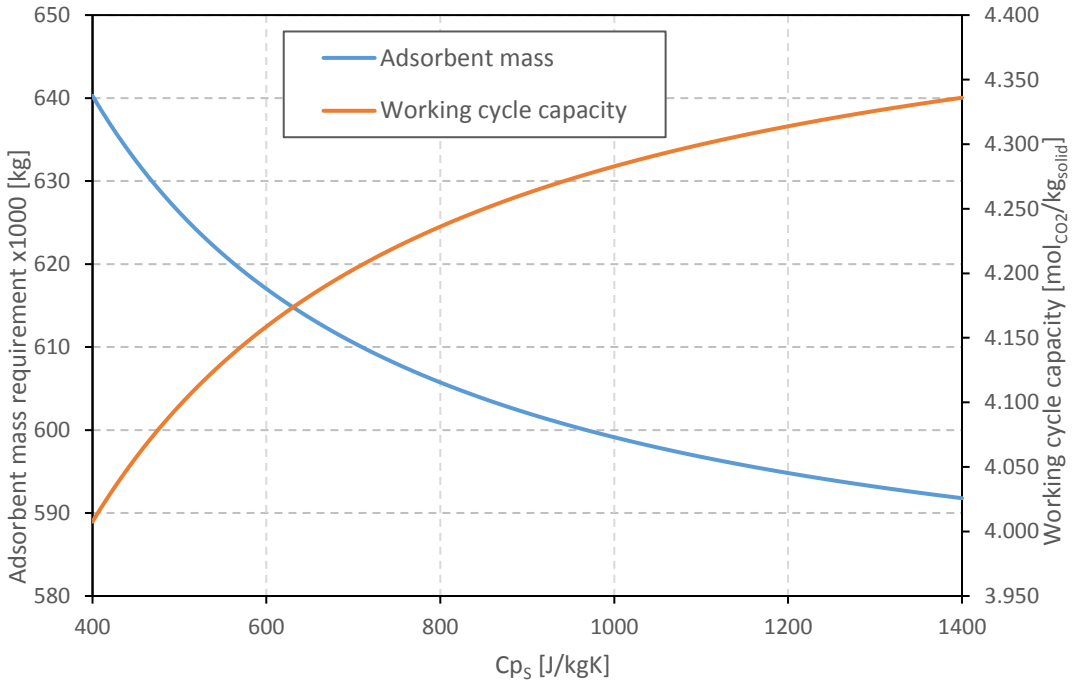

Figure 4-20: Sensitivity of adsorbent mass and working cycle capacity to specific heat capacity Cp_s; flue gas composition for SEGR configuration in parallel; recovery rate 97%

Surface heating area

The heat transfer in the regenerative rotary CO2 transfer wheel is limited by a convective heat transfer resistance, as described in Section 3.4.2 by Equation (3.35) - (3.37). The heat $\dot{Q}$ that can be transferred is given by Equation (4.5).

$$\dot{Q} = h_{cv} \cdot A_s \cdot \Delta T \tag{4.5}$$

With, as previously described, the convective heat transfer coefficient h_{cv}, the total surface heating area A_s and the temperature difference ΔT between the gas and the solid. Typical values of heat transfer coefficients for gases and vapours are in the magnitude of 5 to 150 W/m^{2}K. In the simulation it is assumed to be around 50 W/m^{2}K. Since the surface heating area is a property of the adsorbent, it can be estimated based on the specific surface area of the adsorbent and the amount of adsorbent used.

The specific surface area for the KOH activated carbon has only been measured on an adsorbent sample in powder form as per BET method, therefore the value is not representative of a regenerative rotary CO2 transfer wheel filled with a honeycomb monolith. The value is not available for a honeycomb structure at the time of writing. Therefore, an approximation is made on the basis of literature values for the specific surface area of honeycomb-monolithic activated carbons. The specific surface area typically ranges from 483 m^2/g in (Ribeiro et al. 2008) to 1818 m^2/g in (Querejeta et al. 2017).

The effect of an increasing surface heating area A_s, i.e. the product of adsorbent mass m_s and specific surface area S_{BET} (Equation (4.6)), on the recovery ratio, the flue gas outlet temperature and the CO2-enriched air outlet temperature is shown in Figure 4-21.

The red dotted lines represent, as reference, the surface heating areas given by different specific surface areas reported in literature. For the range of values investigated here, the surface heating area does not have an impact on the recovery rate of the regenerative rotary wheel, the flue gas outlet temperature, or the CO2-

enriched outlet temperature. They match the same values predicted by the model without a resistance to heat transfer. The results suggest that the surface heating area is high enough to not limit heat transfer for honeycomb-monolithic structured activated carbon in the range considered.

$$A_s = S_{BET} \cdot m_s \tag{4.6}$$

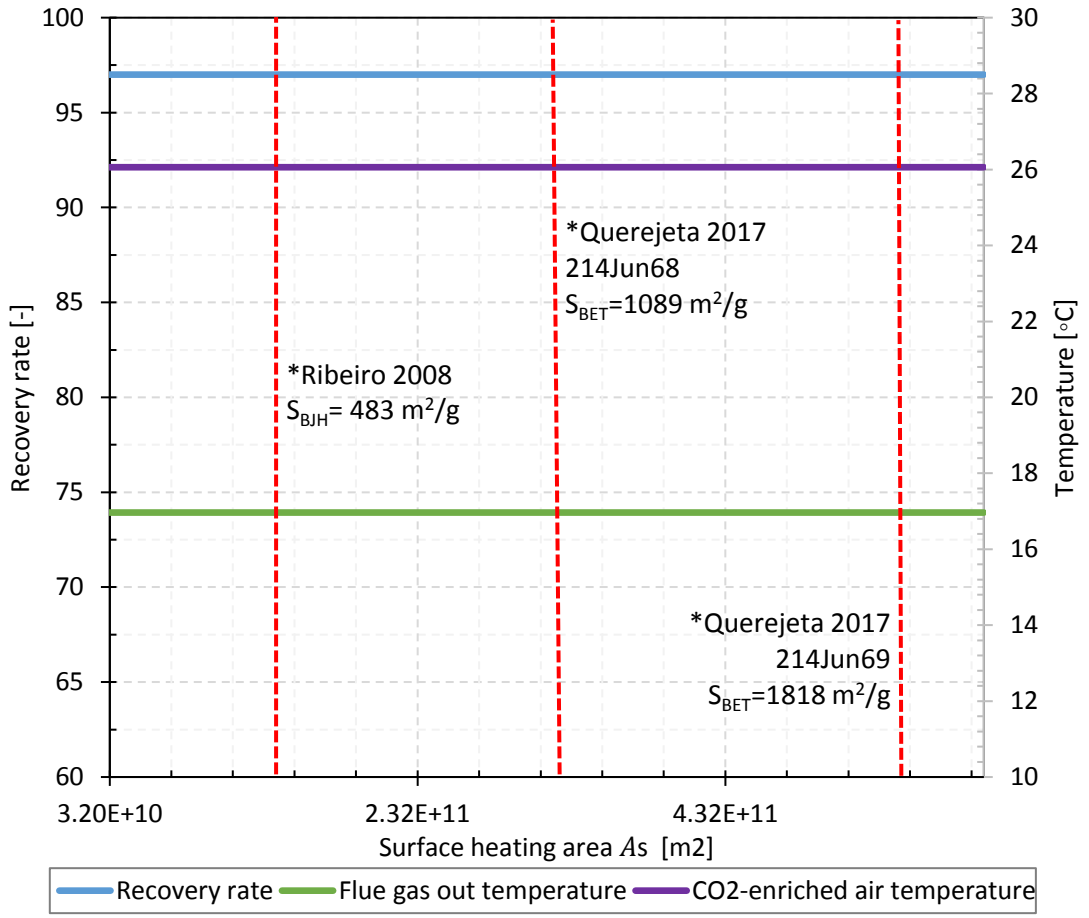

Figure 4-21: Sensitivity of recovery rate, flue gas outlet temperature and CO2-enriched air temperature to surface heating area; flue gas composition for SEGR configuration in parallel; adsorbent mass = 598t

4.2.6 Sensitivity Analysis of Operating Conditions

The objective of this section is to assess operational conditions of the regenerative rotary CO2 transfer device, to either minimise the adsorbent mass requirement, or to push the limits of the recovery rate achievable.

Rotational speed

An increase in rotational speed, while keeping the adsorbent mass constant, leads to an increase in recovery rate in the regenerative rotary CO2 transfer wheel, as illustrated in Figure 4-22. Particularly low recovery rates can be pushed up. An increase from 0.1 to 0.3 rpm increases the recovery ratio by 45%. Each cell, filled with adsorbent, has to treat less flue gas amount, since the contact time is decreased, therefore there is more capacity for CO2 left. That effect can be seen in the comparison of Figure 4-23, showing the adsorbed amount of CO2 per adsorbent cell for a rotational speed of 0.5 rpm, and Figure 4-24, showing the adsorbed amount of CO2 per adsorbent cell for a rotational speed of 1.5 rpm. At recovery rates over 96% the increase in recovery rate with increasing rotational speed reduces significantly (Figure 4-22). The higher the initial design point, based on adsorbent mass, recovery rate and rotational speed, the harder it is to push the recovery rate up by increasing the rotational speed. At the same time the working cycle capacity decreases with increasing rotational speed, due to more adsorbed amount of CO2 remaining on the solid for the same horizontal section.

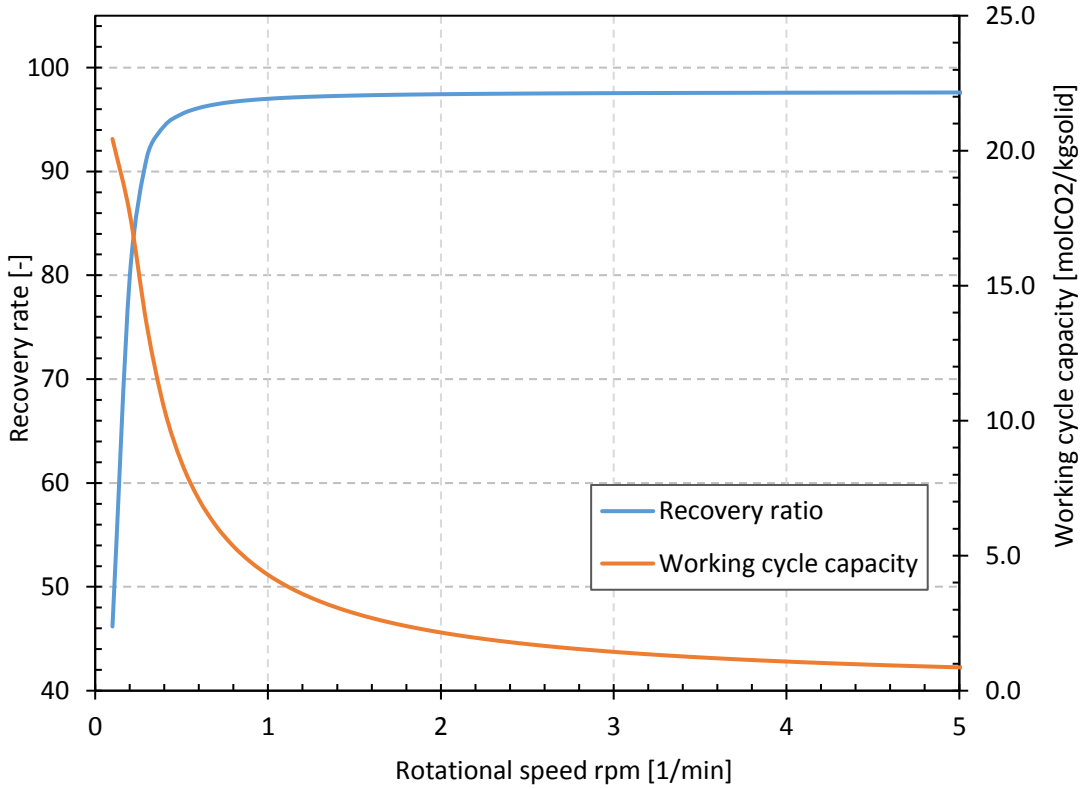

Figure 4-22: Sensitivity of recovery ratio and working cycle capacity to rotational speed of the rotor; flue gas composition for SEGR configuration in parallel; adsorbent mass = 598t

Figure 4-23: Adsorbed amount of CO2 on the solid for a rotational speed of 0.5 rpm; flue gas composition for SEGR configuration in parallel; adsorbent mass = 598t; recovery rate 95.5%

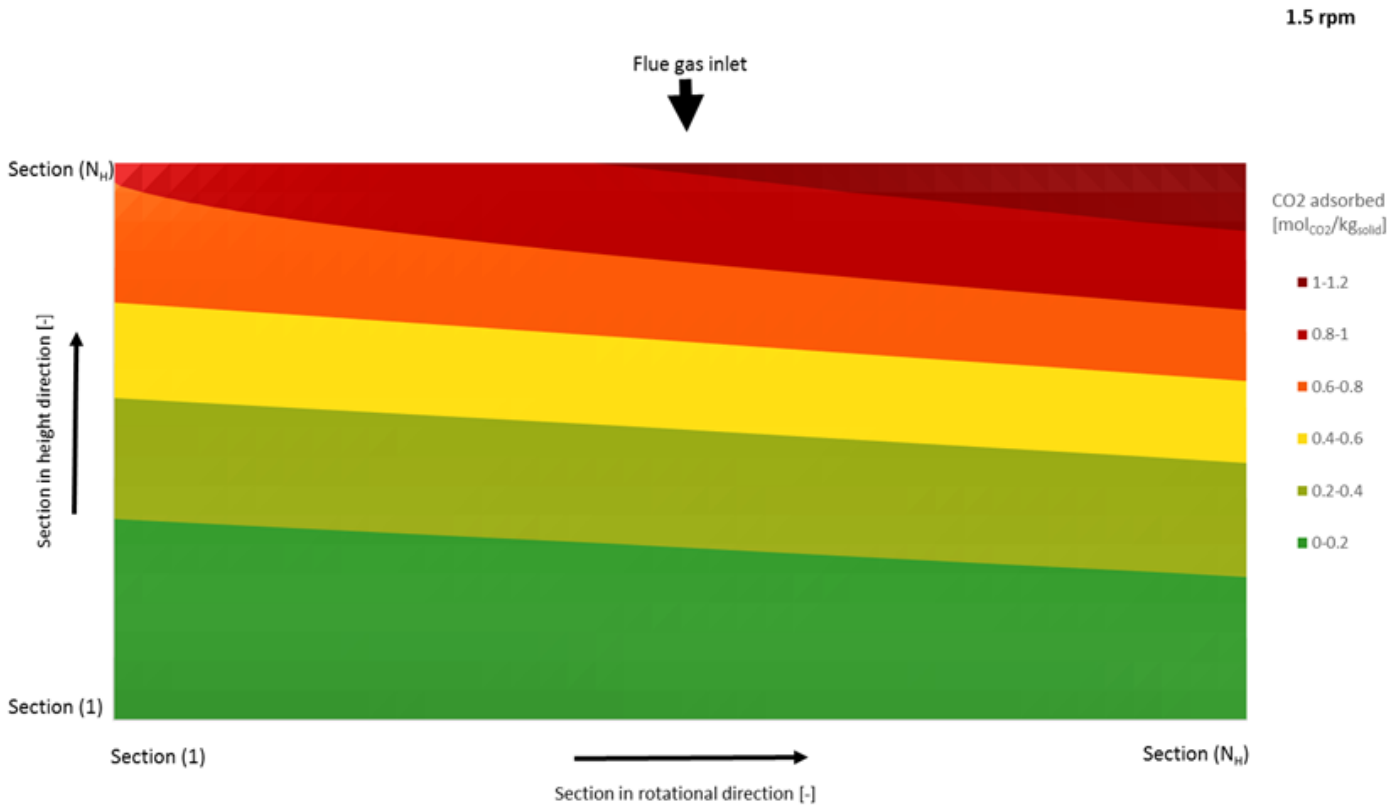

Figure 4-24: Adsorbed amount of CO2 on the solid for a rotational speed of 1.5 rpm; flue gas composition for SEGR configuration in parallel; adsorbent mass = 598t; recovery rate 97.3%

The impact of increasing the rotational speed, while keeping the recovery rate constant, shows an asymptotic decrease in adsorbent mass requirement, as shown in Figure 4-25. The initial design point for the SEGR in parallel configuration with a recovery rate of 97%, is a rotational speed of 1 rpm. Therefore, pushing beyond that point by increasing the rotational speed is challenging, especially at already high recovery rates. The working cycle capacity follows the trend of the adsorbent mass requirement.

The amount of CO2 absorbed per adsorbent cell for two different rotational speeds (0.5 and 1.5 rpm) are illustrated in Figure 4-26 and Figure 4-27. It can be seen, that even though there is more solid per time step available for a rotational speed of 0.5 rpm, the solid is getting into contact with more moles of CO2 in the same time step, than in the case of 1.5 rpm.

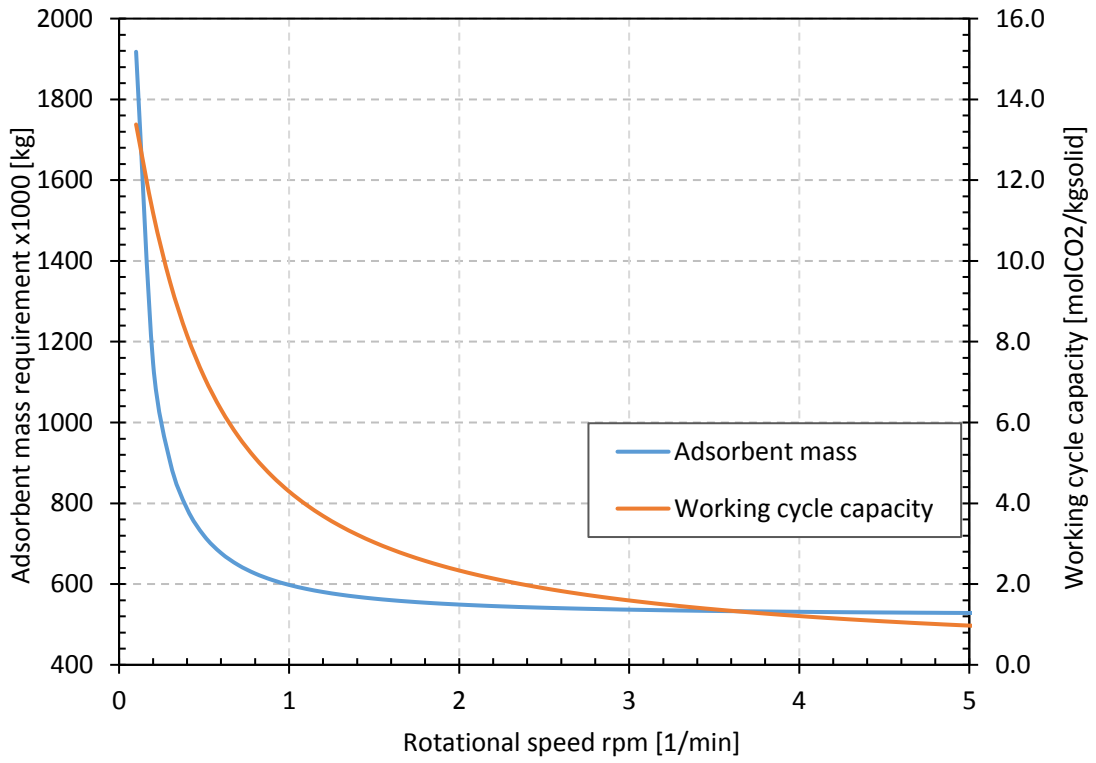

Figure 4-25: Sensitivity of adsorbent mass and working cycle capacity to rotational speed of the rotor; flue gas composition for SEGR configuration in parallel; recovery rate 97%

Figure 4-26: Adsorbed amount of CO2 on the solid for a rotational speed of 0.5 rpm; flue gas composition for SEGR configuration in parallel; recovery rate 97%; adsorbent mass = 710t

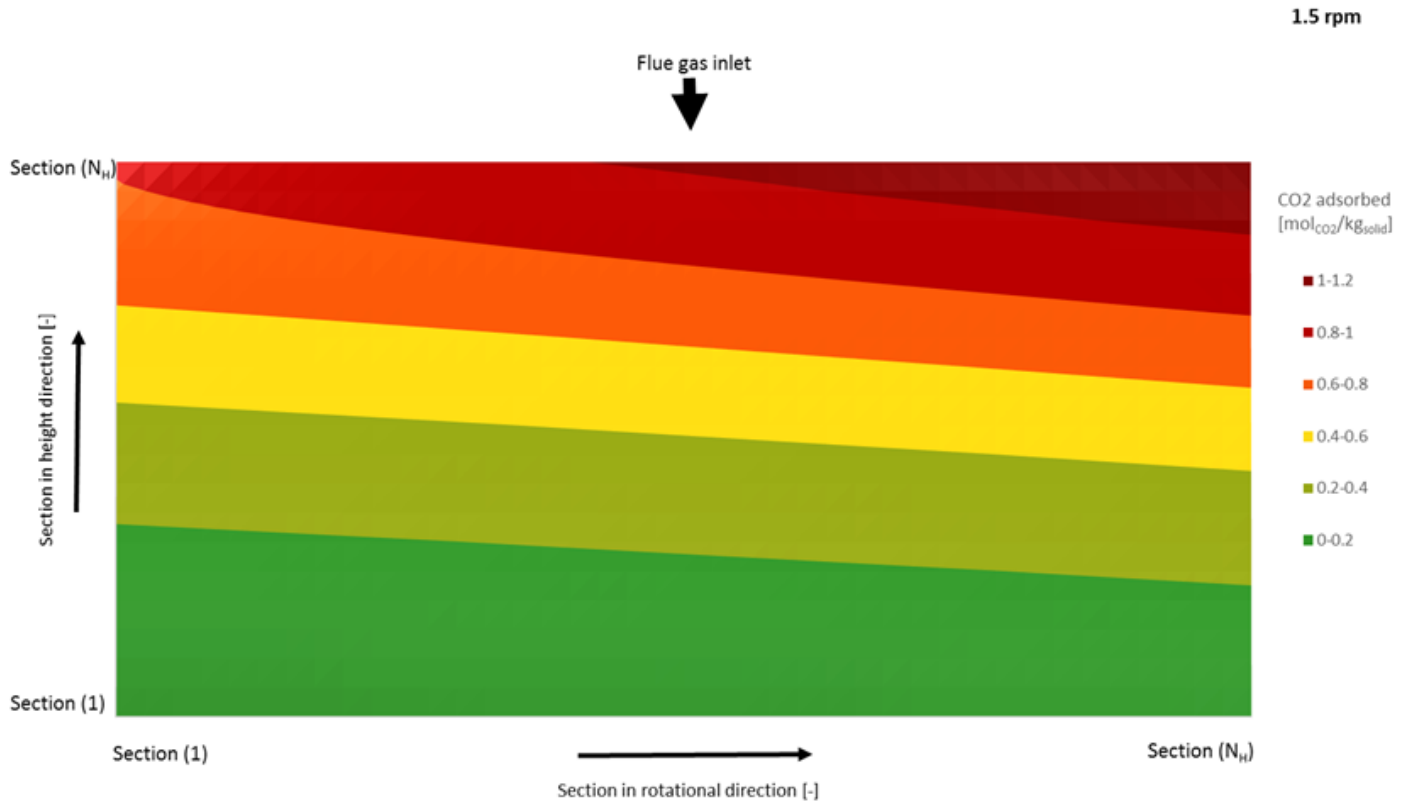

Figure 4-27: Adsorbed amount of CO2 on the solid for a rotational speed of 1.5 rpm; flue gas composition for SEGR configuration in parallel; recovery rate 97%; adsorbent mass = 564t

Air and flue gas inlet temperature

An impact assessment of air inlet and flue gas inlet temperature on the regenerative rotary CO2 transfer wheel, was done previously by Herraiz and co-workers (Herraiz et al. 2019), using the equilibrium model presented under Section 3.3. Since the energy balance was extended by a convective heat transfer resistance term, the impact of air and flue gas inlet temperature need to be re-evaluated.

The effect of a higher air inlet temperature used for regeneration on the adsorbent mass requirement for a constant recovery rate of 97% is shown in Figure 4-28. The adsorbent mass requirement follows a nearly exponential trend, by doubling the required increase in adsorbent mass for each 10°C increase, starting by 5 tonnes more needed mass, or 0.8% of the original mass, for the first 10°C increase. The equilibrium model previously reported a linear trend of adsorbent mass dependency on the air inlet temperature.

Although a higher air temperature assists the regeneration part of the process, it does not lead to a higher recovery rate. The recovery rate, as illustrated in Figure 4-29, drops about 0.6% over the investigated temperature range. This is due to the increase in temperature of the solid entering the adsorption process (Figure 4-30), which is unfavourable for adsorption and therefore decreases the recovery rate. This decrease in recovery rate is minor compared to the range of the investigated temperature, indicating an insensitivity of the recovery rate to the air inlet temperature (Herraiz et al. 2019) and an insensitivity of performance for changing ambient conditions.

The impact of air inlet temperature on the CO2-enriched outlet temperature is shown Figure 4-30. Herraiz (Herraiz et al. 2019) showed an increase of 2°C in CO2-enriched air temperature predicted by the equilibrium model for the range of investigated temperatures. As a consequence, the gas turbine power output is derated by approximately 2MW of ca. 820 MW of total output.

In contrast to that, the kinetic model predicts an increase of 12°C over the investigated temperature range. This would be unacceptable, as the gas turbine compressor inlet temperature needs to be maintained as low as possible. Therefore,

it is even more important to limit any increase in air inlet temperature, to limit an overall detrimental effect on the net power output.

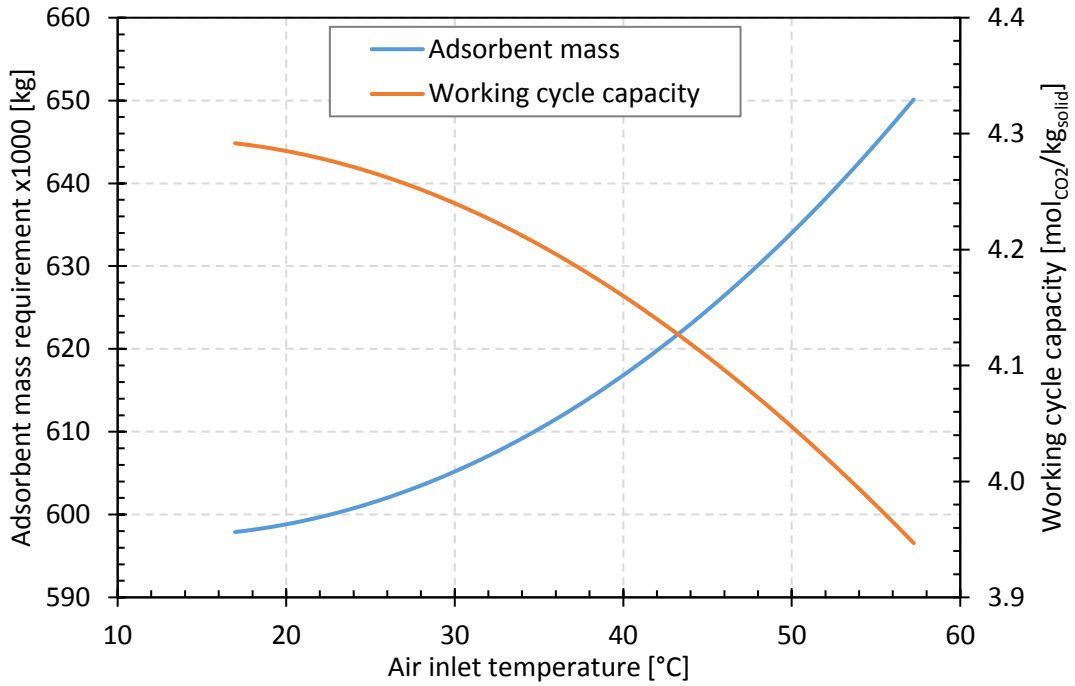

Figure 4-28: Sensitivity of adsorbent mass and working cycle capacity to air inlet temperature; flue gas composition for SEGR configuration in parallel; recovery rate 97%

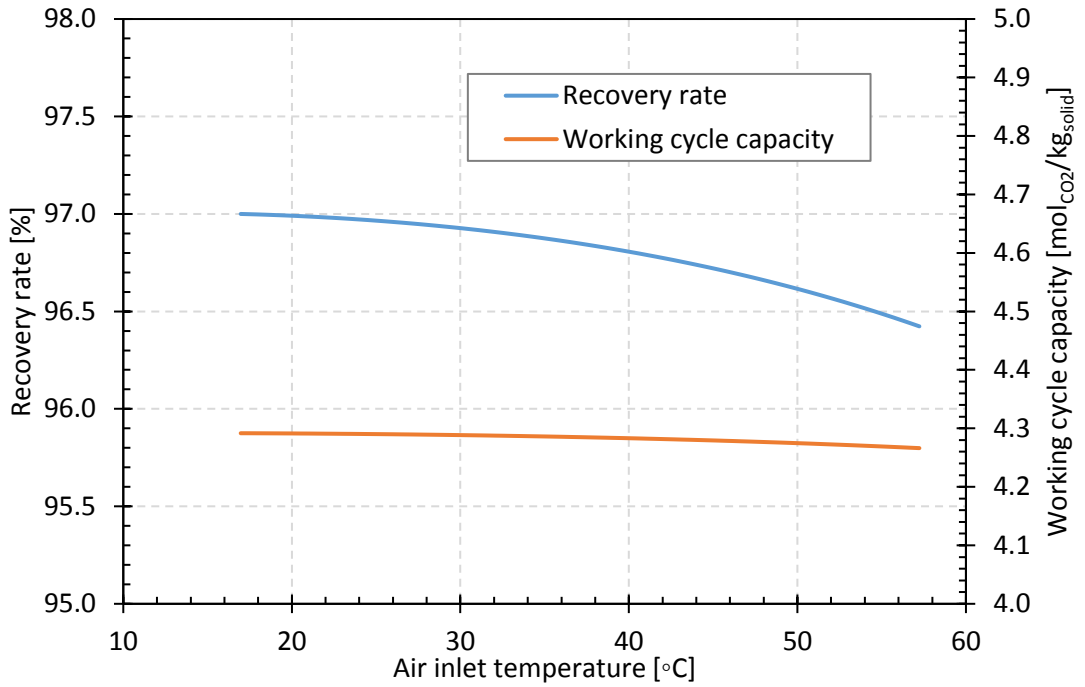

Figure 4-29: Sensitivity of recovery ratio and working cycle capacity to air inlet temperature; flue gas composition for SEGR configuration in parallel; adsorbent mass = 598t

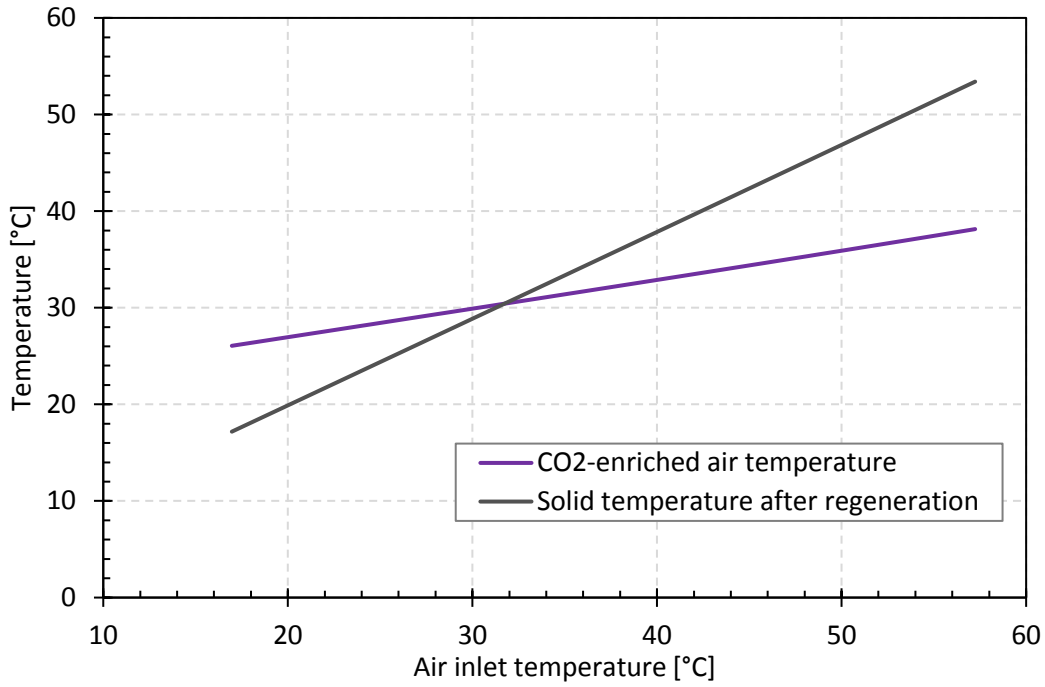

Figure 4-30: Sensitivity of CO2-enriched air and solid temperature to air inlet temperature; flue gas composition for SEGR configuration in parallel; adsorbent mass = 598t

The impact of a change in flue gas inlet temperature on the adsorbent mass requirement and on the temperatures of CO2-enriched air outlet and flue gas outlet are illustrated in Figure 4-31 and Figure 4-32. The change in required adsorbent mass remains marginal. The flue gas outlet temperature does not change in the investigated temperature range, and the CO2-enriched air outlet temperature increases linear with increasing flue gas inlet temperature. For an optimised system, it remains recommended to keep the flue gas inlet temperature as low as possible to minimise the impact on the CO2-enriched air temperature and therefore on the gas turbine compressor.

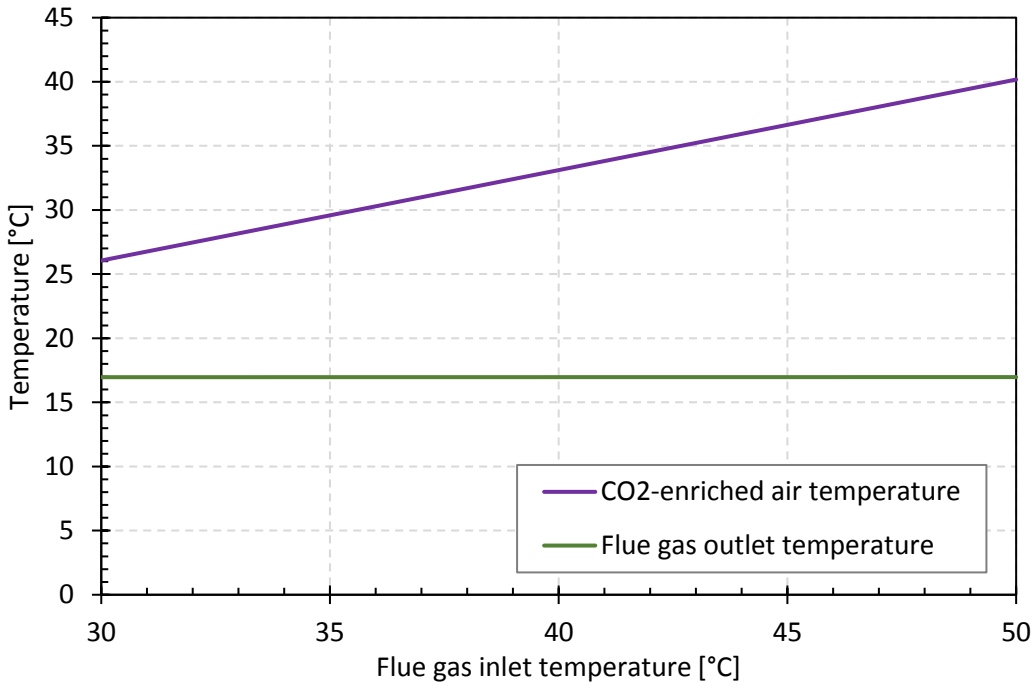

Figure 4-31: Sensitivity of CO2-enriched air and flue gas outlet temperature to flue gas inlet temperature; flue gas composition for SEGR configuration in parallel; adsorbent mass = 598t

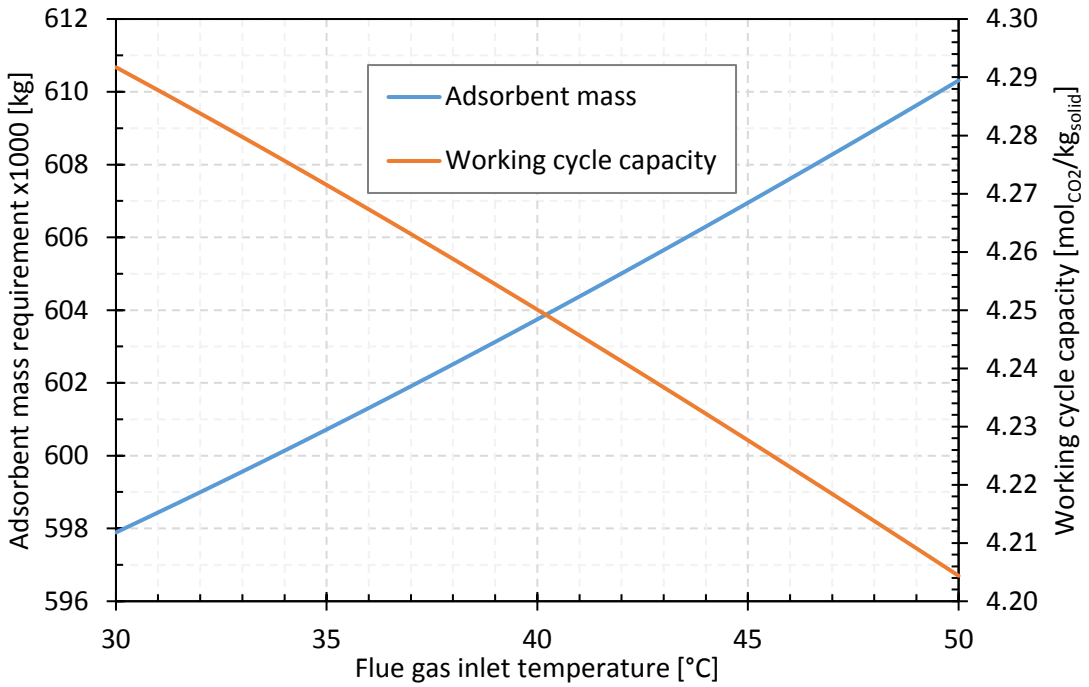

Figure 4-32: Sensitivity of adsorbent mass and working cycle capacity to flue gas inlet temperature; flue gas composition for SEGR configuration in parallel; recovery rate 97%

Partitioning of the wheel

The objective is to investigate the effect of balancing adsorption and desorption by adjusting the partitioning of the wheel. By changing the partitioning, more solid will be available for one of the two process part. This is schematically visualised in Figure 4-33. This allows to evaluate which part of the rotary regenerative CO2 transfer process is the time limiting part of the whole process.

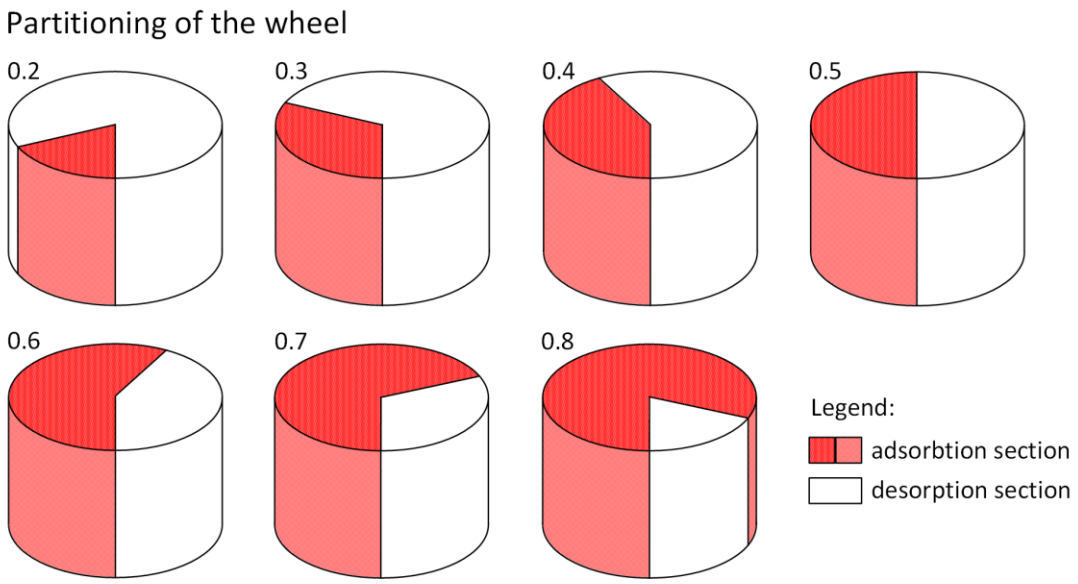

Figure 4-33: Schematic of the different wheel partitions

'Partition of the wheel' refers to the size of the wheel available for the adsorption side. Consequently, the desorption size of the wheel amounts to one minus the value reported.

The sensitivity analysis is carried out to investigate if the overall system would benefit in form of either an increase in recovery rate for a constant adsorbent mass (Figure 4-34), or in form of a decrease in overall adsorbent mass requirement for a constant recovery rate of 97% (Figure 4-35).

Figure 4-34 shows the effect of partitioning on the recovery rate and working cycle capacity at three different rotational speeds. Partitioning the wheel either to have more area available for adsorption and less for desorption, or less area for adsorption and more for desorption, reduces for all the studied cases the recovery rate nearly equally. This leads to a bell-shaped dependency of the recovery rate on the partitioning of the wheel. A slightly better recovery rate is achieved for a reduced adsorption area and a larger desorption area, than the other way round. However, the difference between both sides is less than 0.2% recover rate. The effect of partitioning the wheel on the working cycle capacity is marginal. The sensitivity of adsorbent mass requirement to partitioning is shown in Figure 4-35. Changing the partitioning from 0.5 (50% adsorption / 50% desorption) increases the adsorbent

mass requirement in all rotational speed cases investigated. The working cycle capacity is at its optimum for an equally partitioned wheel. The bell shaped trend of Figure 4-34 and Figure 4-35 can be explained by the fact, that for both, adsorption and desorption, the Langmuir isotherm is used to describe the adsorbed amount as a function of the partial pressure of the gas phase, with the Langmuir isotherm parameter being the same. Therefore, they follow the same dependencies.

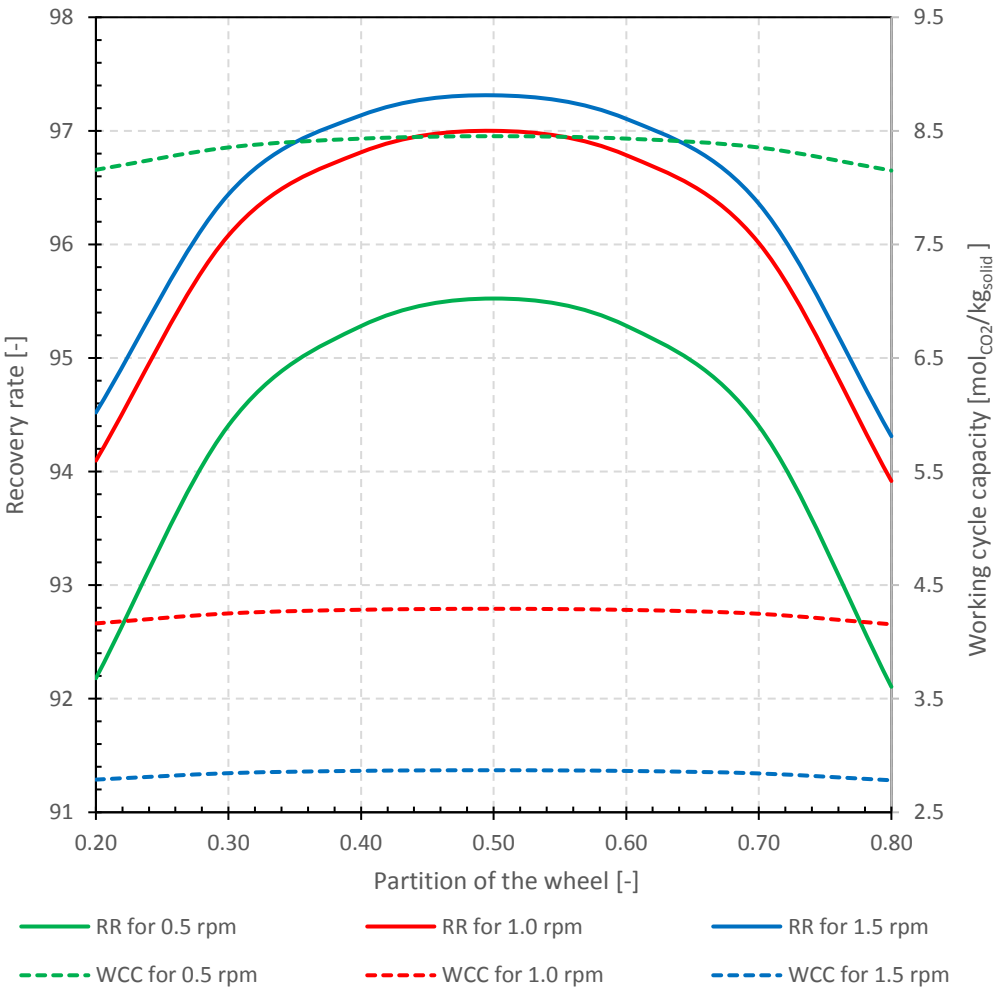

Figure 4-34: Sensitivity of recovery ratio and working cycle capacity to partitioning of the wheel for different rotational speeds; flue gas composition for SEGR configuration in parallel; adsorbent mass = 598t

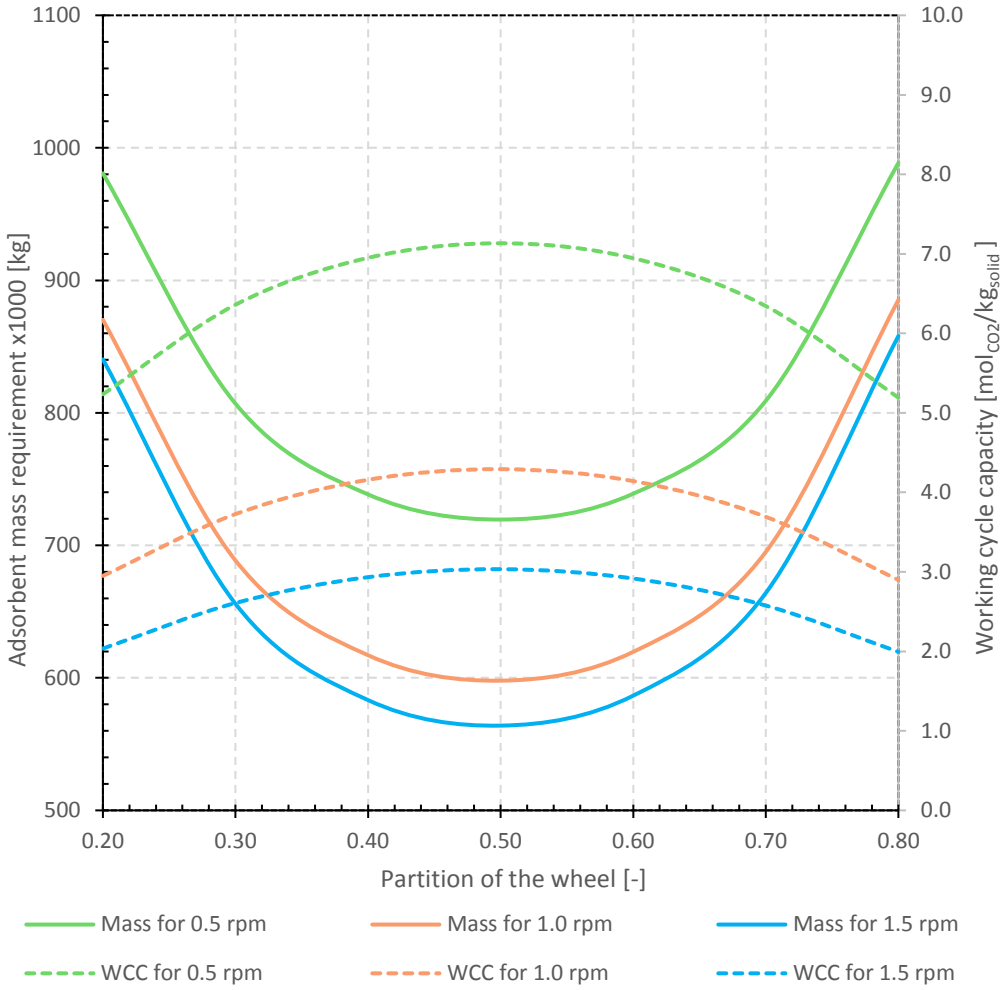

Figure 4-35: Sensitivity of adsorbent mass and working cycle capacity to partitioning of the wheel for different rotational speeds; flue gas composition for SEGR configuration in parallel; recovery rate 97%

4.3 Results of Leakage Considerations

The direction of leakage in the regenerative rotary CO2 transfer wheel can be controlled by choosing the most favourable location for the fans to overcome the pressure drops across the system. The preferred direction for the gap leakages is from the air to the flue gas side. Other important aspects to consider for the positioning of the fans are power consumption and temperature rise due to compression. For the flue gas stream the pressure drop depends on the HRSG, the gas/gas heat exchanger,

the gas conditioning system in form of a direct contact cooler, the regenerative rotary CO2 transfer wheel, the stack and the ducts. For the air stream the pressure drop depends on the regenerative rotary CO2 transfer wheel and the ducts.
In configuration with regenerative rotary CO2 transfer wheels, the booster fan for the flue gas side can be located at three different positions (Position A, B and C), the air fan for the ambient air side can be located at two different positions (Position 1 and 2). All possible locations are illustrated in Figure 4-36 accordingly.

For the flue gas stream these are:

- Downstream of the gas/gas heater and upstream of the DCC. Position A in Figure 4-36.
- Downstream of the DCC and upstream of the regenerative rotary CO2 transfer wheels. Position B in Figure 4-36.
- Downstream of the regenerative rotary CO2 transfer wheels and upstream of the stack. Position C in Figure 4-36.

For the air stream these are:

- Downstream of the regenerative rotary CO2 transfer wheels. Position 1 in Figure 4-36.
- Downstream of the gas turbine and upstream of the regenerative rotary CO2 transfer wheels. Position 2 in Figure 4-36.

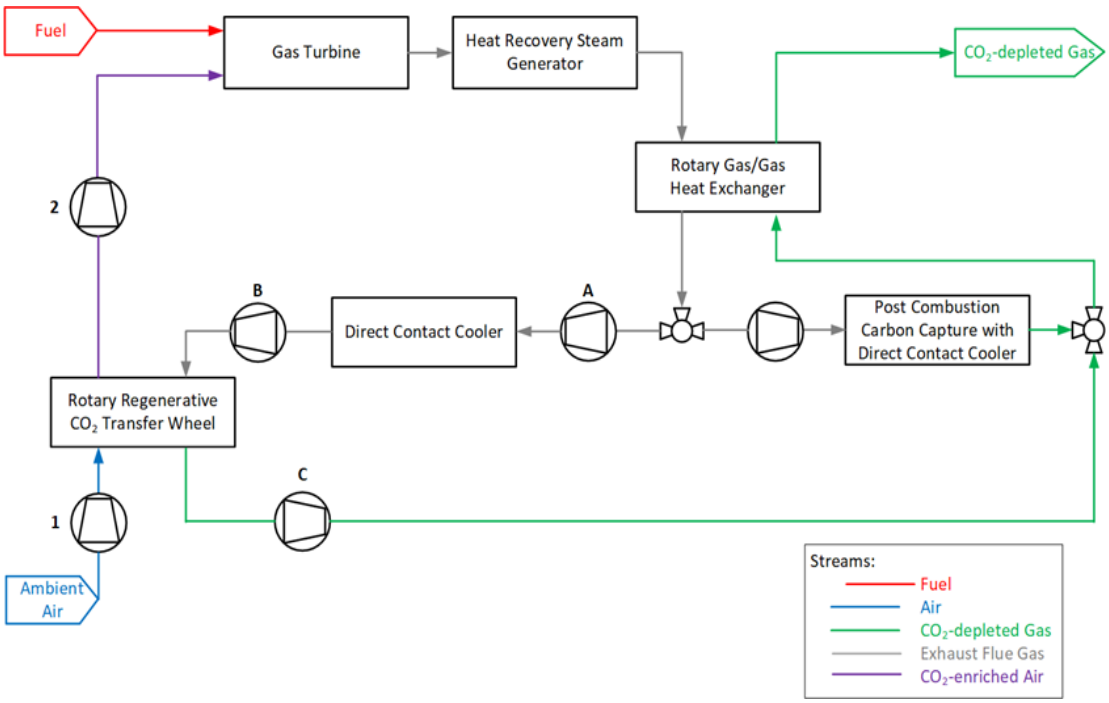

Figure 4-36: Block flow diagram showing all possible locations for the fans

The discussion below is summarized in Table 4-5.

Since lower gas temperatures lead to smaller volumetric flow rate for a given mass flow rate, locating the fan downstream of the DCC (Position B) offers the advantage of a smaller fan size and lower power consumption. However, overcoming the pressure drop of the downstream elements would lead to a higher pressure of the flue gas stream in the wheel leading to higher leakages into the air stream than alternative locations. Additionally, the flue gas inlet temperature into the regenerative rotary CO2 transfer wheel would be more challenging to control. As previously shown in Figure 3-13, the flue gas inlet temperature has a direct effect on the CO2-enriched air temperature. Increasing the CO2-enriched air temperature derates the gas turbine and reduces the gas turbine power output. Therefore, it is important to maintain the lowest temperature possible for the CO2-enriched air entering the gas turbine compressor.

Locating the fan upstream of the DCC (Position A) would allow for better temperature control at the regenerative rotary CO2 transfer device inlet. Likewise for option B, a location upstream of the wheel leads to higher pressure on the flue gas side in the CO2 transfer device and thus leads to leakages from the flue gas to the air stream.
Position C creates a leakage from the air stream to the flue gas stream. Due to a reduced mass flow rate, as a result of the transferred CO2, the power consumption of the fan is lower. However, the CO2-depleted flue gas stream temperature is increased after the adsorption process and would lead to a higher volumetric flowrate and higher power consumption of the fan. Furthermore, operation below atmospheric pressure of the adsorption part of the transfer wheel would marginally counteract the adsorption process itself.
Therefore, Positon A is recommended as the preferential location for the flue gas fan. It results in a better controlled flue gas inlet temperature into the CO2 transfer device and does not affect the adsorption process.

For the air stream there are two possible positions for the fan.
Position 2 is not the preferential option. As a result of the higher temperature of the CO2-enriched air stream, the volumetric flow is higher and leads to a higher power consumption. Due to the CO2 transfer, a higher mass flow rate has to be driven to the gas turbine inlet, leading to a possible larger fan requirement. By creating a sub-atmospheric pressure in the CO2 transfer device, the leakage direction created would be from the flue gas stream to the air stream.
Locating the fan in Position 1 leads to a higher than atmospheric pressure in the regenerative rotary CO2 transfer wheel, creating a leakage direction from the air stream to the flue gas stream. The lower mass flow of the air stream compared to location 2 results in a smaller size of fan. An increase in air temperature is unavoidable, which positively effects the desorption process of the regenerative rotary CO2 transfer wheel and increases the power consumption in the compressor of the gas turbine by increasing the inlet CO2-enriched air temperature.

Table 4-5: Comparison of the advantages and disadvantages of possible fan locations

Fan position	Advantages	Disadvantages
A (downstream of the gas/gas heater)	- Flue gas temperature rises before the DCC because of compression, which allows for a better temperature control for the inlet temperature at the CO2 transfer device	- Higher temperature and volumetric flow - Leakage from flue gas to air stream
B (downstream of the DCC)	- Lower temperature and volumetric flow	- Due to the compression the flue gas temperature rises. Since the rise occurs after the cooler control at the CO2 transfer device inlet is worse - Leakage from flue gas to air stream
C (downstream of the CO2 transfer device)	- Leakage from air stream to flue gas stream	- Below atmospheric operation of the CO2 transfer device has an effect on the adsorption - Higher temperature and volumetric flow after adsorption
1 (upstream of the CO2 transfer device)	- Lower mass flow rate before CO2 transfer - Leakage from air stream to flue gas stream - Higher temperature assists desorption	- Higher temperature at CO2 transfer device inlet
2 (downstream of the gas turbine)		- Higher temperature and volumetric flow after CO2 transfer - Leakage from flue gas to air stream - Higher mass flow rate after CO2 transfer

Assumed values for pressure drops through the different elements within the control volume analysis, as shown in Table 4-6, are used as an initial guess of the pressure rise to be provided by the booster fan. The qualitative representation of the pressure

drop profile within the controlled volume for the preferred flue gas fan position is illustrated in Figure 4-37.

Table 4-6: Assumed pressure drops of the different elements

Element	Assumed pressure drop	Dependencies
HRSG	2-3 kPa	Typical values of pressure drop in a HRSG.
Direct contact cooler	1 kPa	Depending on volumetric flow.
Rotary heat exchanger	2 kPa	Depending on mass flow, velocity and element length. Gas/gas heater up to 2 kPa/side
Rotary regenerative CO2 transfer wheel	3 kPa	Depending on bed height, gas velocities and liquid flow rates.
Ducts	2 kPa	Depending on length, overall assumed value.

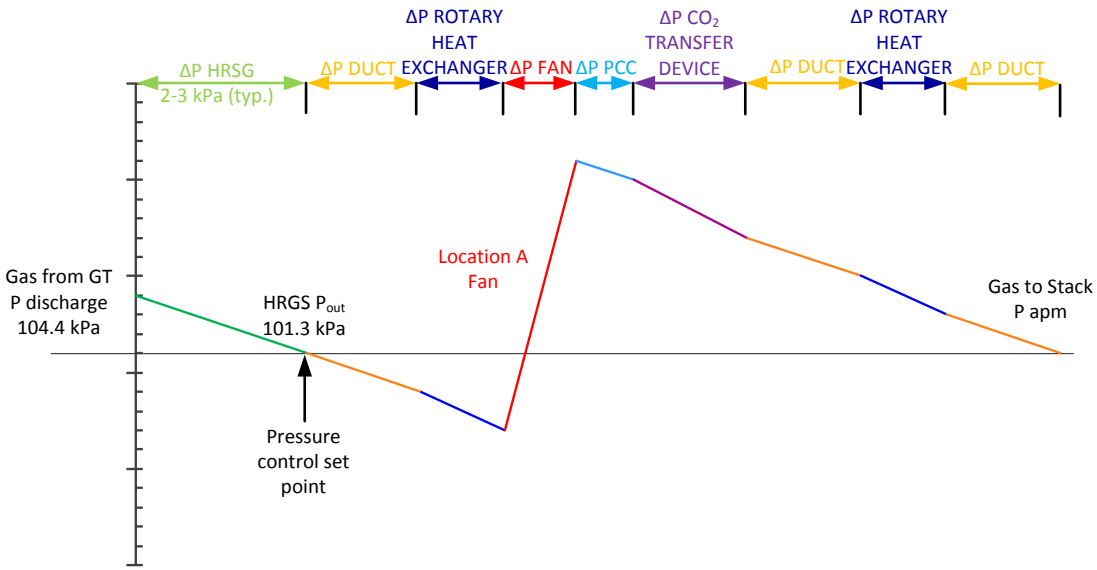

Figure 4-37: Illustrative pressure profile within the analysed control volume for preferred fan Position A

4.4 New Insights

The breakthrough curve measurements for a gas composition similar to the SEGR configuration in parallel (97/96) validate the assumptions made in the kinetic model for the operational conditions. It further shows that kinetic data, obtained through breakthrough measurements of an adsorbent in a laboratory isothermal fixed bed tubular reactor setup and equilibrium parameters can be used to predict the behaviour of the adsorbent in a rotary regenerative CO2 transfer wheel. This makes screening for promising adsorbent material for this kind of technology possible.

The kinetic model shows that the equilibrium model under-predicts the required adsorbent mass for a needed recovery rate of 97% for SEGR in parallel by factor of 3.7. A total mass of KOH activated carbon of 598t per GT-HRSG train will be needed to achieve a recovery rate of 97% at a rotational speed of 1 rpm. It highlights the importance of further development in adsorbent material. Especially in the region of high recovery rates, where the kinetic model predicts an exponential increase in adsorbent mass, better adsorbent materials are needed, to get to a number of wheels that are practical and financially reasonable.
Several adsorbent properties determine the final adsorbent mass requirement. These are:

- Saturation capacity
- Enthalpy of adsorption
- Equilibrium constant
- Temperature independent pre-exponential constant / Diffusion coefficient
- Geometrical factor of the adsorbent structure

To show exemplary in which direction the adsorbent development would need to go to achieve a 20% reduction in adsorbent mass requirement, starting from the activated carbon used to verify the rotary wheel model, the different property values, that would achieve a reduction of 20%, while the others stay constant, are listed in Table 4-7. An increase in saturation capacity by 26%, or an increase in the enthalpy

of adsorption by 3%, an increase in the temperature independent pre-exponential constant by 28%, or an increase in the geometrical factor from 15 to 20 would all be sufficient to achieve the 20% of solid mass reduction. The equilibrium constant in the case of the KOH activated carbon is already at a value achieving a maximum in reduction, so it is not possible to achieve a further reduction of 20% in adsorbent mass requirement by changing the equilibrium constant without changing any other properties.

Table 4-7: Prospective adsorbent property values to achieve a reduction in adsorbent mass requirement; *the geometrical factor is not specific the used adsorbent

Adsorbent properties	Unit	KOH activated carbon	20% Reduction
Saturation capacity (qs)	mol/kg	10.82	13.62
Enthalpy of adsorption (-ΔHads)	KJ/mol	17.44	18.03
Temperature independent pre-exponential constant (DcCO2 0)	S-1	12.995	16.695
Geometrical factor	-	15*	20

In a bottom-up approach the predicted mass by the kinetic model is used to size the regenerative rotary CO2 transfer wheel and determine the number of wheels needed. Two different approaches, are used to calculate the number of wheel devices needed. The classic approach uses the standard maximum currently available diameter of rotary heat exchangers supplied by Howden and adapts the height of the rotor to fit in the bulk volume. It leads to three wheel devices of 24m in diameter and 2.26 m in height needed. The second approached, a design optimisation, assumes a maximum diameter of the wheel based on the practicality of the diameter size, in an attempt to lower the number of wheel devices and the pressure drop, associated with a height increase. This results for the mass of adsorbent predicted by the kinetic model in two wheel devices of 30m in diameter and 2.17 m in height.

The kinetic model is used to assess kinetic adsorbent properties and operational conditions, which have an impact on adsorbent mass requirement and the recovery rate of the regenerative rotary CO2 transfer device, in an attempt to push the limits of process intensification.

The sensitivity analysis shows an optimum value for the temperature independent pre-exponential diffusion constant at 40 m^2/s. Further increases are marginal for both recovery rate increase and adsorbent mass reduction.

The evaluation of the effect of an increased specific heat capacity of the adsorbent on the mass requirement shows only a low to moderate effect.

The optimisation study of the surface heating area, given by the surface of the adsorbent, indicates that a further increase in this adsorbent property is not necessary. It appears to be high enough, to not add any further resistance to heat transfer. This has been shown for a variety of different honeycomb-monolithic activated carbon adsorbents, reported in the literature.

The operation parameter rotational speed can be used to push recovery rate and adsorbent mass reduction. It can be interpreted similar to an increase in L/G ratio in liquid CO2 scrubbing technologies. The increase in rotational speed leads to a higher mass rotation, therefore higher mass flow of adsorbent. Consequently each kg of adsorbent mass has to treat less flue gas and hence has to adsorb less mol of CO2 per time unit. It is however, depending on the previous design point (recovery rate and rotational speed). If the system is built for a high recovery rate of 95% and higher, the effect of an increase in rotational speed on the recovery rate will be marginal, since the driving force of the process limits the recovery rate. In general rotational speeds of 0.5-2 rpm are acceptable and should be considered during design development.

The results of the assessment of flue gas and air inlet temperature remain similar to previous assessment results performed with the equilibrium model. However, the effect of either temperature increase shows a larger impact on the CO2-enriched air outlet temperature, then predicted by the equilibrium model. Since a higher air inlet temperature into the compressor derates the gas turbine power output, measures need to be taken to limit the heat transfer into the CO2-enriched air stream. This can

be achieved by keeping the air inlet and the flue gas outlet temperature as low as possible.

Changing the partitioning of the rotary wheel in either way, towards or away from more adsorbent for adsorption, leads to a loss in recovery rate and an increase in adsorbent mass. This can be explained by the fact that adsorption and desorption in the simulation are using the same parameters for the adsorption equilibrium isotherms and the kinetics. Therefore the trend shown in the sensitivity analysis for partitioning of the wheel would be looking different, if the isotherm for adsorption and isotherm for desorption would look different, which would be the case for example with a desorption hysteresis in the isotherm.

Chapter 5 Integrated System Design and Performance Modelling

To assess the performance of a SEGR devices using adsorption technology on new build CCGTs with integrated PCC and on existing CCGTs with integrated PCC and retrofitted SEGR devices, a rigorous integrated model of the different parts of the power plant, flue gas conditioning system, selective CO2 transfer unit, capture plant and compression train is necessary. The models are developed in gCCS v1.1.0 (Process Systems Enterprise) (PSE Enterprise 2016a), an add-on built on the wider gPROMS modelling platform, using provided model libraries, or the gPROMS language interface in gCCS for model developers.

The developed rotary regenerative CO2 transfer wheel model, used as SEGR unit, is covered in the previous Section 3.4 and the results of the optimisation of the model are described in Chapter 4.

This section focuses on models used to evaluate the overall power plant performance. A schematic overview of the overall process model is given in Figure 5-1. The overview follows the flow of the CO2 through the different models. The page number in the figure indicate the position of the detail process flowsheet of the sub-models. Other variables, which are not shown in the overview, are process water, steam and power. For illustrative reasons parallel trains are not shown in the diagram.

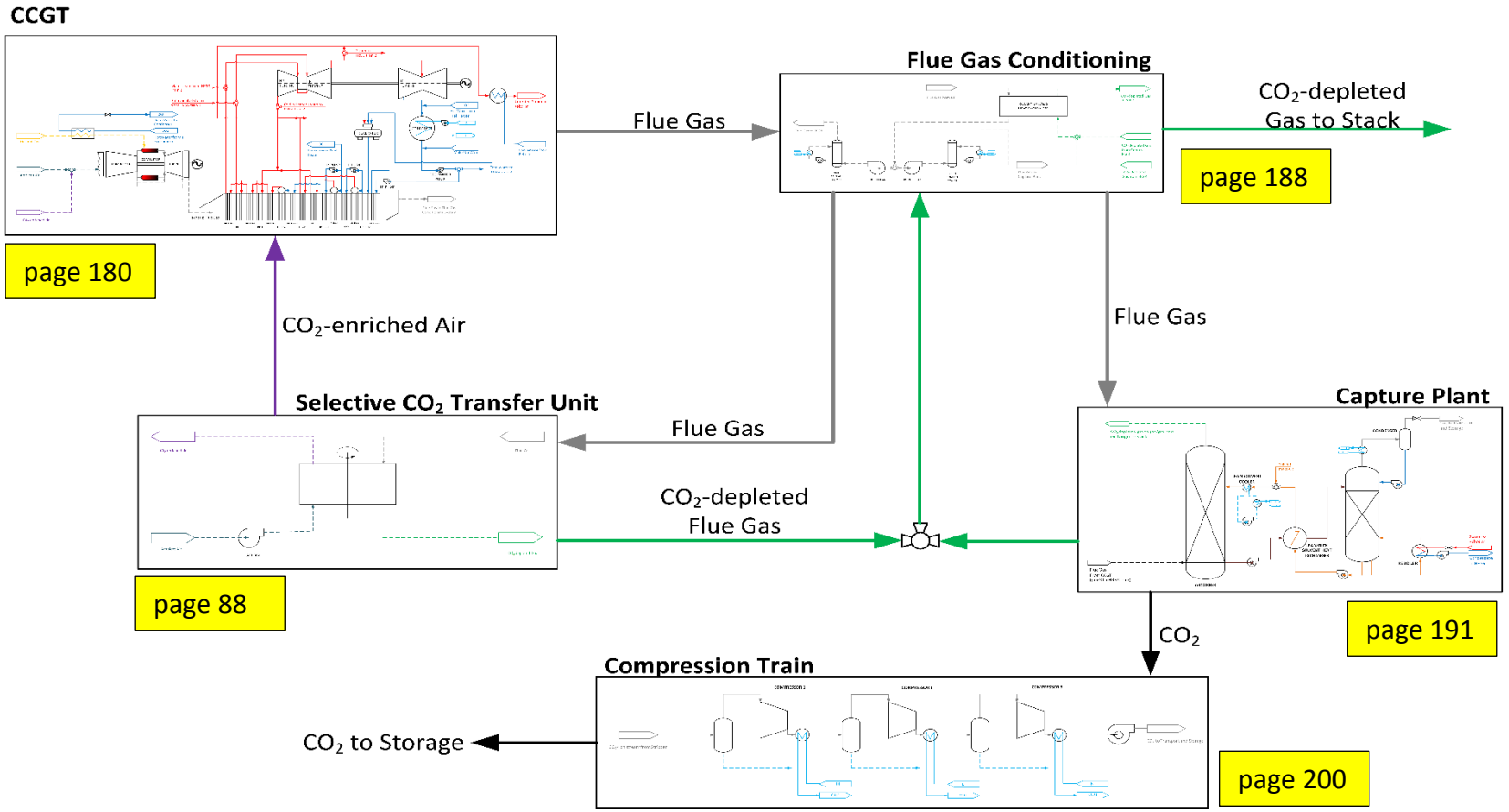

Figure 5-1: **Schematic overview of the integrated power plant, SEGR unit, capture plant unit and compression train of the modelled CCGT with CCS and SEGR power station. Parallel trains are not shown in the diagram. Considered configurations consist of two parallel GT, HRSG, PCC and compression trains. The steam turbines are shared between both trains**

5.1 Overview of the Base Case Configurations

The considered base case configurations consist of two parallel GTs, HRSGs, flue gas conditioning systems and compression trains, sharing one set of steam turbines between both trains. The capture plant unit consists either of:

- One absorber and stripper column per gas turbine train, illustrated in the block flow diagram in Figure 5-2 and referred to as the case Full Scale Capture Plant (Full Scale CP).
- Two absorber and two stripper columns per gas turbine train, illustrated in the block flow diagram in Figure 5-3 and referred to as the case Half Scale Capture plant (Half Scale CP). The case Half Scale CP features the possibility to interconnect the solvent flows of the system, making it possible to switch one absorber off, while supplying the full amount of available solvent flow rate to one absorber and regenerating the solvent using both strippers.

The assumption regarding the number of capture plants for the base cases is based on two FEED studies. The FEED study by Gassnova to retrofit CCS to the existing CCGT at Kårstø power plant, Norway, assumes two absorber to treat the flue gases (Gassnova 2019). The study by the UK Energy Technology Institute for new build thermal power with CCS on five different locations in the UK, assumes one absorber per GT train to treat the flue gases (ETI 2017).

The rotary regenerative CO2 transfer device is fitted to both configurations to study the option of retrofitting CO2 recycling and the associated limitations in Chapter 7.

The configurations are then referred to as Full Scale Capture Plant with SEGR and Half Scale Capture Plant with SEGR.

In the assessment of the effect of the rotary regenerative CO2 transfer device on a new build CCGT with PCC, the SEGR device is fitted to the Full Scale Capture Plant configuration and is then referred to as New Build.

The net power output of the CCGT with post-combustion capture $\dot{W}_{CCGT,net}$ depends on the electrical power generated in the gas turbine $\dot{W}_{GT}$ and steam turbine $\dot{W}_{ST}$, the auxiliary power consumption of all the elements of the power plant $\dot{W}_{aux}$ and the efficiency of the generator $\eta_{generator}$, as shown in Equation (5.1). The auxiliary power consumption is given by water pumps for process and cooling water $\dot{W}_{water\ pumps}$, the fuel compressor $\dot{W}_{fuel\ compressor}$, fans $\dot{W}_{fans}$, the energy needed in the post-combustion capture plant $\dot{W}_{aux\ PCC}$ and the compression of the CO2 for transport $\dot{W}_{CO2\ compression}$ (Equation (5.2)).

$$\dot{W}_{CCGT,net} = (\dot{W}_{GT} + \dot{W}_{ST} - \dot{W}_{aux}) \cdot \eta_{generator} \quad (5.1)$$

$$\dot{W}_{aux} = \dot{W}_{water\ pumps} + \dot{W}_{fans} + \dot{W}_{fuel\ compressor} + \dot{W}_{aux\ PCC} + \dot{W}_{CO2\ compression} \quad (5.2)$$

The energy consumption of the drive for the regenerative rotary transfer wheel has to be added to the auxiliary power consumption. However, the drive's power consumption is with 20-25kW negligible.

The thermal efficiency of the CCGT with PCC $\eta_{th,CCGT}$ can be evaluated according to Equation (5.3) and (5.4).

$$\eta_{th,CCGT} = \frac{\dot{W}_{CCGT,net}}{\dot{Q}_{in,LHV}} \quad (5.3)$$

$$\dot{Q}_{in,LHV} = \dot{m}_{fuel} \cdot LHV \quad (5.4)$$

With $\dot{Q}_{in,LHV}$, the heat input into the CCGT with PCC and $\dot{m}_{fuel}$, the mass flow rate of the fuel and LHV, the low heating value of natural gas.

The interfaces of the CCGT with integrated post-combustion carbon capture and SEGR are:

- Flue gas to capture plant, flue gas to SEGR unit, flue gas out of the capture plant and flue gas out of the SEGR unit

- Low pressure steam extraction to supply reboiler of the capture plant and recycling into the steam cycle.
- Air for combustion in the GT passing through the SEGR unit.
- CO2-depleted gas of the SEGR unit and the capture plant to the flue gas conditioning system.

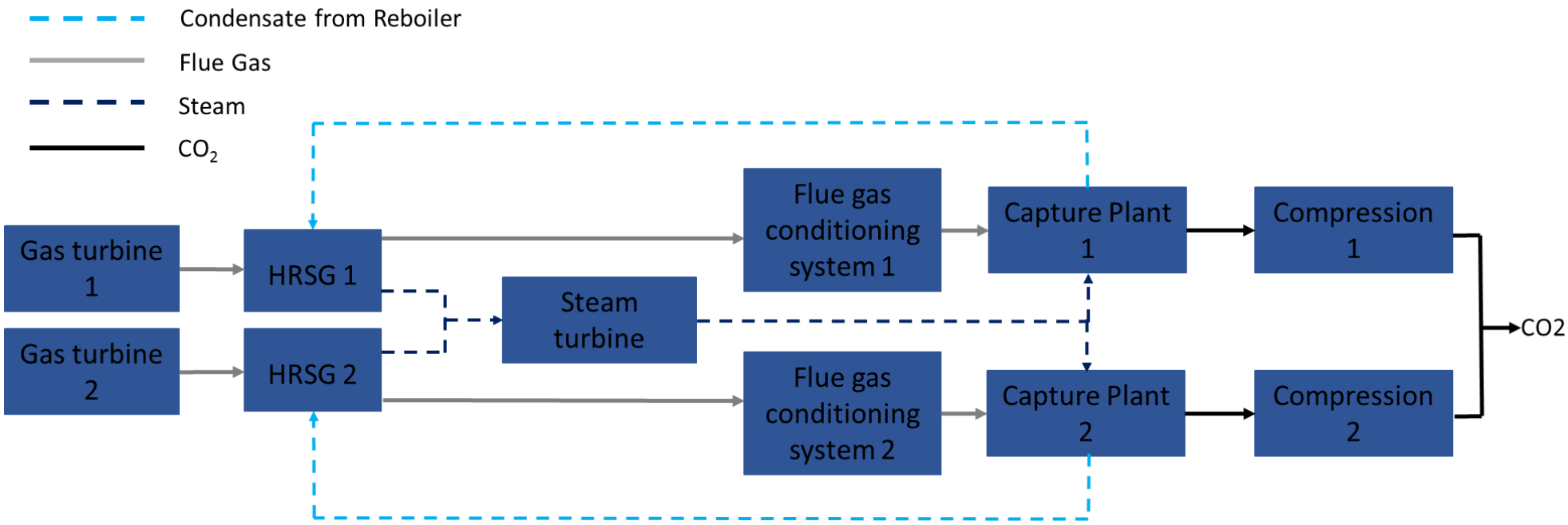

Figure 5-2: Block flow diagram of case Full Scale CP, an integrated CCGT with flue gas conditioning, capture plant and compression train

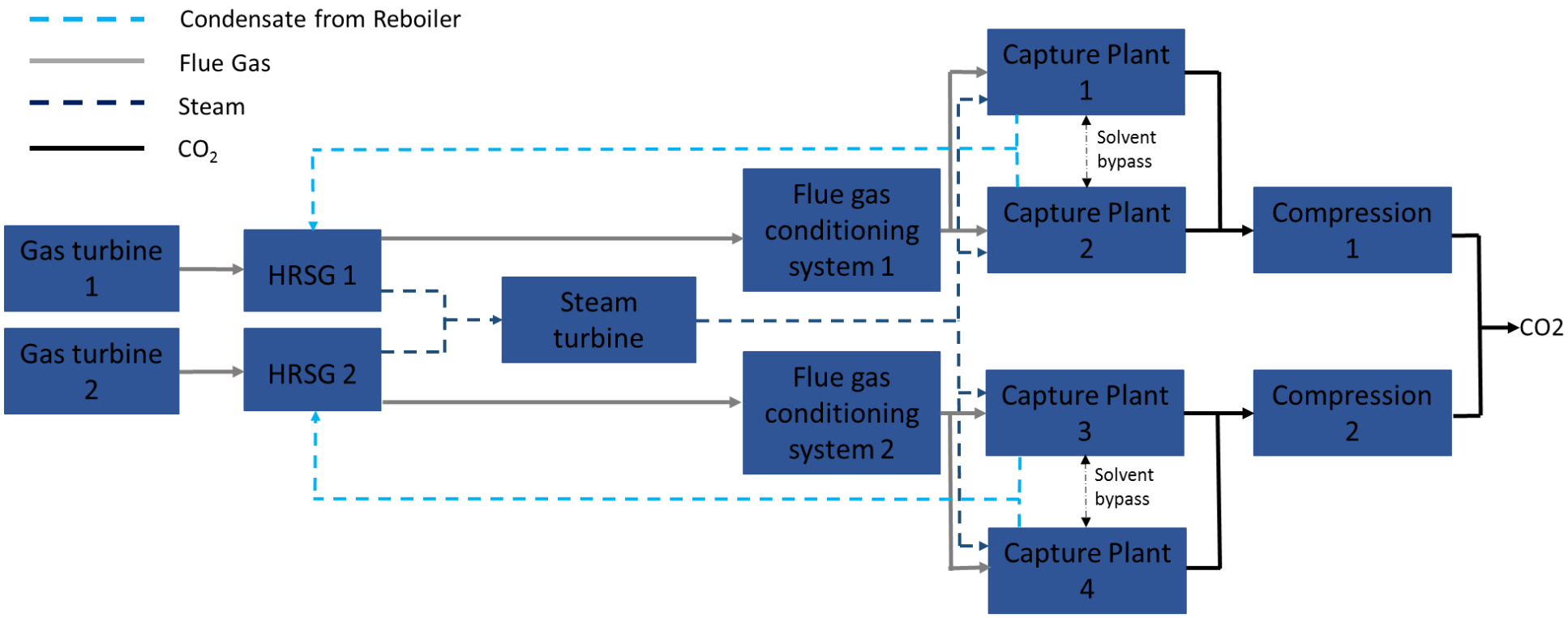

Figure 5-3: Block flow diagram of case Half Scale CP, an integrated CCGT with flue gas conditioning, capture plant and compression train

5.2 Combined Cycle Gas Turbine Power Plant

5.2.1 Process Description

The investigated large CCGT plant, with a net power output of 800 MWe, follows the configuration proposed by IEAGHG (IEAGHG 2012). It is a 2-in1 configuration of two General Electrics (GE) Class F (GE9371) gas turbines producing exhaust gas for their HRSGs. The gas turbine at 100% load has a pressure ratio of 18, a turbine inlet temperature of 1370◦C and an air fuel ratio (AFR) of 40.5 on mass basis at ISO ambient condition (Herraiz et al. 2018). In the two HRSGs, steam for the bottoming cycle is jointly generated. Parallel trains are shown in the previous block flow diagrams in Figure 5-2 and Figure 5-3.

The process flow diagram of the CCGT is illustrated in Figure 5-4. For illustrative reasons parallel trains are not shown in the flow diagram.

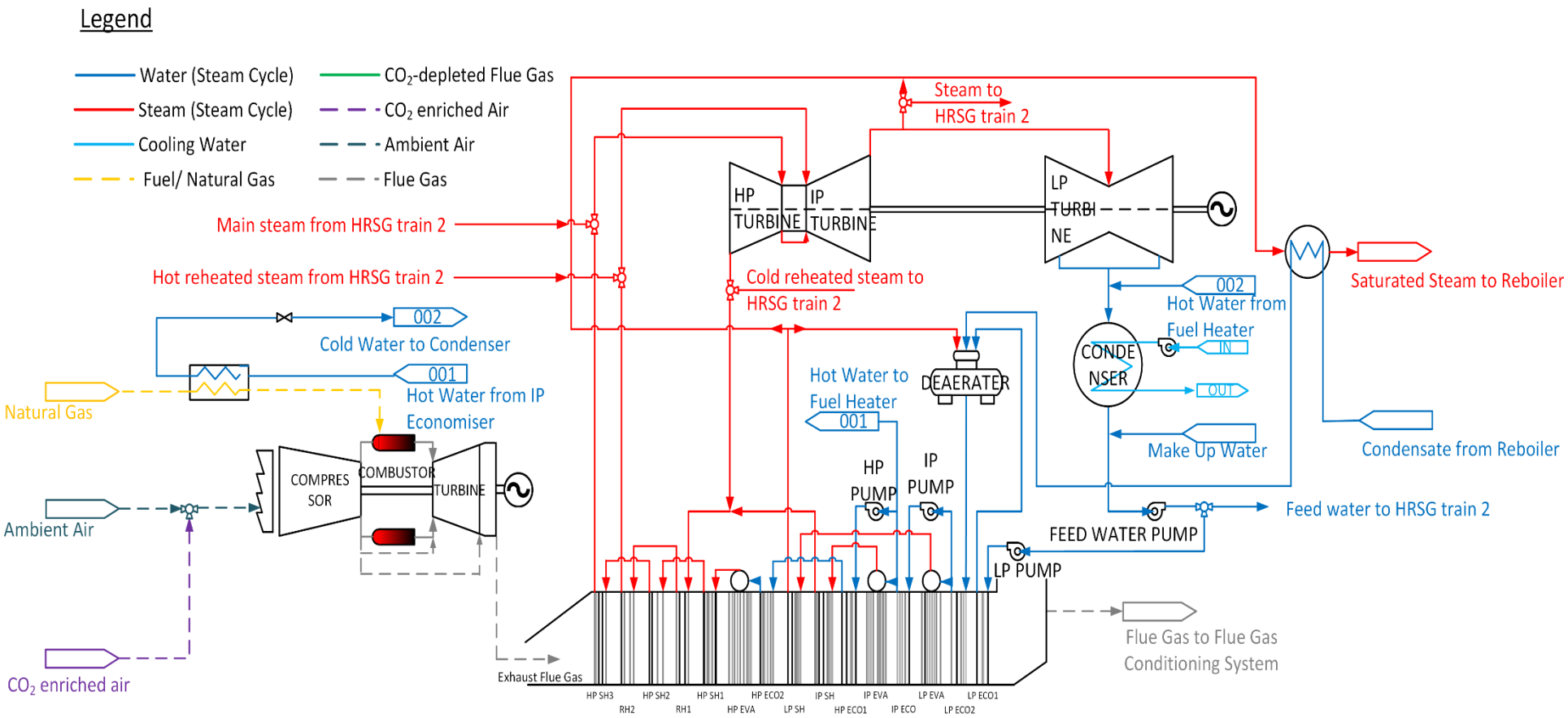

Figure 5-4: Process flow diagram of the CCGT (adapted from (Herraiz et al. 2018))

5.2.2 Model Description

The CCGT power plant model, consisting of customised models for each piece of equipment, was built by (Herraiz 2016) in gPROMS Model builder. It is integrated, for this work, in gCCS with a flue gas conditioning system, the CO2 capture plant, the CO2 compression train and the rotary regenerative CO2 transfer wheel. A detail description of the CCGT plant model can be found in (Herraiz 2016). In the following, the most relevant aspects of the model are summarised.
Additional technical data and assumption to perform the simulations are included in Appendix D.

Gas Turbine

The gas turbine is validated by (Herraiz 2016) to match reported technical specifications for GE F-class engines (General Electric Power Generation 2016).
Exhaust gas composition and flow rates are gas turbine engine specific, since design parameters, such as turbine inlet temperature, define excess of air (Herraiz 2016). However (Herraiz 2016) assessed the performance of the gas turbine at off-design operation based on a dimensionless analysis to provide results extendable to other gas turbine technology. Details can be found in (Herraiz 2016) and (Herraiz et al. 2018).

The gas turbine consists of three parts. The air compressor, the combustor, and the turbine. The net power output of the gas turbine $\dot{W}_{GT,net}$ depends on the difference between the power generated in the turbine section $\dot{W}_t$ and the work input to compress the air $\dot{W}_c$ for the combustion of the fuel and for the cooling of the blades in the turbine section as shown in Equation (5.5). Where, η_{mech} is the mechanical efficiency of the compressor.

$$\dot{W}_{GT,net} = (\dot{W}_t - \frac{\dot{W}_c}{\eta_{mech}}) \quad (5.5)$$

In the compression section the total pressure of air entering the combustor of the GT is increased to achieve a design pressure ratio, through a series of stages.

The compressor work $\dot{W}_c$ is calculated based on the mass flow of air $\dot{m}_{air}$ swallowed by the compressor and the change in enthalpy of the air between the inlet $h_{0\ air,in}$ and the outlet $h_{0\ air,out\ isentropic}$, divided by the isentropic efficiency η_c (Equation (5.6)). The isentropic efficiency of the compressor is calculated according to Equation (5.7).

$$\dot{W}_c = \dot{m}_{air} \cdot \frac{h_{0\ air,out\ isentropic} - h_{0\ air,in}}{\eta_c} \tag{5.6}$$

$$\eta_c = \frac{h_{0\ air,out\ isentropic} - h_{0\ air,in}}{h_{0\ air,out} - h_{0\ air,in}} \tag{5.7}$$

In the combustor the fuel is burned under lean conditions (pre-mixed Dry Low NOx). The air in the combustor is controlled to have an optimal air-fuel-ratio.

Two design parameters are used in the gas turbine model. The combustor outlet temperature (COT) and the turbine inlet temperature (TIT).

The maximal turbine inlet temperature is given by the GT manufacturer and is the temperature resulting after the combustion gases are mixed with cooling air to limit the turbine inlet temperature. Assumptions applied in the model by (Herraiz 2016) are based on literature (Eldrid, Kaufman, and Marks 2001; Walsh and Fletcher 2004). Those assumption are a TIT of 1370◦C, a constant combustion efficiency of 99.8% and an exhaust gas composition based on a complete combustion.

The combustion gases drive, at a high temperature and pressure, the turbine blades, supplying power to drive the compressor and the electrical generator. The turbine work $\dot{W}_t$ is described as the difference in stagnation enthalpy as the exhaust flue gases expand, multiplied by the mass flow of the exhaust flue gases $\dot{m}_{EFG}$ (Equation (5.8)). The actual work and outlet temperature are evaluated based on the isentropic efficiency η_t of the turbine, as indicated in Equation (5.8).

$$\dot{W}_t = \dot{m}_{EFG} \cdot (h_{EFG,out} - h_{EFG,in}) \tag{5.8}$$

$$\eta_t = \frac{h_{EFG,out} - h_{EFG,in}}{h_{EFG,out\ isentropic} - h_{EFG,in}} \quad (5.9)$$

Further considered in the model by (Herraiz 2016) are turbine blade cooling and pressure loss. The swallowing capacity of the turbine is calculated based on the pressure drop in the combustion chamber.

For a fixed compressor geometry, as assumed by the model, the mass flowrate swallowed by the compressor will change with changing density, temperature or composition of the CO2-enriched air. The inlet air mass flow rate is therefore calculated in the model as a function of the density of CO2-enriched air. Fuel mass flow and cooling air flow rate will be matched to maintain the same combustor outlet temperature and turbine inlet temperature.

Steam cycle

The steam cycle consist of two three pressure level HRSGs with double reheat and a turbine train with high (HP), intermediate (IP) and low pressure (LP) cylinders, connected to a 50Hz fixed-speed generator. The arrangement of the heat transfer banks and design parameter are according to (Herraiz 2016) modelled and sized to IEAGHG standard.

The steam generated in both HRSGs are fed to one steam turbine. The design inlet temperature of the steam is 600◦C and is kept constant. Admission and discharge pressure are defined by the pressure levels in the HRSG. The temperature difference between the HP superheated and reheated steam and the flue gas entering the high-pressure superheater and reheater, the so called approach temperatures, will vary with changing flue gas outlet temperature coming from the GT. The inlet pressure to the HP steam turbine is 170 bar. The inlet temperature to the IP steam turbine is 40 bar. The pressure in the IP-LP crossover and in the LP steam turbine matches the requirement in the reboiler of the capture plant, which is saturated steam 3 bar, plus 1 bar pressure loss along the pipe.

The power generated in the steam cycle $\dot{W_{ST}}$ is calculated according to Equation (5.10), as the sum of the power of each steam turbine (j ϵ HP,IP,LP), which

is given by the change in enthalpy of the steam at the inlet $h_{steam,in}$ and outlet $h_{steam,out}$, multiplied by the mass flow of steam in each turbine $\dot{m}_{steam,j}$. The isentropic efficiency of the steam turbines is given by Equation (5.11).

$$\dot{W_{ST}} = \sum_j \dot{m}_{steam,j} \cdot (h_{steam,in} - h_{steam,out})_j \quad (5.10)$$

$$\eta_{ST} = \frac{h_{steam,in} - h_{steam,out}}{h_{steam,in} - h_{steam,out\ isentropic}} \quad (5.11)$$

Both base case power plants lead to the same technical and operational parameters for the CCGT plant. The CCGT power outputs and thermal efficiencies are shown in Table 5-1. The gas turbine technical and operational parameters are listed in Table 5-2. The parameters of the HRSG are shown in Table 5-3, and Table 5-4 lists the technical and operational parameters of the steam turbine.

The net power output of the CCGT with PCC is 795 MWe with a net thermal efficiency of 53%. The gas turbine has an air to fuel ratio of 40.5 at 100% load, leading to a net power output of 285.8 MWe with a net thermal efficiency of 38.2%.

Table 5-1: CCGT power output and thermal efficiencies for Case Full Scale CP and Case Half Scale CP

CCGT	Units	
Gas turbine net power per GT-HRSG train	MWe	285.8
Gas turbine net power	MWe	571.6
Open Cycle thermal efficiency	%LHV	38.2
Steam turbine power	MWe	257.4
Fuel heat input per GT-HRSG train	MWth	748.4
CCGT gross power	MWe	834.6
CCGT gross thermal efficiency	%LHV	55.8
CCGT net power output	MWe	795.0
CCGT net thermal efficiency	%	53.1

Table 5-2: The gas turbine technical and operational parameters for Case Full Scale CP and Case Half Scale CP

Gas turbine	**Units**	
Model		GE 9371FB
Air mass flow rate	kg/s	641.8
Fuel mass flow rate	kg/s	16.1
Compressor		
Inlet pressure drop	kPa	1
Pressure ratio	-	18.1
Compressor isentropic efficiency	%	79.5
Combustor		
Pressure drop	%	5.01
Combustor efficiency	%	99.80
Pressure fuel in	bar	27.20
Temperature fuel in	◦C	117
Turbine		
Turbine back pressure	bar	1.039
Turbine inlet temperature	◦C	1371
Turbine isentropic efficiency	%	92.1
Exhaust flue gas		
Pressure	kPa	1.039
Temperature	◦C	643
Exhaust flue gas flow rate	mol/s	23178.5
Exhaust flue gas flow rate	kg/s	657.9
Composition:		
CO_2	%vol	4.21
H_2O	%vol	8.82
N_2	%vol	74.21
O_2	%vol	11.87
Ar	%vol	0.89
Molar mass	g/mol	28.38
Gas turbine performance		
Net power	MW	285.8
Net thermal efficiency	%	38.2
Net heat rate	kJ/kWh	9428.1

Table 5-3: Heat recovery steam generator technical and operational parameters for Case Full Scale CP and Case Half Scale CP

Heat Recovery steam generator	Units	
Flue gas mass flow	kg/s	657.9
Gas inlet temperature	◦C	643
Gas stack temperature	◦C	114.
Feed water temperature	◦C	32
Gas inlet pressure	bar	1.039
Gas outlet pressure	bar	1.013

Table 5-4: Steam turbine technical and operational parameters for Case Full Scale CP and Case Half Scale CP

Steam turbine	Units	
HP steam turbine		
Live steam molar flow	mol/s	9586.6
Live steam mass flow	tn/h	621.6
Pressure in	bar	170.0
Temperature in	◦C	600
Pressure out	bar	45.2
Temperature out	◦C	394
Isentropic efficiency	%	88.1
IP steam turbine		
Hot reheated molar flow	mol/s	10445.1
Hot reheated mass flow	tn/h	677.2
Pressure in	bar	40
Temperature in	◦C	600
Pressure out	bar	3.8
Temperature out	◦C	267
Isentropic efficiency	%	92.4
LP steam turbine		
Turbine exhaust molar flow	mol/s	6205.1
Turbine exhaust mass flow	tn/h	402.3
Pressure in	bar	3.8
Temperature in	◦C	267
Pressure out	bar	0.048
Exhaust steam quality	%	91.9
Isentropic efficiency	%	88.0

5.3 Flue Gas Conditioning System

5.3.1 Process Description

The flue gas exiting the HRSG is entering the flue gas conditioning system. The conditioning system is needed to adjust flue gas conditions, namely water content and temperature, to the operation of the capture plant and to the power plant stack. It consists of a gas/gas rotary heat exchanger and two booster fans and direct contact coolers (DCC) operating in parallel, one for the flue gas stream entering the capture plant and one for the flue gas stream entering the CO2 transfer unit. This is illustrated in Figure 5-5.

In work conducted by (Herraiz et al. 2015) a gas/gas rotary heat exchanger is introduced as a heat integration option for reducing cooling water requirements. Therefore, a gas/gas heat exchanger is also utilised in the process simulation presented in this work. In the gas/gas rotary heat exchanger, sensible heat from the flue gas is transferred to the CO2-depleted gas. Booster fans to overcome the pressure loses of the system upstream and direct contact coolers are implemented to condition the flue gas to the process inlet condition requirements of the systems upstream, capture plant and CO2 transfer unit.

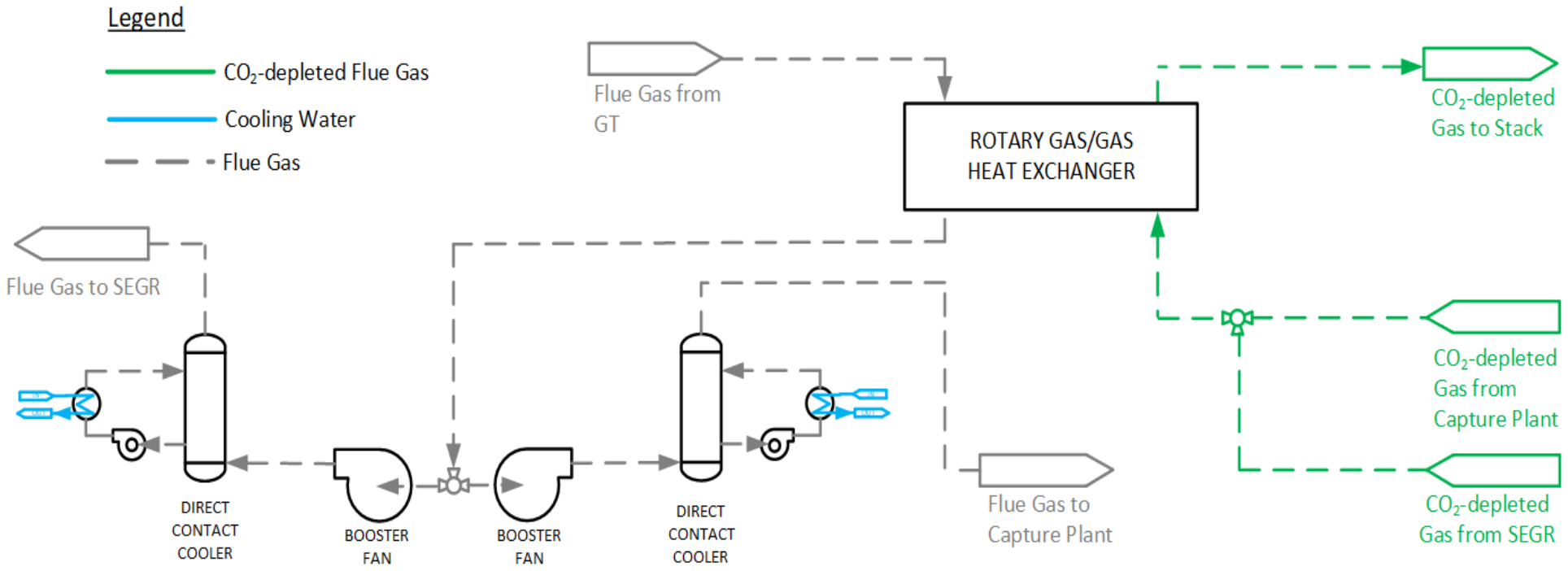

Figure 5-5: Process flow diagram of the flue gas conditioning system

5.3.2 Model Description

The model for the rotary gas/gas heat exchanger in the overall process flow simulation was developed by (Herraiz et al. 2015) in gPROMS and is implemented for this work in gCCS as a simplified heat exchanger, using a pinch approach of 20°C.

After the rotary gas/gas heat exchanger the flue gas is split according to the SEGR ratio to leave either for the capture plant or the SEGR unit.

The flue gas leaving for the capture plant is conditioned to 1.05 bar and 40°C by booster fan and DCC.

The flue gas leaving for the rotary regenerative CO2 transfer wheel is conditioned to 1.03 bar and 30°C by the booster fan and the DCC. This part is switched of for the base case configurations.

This system partly contributes to the auxiliary plant losses in form of $\dot{W}_{fans}$, the work required to operate the booster fans.

5.4 Post-Combustion Capture Plant

5.4.1 Process Description

As reference system, a benchmark post-combustion solvent capture system of a conventional 30%wt MEA based chemical absorption process is utilised, as illustrated in Figure 5-6.

Flue gas from the flue gas conditioning system downstream the HRSG is entering the capture plant through the absorber. In the absorber the flue gas gets into contact with the solvent and CO2 is chemically bond to the solvent and leaves the absorber as CO2 loaded solvent/ CO2 rich solvent at the bottom. The CO2-depleted flue gas leaves the capture plant through the top of the absorber. The CO2 loaded solvent is heated up in the lean/rich solvent heat exchangers before entering the stripper section. In the stripper the solvent is regenerated with the heat provided in the reboiler. The energy is needed to provide sensible heat required to heat up the solvent, heat to desorb the CO2 from the solvent and latent heat to evaporate the water. To provide the heat necessary in the reboiler, low-pressure steam is extracted

after the intermediate-pressure turbine of the steam turbine cycle and returned into the cycle after the condenser. A stream mixture of CO2 and water vapour leaves the top of the stripper. The vapour is then condensed in the condenser, separated from the gas phase and recycled back into the top of the stripper. The CO2-rich stream leaves the capture plant in the direction of the compression train. The regenerated lean solvent is pumped back to the absorber top, passing through the lean/rich solvent heat exchanger, and being conditioned in the lean solvent cooler.

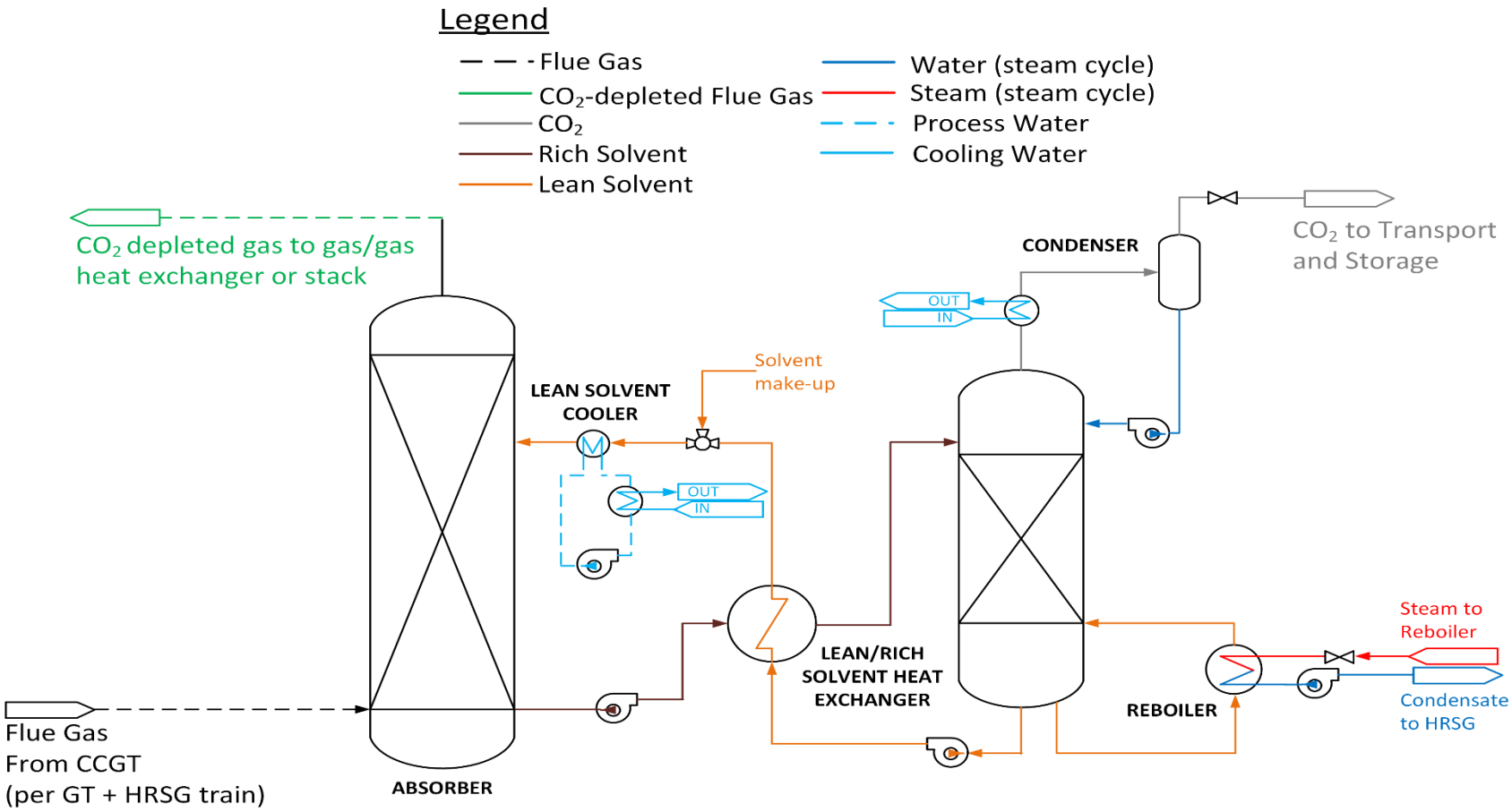

Figure 5-6: Process flow diagram of the post-combustion CO2 capture plant

5.4.2 Model Description

The capture plant is modelled using the gCCS library models. The thermodynamic package used for predicting the physical properties of CO2 in MEA is gSAFT (PSE Enterprise 2016c).

Absorber and stripper are rate-based separation models, taking resistance to mass and heat transfer into account. The structured packing chosen is Mellapak 250Y. The capture plant design has been validated against a design examined by (IEAGHG 2012). The methodology applied for sizing absorber and stripper follows (Herraiz et al. 2018; Oexmann 2011; González Díaz 2016; Sanchez Fernandez et al. 2016; Freguia and Rochelle 2003) and is presented in Section 5.4.3.

Reboiler and condenser temperatures and pressures were adopted from (Herraiz et al. 2018).

The capture plant contributes to the auxiliary plant losses in form of the work required to pump the solvent around ($\dot{W}_{solvent\ pumps}$) and in form of the reboiler duty $\dot{W}_{reboiler\ duty}$ to regenerate the solvent (Equation (5.12)).

$$\dot{W}_{aux\ PCC} = \dot{W}_{solvent\ pumps} + \dot{W}_{reboiler\ duty} \tag{5.12}$$

The specific reboiler duty is defined as the thermal energy required to regenerate the solvent per unit of mass of CO2 recovered, as shown in Equation (B.1).

$$\dot{W}_{reboiler\ duty} = \frac{Thermal\ energy\ rate}{CO2\ mass\ flow} \tag{5.13}$$

5.4.3 Sizing and Optimisation

As previously mentioned, the methodology applied for sizing absorber and stripper follows (Herraiz et al. 2018; Oexmann 2011; M. E. Diego, Bellas, and Pourkashanian 2018; González Díaz 2016; Sanchez Fernandez et al. 2016; Freguia and Rochelle 2003).

The absorber diameter is established for a flue gas velocity corresponding to 75% of the flooding-point velocity. The flooding point is reached, when the mass flow of the gas is high enough to carry away upwards all the solvent liquid.

To determine the optimum absorber height, the established diameter of the absorber and the capture rate (90%) are kept constant, while the packing height is increased in increments. Increasing the packing height leads to a higher contact area between the flue gas and the solvent, which in return leads to a higher CO2 solvent loading at the bottom of the absorber. This results in an increased solvent capacity and therefore to a reduction in solvent amount for the same CO2 capture rate. The reduced amount of solvent flow leads to a reduction in reboiler duty. The maximum in CO2 loading corresponds to the equilibrium value of the partial pressure of CO2 in the flue gas. The optimum height is reached when a further increase in adsorbent height leads to an only marginal gain in solvent loading (<0.2%). The results of such an optimisation for the large absorber in Case Full Scale CP can be seen in Figure 5-7. The black dotted line marks the optimum height of the absorber. The optimised absorbent height for the large absorber in Case Full Scale CP and the two smaller absorbers in Case Half Scale CP is 14 m, with an absorber diameter of 19.6 m in Case Full Scale CP and 13.8 m in Case Half Scale CP.

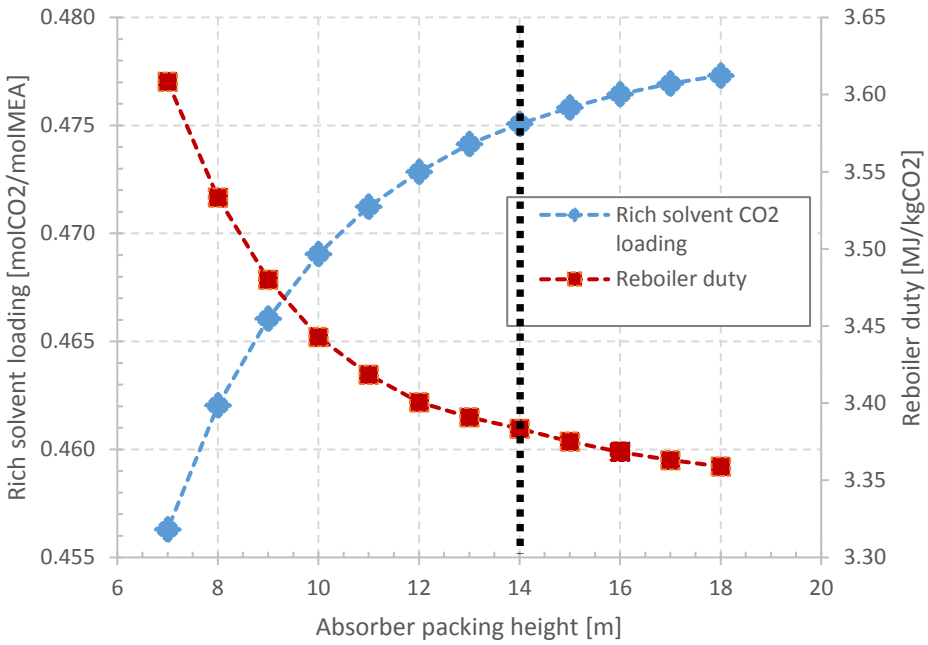

Figure 5-7: Height optimisation of the absorber of Case Full Scale CP for a constant capture rate of 90%

Sizing of the stripper follows the same approach as for the absorber. First the diameter is established corresponding to 75% of the flooding-point velocity, followed by the height optimisation based on the change in lean solvent loading reaching less than 0.2% change in loading with increasing height of the stripper, for a constant capture rate of 90%. This leads to a stripper height of 8 m and stripper diameter of 8 m for the capture plant of Case Full Scale CP and to a stripper height of 8 m and stripper diameter of 5.7 m for the capture plant in Case Half Scale CP.

Reboiler duty and compression work are sensitive to the stripper pressure. The energy penalty of the capture plant is however more sensitive to the energy requirement to regenerate the solvent, linked to the reboiler duty than to the work requirement to compress the CO2 up to transportation and storage pressure. Therefore, although a higher outlet pressure at the top of the stripper reduces the compression work, the maximum power output of the overall CCGT with PCC is achieved for a minimum reboiler duty. (Sanchez Fernandez et al. 2016)

Hence, to determine the minimal reboiler duty, a sensitivity analysis of the stripper pressure is performed. The stripper pressure is increased in increments, while the solvent mass flow is adjusted to the design capture rate of 90%, leading to a change in liquid solvent to flue gas ratio, which is called L/G ratio. (Freguia and Rochelle 2003; Herraiz et al. 2018)

The results of this sensitive analysis for the capture plant of Case Full Scale CP are depicted in Figure 5-8. The minimum reboiler duty is achieved for a stripper pressure of 1.94 bar, corresponding to a L/G ratio of 1.3. The same results are achieved for Case Half Scale CP.

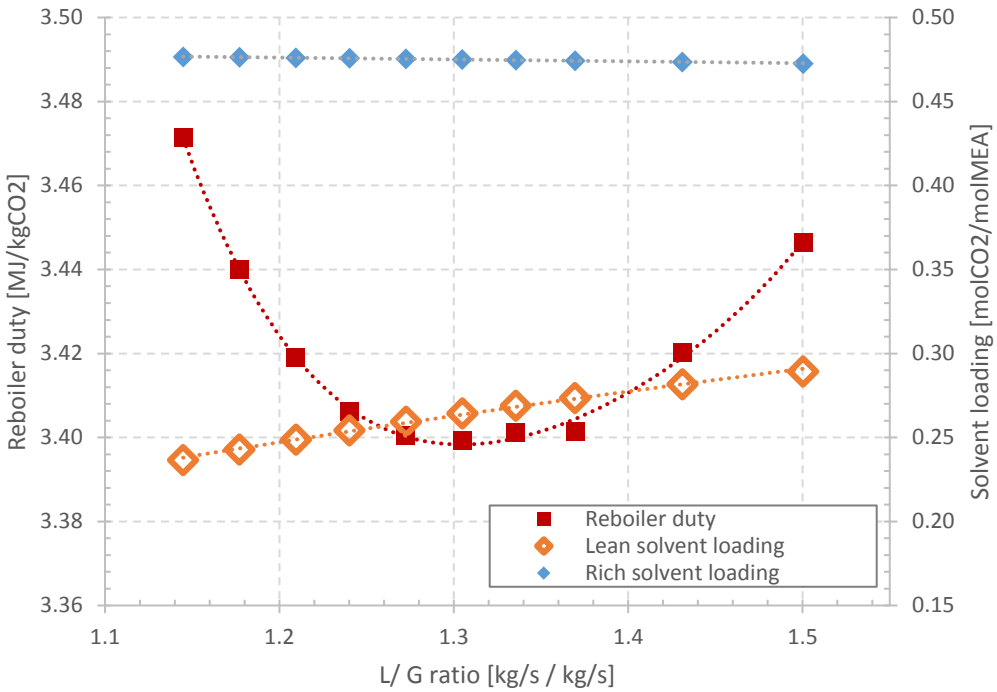

Figure 5-8: Optimisation of the reboiler duty of Case Full Scale CP for a constant capture rate of 90%

Table 5-5 provides a summary of the relevant process conditions and design parameters associated with the capture plants of Case Full Scale CP and Case Half Scale CP.

Table 5-5: Technical and operational parameters of the CO2 capture plants of Case Full Scale CP and Case Half Scale CP, per GT-HRSG train

Case		Full Scale CP	Half Scale CP
	Units		
Flue gas temperature to absorber	°C	40	40
Flue gas pressure to absorber	bar	1.05	1.05
Flue gas mass flow rate per absorber	kg/s	649.9	324.9
CO2 concentration in the flue gas	mol%	4.29	4.29
Capture rate	%	90	90
Absorber flooding fraction	%	75	75
Absorber packing height	m	14	14
Absorber diameter	m	19.6	13.8
No. of absorbers	-	1	2
Total packing volume per train	m^3	4207	4188
Lean solvent temperature to absorber	°C	40	40
Stripper flooding fraction	%	75	75
Stripper packing height	m	8	8
Stripper diameter	m	8	5.7
No. of strippers	-	1	2
Total packing volume per train	m^3	402	401
Stripper pressure	bar	1.94	1.94
Reboiler solvent temperature	°C	120	120
Reboiler pressure	bar	3	3
Reboiler duty	MJ/kg_{CO2}	3.40	3.40
Lean loading	mol_{CO2}/mol_{MEA}	0.264	0.264
Rich loading	mol_{CO2}/mol_{MEA}	0.475	0.475
L/G ratio	-	1.30	1.30
Overhead condenser temperature	°C	40	40

5.4.4 Operating Parameters and Strategies for SEGR Retrofitting

Operating parameters and strategies need to be established in the context of a reduced flue gas flow towards the capture plant for SEGR retrofits in parallel.

Loading point

The operating parameter loading point of the absorber needs to be considered for lower gas mass flow rates. The loading point of an absorber is reached, when the gas velocity is high enough to restrict the flow of the solvent liquid. This can be

established by observing the pressure drop in the absorber. When the loading point is reached, the pressure drop increases at a higher rate until it reaches a further increase in pressure drop corresponding to the flooding point. Both points mark the start and end of the entrainment regime of a column. Hence, the absorber needs to be operated between those two points. The corresponding plots of F-Factor vs pressure drops per height of packing for Mellapak 250Y for different head pressures is provided by Sulzer (Sulzer Chemtech 2016) and is illustrated in Figure 5-9.

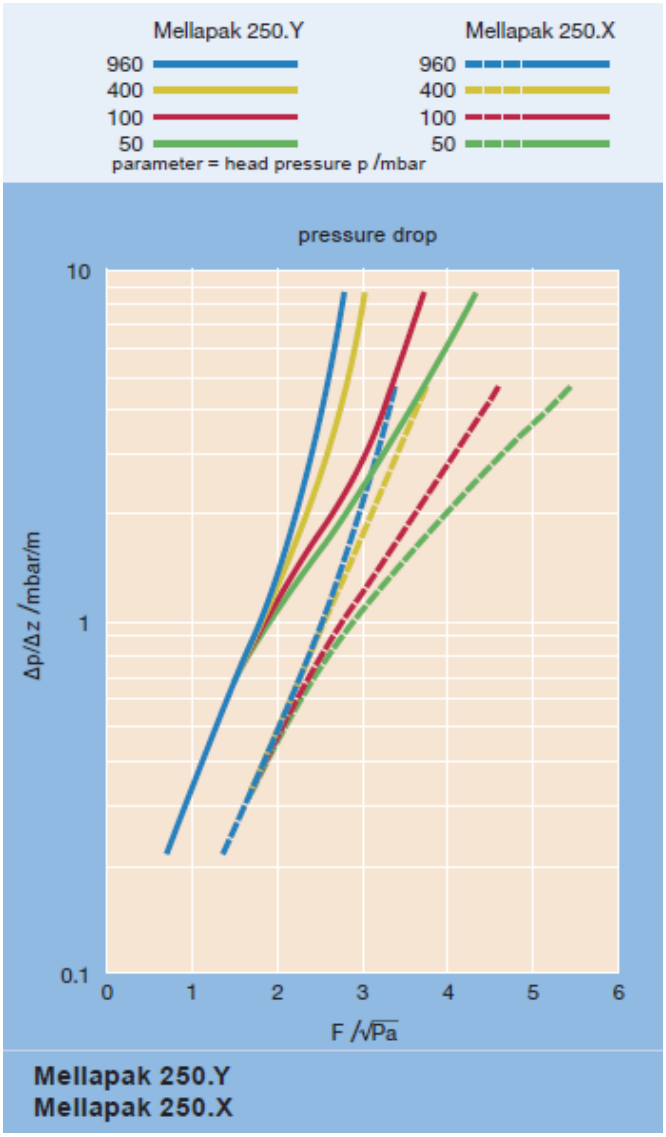

Figure 5-9: **F-Factor of the gas vs the pressure drop per m height of packing for Mellapak 250 Y and 250 X** (Sulzer Chemtech 2016)

The F-factor is defined as the product of gas velocity v_g and the square root of the gas density ρ_g as shown in Equation (5.14).

$$F = v_g \cdot \sqrt{\rho_g} \tag{5.14}$$

The F-factor corresponding to the loading point for Mellapak 250Y is 1.5 (Sulzer Chemtech 2016).

Operating mode

To operate the capture plant during a reduced gas mass flow encountered with SEGR in parallel, an operating mode for retrofitted capture plants needs to be chosen.

Possible operating modes follow the strategies developed for operating capture plants at part-load.

Three different strategies for part-load are proposed by (Sanchez Fernandez et al. 2016):

- Constant stripper pressure
- Constant L/G ratio in adsorber
- A combination of both above strategies

(Sanchez Fernandez et al. 2016) concludes, after assessing all three options, that the most efficient one is to keep the stripper pressure constant. For lower pressure and temperature in the stripper, more energy is required per kg of CO2 to achieve the same degree of solvent regeneration. Additionally, it increases the work required by the compression train to achieve the final transportation pressure.

Therefore, in the context of retrofitting SEGR to an existing capture plant, which decreases flue gas mass flow rates and increases CO2 flue gas concentration, a constant stripper pressure strategy will be followed.

5.5 CO_2 Compression Train

5.5.1 Process Description

A stream, consisting of desorbed CO2 (96 %vol) and water vapour leaves the condenser of the stripper at 40°C and 1.9 bar and enters the compression train. The compression train consists of a series of compressors, heat exchangers for intercooling and knock-out drums to condition the CO2 stream up to a purity of 99% at 110 bar for transport and storage.

5.5.2 Model Description

The model is developed in gCCS. The selected CO_2 compression system configuration consists of one train per GT-HRSG train. It is based on the European Benchmarking Task Force (EBTF) developed common framework 'European best practice guidelines for assessment of CO2 capture technologies' under the project acronym CAESAR (EBTF 2011). It comprises three compressor stages with appendant intercooling and water knock-out between each compression stage to lower power consumption for the compressor drive, followed by a pump. The flow diagram of the compression train is shown in Figure 5-10. The compressor stages increase the CO2 stream pressure up to critical pressure, at which CO2 is liquefied (~73 bar). The pump stage delivers the final transport pressure of 110 bar. Technical and operation parameters of the compression system are listed in Table 5-6.

The compression train contributes to the auxiliary plant losses in form of the work required to operate the compressors $\dot{W}_{CO2\ compression}$.

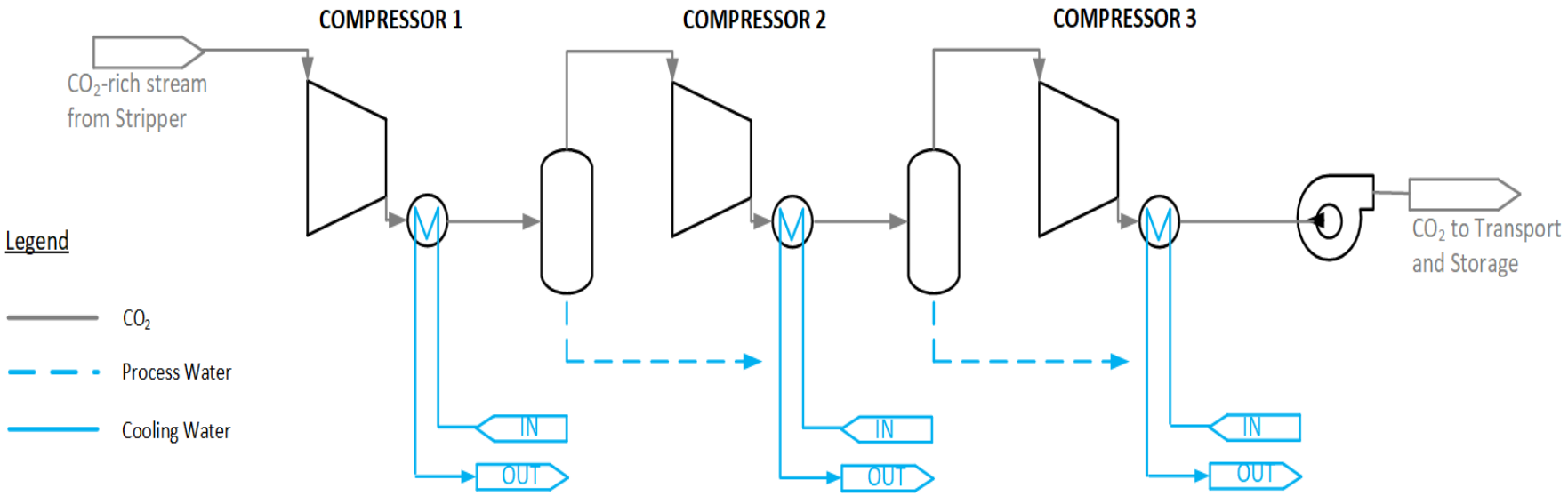

Figure 5-10: Process flow diagram of the CO2 compression train

Table 5-6: Technical and operational parameters of the compression systems (assumptions based on (EBTF 2011)**)**

Pressure for transport	110	bar
CO2 purity	99.9	%
Compression stages pressure ratios	2.9 / 4.34 / 4.33	-
Compressor polytropic efficiencies stage 1 and 2	80	%
Compressor polytropic efficiency stage 3	75	%
Intercooler stages	3	-
Intercooling outlet temperature	28	◦C
Pump efficiency	75	%
Cooling water temperature	18	◦C

Chapter 6 Integrated New-Build CCGT with PCC and Regenerative Rotary CO2 Transfer Wheel

In this chapter a configuration for a new build CCGT power plant with post-combustion capture and regenerative rotary CO2 transfer wheel in parallel, optimised for a 90% overall capture rate is investigated. The configuration will be referred to as 'New-Build'.

The aim is to assess the overall performance of the CCGT power plant and possible energy penalty savings and equipment size reduction in the capture plant, by adding regenerative rotary CO2 transfer devices.

To achieve an overall capture rate of 90% at a SEGR ratio of 70%, a selective CO2 transfer recovery rate of 97% and a capture rate in the capture plant of 96% need to be achieved.

The absorber of the capture plant is optimised for the flue gas mass flow rate corresponding to a SEGR ratio of 70% and a capture rate of 96%.

The results of the integrated simulations of a new build CCGT with PCC and regenerative CO2 transfer device are compared to the results of a conventional CCGT with PCC, as reported in Chapter 5 as Full Scale Capture Plant (Full Scale CP) configuration.

A block flow diagram of both studied cases including the characteristics of the main process streams can be found in Appendix G.

The chapter is divided into the following sections.

First, the New-Build configurations investigated is described in Section 6.1.

In Section 6.2, the adsorbent mass requirement for the SEGR unit in the New-Build configuration is established and the design parameters of the regenerative rotary CO2 transfer wheels for the New-Build application are reported.

Next, effect on the gas turbine (Section 6.3) and the steam cycle (Section 6.4) are investigated for the New Build configuration and compared to the gas turbine and steam cycle of a conventional CCGT with PCC.

Section 6.5 investigates the effect and design changes on the capture plant for the New-Build configuration, compared to the conventional configuration. Reductions in absorber packing volume and reboiler duty reductions are evaluated for a chemical absorption post-combustion capture system using an aqueous solution of 30 wt% MEA, as benchmarking solvent.

Finally, the overall effect on the power plant in form of power output is summarised and presented in Section 6.6.

6.1 Description of the New-Build Configurations

The considered New-Build configurations consist of two parallel trains of GT, HRSG, flue gas conditioning system, CO2 transfer devices, capture plant and compression trains, sharing one set of steam turbines between both trains.

The block flow diagram of the New-Build configurations is illustrated in Figure 6-1.

Exhaust gas leaving the HRSG passes through the heat recovery unit and is split according to a SEGR ratio to either pass through a blower and DCC towards the selective CO2 transfer device, or through a blower and DCC towards the capture plant. The conditions for the flue gas entering the capture plant is 40◦C and 1.05 bar. The flue gas entering the rotary regenerative CO2 transfer device is conditioned to 30◦C and 1.03 bar.

Air used for the combustion of the natural gas passes first through the selective CO2 transfer device, where it is enriched with CO2. The CO2-depleted gas streams from the selective CO2 transfer device and the capture plant are mixed and passed through the rotary gas/gas heat exchanger, being heated up before leaving to the stack.

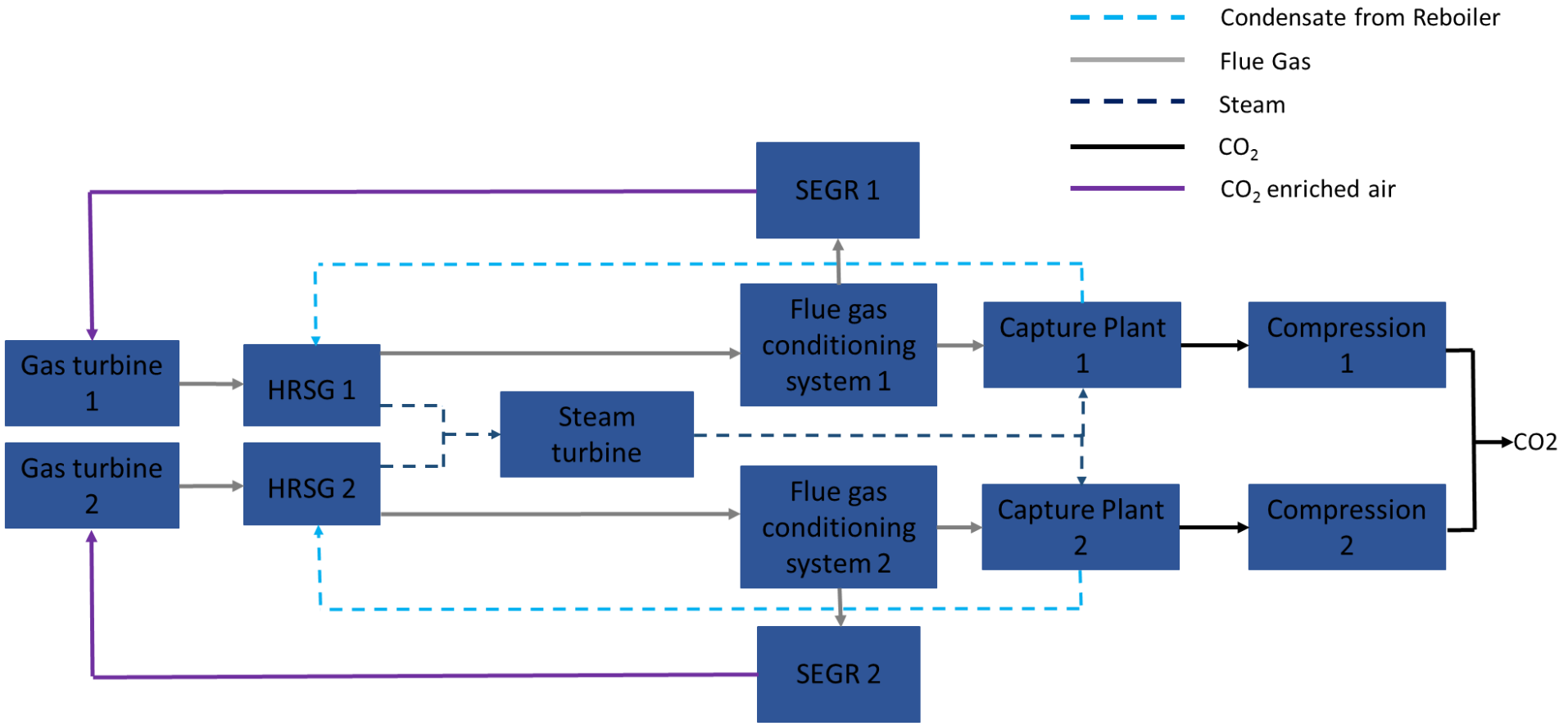

Figure 6-1: Block flow diagram of the configuration New-Build with SEGR; an integrated CCGT with flue gas conditioning, SEGR device, capture plant and compression train

6.2 Design of the Rotary CO2 Transfer Wheel

The regenerative rotary CO2 transfer wheel is sized to transfer 97% of the CO2 of the CCGT flue gas composition, for a SEGR ratio of 70%. Before entering the rotary regenerative CO2 transfer wheels, the flue gas is conditioned to 30◦C and 1.03 bar.

The exhaust gas stream variables entering the rotary wheel device for a fully integrated power plant with PCC and SEGR at a SEGR ratio of 70% are listed in Table 6-1.

Table 6-1: Exhaust flue gas stream variables entering the SEGR unit

Flue gas towards SEGR unit		
Temperature	°C	30
Pressure	bar	1.033
Molar flow rate	mol/s	14969.3
Composition:		
CO2	%mol	14.8109
H2O	%mol	4.1113
N2	%mol	70.4247
O2	%mol	9.80896
Ar	%mol	0.84

As solid adsorbent, the KOH activated carbon of Chapter 4 is utilised.

A rotational speed of 2rpm and a wheel partitioned equally in adsorption and desorption section are chosen for the regenerative rotary wheel to reduce the solid mass requirement, following the analysis of Section 4.2.6. The solid mass required for those flue gas conditions and composition for a recovery rate of 97% is 551 tonnes of solid KOH activated carbon. Applying the procedure detailed in Section 3.4.3, the number of needed wheel devices are calculated based on a honeycomb wall thickness of 1 mm and a pitch of 4.5 mm, leading to a bulk void fraction of 0.77. For a wheel diameter of 30 m and height of 2 m, two rotary wheel devices per GT/HRSG train are necessary for the predicted mass of adsorbent. The dimensions of the rotary CO2 transfer device are reported in Table 6-2.

Table 6-2: Requirements for the regenerative rotary CO2 transfer device for SEGR in parallel for the New-Build configuration

Flue gas		S-EGR Parallel
SEGR ratio	%	70
CO2 conc. at SEGR unit	mol%	14.8
Recovery rate	%	97.0
Adsorbent		
Material	-	KOH activated carbon
Mass x 1000	kg	551
Particle and Bulk		
Particle density	kg / m^3	952
Particle Volume	m^3	579
Bulk void fraction	-	0.77
Bulk volume	m^3	2516
Rotary wheel		
External diameter	m	30
Height	m	2
Basket Factor [Howden]	-	0.89
Rotor volume	m^3	1260
No. of devices	-	2

6.3 Effect on the Gas Turbine

Two GE Class F (GE9371) gas turbines are utilised in the model of the 2-in-1 configuration of a CCGT, with a compressor initially designed to operate with air.

As discussed in Section 5.1, the compressor of the gas turbine swallows a constant volume of air at full load (531.25 m^3/s), for a fixed compressor geometry. Therefore, the mass flowrate swallowed by the compressor will change with changing density, temperature or composition of the CO2-enriched air. At the same time the specific heat of the working fluid decreases with higher CO2 concentration. For illustration of the changes in specific heat and density, the sensitivity analysis on the change in working fluid properties with increasing SEGR ratio performed by Herraiz, can be found in the Appendix E, Figure E-1.

The air stream variables entering the compressor of the gas turbine are listed in Table 6-3. The CO2-enriched air temperature, coming from the rotary CO2 transfer wheels, rises by 9°C, compared to the configuration without SEGR. The CO2-enriched air has a CO2 concentration of 9.97 %mol compared to the 0.03 %mol in the not enriched air. Due to the changed flue gas composition the molecular weight of the gas changes, decreasing the molar flow rate by 3%. The density of the air enriched with CO2 increases by 2% for the New-Build configuration with an SEGR ratio of 70%.

Table 6-3: Air stream variables entering the compressor for the Full Scale CP and New-Build configuration, per GT-HRSG train

Air swallowed by GT compressor			
Configuration		Full Scale CP	New-Build
SEGR ratio	%	0	70
Temperature	°C	15	24
Pressure	bar	1.0030	1.0028
Air density	kg/m^3	1.209	1.237
Specific heat ration (C_p/C_v)	-	1.402	1.387
Molar flow rate	mol/s	22243.0	21623.7
Composition:			
CO2	%mol	0.0315	9.9739
H2O	%mol	1.0101	0.9097
N2	%mol	77.2953	69.6079
O2	%mol	20.7360	18.6737
Ar	%mol	0.9270	0.8348

Fuel mass flow and cooling air flow rates are matched to maintain the same combustor outlet temperature and turbine inlet temperature. Although the CO2-enriched air enters at 9°C hotter than the not enriched air, the lower specific heat ratio, caused by the addition of CO2, results in a lower compressor outlet temperature of 452°C instead of 464°C. This requires an increase in fuel mass flow rate of 4.3% in the combustor of the New-Build configuration compared to the configuration Full Scale CP. Resulting fuel mass flow rates as well as air fuel ratios in the combustor and flue gas stream variables at the turbine inlet are shown for both configuration in comparison in Table 6-4.

The higher mass flow rate through the turbine increases the gas turbine net power output by 4.3 MWe per GT-HRSG train, or 8.5 MWe for both gas turbines combined.

Table 6-4: Fuel mass flow rates, AFR and flue gas stream variables entering the turbine for the Full Scale CP and New-Build configuration, per GT-HRSG train

Flue gas after combustion			
Configuration		Full Scale CP	New-Build
SEGR ratio	%	0	70
Combustor			
Specific heat ration at inlet (C_p/C_v)	-	1.362	1.337
Fuel mass flow rate	kg/s	16.10	16.79
AFR		24.89	23.20
Combustion outlet temperature	◦C	1626	1626
Turbine inlet			
Turbine inlet temperature	◦C	1371	1371
Inlet pressure	bar	17.228	17.376
Inlet density	kg/m^3	3.565	3.774
Specific heat ration (C_p/C_v)	-	1.281	1.263
Molar flow rate	mol/s	22479.4	21919.5
Mass low rate	kg/s	637.7	652.7
Composition:			
CO2	%mol	4.3419	14.1403
H2O	%mol	9.0613	9.5230
N2	%mol	74.1140	66.5483
O2	%mol	11.5944	8.9907
Ar	%mol	0.8885	0.7977

6.4 Effect on the Steam Cycle

Exhaust gas, with changed composition, leaves the gas turbine at a higher mass flow rate and a higher temperature for the New-Build configuration. This results in a larger amount of heat available in the HRSG, leading to a higher steam mass flow rate for the steam turbines. For both configurations the exhaust gas stream variables entering the HRSG are listed in Table 6-5.

Table 6-5: Exhaust flue gas stream variables entering the HRSG for the Full Scale CP and New-Build configuration, per GT-HRSG train

Turbine exhaust gas towards HRSG			
Configuration		Full Scale CP	New-Build
SEGR ratio	%	0	70
Temperature	◦C	643	670
Pressure	bar	1.039	1.039
Density	kg/m^3	0.387	0.395
Specific heat C_p	J/mol·K	33.92	36.11
Mass flow rate	kg/s	657.9	673.3
Composition:			
CO2	%mol	4.2119	14.0150
H2O	%mol	8.8185	9.2640
N2	%mol	74.2099	66.6404
O2	%mol	11.8701	9.2819
Ar	%mol	0.8896	0.7988

A comparison of the heat transfer diagram of the heat recovery steam generators is presented in Figure 6-2. As illustrated, the steam turbine net power output increases by 32 MW. Due to the limitation of the superheated high pressure steam inlet temperature to 600°C, the approach temperature for the Full Scale CP is 43°C, compared to 70°C for the New-Build configuration, an increase of 39%. Yet, the Rankine efficiency increases for the New-Build configuration from 66% to 68%, due to the higher amount of heat recovered in the case of the New-Build configuration.

The steam cycle, as it is simulated here for the New Build case, uses the same pressure level as the steam cycle in the Full Scale CP. However, more thermal energy in form of higher temperature and higher mass flow rate, is available. Consequently, the steam cycle is not any longer optimised for the new process conditions. A re-design of the steam cycle adapting pressure levels and approach temperatures in the cycle would open up the possibility to access higher Rankine efficiency for the steam cycle. According to (González Díaz 2016) a supercritical HRSG could lead to an increase in LHV efficiency of up to 2.5 %. This should be considered for future work.

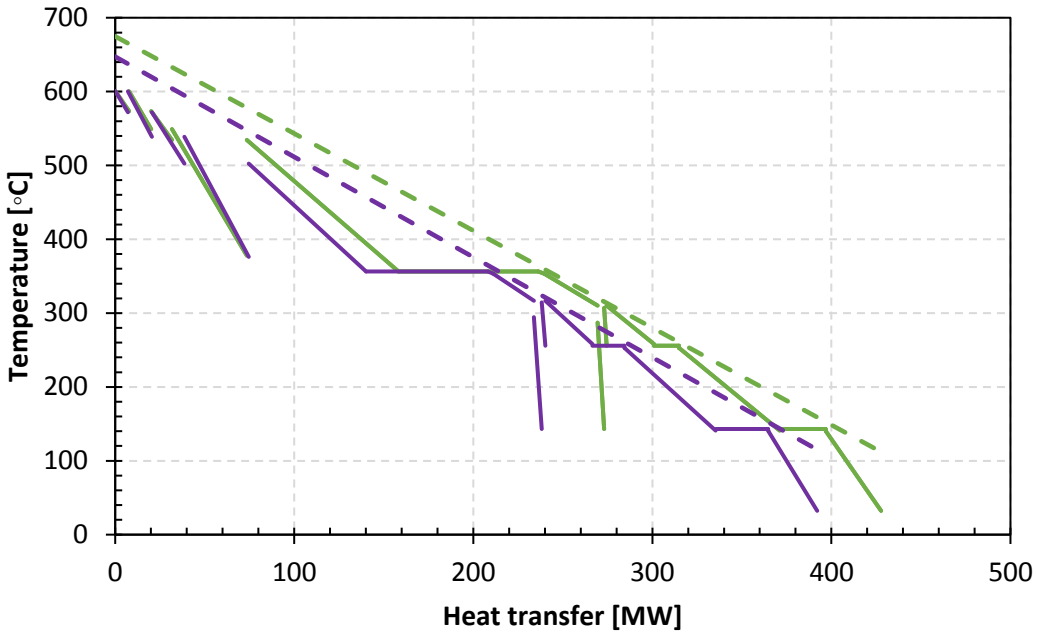

Figure 6-2: **Heat transfer versus temperature diagram for the New-Build configuration with a SEGR ratio of 70% (green lines), compared to the Full Scale CP configuration without SEGR (purple lines)**

6.5 Design of and Effect on the Capture Plant

The capture plant of the New-Build configuration utilises a 30%wt aqueous MEA solution as solvent, similar to the base case.

Before entering the capture plant, the flue gas is conditioned to 40°C and 1.05 bar. The exhaust gas stream variables entering the capture plant for a fully integrated power plant with PCC and SEGR at a SEGR ratio of 70% are listed in Table 6-6, next to the exhaust gas stream variables of the integrated power plant without SEGR. The CO2 concentration in the New-Build configuration is 3.3 times higher than the CO2 concentration in the base case. The mass flow rate is reduced by a factor of 3.3, compared to the Full Scale CP configuration.

The methodology applied to size and optimise the capture plant for the New-Build configuration follows the procedure described in Section 5.4.3.

Table 6-7 provides a summary of the relevant process conditions and design parameters associated with the capture plants of the configuration Full Scale CP and New-Build.

For the New-Build configuration, the capture plant has to achieve a capture rate of 96% to achieve an overall capture rate of 90%. The capture plant of the Full Scale CP needs to achieve a capture rate of 90%. The higher CO2 inlet concentration presents a higher driving force, leading to a higher rich solvent CO2 loading of 0.488 mol_{CO2}/mol_{MEA}, compared to a rich loading of 0.475 mol_{CO2}/mol_{MEA} in the Full Scale CP configuration. The lean CO2 loading for the New-Build configuration is 0.252 mol_{CO2}/mol_{MEA}, compared to 0.264 mol_{CO2}/mol_{MEA}. This results in different solvent capacities in both cases. The solvent in the New-Build configuration has a capacity of 0.236 mol_{CO2}/mol_{MEA}, compared to the solvent capacity in the Full Scale CP configuration of 0.211 mol_{CO2}/mol_{MEA}. The higher capacity is necessary to capture 96% of the CO2 inlet concentration. The solvent flow rate in the New-Build configuration is reduced from 848 kg/s to 788 kg/s. However, this results in a L/G ratio of 3.96, compared to a L/G ratio of 1.3 in the Full Scale CP configuration. The reboiler duty is reduced by 2.7%.

The absorber for the New-Build configuration is 5 m higher. This is necessary due to the higher absorber capture rate required for the New-Build configuration. The diameter however can be reduced by 6.8m, due to the reduced flue gas mass flow rate. Overall this leads to a reduction in packing volume by 42%.

Table 6-6: Exhaust flue gas stream variables entering the capture plant for the Full Scale CP and New-Build configuration, per GT-HRSG train

Flue gas towards capture plant			
Configuration		Full Scale CP	New-Build
SEGR ratio	%	0	70
Temperature	◦C	40	40
Pressure	bar	1.05	1.05
Mass flow rate	kg/s	649.9	199.1
Composition:			
CO2	%mol	4.2943	14.3596
H2O	%mol	7.0333	7.0333
N2	%mol	75.6629	68.2787
O2	%mol	12.1025	9.5101
Ar	%mol	0.9070	0.8184

Table 6-7: Technical and operational parameters of the CO2 capture plants of configurations New-Build and Full Scale CP, per GT-HRSG train

Configuration		Full Scale CP	New-Build
	Units		
Flue gas temperature to absorber	◦C	40	40
Flue gas pressure to absorber	bar	1.05	1.05
Flue gas mass flow rate per absorber	kg/s	649.9	199.1
CO2 concentration in the flue gas	mol%	4.29	14.4
Capture rate	%	90	96
Absorber flooding fraction	%	75	75
Absorber packing height	m	14	19
Absorber diameter	m	19.6	12.8
No. of absorbers	-	1	1
Total packing volume per train	m^3	4207	2426
Lean solvent temperature to absorber	◦C	40	40
Stripper flooding fraction	%	75	75
Stripper packing height	m	8	8
Stripper diameter	m	8	7.85
No. of strippers	-	1	1
Total packing volume per train	m^3	402	387
Stripper pressure	bar	1.94	1.92
Reboiler design temperature	◦C	120	120
Reboiler pressure	bar	3	3
Solvent flow rate	kg/s	848	788
Reboiler duty	MJ/kg_{CO2}	3.40	3.31
Lean loading	mol_{CO2}/mol_{MEA}	0.264	0.252
Rich loading	mol_{CO2}/mol_{MEA}	0.475	0.488
L/G ratio	-	1.30	3.96
Overhead condenser temperature	◦C	40	40

6.6 Overall Effect and Discussion

The power output of the power plant parts, the overall power output and the thermal efficiency of the New Build and the conventional Full Scale CP configuration are reported Table 6-8.

The increased density of the CO2-enriched air leads to less mass flow of air being swallowed by the compressor for the New Build configuration. At the same time, the specific heat of the working fluid decreases, leading to a lower compressor outlet temperature. To keep the combustor exit temperature and turbine inlet temperature constant, more full mass flow is needed. That increases the total mass flow rate through the turbine, increasing the turbine net power output for the New Build configuration by 8.5MW, in comparison to the conventional configuration Full Scale CP, as discussed in Section 6.3. However, the thermal efficiency of the turbine decreases by 1%, due to the higher heat input requirement to maintain the turbine inlet temperature.

The exhaust flue gas enters the HRSG with a higher temperature and higher mass flow rate. This results in more heat being available for the generation of steam, which in turn increases the power output of the steam cycle in the New Build configuration by 32 MW, as shown in detail in Section 6.4.

The higher CO2 concentration and lower mass flow rate (due to SEGR ratio of 70%), reduces the required absorber packing volume by 42% and reboiler duty by 2.7%, as evaluated in Section 6.5.

The CCGT net power output increases by 39MWe, resulting in an increase of the CCGT net thermal efficiency from 53.1 % in the conventional configuration to 53.4% in the New Build configuration.

Table 6-8: Power and thermal efficiencies for the investigated retrofit configurations

	Units		
Configuration		Full Scale CP	New Build
SEGR ratio	%	0.0	70.0
SEGR transfer rate	%	-	97
Capture rate	%	90	96
Overall capture rate	%	90	90
Air fan x2	MWe	-	0.75
Booster fan for PCC x2	MWe	2.64	0.75
Booster fan for SEGR x2	MWe	-	0.95
Gas turbine net power per GT-HRSG train	MWe	285.8	290.1
Gas turbine net power	MWe	571.6	580.1
Open cycle thermal efficiency	%LHV	38.2	37.2
Fuel heat input per GT-HRSG train	MWth	748	780
Fuel input per GT-HRSG train	kg/s	16.1	16.8
Fuel LHV	kJ/kg	46476	46476
Steam turbine power	MWe	257.4	289.4
CCGT gross power	MWe	834.6	876.0
CCGT gross thermal efficiency	%LHV	55.8	56.1
CCGT net power output	**MWe**	**795.0**	**834.0**
CCGT net thermal efficiency	**%**	**53.1**	**53.4**

Chapter 7 SEGR Retrofitting Strategies for CCGTs with PCC

In this chapter SEGR retrofit options for two different configurations of CCGT with PCC optimised for a CO2 capture rate of 90% are investigated.

As previously stated, in the context of achieving net zero emissions, it is important to give consideration to the marginal cost of increasing capture levels on existing CCS facilities, beyond initial capture levels. In this chapter the possibility to achieve such an increase in capture levels, beyond the initial design of 90% capture rate in the capture plant, by means of SEGR, is assessed. The intent is to assess the performance of CCGT with PCC and SEGR to get as close as possible to net-zero emissions. A cost analysis is not part of the scope.

The objective is to identify the operational framework of existing CCGT with PCC, utilising amine based scrubbing technology, retrofitted with regenerative rotary CO2 transfer devices. Limiting factors for retrofit deployment of SEGR in CCGTs with PCC are investigated and CO2 concentrations in the exhaust flue gas for achievable SEGR ratios are established. The intention is to assess possible increases in the overall capture rate of existing CCGT with PCC by adding regenerative rotary CO2 transfer in parallel to the capture plant and to minimise energy penalties for the capture plant.

Adding SEGR in parallel increases the CO2 concentration in the exhaust flue gas and reduces the flue gas mass flow rate to the capture plant.

(Herraiz et al. 2018) showed through process model simulations, that the current class of gas turbine engines can operate at higher CO2 inlet concentration without a significant deviation in the compressor and the turbine performance from the design conditions. Similar deviations are reported by (K. Jonshagen 2011) for F-class GE engine, and by (Sander et al. 2011) for Alstom GT26 engine for different EGR ratios. This will not be further assessed here.

The structure of this chapter is as follows.

First, the two retrofit configurations investigated are described in Section 7.1, followed by the design of the regenerative rotary CO2 transfer wheel for retrofit application (Section 7.2).

Next, the operational limits for retrofitting SEGR to existing CCGT with PCC in a bottom-up approach are established by observing the entrainment regime of the absorber columns, while the CO2 concentration in the flue gas increases and the flue gas mass flow rate decreases (Section 7.3).

In a top-down approach, the optimum SEGR ratio reported in Section 7.3 is used and options to increase the overall capture rate further by adapting lean solvent mass flow rate and reboiler pressure are investigated in Section 7.4. The CCGT power output for the case is reported and compared to CCGT power output of the base case without SEGR applying the same options to increase the capture level.

Finally, a summary and discussion of the results is presented in Section 7.5.

7.1 Description of the Retrofit Configurations

The considered retrofit configurations are based on the two base cases, introduced in Section 5.1. The retrofit configurations consist of two parallel GT, HRSG, flue gas conditioning systems, SEGR units, capture plants (one in the Full Scale configuration, two parallels in the Half Scale configuration) and compression trains, sharing one set of steam turbines between both trains.

The block flow diagrams of the retrofit configurations Full Scale CP with SEGR is illustrated in Figure 7-1, and the block flow diagrams of the retrofit configurations Half Scale CP with SEGR is shown in Figure 7-2. The configuration Half Scale CP with SEGR features the possibility to interconnect the solvent flows of the two parallel capture plants, switching off one absorber, but still using both strippers to regenerate the solvent mass flow. This feature can be applied when the flue gas mass flow, that needs to be treated by the capture plant, reaches 50% of the flue gas mass flow produced during full load operation without SEGR.

The SEGR device operates in parallel to the capture plant. Flue gas coming out of the HRSG passes through the gas/gas heater and is split according to a SEGR ratio to either pass through a blower and DCC towards the SEGR unit, or through a blower and DCC towards the capture plant. The SEGR ratio is defined as the ratio of flue gas flow rate that is diverted to the SEGR unit. The flue gas entering the capture plant is, as in the base case, conditioned to 40◦C and 1.05 bar. The flue gas entering the rotary regenerative CO2 transfer device is conditioned to 30◦C and 1.03 bar.

Air passing through the SEGR unit is enriched with CO2. It is then swallowed by the gas turbine compressor and used as comburent in the combustion of the natural gas. The CO2-depleted gas streams from the SEGR unit and the capture plant are mixed and passed through the rotary gas/gas heat exchanger, being heated up before leaving to the stack.

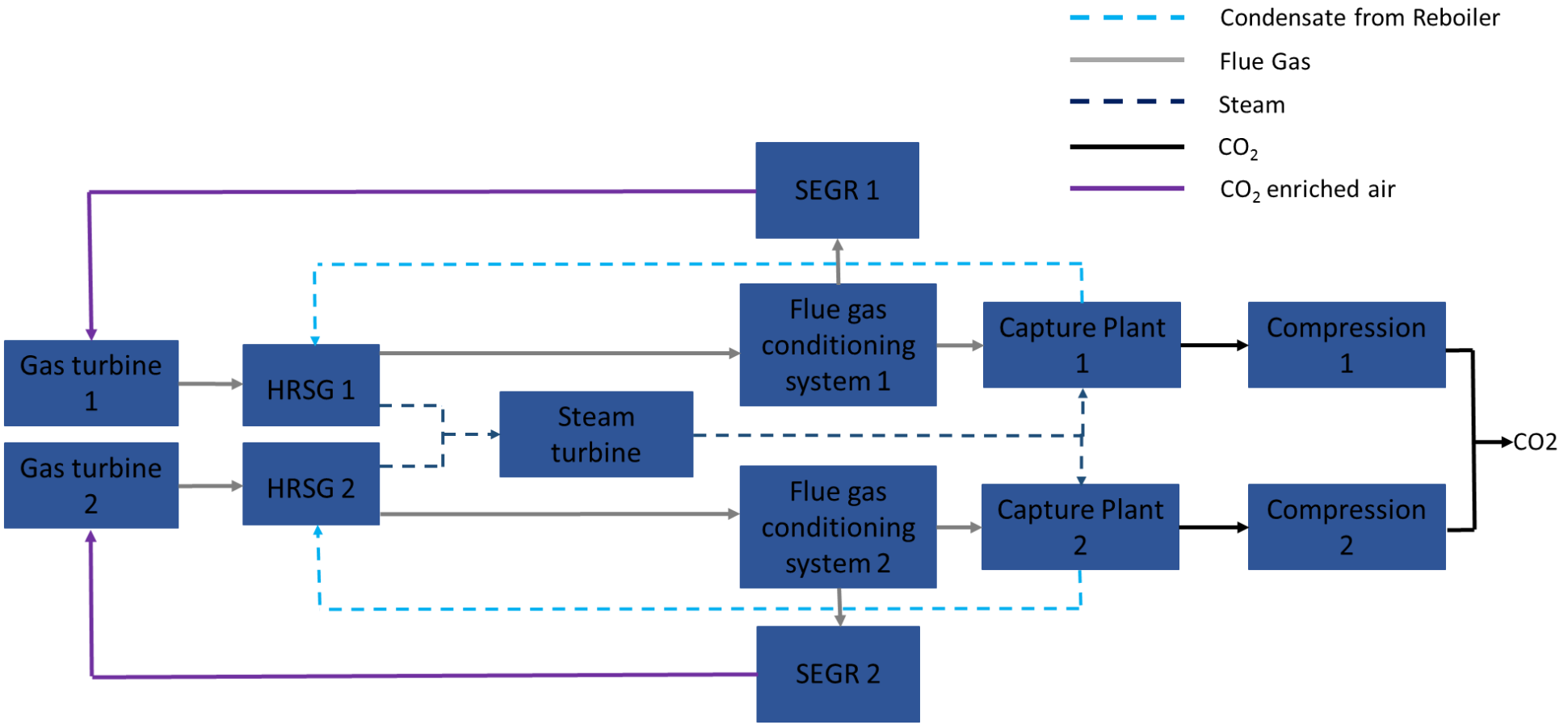

Figure 7-1: Block flow diagram of Case Full Scale CP with SEGR, an integrated CCGT with flue gas conditioning, SEGR unit, capture plant and compression train

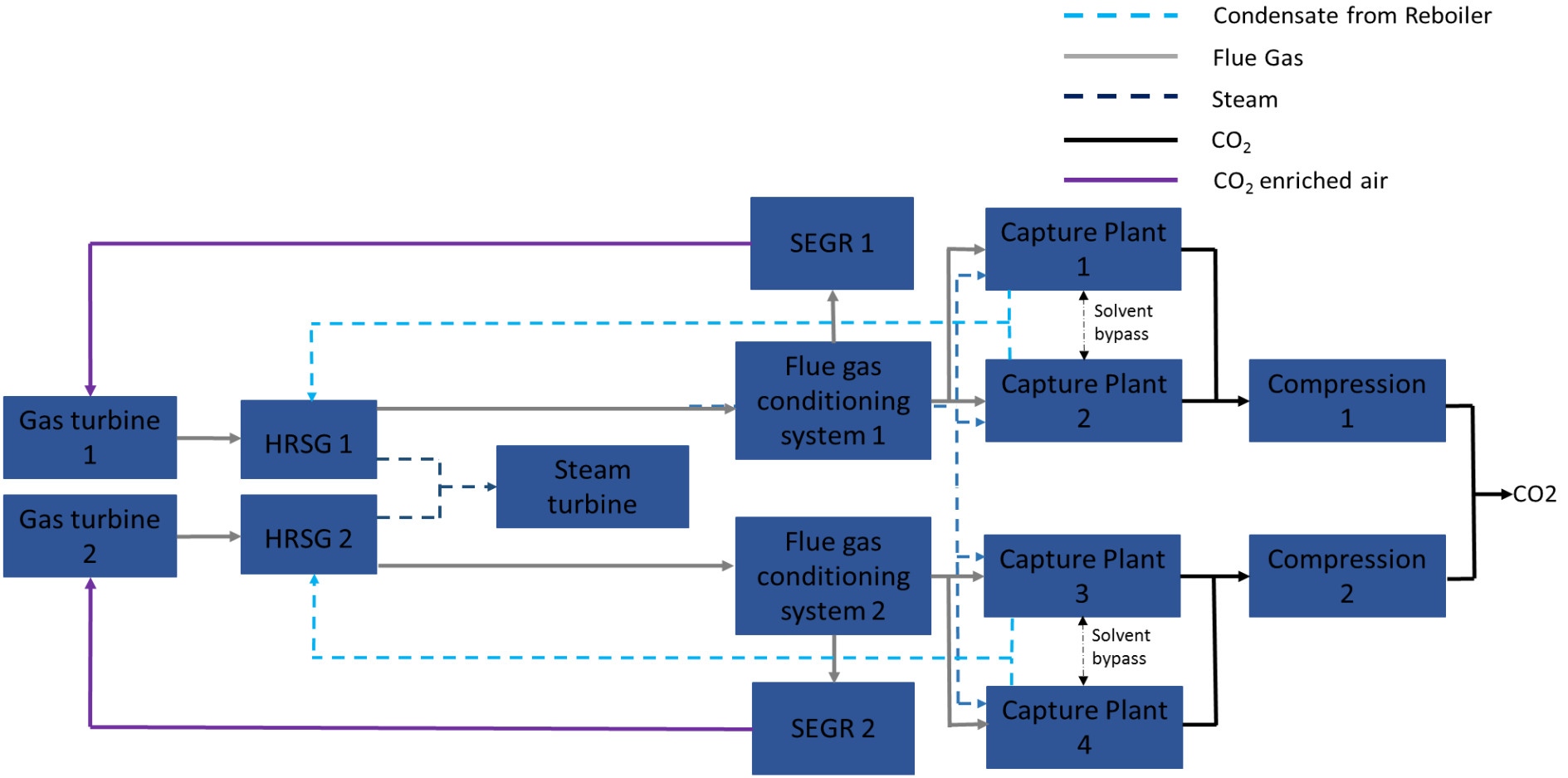

Figure 7-2: Block flow diagram of Case Half Scale CP with SEGR, an integrated CCGT with flue gas conditioning, SEGR unit, capture plant and compression train

7.2 Design of the Rotary CO2 Transfer Wheel for Retrofit Application

The design parameters of CCGT, HRSG, PCC, flue gas conditioning and compression train are the same as in the base cases. The design, technical and operational parameters of the rotary regenerative CO2 transfer wheel are described in hereinafter.

The regenerative rotary CO2 transfer wheel is sized for the retrofit configurations to transfer 99% of the CO2 in the CCGT flue gas composition, reported by (Herraiz et al. 2018) for a SEGR ratio of 70%. The high recovery rate was chosen to not limit the overall capture rate by the transfer rate of the SEGR unit. The CO2 overall capture rate of the system, as shown in Equation (2.5) in Chapter 2, depends on both, the capture rate of the capture plant and the recovery rate of the SEGR unit. The overall capture rate of the system is defined as the amount of CO2 captured in the overall process in relation to the generated CO2 in the combustion. This leads to an oversized regenerative rotary CO2 transfer device for lower SEGR rates.

As solid adsorbent, the KOH activated carbon, used to validate the system (Section 4.2.2), is utilised. The condition of the ambient air and technical parameters of the air fan, used to size the wheel, are reported in the Appendix E. The flue gas conditions and the dimensions of the rotary CO2 transfer device are reported in Table 7-1.

The solid amount of the KOH activated carbon necessary to transfer 99% of the CO2 concentration in the flue gas is 1063tn, for a regenerative rotary wheel partitioned equally in adsorption and desorption section and a rotational speed of 1 rpm. The rotational speed of 1 rpm was chosen in the case of a drop in recovery rate. A higher rotational speed of 2 rpm would have reduced the necessary amount of solid adsorbent, however a further increase to adapt to sudden changes in recovery ratio would not be possible, since a higher rotational speed for such large rotating devices is not recommended. In case of a drop in recovery rate in the integrated model, the operational strategy to increase the rotational speed can be applied to increase the recovery rate.

Applying the procedure detailed in Section 3.4.3, the number of needed wheel devices are calculated based on a honeycomb wall thickness of 1 mm and a pitch of 4.5 mm, leading to a bulk void fraction of 0.77. For a maximum diameter, from a practical point of view, as discussed in Section 3.4.3., that leads for the predicted mass of adsorbent to three wheel devices of 30m in diameter and 2.56 m in height.

Table 7-1: Retrofitting requirements for the regenerative rotary CO2 transfer device for SEGR in parallel

Flue gas		**S-EGR Parallel**
SEGR ratio	%	70
CO2 conc. at SEGR unit	mol%	14.8
Flue gas molar flow rate	mol/s	14904
Flue gas inlet temperature	◦C	30
Flue gas inlet pressure	bar	1.033
Recovery rate	%	99.0
Adsorbent		
Material	-	KOH activated carbon
Mass x 1000	kg	1063
Particle and Bulk		
Particle density	kg / m^3	952
Particle Volume	m^3	1117
Bulk void fraction	-	0.77
Bulk volume	m^3	4855
Rotary wheel		
External diameter	m	30
Height	m	2.56
Basket Factor (Hogg 2016)	-	0.89
Rotor volume	m^3	1612
No. of devices	-	3

7.3 Operational Limits for Retrofitting SEGR

During SEGR in parallel operation, the amount of flue gases passing through the capture plant will be decreased. This can lead to velocity and pressure drop restrains in the capture plant. Therefore, to establish operational limits for retrofitting SEGR to CCGT with PCC, the SEGR ratio in the integrated model is increased step wise and the effect of the reduced flue gas flow rate coupled with the increased CO2 concentration

on the F-factor (Equation (5.14)) over the pressure drop in the absorber column is investigated.

For both retrofit configurations the methodology is to increase the SEGR ratio step wise, while keeping the solvent mass flow rate (Full Scale CP solvent mass flow rate = 848 kg/s; Half Scale CP solvent mass flow rate = 424 kg/s) and stripper pressure (1.94 bar) in the capture plant fixed to the values for SEGR ratio = 0, except when reported otherwise.

In cases where the solvent flow rate cannot be kept at maximum, it is adapted to keep the constrain of a flooding fraction of 75% for absorber and stripper. If the SEGR ratio leads to an F-factor below the loading point of Mellapak 250Y (F-factor > 1.5), the lower limit of the entrainment regime of a column is reached. A further increase in SEGR ratio and therefore a further decrease in flue gas mass flow rate would not be able to be processed by the absorber column.

7.3.1 Configuration Full Scale CP with SEGR

In this section, the strategy detailed above is applied to the configuration Full Scale CP with SEGR. Reported values are given for one GT train of the overall CCGT with PCC and SEGR configuration.

The CO2 concentration in the exhaust flue gas entering the capture plant increases with increasing S-EGR ratio. At the same time the flue gas mass flow rate decreases, while the solvent flow stays constant at a mass flow rate of 848 kg/s. Corresponding CO2 concentrations and total mass flow rates at the inlet of the absorber for different SEGR ratios of the retrofit configuration Full Scale CP with SEGR, obtained from the integrated CCGT with PCC and SEGR model, are given in Table 7-2. While the flue gas concentration rises from 4.29 mol% in the base case without SEGR (SEGR ratio = 0%) to 6.29 mol% for a SEGR ratio of 30%, the mass flow rate of flue gas decreases from 650 kg/s to 452 kg/s. This leads to a change in the gas velocity (29% change) and density in the absorber (1% change), as shown in Figure 7-3 for the averaged gas velocity and average gas density of the absorber column for SEGR ratios from 0-30%.

This in turn is affecting the operational F-Factor and pressure drop in the absorber column.

A sensitivity analysis of the pressure drop per unit of length of packing height to the F-factor, based on the inlet CO2 concentration and flue gas mass flow rate of the different SEGR ratios, is illustrated in Figure 7-4. Each colour represents the absorber at a different SEGR ratio. Each point of the same colour represents one section of the absorber height. The red region in Figure 7-4 illustrates the area where the F-Factor falls below the value for the loading point of the packing and therefore under the entrainment regime of the column. Figure 7-4 indicates that the pressure drop in the absorber decreases with increasing SEGR ratio. Over the investigated SEGR ratio the change in pressure drop amounts to 48%, the change in F-factor to 30%. For a SEGR ratio of 30% and higher, the absorber is operated under the loading point, therefore beyond the entrainment regime of the absorber. Consequently, it can be concluded, for the retrofit configuration Full Scale CP with SEGR that the maximum SEGR ratio the CCGT with PCC and SEGR can be operated in is 20%, leading to a CO2 concentration entering the absorber column of 5.39 mol%.

Table 7-2: CO2 concentrations and mass flow rates towards the capture plant for different SEGR ratios for the retrofit configuration Full Scale CP with SEGR

	Units				
SEGR ratio	%	0	10	20	30
CO2 concentration	mol%	4.29	4.78	5.39	6.29
Total flue gas mass flow rate	kg/s	650	582	517	452

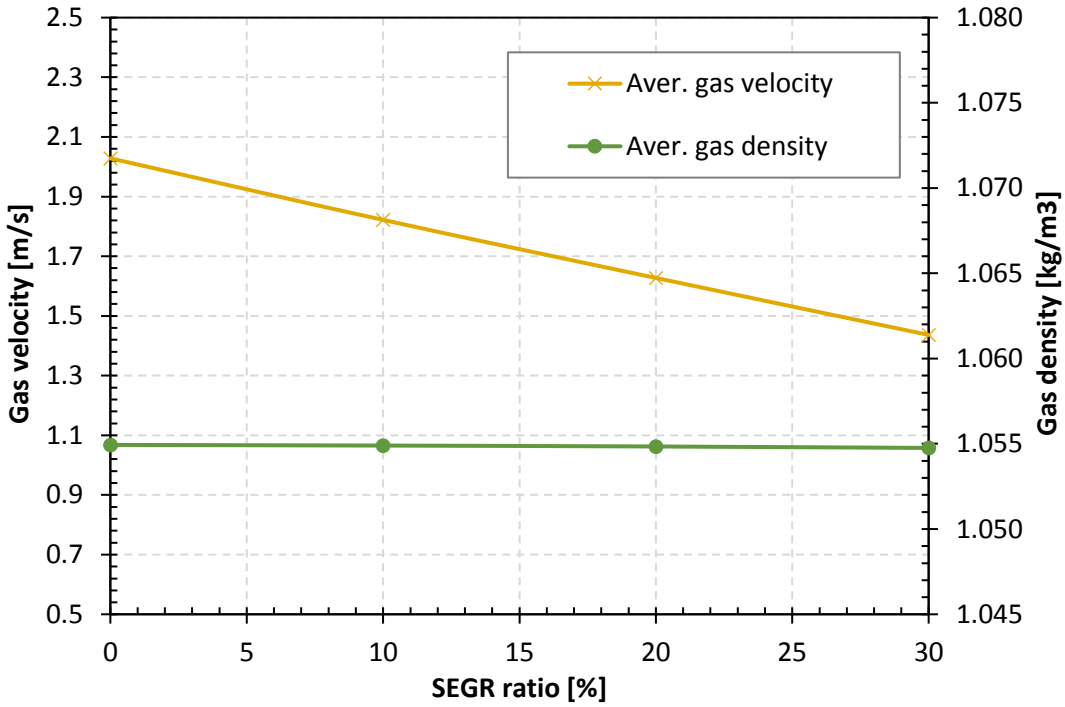

Figure 7-3: **Change in average gas velocity and average gas density with increasing SEGR ratio**

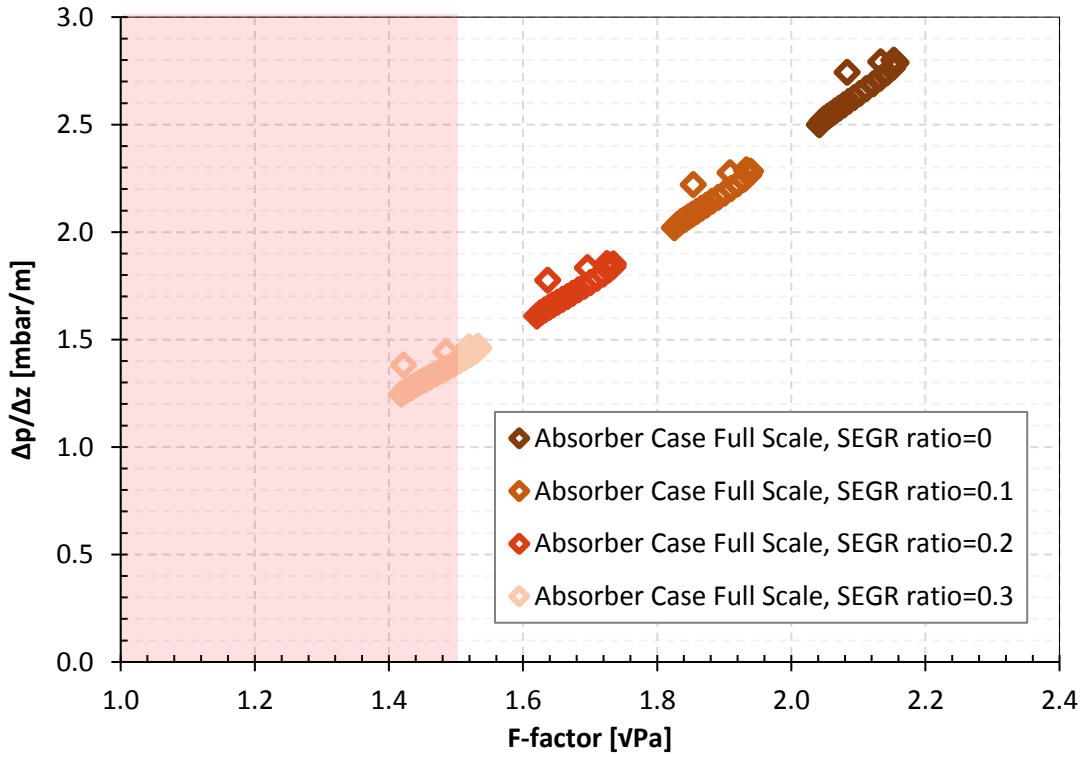

Figure 7-4: **Sensitivity analysis of the absorber pressure drop depending on the SEGR ratio for the retrofit case Full Scale CP with SEGR; the red area marks the area where the loading point of the packing is reached**

7.3.2 Configuration Half Scale CP with SEGR

The same strategy as for the configuration Full Scale CP with SEGR is applied to the configuration Half Scale CP with SEGR. However, this configuration has two operational modes. When the total mass flow rate of the flue gas reaches the mass flow rate that can be treated by one absorber (SEGR ratio = 50%), the second absorber is switched off, and the solvent bypass is switched on. This leads to an operation, where the flue gas is treated by one absorber and the rich solvent is treated by two strippers. Consequently, operational higher SEGR ratios are achievable in the configuration Half Scale CP with SEGR, compared to the configuration Full Scale CP with SEGR. Reported values refer to one GT train of the overall CCGT with PCC and SEGR configuration.

The change in CO2 concentrations and total flue gas mass flow rates for different SEGR ratios for the retrofit configuration Half Scale CP with SEGR, obtained from the integrated CCGT with PCC and SEGR model, are given in Table 7-3. The flue gas concentration rises from 4.29 mol% in the base case without SEGR (SEGR ratio = 0%) to 15.10 mol% for a SEGR ratio of 70%, while the mass flow rate of flue gas decreases from 650 kg/s to 200 kg/s.

Table 7-3: CO2 concentrations and total mass flow rates for different SEGR ratios for the retrofit configuration Half Scale CP with SEGR

	Units								
SEGR ratio	%	0	10	20	30	40	50	60	70
CO2 concentration	%	4.29	4.78	5.39	6.19	7.27	8.81	11.20	15.10
Total flue gas mass flow rate	kg/s	650	582	517	452	389	325	262	200

At a flue gas mass flow rate of 325 kg/s, corresponding to a SEGR ratio of 50%, one absorber is switched off and the solvent flow of the switched off absorber bypasses towards the operating absorber. The maximum solvent flow rate for the SEGR ratios with solvent bypass is determined based on the flooding fraction constrain of 75% for the operating absorber. Resulting flue gas and solvent mass flows per absorber/ stripper column are reported in Table 7-4.

Table 7-4: Flue gas mass flow rate per absorber and solvent mass flow rate per stripper for different SEGR ratio for the retrofit configuration Half Scale CP with SEGR

	Units								
Capture plant operational mode		two absorbers two strippers					one absorber two strippers		
SEGR ratio	%	0	10	20	30	40	50	60	70
CO2 concentration	%	4.29	4.78	5.39	6.19	7.27	8.81	11.20	15.10
Flue gas mass flow rate per absorber	kg/s	325	291	258	226	194	325	262	200
Solvent mass flow rate per stripper	kg/s	424	424	424	424	424	220	380	424

The change in the flue gas and solvent mass flow rates are again affecting the operational F-Factor and pressure drop in the absorber column. The sensitivity analysis of the pressure drop per m packing height to the F-factor, for SEGR ratios of 0% to 30% ratios, for the operation of two absorber and two strippers, is depicted in Figure 7-5. The sensitivity analysis of the pressure drop per m packing height to the F-factor, based on SEGR ratios of 50% to 70%, for the operation of one absorber and two strippers, is shown in Figure 7-6. Each colour represents the absorber at a different SEGR ratio. Each point of the same colour represents one section of the absorber height. The red region in both figures illustrates the area where the F-Factor falls below the value for the loading point of the packing and therefore under the entrainment regime of the column.

Figure 7-5 indicates that the pressure drop in each of the two absorbers decreases with increasing SEGR ratio. Over the investigated SEGR ratio (0-30%), the change in pressure drop amounts to 48%, the change in F-factor to 30%. For a SEGR ratio of 30% and higher the absorber is operated under the loading point, thus beyond the entrainment regime of the absorber. Therefore, a SEGR ratio of 40% is as well under the loading point of the packing, but at the same time the flue gas mass flow rate is too high to be treated in the operation of one absorber. As a result, the operational SEGR ratio of 40% cannot be operated at all in the retrofit configuration Half Scale CP with SEGR.

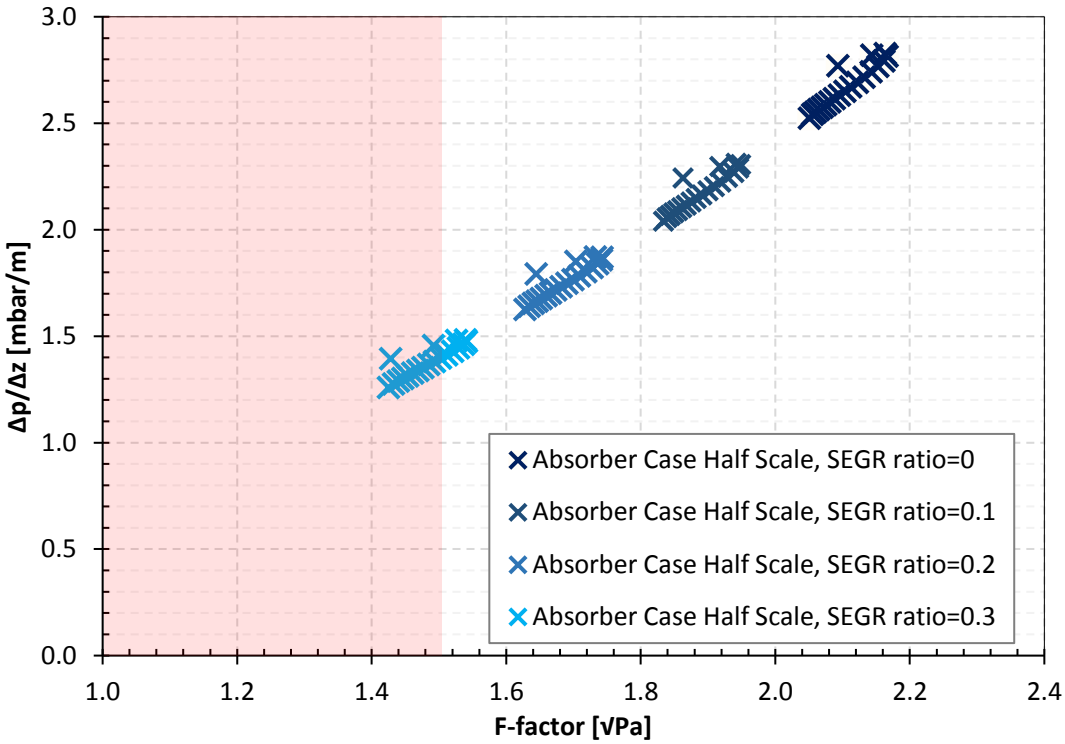

Figure 7-5: Sensitivity analysis of the absorber pressure drop depending on the SEGR ratio (0%-30%) for the retrofit case Half Scale CP with SEGR; two absorber and stripper are in operation; the red area marks the area where the loading point of the packing is reached

The sensitivity analysis of the absorber pressure and F-factor, presented in Figure 7-6, for the operation of the configuration Half Scale CP with SEGR under the operation of one absorber and two stripper for the investigated SEGR ratios of 50-70%, shows a change in pressure drop of 60% and a change in F-factor of 38%. The highest SEGR ratio achievable in the limits of the entrainment regime of the absorber is 60%.

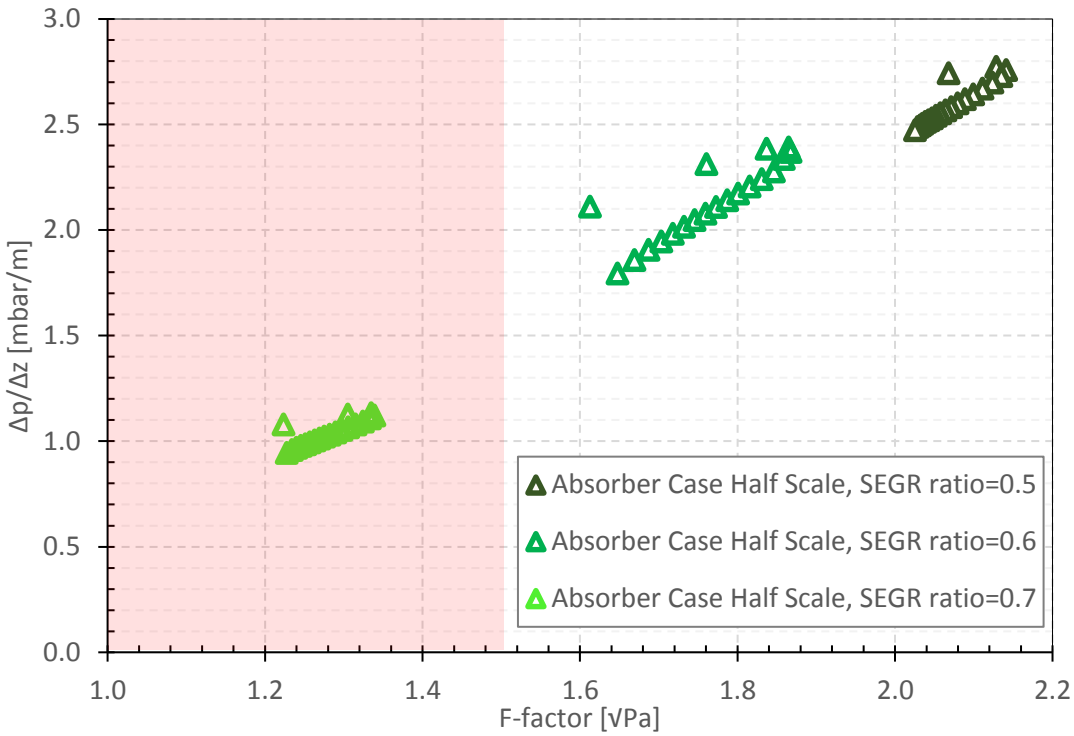

Figure 7-6: Sensitivity analysis of the adsorber pressure drop depending on the SEGR ratio (50-70%) for the retrofit case Half Scale CP with SEGR; one absorber and two stripper are in operation; the red area marks the area where the loading point of the packing is reached

For the retrofit configuration Half Scale CP with SEGR two different maximum SEGR ratios are possible, depending on the total amount of flue gas. If the flue gas flow rate is above the flow rate treatable in one absorber, the maximum SEGR ratio is 20%, corresponding to a CO2 concentration of 5.39 mol% at the inlet of the absorbers. If the flue gas mass flow rate drops under 50% of the maximum flue gas mass flow rate (SEGR ratio=0%), one of the absorbers can be switched off and the solvent bypass can be activated. In this operational mode the maximum SEGR ratio for the retrofit configuration Half Scale CP with SEGR is 60%, corresponding to a CO2 concentration of 11.2 mol% at the absorber inlet.

7.3.3 Effect on the Overall System

For a given SEGR recovery rate the CO2 generated in the combustion increases, at the same time, the absolute amount of CO2 leaving the power plant with the CO2-depleated stream increases. To increase the overall capture rate, the capture rate of the PCC has to increase. Therefore, the efficiencies of both, capture plant and SEGR device, are limiting the overall capture rate.

The performance of a regenerative rotary CO2 device, designed to transfer 99% of CO2 for a recirculation ratio of 70%, changes drastically when lower recirculation ratios and therefore lower flue gas mass flows rates with lower CO2 inlet concentration as the design point are applied. The corresponding technical and operational variables for the transfer device at design and at the maximal operational SEGR ratio for retrofit operation (20% and 60%) are listed in Table 7-5.
The cyclic capacity of the CO2 transfer wheel drops for a SEGR ratio of 20% by 89% and for a SEGR ratio of 60% by 32%. This can be explained by the ratio of solid adsorbent to available adsorbat. This however, also means that most of the solid is not utilised in a process where SEGR is used as a retrofit option to chase residual CO2 emissions.

Table 7-5: Technical and operational variables for the regenerative rotary CO2 transfer device at design point and at the maximal operational SEGR ratio of 20% and 60%

	Units			
SEGR ratio	%	70	60	20
Flue gas molar flow rate	mol/s	14904	12882	4356
CO2 concentration	mol%	14.8	11.5	5.6
SEGR recovery rate	%	99.00	99.50	99.45
Cyclic capacity	mol_{CO2}/kg solid	2.464	1.668	0.272

Corresponding technical and operational variables for the CO2 capture plants at design and the overall capture rate are reported in Table 7-6 for the configuration Full Scale CP and in Table 7-7 for the configuration Half Scale CP. Design parameters

are a flooding fraction for absorber and stripper of 75%, a stripper pressure of 1.94 bar and a maximum solvent flow rate given by the base case configuration, except for cases where flooding fraction constrains are reached.

The implementation of a rotary regenerative CO2 transfer device with a SEGR ratio of 20% (with a recovery rate above 99% due to oversizing) leads, in the case of the Full Scale CP, to an increase in the overall capture rate of 2% and a marginal reboiler duty reduction of below 1%. The same results are presented for the implementation of a rotary regenerative CO2 transfer device with a SEGR ratio of 20% in the case of the Half Scale CP. That increase may not constitute a sufficiently large increase to justify the additional costs of retrofitting SEGR.

In the case of the implementation of a CO2 transfer wheel with a SEGR ratio of 60% for the configuration Half Scale CP with SEGR, the overall capture rate decreases to 84%. There are two reasons for the decrease in overall capture level. First, the overall solvent mass flow rate is decreased for 10% due to flooding fraction limitations of the one absorber in operation. And secondly, the absorber gets pinched for the operation at a SEGR ratio of 60%, as shown in Figure 7-7. The temperature of the gas leaving the absorber at the top is relatively high. The absorption process itself depends on the thermodynamics and kinetics of the process and therefore on the solvent. The heat of absorption reaches a maximum, leading to a bulging in the gas temperature profile. The cool lean solvent entering at the top of the absorber cools the gas down, leading to an increase in mass transfer at the top, which is exponential, since the CO2 concentration is still high at the top. For a SEGR ratio of 60% the effect of SEGR is limited by the equilibrium of the solvent used, which is 30 %wt MEA.

Table 7-6: Technical and operational variables for the CO2 capture plant for the configuration Full Scale CP and Full Scale CP with SEGR at the maximal operational SEGR ratio of 20% , using a 30% MEA aqueous solution

	Units		
Configuration		Full Scale CP	Full Scale CP with SEGR
SEGR ratio	%	0	20
CO2 concentration	mol%	4.29	5.39
Total flue gas mass flow rate	kg/s	650	517
Capture rate of the PCC	%	90.0	92.2
SEGR recovery rate	%	-	99.4
Overall capture rate	**%**	**90.0**	**92.0**
Total solvent mass flow rate	kg/s	848	848
Stripper pressure	bar	1.94	1.94
Reboiler duty	MJ/kg_{CO2}	3.40	3.37
Lean solvent loading	mol_{CO2}/mol_{MEA}	0.264	0.264
Rich solvent loading	mol_{CO2}/mol_{MEA}	0.475	0.478

Table 7-7: Technical and operational variables for the CO2 capture plant for the configuration Half Scale CP and Half Scale CP with SEGR at the maximal operational SEGR ratio of 20% and 60%, using a 30% MEA aqueous solution

	Units			
Configuration		Half Scale CP	Half Scale CP with SEGR	
SEGR ratio	%	0	20	60
CO2 concentration	mol%	4.29	5.39	11.20
No. of absorber	-	2	2	1
Flue gas mass flow rate per absorber	kg/s	325	258	262
Capture rate of the PCC	%	90.0	92.2	85.0
SEGR recovery rate	%	-	99.4	99.5
Overall capture rate	**%**	**90.0**	**92.0**	**84.3**
Solvent mass flow rate per absorber	kg/s	424	424	760
Stripper pressure	bar	1.94	1.94	1.94
Reboiler duty	MJ/kg_{CO2}	3.40	3.37	3.26
Lean solvent loading	mol_{CO2}/mol_{MEA}	0.264	0.264	0.264
Rich solvent loading	mol_{CO2}/mol_{MEA}	0.475	0.478	0.488

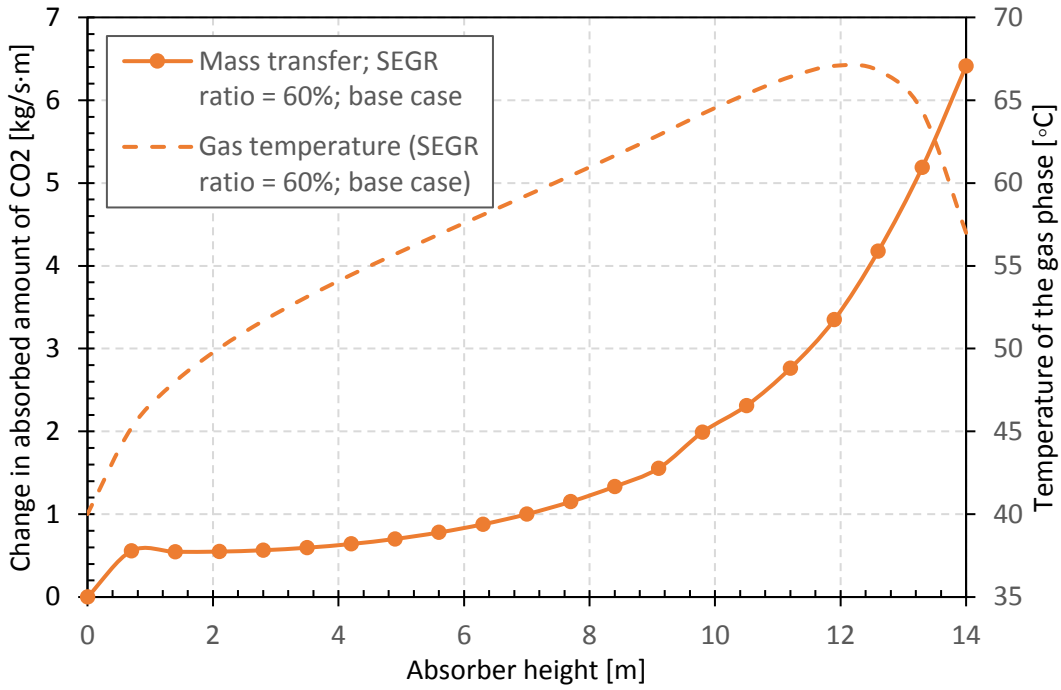

Figure 7-7: Mass transfer (continuous line) and temperature profile of the gas phase (dashed line) in the absorber of the configuration Half Scale CP with SEGR at a SEGR ratio of 60%, using a 30% MEA aqueous solution

The effect on the power output of the power plant parts and overall power output is reported Table 7-8. However, for the SEGR ratio of 60% in the configuration Half Scale CP the results are not generic, since the solvent used is limiting the effect of the increased CO2 concentration.

The gas turbine swallows a constant volume of air at full load. Therefore, the density of the air at the compressor inlet defines the mass flow through the GT. With increasing SEGR ratio the CO2 concentration and air temperature increase at the inlet of the GT compressor. Higher temperatures decrease the working fluid density, while higher CO2 concentrations increase working fluid density. The resulting density will be a mixture of both these effects. At the same time the specific heat of the working fluid decreases at higher CO2 concentration, which however is counteracted by the increase in CO2-enriched air inlet temperature. Overall the turbine inlet temperature can be maintained constant for a large range of SEGR ratios with only little changes in fuel mass flow rates. For illustration of the changes in specific heat and density, the

sensitivity analysis on the change in working fluid properties with increasing SEGR ratio performed by Herraiz, can be found in the Appendix E, Figure E-1.

For marginal lower density for a SEGR ratio of 20% in both retrofitted configurations (Full Scale with SEGR and Half Scale with SEGR) and a marginal change in specific heat compared to the increase in CO2-enriched air inlet temperature of 3◦C, the fuel mass flow needs to be slightly decreased to keep the turbine inlet temperature constant at 1371◦C. This leads to a slight reduction in mass flow rate through the turbine and therefore a reduction in gas turbine net power by 6 MWe, compared to the base case without SEGR. However, due to a reduced reboiler duty in in the capture plant, the steam turbine power output is increased by 2 MWe. The net power output of the CCGT in both retrofit configurations for a SEGR ratio of 20% is reduced by 7MWe, leading to a reduction in net thermal efficiency of 1%.

For the retrofit configuration Half Scale with SEGR at a SEGR ratio of 60% the CO2-enriched air inlet temperature increases by 7◦C. However, the increased CO2 concentration has a bigger effect on the density of the CO2-enriched leading to an overall increase in density at the compressor inlet. Therefore, the mass flow at compressor inlet is reduced to keep the volume flow rate constant. The increase in CO2-enriched air is counteracted by the decrease in specific heat, so that more fuel mass flow is needed to keep the turbine inlet temperature constant. This leads to a higher mass flow rate through the turbine, increasing the gas turbine net power by 1MWe. Since the reboiler duty in the capture plant is further decreased for a SEGR ratio of 60%, the steam turbine power outlet is increased by 27 MWe, leading to a CCGT net power output increase of 29MWe. However, this increase needs to be seen in the context that the CO2 overall capture level is decreased to 84% of previously 90%, emitting more CO2 to the environment than before.

The auxiliary power consumption increases with SEGR 20% and decrease again with SEGR 60%, due to the fact that only one capture plant per CCGT train is used for the SEGR case 60%. Therefore, several pumps and fans can be switched off for the unused capture plant.

Table 7-8: Power and thermal efficiencies for the investigated retrofit configurations

	Units					
Configuration		Full Scale		Half Scale		
SEGR ratio	%	0	20	0	20	60
Fuel mass flow rate	kg/s	16.10	16.00	16.10	16.00	16.46
Gas turbine net power per GT-HRSG train	MWe	285.8	282.5	285.8	282.5	286.4
Gas turbine net power	MWe	571.6	564.9	571.6	564.9	572.7
Open cycle thermal efficiency	%LHV	38.2	38.0	38.2	38.0	37.4
Steam turbine power	MWe	257.4	259.1	257.4	259.1	284.5
Fuel heat input per GT-HRSG train	MWth	748.4	743.7	748.4	743.7	765.1
CCGT gross power	MWe	829	824	829	824	857
CCGT gross thermal efficiency	%LHV	55.8	55.8	55.8	55.8	56.4
CCGT net power output	MWe	795.0	788.4	795.0	788.4	823.6
CCGT net thermal efficiency	**%**	**53.1**	**53.0**	**53.1**	**53.0**	**53.8**

7.4 Increasing the Overall Capture Rate

To reduce CO2 emissions in future CO2 capture plants beyond the initial design of 90% capture rate, different strategies can be applied, which only imply marginal increase in operational costs.

Possible operational changes to increase the capture rate and the overall capture rate respectively, as discussed under Section 5.4.4, further include:

- Allowing flooding fractions in absorber and stripper to reach up to 80%, and thereby being able to increase the solvent mass flow rate.
- Decreasing the stripper pressure, allowing a leaner solvent loading entering the absorber.

These strategies could also be applied together, however an independent assessment of the effect would then not be possible.

The effect of these operational changes on the technical and operational variables of the capture plant and the CCGT net power output for the base case configuration Half

Scale CP are provided in Table 7-9. Corresponding analysis of the mass transfer and the gas temperature in the absorber to an increased solvent mass flow rate and decreased stripper pressure is illustrated in Figure 7-8. It shows, that the CO2 capture rate of the capture plant can be increased by up to 7% with only a marginal decrease in CCGT net thermal efficiency of around 1%.

Table 7-9: Technical and operational variables of the capture plant and CCGT net power output for the configuration Half Scale CP for different operational strategies

	Unit			
Configuration		Half Scale CP		
SEGR ratio	%	0		
Intensification strategy		original design	higher solvent mass flow rate	lower stripper pressure
Solvent mass flow rate	kg/s	424	460	424
Stripper pressure	bar	1.94	1.94	1.89
Reboiler duty	MJ/kg_{CO2}	3.40	3.48	3.67
Lean solvent loading	mol_{CO2}/mol_{MEA}	0.264	0.264	0.236
Rich solvent loading	mol_{CO2}/mol_{MEA}	0.475	0.468	0.465
Capture rate of the PCC	%	**90.0**	**95.5**	**97.0**
CCGT net power output	MWe	795.0	787.6	781.9
CCGT net thermal efficiency	**%**	**53.1**	**52.6**	**52.2**

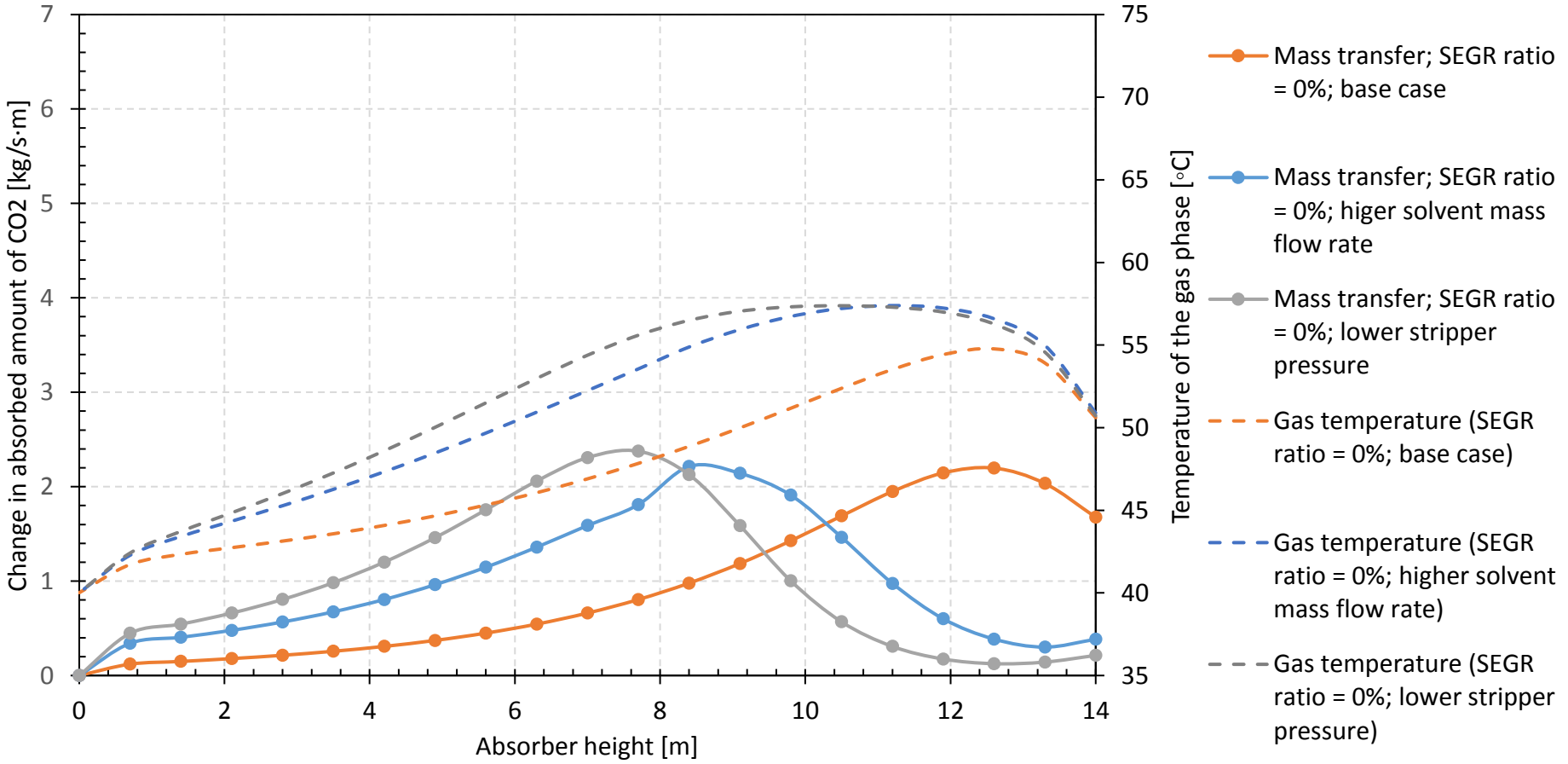

Figure 7-8: Mass transfer (continuous line) and temperature profile of the gas phase (dashed line) in the absorber of the configuration Half Scale CP, using a 30% MEA aqueous solution, for different operational changes

It still needs to be determined, if those operational changes including applying SEGR would increase the overall capture levels even further than the operational changes alone for the base case.

Based on the hydraulic limitation two different SEGR ratios for retrofitting SEGR have been established in Section 7.3.1 and 7.3.2:

- SEGR ratio of 20% for the retrofit configuration Full Scale CP with SEGR.
- SEGR ratio of 20% for the retrofit configuration Half Scale CP with SEGR, both capture plants per GT train in operation.
- SEGR ratio of 60% for the retrofit configuration Half Scale CP with SEGR, one capture plant with solvent bypass of the second capture plant per GT train in operation.

As shown in Section 7.3.3, there is no significant benefit in doing SEGR for a SEGR ratio of 20%, which only increases the CO2 concentration in the flue gas entering the capture plant by 1%. Especially in the context that this CO2 concentration can be achieved with EGR and therefore without the need of a further transfer device.

A SEGR ratio of 60%, hydraulically achievable in the configurations Half Scale CP with SEGR, since one absorber can be switched off, showed, that MEA is limiting the beneficial effect SEGR could have due to the higher concentration of CO2 in the flue gas entering the capture plant. The high enthalpy of adsorption of MEA leads to high gas temperatures limiting the mass transfer of CO2. The change in operational conditions might however have an optimising effect on the performance of MEA. This will be assessed here. Yet, the results will be solvent specific.

A summary of the results for the configuration Half Scale CP with SEGR and without SEGR for comparison is provided in Table 7-10.

The illustrated results in Figure 7-9, show a comparison of the changes in solvent mass flow rate, reboiler duty and overall capture rate for the operational strategy ‘increased solvent mass flow rate’ as changes to the base case without SEGR in percentages.

The solvent flow rate in the configuration Half Scale CP (base case) can be increased by 9% before reaching a flooding fraction of 80%, which increases the overall capture rate to 96% from originally 90%. The higher solvent flow results in an increased reboiler duty of 2%.

For the retrofit configuration Half Scale CP with SEGR at a SEGR ratio of 60%, the solvent mass flow rate can be increased by 17%, which increases the overall capture rate to 94%, from originally 84%. Compared to the base case, this results in an increase in the overall capture rate of 4%. Yet, the reboiler duty decreases in comparison to the base case by 1% for the configuration with SEGR at a SEGR ratio of 60%.

The decrease in net thermal efficiency of the CCGT is linked to the change in reboiler duty. For the Half Scale configuration without SEGR the net efficiency decreases by 0.5%, for an overall capture level of 96%. For the retrofit configuration with SEGR at a SEGR ratio of 60% the decrease is 0.1%, for an overall capture level of 94%.

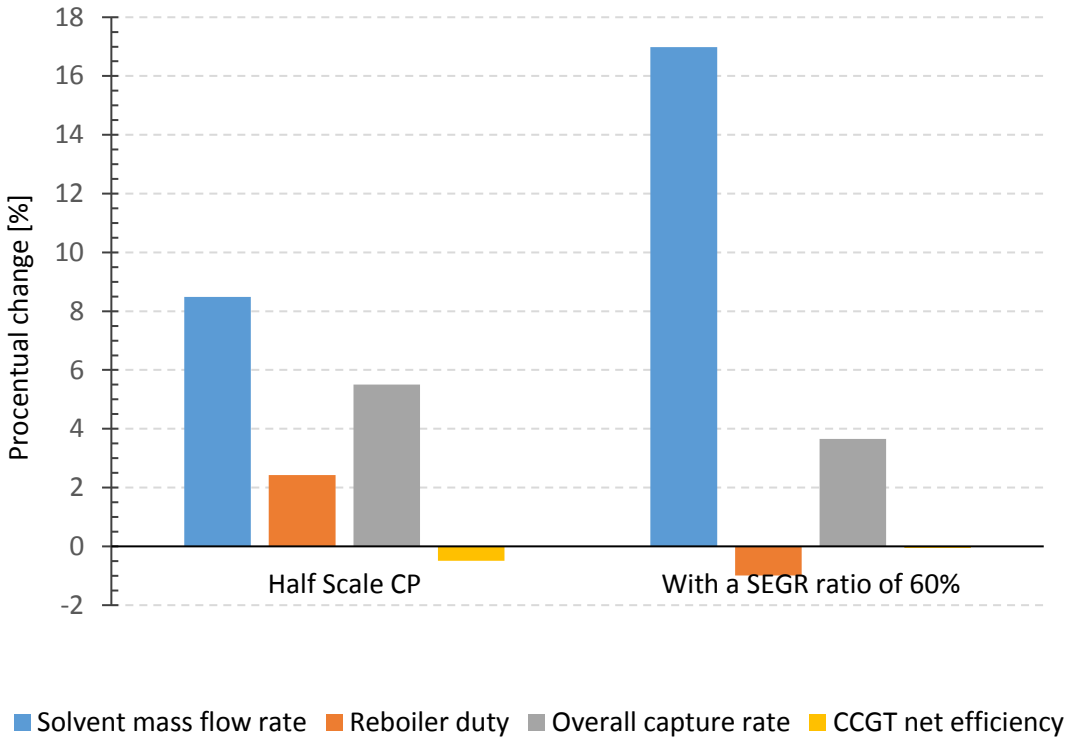

Figure 7-9: Changes in solvent mass flow rate, reboiler duty, overall capture rate and CCGT net thermal efficiency to the base case without SEGR, due to the intensification strategy 'increased solvent mass flow rate', for the configuration Half Scale CP

The effect of the intensification strategy 'decreased stripper pressure' is illustrated in Figure 7-10 as changes to the base case in percentages. A decrease in the stripper pressure for the base case from 1.94 bar to 1.89 bar, increases the overall capture rate to 97%. For the retrofitted configuration at a SEGR ratio of 60%, the same decrease in stripper pressure leads to an increase of the overall capture rate to 94%. The reboiler duty increases for the configuration without SEGR compared to the base case by approximately 8%. For the configuration with SEGR at a SEGR ratio of 60% the reboiler duty does not increase at all, compared to the base case. The CCGT net thermal decrease for the Half Scale configuration without SEGR is 0.9%, for an overall capture level of 97%. For the retrofit configuration with SEGR at a SEGR ratio of 60% the decrease is 0.1%, for an overall capture level of 94%.

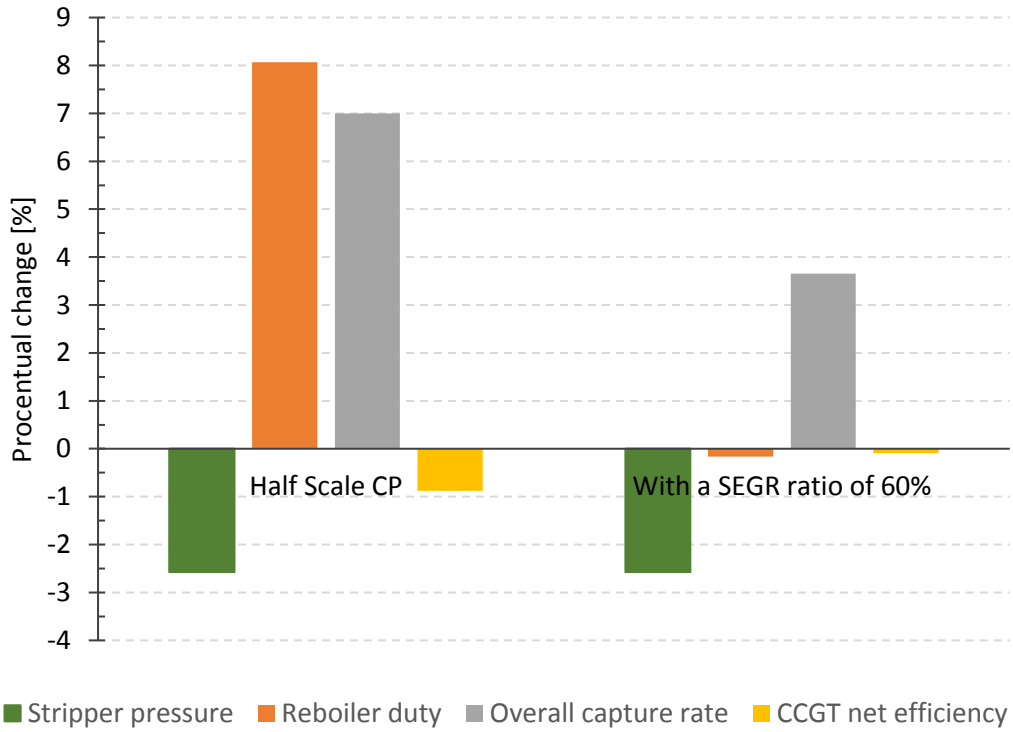

Figure 7-10: Changes in stripper pressure, reboiler, overall capture rate and CCGT net thermal efficiency to the base case without SEGR, due to the intensification strategy 'decreased stripper pressure', for the configuration Half Scale CP'

Figure 7-11 is illustrating the effect of the different operational strategies on the mass transfer and the gas temperature in the absorber for the configuration Half Scale CP

with SEGR at a SEGR ratio of 60%. The results show, that a change in the operational strategy can optimise the mass transfer performance of MEA for flue gas conditions under SEGR in parallel at a SEGR ratio of 60%, increasing the overall capture rate up to 94%. However, the gas temperatures in the absorber are getting even hotter and therefore are limiting the achievable mass transfer even further.

The difference in CCGT net efficiency between the configurations Half Scale CP without SEGR to the configuration Half Scale CP with SEGR, under all investigated operational strategies to increase the capture level of the power plant, is 1%. However, the maximal achievable overall capture rate in the cases without SEGR is 97%, compared to the 94% in the cases with SEGR.

Though, the net thermal efficiency of the configuration cases with SEGR is higher, the overall CO2 emissions increase drastically for all the investigated SEGR configuration cases (see Table 7-10). Considering the configuration CCGT with PCC without any intensification strategy applied as base case, the CO2 emission increase for the configuration cases with SEGR and intensification strategy applied by nearly 30%. That leads to a CO2 emission per net power output of the CCGT of 0.012 tCO2/MWh (CCGT with PCC and SEGR and intensification strategy applied) in comparison to 0.010 tCO2/MWh for a conventional CCGT with PCC.

In contrast to the intensification strategy ‘higher solvent mass flow rate’ without SEGR, the CO2 emissions drop by 55% and for the intensification strategy ‘lower stripper pressure’ by even 70%, respectively, leading to a CO2 emission per net power output of the CCGT 0.004 and 0.003 tCO2/MWh.

Table 7-10: Technical and operational variables of the capture plant and CCGT net power output for the configuration Half Scale CP and Half Scale CP with SEGR at a SEGR ratio of 60% for different operational strategies

	Unit						
Configuration		Half Scale CP			Half Scale CP with SEGR		
SEGR ratio	%	0			60		
Intensification strategy		original design	higher solvent mass flow rate	lower stripper pressure	original design	higher solvent mass flow rate	lower stripper pressure
Solvent mass flow rate	kg/s	424	460	424	760	884	760
Stripper pressure	bar	1.94	1.94	1.89	1.94	1.94	1.89
Reboiler duty	MJ/kg_{CO2}	3.40	3.48	3.67	3.26	3.37	3.39
Lean solvent loading	mol_{CO2}/mol_{MEA}	0.264	0.264	0.236	0.264	0.263	0.236
Rich solvent loading	mol_{CO2}/mol_{MEA}	0.475	0.468	0.465	0.489	0.479	0.486
Capture Rate of the PCC	%	90.0	95.5	97.0	85.0	94.4	94.4
Overall CO2 emissions	t_{CO2}/h	**7.7**	**3.5**	**2.3**	**24.7**	**10.0**	**10.0**
CO2 emissions per net power output	t_{CO2}/MWh	**0.010**	**0.004**	**0.003**	**0.030**	**0.012**	**0.012**
SEGR recovery rate	%	-	-	-	99.5	99.5	99.5
Overall capture rate	**%**	**90.0**	**95.5**	**97.0**	**84.3**	**93.7**	**93.7**
CCGT net power output	MWe	795.0	787.6	781.9	823.6	811.9	811.3
CCGT net thermal efficiency	**%**	**53.1**	**52.6**	**52.2**	**53.8**	**53.1**	**53.0**

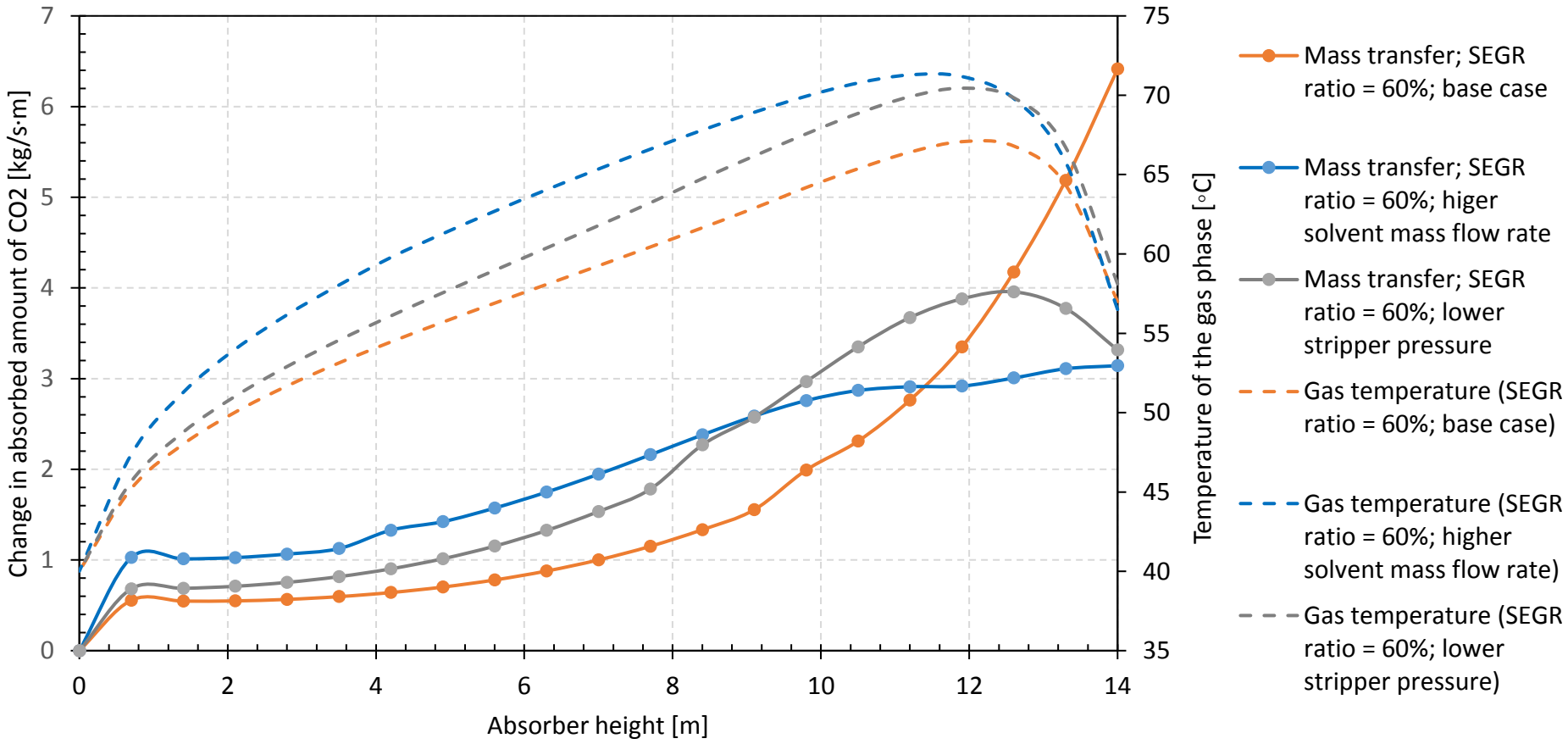

Figure 7-11: Mass transfer (continuous line) and temperature profile of the gas phase (dashed line) in the absorber of the configuration Half Scale CP with SEGR for a SEGR ratio of 60%, using a 30% MEA aqueous solution, for different operational changes

7.5 Summary and Discussion of the Results

Results obtain from the assessment of the capture plant and overall capture rate of process simulations of CCGT power plants with PCC, using MEA aqueous solution, and retrofitted regenerative rotary CO2-transfer devices, for SEGR in parallel application, are summarised and discussed in this section.

An important parameter for SEGR retrofit configurations is the overall capture rate of the power plant. Since CO2 will not only leave the system boundary at the capture plant, but as well at the SEGR unit, the capture rate of the PCC is not any longer the only parameter to be considered when reporting CO2 emissions.

To mitigate detrimental effects of the efficiency of the SEGR unit, the retrofitted regenerative rotary CO2 transfer device needs to be oversized in means of adsorbent mass requirement.

For the reported retrofit configurations that leads to a mass requirement of 1063 tonnes for the used KOH activated carbon. This mass can be distributed in four wheels of 30m diameter and 2.6 m height, per CCGT train.

This large mass requirement and associated costs for a transitioning towards SEGR need to be justified in the context of a higher overall capture level, a smaller penalty in net thermal efficiency of the CCGT and reduced overall CO2 emissions.

There are several further points to be considered in this context.

The 99% transfer efficiency approach does not take into account the large footprint such a large amount of solid would generate in form of several rotary devices per CCGT train. CCGT power plants are designed to fit on a rather small piece of property. To accommodate eight wheels of 30 m in diameter might be more than challenging on an existing side.

Moreover, a large amount of the solid adsorbent is not utilised efficiently in a process where SEGR is used as a retrofit option to chase residual CO2 emissions. Since the flue gas variables and properties at a SEGR ratio of 20% as well as 60% are off design, this leads to an inefficient CO2 transfer process.

Furthermore, the current rotary transfer model does not consider pressure drop. Taking into account that the flue gas mass flow rate would be distributed over four very large wheels per CCGT train, reducing the effective flue gas flow rate to a quarter, the effect of pressure drop increase over the adsorbent bed would increase the energy penalty significantly. Those associated the auxiliary losses are not accounted for at the in current version of the regenerative CO2 transfer wheel model. Hence, it seems not justifiable to apply adsorption based SEGR as a retrofit to existing CCGTs.

In general, the operation of the absorber column at reduced gas velocity is shown to be detrimental to retrofitting selective CO_2 recycling to existing CCGT plants with solvent-based capture.

Possible operational SEGR ratios for the two different retrofit configurations are:

- For a retrofit configuration Full Scale CP with SEGR, SEGR ratios of up to 20% can be achieved in the limitation of the entrainment regime of the absorber column.
- For a retrofit configuration Half Scale CP with SEGR, SEGR ratios of up to 20% can be achieved in the limitation of the entrainment regime of the absorber column when both capture plants are operated separately.
- For a retrofit configuration Half Scale CP with SEGR, SEGR ratios from 50% up to 60% can be achieved in the limitation of the entrainment regime of the absorber column, when the absorber column of one capture plant is switched off and the solvent bypass is activated.

An increase of the overall capture level beyond the initial design of 90% capture is achievable for some SEGR ratios at constant design and operation parameters.

For design variables kept constant (flooding fraction 75% and stripper pressure 1.94bar), an increase in overall capture rate to 92% for both retrofit configurations for a SEGR ratio of 20% is possible. The resulting CO2 concentration at absorber inlet is just around 1% point higher than in the configurations without SEGR. This increase may not constitute a sufficiently large increase to justify the additional costs of

retrofitting SEGR, especially in the context that these CO2 concentrations are achievable with EGR instead of SEGR.

The retrofit configuration Half Scale CP with SEGR at a SEGR ratio of 60% is only achieving an overall capture rate of 84% at design point, due to reaching the flooding constrain for the higher solvent flow rate through one absorber and the absorber getting pinched. This clearly shows that SEGR retrofitted to post-combustion carbon capture plants using MEA as solvent is not beneficial.

Assessing CO2 emission reductions in future CO2 capture plants beyond the initial design of 90% capture rate, by different intensification strategies, lead to higher overall capture rates for all investigated configurations with only marginal increase in operational costs.

The mass transfer limitation for MEA for a SEGR ratio of 60% in the retrofit configuration can be partially overcome. However, the maximal achievable overall capture rate with SEGR is 94%, compared to the 97% in the cases without SEGR. A difference in CCGT net efficiency of 1% between the configurations Half Scale CP without SEGR to the configuration Half Scale CP with SEGR is not sufficient to justify the additional cost associated with SEGR. Yet, these results are MEA specific due to the high enthalpy of adsorption associated with MEA.

However, the purpose of retrofitting SEGR to an existing CCGT with PCC is to chase residual CO2 emission. Therefore, the most important factor considered should be the overall CO2 emissions in each case. In all considered SEGR cases the CO2 emissions increase drastically, with the best considered intensification strategy (higher solvent mass flow rate) increasing CO2 emissions by 30% in comparison to an existing CCGT with PCC and no further intensification strategy applied. Therefore, it seems that applying SEGR as retrofit to existing CCGTs with PCC is not justifiable.

Chapter 8 Conclusions and Recommendations

This thesis aims at improving the understanding of the implications and effects of adding selective CO2 transfer devices to combined cycle gas turbines with post-combustion carbon capture technologies, in the context of process intensification of carbon capture, by utilizing a kinetic-based model of CO2 adsorption in a honeycomb structure, regenerative, rotary wheel. It further aims to improve the understanding of the potential gain of retrofit SEGR to existing CCGT with PCC.

8.1 Conclusions

8.1.1 Regenerative Rotary CO2 Transfer Wheel

A new kinetic based model of CO2 adsorption in a honeycomb structure, regenerative, rotary wheel is s developed to assess the potential of using adsorption for selective CO2 exhaust gas recycling. The results are presented in Chapter 4. The kinetic-based model is used to size the rotary wheel for an 800MW combined cycle gas turbines power plant with PCC, using kinetic and equilibrium properties of an activated carbon material (presented in Section 3.4.1), with suitable equilibrium properties.

- The KOH activated carbon is experimentally assessed under SEGR flue gas conditions and presents no sensitivity to water for the investigated conditions, an important factor due to the relative high amount of water vapour in the flue gas of CCGTs. The generated breakthrough curve measurements for a feed gas flow similar to the expected flue gas conditions in CCGTs with SEGR in parallel at a SEGR ratio of 70% are used to validate the kinetic model of the rotary regenerative CO2 transfer wheel.
- The validation shows that kinetic data, obtained through breakthrough measurements of an adsorbent in a laboratory isothermal fixed bed tubular reactor setup and equilibrium parameters can be used to predict the

behaviour of the adsorbent in a rotary regenerative CO2 transfer wheel. This enables screening for promising adsorbent materials for this kind of technology.

- An attempt to regenerate the KOH activated carbon with air is performed. The results indicate that a full regeneration is not achieved under the limitation of a ratio of desorption air to flue gas mass flow of 1.12. However, this is acceptable for the regenerative rotary CO2 transfer wheel as the reduced adsorption capacity can be overcome with a higher mass of solid adsorbent.
- The kinetic model shows that a previously developed equilibrium model of the rotary wheel underestimates the required adsorbent mass for a needed recovery rate of 97% for SEGR in parallel by factor of 3.7. A total mass of KOH activated carbon of around 598 tonnes per GT train will be needed to achieve a recovery rate of 97%.
- A rigorous design assessment concludes, that the amount of adsorbent material required for SEGR in parallel and a SEGR ratio of 70% could be accommodated in two wheel devices of 30 m in diameter and 2.17 m in height. The sizing is not dissimilar to regenerative rotary heat exchanger used in large thermal coal-fired power plants for preheating combustion air.
- Nonetheless, it highlights the importance of further research in adsorbent material to reduce sizes, and by extension costs. Especially in the region of high recovery rates, where the kinetic model predicts an exponential increase in adsorbent mass, better adsorbent materials are needed to reduce the adsorbent mass requirement and therefore the number of wheels needed.
- A sensitivity analysis of kinetic adsorbent properties and operational conditions is performed in an attempt to push the limits of process intensification. It shows a maximal optimum value for the temperature independent pre-exponential diffusion constant at 40 m^2/s. Further increases improve recovery rate or adsorbent mass requirement only marginally. A reduction of 20% in adsorbent mass requirement could, however, be already achieved by a change in the temperature independent pre-exponential

diffusion constant of the KOH activated carbon from 13 to 16.7 m^2/s. The same reduction can be achieved by either increasing the saturation capacity from 10.8 to 13.6 mol/kg, or by increasing the enthalpy of adsorption from 17.4 to 18.0 kJ/mol.

- The sensitivity analysis on the geometrical factor, which is simplified in the model to the value for a packed bad, shows the importance of the development of an optimal structured adsorbent for this kind of application.
  It clearly demonstrations a large effect on adsorbent mass requirement. An increase of the factor from 15 to 20 leads to a significant decrease in adsorbent mass requirement of 20.2%.
- The sensitivity analysis on the specific heat capacity of the adsorbent material shows over the investigated range of Cp_s values (400-1400 J/kg·K), a moderate reduction in adsorbent mass requirement of 8.2% for a constant recovery ratio of 97%. However, the reduction effect is limited and not significant for values above 70.
- The sensitivity analysis of the surface heating area, given by the surface of the adsorbent, indicates that a further increase in this adsorbent property is not necessary. It appears to be high enough, to not add any further resistance to heat transfer.
- The sensitivity analysis of the operational parameter rotational speed shows, that the rotational speed can be used to push recovery rate and adsorbent mass reduction. For the investigated case of SEGR in parallel with a recovery rate of 97% and a SEGR ratio of 70%, the optimal rotational speed is found to be 2 rpm. It leads to an adsorbent mass requirement of the KOH activated carbon of around 550 tonnes per GT train. This amount of adsorbent material could be accommodated in two wheel devices of 30 m in diameter and 2 m in height per GT train.
- The sensitivity analysis performed on the partitioning of the rotary wheel in adsorption and desorption shows that any change in either way of the partitioning leads to a loss in recovery rate and an increase in adsorbent mass.

This is true for adsorbents that follow the same behaviour in adsorption and desorption. For the investigated case of SEGR in parallel with a recovery rate of 97% and a SEGR ratio of 70% using the KOH activated carbon, the optimal partitioning is given by dividing the wheel in equal sections between adsorption and desorption.

- The sensitivity analysis performed on the temperatures of the flue gas and the air stream shows a small effect on the adsorbent mass and the recovery rate. However, the effect of either temperature increase shows a larger impact on the CO2-enriched air outlet temperature. Since a higher air inlet temperature into the compressor derates the gas turbine power output, measures need to be taken to limit the heat transfer into the CO2-enriched air stream. This can be achieved by keeping the air inlet and the flue gas outlet temperature as low as possible.
- Leakage considerations show a preferred direction of gap leakages from the air to the flue gas side. This can be achieved by choosing the position of the booster fans accordingly, to achieve a higher pressure in the desorption section than in the adsorption section.

8.1.2 Effects of a Regenerative Rotary CO2 Transfer Device on a new build CCGT Power Plant with PCC

For the first time, a kinetic model of a regenerative rotary CO2 transfer wheel, using adsorption technology to transfer CO2 in a parallel configuration, is integrated with a model of a new build CCGT power plant with post-combustion capture. It is used to assess the effect of SEGR on a new build CCGT plant with PCC. The results are presented in Chapter 6.

- SEGR operated in parallel to the CO2 PCC plant increases the CO2 concentration in the flue gas of a CCGT power plant significantly, while slightly reducing oxygen levels in the combustor of the gas turbine. The O2

concentration drops in the CO2-enriched air used for combustion from originally 21 vol% in ambient air to 19 vol%, for a maximal SEGR ratio of 70%.

- For a maximal SEGR ratio of 70%, the selective CO2 transfer device needs to achieve a recovery rate of 97%, while the post-combustion capture plant needs to operate at a capture rate of 96% to achieve an overall CO2 capture rate of 90%. The resulting CO2 concentration at the post-combustion capture plant is 14.4 vol%, compared to 4.3 vol% in a conventional air fired CCGT with PCC.
- To achieve a recovery rate of 97%, a total amount of 551 tonnes of the KOH activated carbon, introduced in Section 3.4, is required per GT train, at an optimised rotational speed of the CO2 transfer wheel of 2 rpm. That amount can be accommodated in two wheels of 30m in diameter and 2 m in height per GT train as honeycomb structured adsorbent, with a wall thickness of 1 mm and a pitch of 4.5 mm.
- The CO2-enriched air entering the gas turbine compressor has a CO2 concentration of 9.97 vol%, compared to the 0.03 vol% in the non-enriched air. The temperature of the CO2-enriched air rises by 9°C to 24°C, and the density increases by 2%, respectively.
- The gas turbine net power output of the new build power plant with SEGR is increased by 4.3 MWe per GT train, or 8.5 MWe for both gas turbines combined, due to the higher density of the CO2-enriched air. However, the thermal efficiency of the turbine decreases by 1%. That offset can be explained by the effect that, although the CO2-enriched air enters the compressor at 9°C hotter, than the non-enriched air, the addition of CO2 results in a lower specific heat ratio, leading to a lower compressor outlet temperature. To keep the turbine inlet temperature constant, more fuel is required, resulting in an increase in fuel mass flow rate of 4.3%.
- The exhaust flue gas enters the heat recovery steam generator at a higher temperature and higher mass flow rate, resulting in more heat being available for the generation of steam. Consequently, the power output of the steam

cycle is increased by 32 MW. However, due to the limitation of the superheated high pressure steam inlet temperature to 600°C, the approach temperature is increased by 39% (70°C). Yet, simultaneously more heat is recovered leading to an increase in Rankine efficiency by 2% point up to 68% point in total. However, more thermal energy, in form of higher temperature and higher mass flow rate, is available. By redesigning the steam cycle to be optimised for the new flew gas condition a further increase in Rankine efficiency can be expected.

- SEGR in parallel with a SEGR ratio of 70 %, decreases the flue gas mass flow rate to the capture plant by around 70%, and increases the CO2 concentration from 4.3 vol% to 14.4 vol%. To achieve an overall CO2 capture rate of 90% the post-combustion capture plant requires to capture 96% of the CO2 entering the capture plant.
- For solvent-based systems, the diameter of the absorber column can be designed 35% smaller, due to the reduced flue gas mass flow rate. However, due to the higher required capture rate, the absorber height needs to be increased by 35%. Yet, the overall packing volume can be reduced from 4207 m^3 to 2426 m^3, a saving in packing volume of 42%. The specific reboiler duty reduces at the same time by 2.7%.
- The net power output of the new build CCGT with PCC and SEGR is evaluated based on the electrical power generated in the gas turbines and steam turbine, considering energy penalties due to steam extraction for the regeneration of the solvent, due to auxiliary power consumption in the power plant and in the capture plant, and due to power consumption for compressing the CO2 for transport and storage. The CCGT net power output increases by 39MWe to 834 MWe, increasing the CCGT net thermal efficiency from 53.1 % to 53.4% for a new build CCGT with PCC and SEGR, when compared to a conventional CCGT with PCC.

8.1.3 Effects of SEGR on a CCGT Plant with PCC Retrofitted with Regenerative CO2 Transfer Devices

For the first time, SEGR retrofit options to existing CCGTs with PCC are investigated. The aim is to explore the possibility to increase the overall capture level beyond the initial design of 90% capture by adding regenerative rotary CO2 transfer in parallel to the capture plant. Two different capture plant configurations are investigated for the retrofit studies. The results are presented in Chapter 7.

- The regenerative rotary CO2 transfer device for the retrofit configurations is sized to transfer 99% of the CO2 in the CCGT flue gas composition for a SEGR ratio of 70%. The high recovery rate is chosen to not limit the overall capture rate by the transfer rate of the SEGR unit. An amount of around 1063 tonnes of the KOH activated carbon is necessary to transfer 99% of the CO2 concentration in the flue gas. This amount can be accommodated in three wheels of 30 m in diameter and 2.56 m in height per GT train as honeycomb structured adsorbent, with a wall thickness of 1 mm and a pitch of 4.5 mm.
- The entrainment regime of the absorbers in the capture plant and therefore hydraulics, is the limiting factor for achievable SEGR ratios. For very low flue gas mass flow rates, as encountered for very high SEGR ratios, the loading point of the absorber packing is not reached, and therefore not enough contact between flue gas and solvent is generated.
- Achievable SEGR ratios for the two studied retrofit configuration, in accordance with the entrainment regime of the absorber column, are:
    - Retrofit configuration Full Scale CP with SEGR: A SEGR ratio of 20%, resulting in a CO2 concentration at the absorber inlet of 5.39 mol%.
    - Retrofit configuration Half Scale CP with SEGR (both capture plants per GT train in operation): A SEGR ratio of 20%, resulting in a CO2 concentration at the absorber inlet of 5.39 mol%
    - Retrofit configuration Half Scale CP with SEGR (one capture plant with solvent bypass of the second capture plant per GT train in operation):

A SEGR ratio of 60%, resulting in a CO2 concentration at the absorber inlet of 11.2 mol%.

- The implementation of a rotary regenerative CO2 transfer device with a SEGR ratio of 20% leads, in both studied configurations, to an increase of only 1 mol% in CO2 concentration. This in turn leads only to an increase in the overall capture rate of 2% and a marginal reboiler duty reduction of below 1%. That increase may not constitute a sufficiently large increase to justify the additional costs of retrofitting SEGR.
- In the case of the implementation of a CO2 transfer wheel with a SEGR ratio of 60% for the configuration Half Scale CP with SEGR, the overall capture rate decreases to 84%. This is due to a reduced overall solvent mass flow rate of 10%, limited by the flooding fraction of the one absorber in operation and by the absorber getting pinched, limiting the CO2 mass transfer. This is a problem specific for the solvent used, which is 30 wt% MEA.
- Analysing the cycle capacity of the wheel for an off design application at a SEGR ratio of 20% and 60%, indicates that a large amount of the solid adsorbent is not utilised efficiently in the SEGR retrofit option. To apply an inefficient CO2 transfer process, with possible higher pressure losses, to chase residual emission seems therefore not justifiable.
- In general, the operation of the absorber column at reduced gas velocity is shown to be detrimental to retrofitting selective CO_2 recycling to existing CCGT plants with solvent-based capture.
- Comparing achievable overall capture levels of a CCGT with PCC, utilizing 30 wt% MEA, and retrofitted SEGR, pushed to reduce CO2 emissions beyond design level, with a conventional CCGT with PCC, utilizing 30 wt% MEA, pushed to reduce CO2 emission, shows that the achievable capture levels with SEGR do not overcome the achievable capture levels in a conventional CCGT with PCC pushed to achieve higher capture levels. This is a solvent specific problem. Therefore, using SEGR as retrofit to push for higher capture levels and lower

CO2 emissions is not a suitable option for post-combustion carbon capture plants using MEA.

8.2 Future Work

There are several ways to further improve the understanding of the implications and effects of selective CO2 transfer on power plants, capture technologies and the associated challenges. Some relevant recommendations and direction for further research are listed here:

- The combustion process has been experimentally assessed in a premixed DLE swirl burner with a CO2-enriched oxidant at 1.1 bar and 2.2 bar (Marsh et al. 2016) and the in a premixed HPGSB 2 swirl burner with a CO2-enriched oxidant at 5.5 bar (Giles et al. 2019). However, even the experiments at 5.5 bar are still below the operational pressure of large scale gas turbines (over 18bar), so further experiments are necessary to investigate the effect on flame stability, burner operation and emissions.
- Although a proof of concept for the desorption of the CO2 loaded adsorbent with air was performed in this work, a much better understanding of the limitations of desorption with air is necessary. These experiments need to be performed qualitatively and quantitatively, to produce data to predict the desorption behaviour of CO2 from adsorbents with air. Those data can then be implemented into the kinetic model of the regenerative rotary wheel to reassess the performed sensitivity analysis of the partitioning of the wheel. Those experimental tests should include repeated cycling over several weeks to assess the life time of the adsorbent and the working cycle capacity reduction over time.
- It is recommended to proof the concept of the regenerative wheel at lab scale, by building a demonstrator of the proposed concept.
- The operational profiles of the adsorbent in the wheel, generated in this work using the developed kinetic model, indicate, that it may be possible to use different adsorbent materials across the height of the rotary wheel, in order

to maximise working capacity. This could lead to a reduction in the adsorbent mass requirement and to the use of adsorbents with properties tailored to their location in the wheel. This might be a further step in the optimisation of the wheel and should be investigated.

- A rigorous screening of available adsorbent materials, applying the methodology used for validation of the wheel is recommended. This work here provides guidelines for adsorbent material development for SEGR application, which currently is focused on adsorbent for CO2 capture. The guidelines allow to screen literature for promising adsorbent materials. However, although often equilibrium properties and data of adsorbents can be found in the literature, diffusion data and kinetic properties are often not reported. Yet, breakthrough curve measurements can be found. As shown by the performed validation of the system, those breakthrough curve measurements can be used by fitting the rotary wheel simulation to predict the behaviour of the adsorbent material in the SEGR application, as long as equilibrium data of the material are available.
- The assessment of the selective CO2 transfer system is performed with a model taking mass and heat transfer resistances into account. The next step to improve the prediction of the model and to better evaluate energy penalties related to the operation of the wheel, is the implementation of a pressure drop equation along the height of the CO2 transfer wheel.
- Fitting regenerative CO2 transfer devices in parallel with a SEGR ratio of 70% to new build CCGTs with PCC show, due to the low volume of flue gas and the increased CO2 concentration, great potential for process intensification. However, a more detail assessment of the costs related to using adsorption technology for SEGR application is a needed next step to evaluate its competitiveness to other process intensification strategies.
- Limiting factors in the retrofit study, performed in this work, are the entrainment regime of adsorber column and the absorber getting pinched. Several further investigations are needed in this context. An assessment to

which degree an intercooling step in the absorber column could improve the performance of the solvent studied (30 %wt MEA) and hence the overall CO2 capture rate should be performed. Furthermore, it might be worth assessing solvents with slower mass transfer rate, higher CO2 capacities and smaller enthalpy of adsorption in the context of higher CO2 concentrations achievable with SEGR.

- There is a growing consensus (IEAGHG 2017; National Grid 2019) that the primary role of fossil fuel power stations will shift away from providing base-load power to flexible dispatchable power as well as inertia, to balance and support the high levels of intermittent renewable penetration. Particularly, in low carbon emission intensity scenarios power stations with PCC are required to operate in a highly flexible manner.(IEAGHG 2017) This will affect both the CO2 capture plant that will consequently need to capture CO2 from the varying amounts of fossil fuel that is burned throughout the day, and the SEGR device that will have to work with lower mass flow rates of flue gas and therefore a lower amount of CO2. CCS systems are highly flexible systems in terms of their design yet operating off design increases operational cost and therefore CO2 capture cost. The ability and effect of rotary regenerative CO2 transfer devices and of integrated CCGT with PCC and SEGR to regularly operate in a flexible manner is to date not understood or assessed. Therefore, further research in the context of flexible operation of the regenerative rotary CO2 transfer device is recommended.

  In its current form the rotary wheel model does not provide the ability to assess the start-up, shutdown and load following behaviour of the wheel. Though, the performance result of the rotary regenerative wheel to operate under different SEGR ratios for the retrofit study gives a first insight into this topic. The results show that the system is able to function with lower flue gas flow rates. Consequently, the CO2 concentration in the flue gas will change, affecting the capture plant efficiency, as demonstrated for retrofit analysis. The same holds true for the SEGR device, where the cyclic capacity shows a

drastic reduction for lower SEGR ratios. If the power plant has to adapt its load, the air through the rotary system would be dictated by the changing swallowing capacity of the GT compressor. That would reduce the transfer efficiency of the system to a lower driving force in the regeneration section of the wheel. To increase the performance in such a situation the rotational time of the wheel could be adapted. A longer rotational time (lower rpm) would lead to a longer contact time of solid mass with a higher amount of regenerating air, providing more driving force per each section of solid.

- The learnings of regenerative rotary CO2 transfer should be extended to coal fired power plants, to assess the possibility of process intensification for the coal power plants equipped with post-combustion capture technology. Different integration strategies need to be developed due to changed composition, contaminations and particle content in the flue gas
- Finally, extending the current study and methodology to other industrial applications, where CO2 capture will be essential in the near future to mitigate climate change, might offer great potential. A significant amount of CO2 emissions is produced in industrial processes, contributing to 25% of the global CO2 emissions (GCCSI 2016). Utilising CCS in decarbonising the industrial sector, with a focus on the key emitters like iron and steel production, cement and oil refining and petrochemicals, will need to go hand in hand with different aspects of process intensification, to keep CO2 capture penalty costs low and thereby keeping those industries competitive on the market. Many of the processes include several stages of burners and heaters to provide heat, steam or energy to different process steps. Increasing in those combustors the CO2 concentration and therefore the CO2 concentration in the exhaust gases, by means of SEGR, might reduce the cost of CO2 capture for those processes.

References

Abanades, J. C., B. Arias, A. Lyngfelt, T. Mattisson, D. E. Wiley, H. Li, M. T. Ho, E. Mangano, and S. Brandani. 2015. “Emerging CO2 Capture Systems.” *International Journal of Greenhouse Gas Control* 40: 126–66. https://doi.org/10.1016/j.ijggc.2015.04.018.

Abbas Abdulkareem Mahmood, Al-Farraji. 2017. “Chemical Engineering and Reactor Design of a Fluidised Bed Gasifier.” Cardiff University. https://orca.cf.ac.uk/104985/1/2017Al-FarrajiAAMPhD.pdf.

Aboudheir, Ahmed, and Walid ElMoudir. 2009. “Performance of Formulated Solvent in Handling of Enriched CO2 Flue Gas Stream.” *Energy Procedia* 1 (1): 195–204. https://doi.org/10.1016/j.egypro.2009.01.028.

Abu-Zahra, M. R.M., A. Sodiq, and P. H.M. Feron. 2016. *Commercial Liquid Absorbent-Based PCC Processes*. *Absorption-Based Post-Combustion Capture of Carbon Dioxide*. Elsevier Ltd. https://doi.org/10.1016/B978-0-08-100514-9.00029-9.

Adderley, B., J. Carey, J. Gibbins, M. Lucquiaud, and R. Smith. 2016. “Post-Combustion Carbon Dioxide Capture Cost Reduction to 2030 and Beyond.” *Faraday Discussions* 192: 27–35. https://doi.org/10.1039/c6fd00046k.

Ågren, N. D., M. O. Westermark, M. A. Bartlett, and T. Lindquist. 2002. “First Experiments on an Evaporative Gas Turbine Pilot Power Plant: Water Circuit Chemistry and Humidification Evaluation.” *Journal of Engineering for Gas Turbines and Power* 124 (1): 96–102. https://doi.org/10.1115/1.1397778.

Akram, M., U. Ali, T. Best, S. Blakey, K. N. Finney, and M. Pourkashanian. 2016. “Performance Evaluation of PACT Pilot-Plant for CO2 Capture from Gas Turbines with Exhaust Gas Recycle.” *International Journal of Greenhouse Gas Control* 47: 137–50. https://doi.org/10.1016/j.ijggc.2016.01.047.

Aqua-Cache. 2020. “AquaStream Modular Filter Arrays.” 2020. http://aqua-cache.com/components/wpu.

Arrieta, Felipe R.Ponce, and Electo E.Silva Lora. 2005. “Influence of Ambient

Temperature on Combined-Cycle Power-Plant Performance." *Applied Energy* 80 (3): 261–72. https://doi.org/10.1016/j.apenergy.2004.04.007.

Bae, Tae Hyun, Matthew R. Hudson, Jarad A. Mason, Wendy L. Queen, Justin J. Dutton, Kenji Sumida, Ken J. Micklash, Steven S. Kaye, Craig M. Brown, and Jeffrey R. Long. 2013. "Evaluation of Cation-Exchanged Zeolite Adsorbents for Post-Combustion Carbon Dioxide Capture." *Energy and Environmental Science* 6 (1): 128–38. https://doi.org/10.1039/c2ee23337a.

Bae, Youn Sang, and Randall Q. Snurr. 2011. "Development and Evaluation of Porous Materials for Carbon Dioxide Separation and Capture." *Angewandte Chemie - International Edition* 50 (49): 11586–96. https://doi.org/10.1002/anie.201101891.

Baker, R.W. 2004. *Membrane Technology and Applications*. 2nd ed. John Wile & Sons.

Baker, Richard W, Johannes G Wijmans, Timothy C Merkel, Haiqing Lin, Ramin Daniels, and Scott Thompson. 2011. Gas separation process using membranes with permeate sweep to remove CO2 from combustion gases. US Patent 7964020B2, issued 2011.

Bansal, Roop Chand, and Meenakshi Goyal. 2005. *Activated Carbon Adsorption*. Boca Raton, USA: CRC Press.

Bathen, Dieter, and Marc Breitbach. 2001. *Adsorptionstechnik*. Berlin; Heidelberg; New York; Barcelona; Hongkong; London; Mailand; Paris; Tokio: Springer.

Ben-Mansour, R., M. A. Habib, O. E. Bamidele, M. Basha, N. A.A. Qasem, A. Peedikakkal, T. Laoui, and M. Ali. 2016. "Carbon Capture by Physical Adsorption: Materials, Experimental Investigations and Numerical Modeling and Simulations - A Review." *Applied Energy* 161: 225–55. https://doi.org/10.1016/j.apenergy.2015.10.011.

Betancur Arroyave, Adrian Alberto, D. Camargo-Trillos, Farid Chejne Janna, and Francisco Carrasco-Marin. 2013. "Activated Carbon Monolith Production By Organic Binders To Capture CO2." In *Annual World Conference on Carbon*.

Bianchi, M., L. Branchini, A. De Pascale, F. Melino, A. Peretto, R. K. Bhargava, and M.

A. Chaker. 2010. “Gas Turbine Power Augmentation Technologies: A Systematic Comparative Evaluation Approach.” *ASME Turbo Expo 2010: Power for Land, Sea, and Air*.

Biliyok, Chechet, and Hoi Yeung. 2013. “Evaluation of Natural Gas Combined Cycle Power Plant for Post-Combustion CO2 Capture Integration.” *International Journal of Greenhouse Gas Control* 19: 396–405. https://doi.org/10.1016/j.ijggc.2013.10.003.

Boyce, M. P. 2012. *Advanced Industrial Gas Turbines for Power Generation*. *Combined Cycle Systems for Near-Zero Emission Power Generation*. Elsevier Masson SAS. https://doi.org/10.1016/B978-0-85709-013-3.50002-X.

BP. 2017. “BP Energy Outlook 2017- Middle East.” https://doi.org/10.1177/107110079501600609.

Brandani, F., A. Rouse, S. Brandani, and D. M. Ruthven. 2004. “Adsorption Kinetics and Dynamic Behavior of a Carbon Monolith.” *Adsorption* 10 (2): 99–109. https://doi.org/10.1023/B:ADSO.0000039866.37214.6a.

Brigman, Natasha, Muhammad I. Shah, Olav Falk-Pedersen, Toine Cents, Vian Smith, Thomas De Cazenove, Anne K. Morken, et al. 2014. “Results of Amine Plant Operations from 30 Wt% and 40 Wt% Aqueous MEA Testing at the CO2 Technology Centre Mongstad.” *Energy Procedia* 63: 6012–22. https://doi.org/10.1016/j.egypro.2014.11.635.

Broekhoff, J.C.P. 1979. “Mesopore Determination from Nitrogen Sorption Isotherms: Fundamentals, Scope, Limitations.” *Studies in Surface Science and Catalysis* 3 (January): 663–84. https://doi.org/10.1016/S0167-2991(09)60243-3.

Brooks, F.J. 2000. “GE Gas Turbine Performance Characteristics.” *GE Power Systems*.

Bui, Mai, Claire S. Adjiman, André Bardow, Edward J. Anthony, Andy Boston, Solomon Brown, Paul S. Fennell, et al. 2018. “Carbon Capture and Storage (CCS): The Way Forward.” *Energy and Environmental Science* 11 (5): 1062–1176. https://doi.org/10.1039/c7ee02342a.

CCC. 2019. “Net Zero Technical Report.” *Committee on Climate Change*, 2019.

www.theccc.org.uk/publications.

Chua, Hui Tong, Anutosh Chakraborty, and Xiao Lin Wang. 2004. “The Specific Heat Capacity of Adsorbate- Adsorbent System.” *International Refrigeration and Air Conditioning Conference*, Paper 662. http://docs.lib.purdue.edu/iracc%5Cnhttp://docs.lib.purdue.edu/iracc/662.

Cooper, Jim. 1991. “Booster Fans and Gas Reheaters for Wet Flue-Gas Desulphurisation Systems.” In *International Power Generation Conference, ASME, 91-JPGC-Pwr-45*.

———. 2013. “Howden Heater Technology - Leakage and Heater Sealing Solutions.” In *Confidential Presentation*.

Dantas, T. L.P., F. M.T. Luna, I. J. Silva, A. E.B. Torres, D. C.S. De Azevedo, A. E. Rodrigues, and R. F.P.M. Moreira. 2011. “Modeling of the Fixed-Bed Adsorption of Carbon Dioxide and a Carbon Dioxidenitrogen Mixture on Zeolite 13X.” *Brazilian Journal of Chemical Engineering* 28 (3): 533–44. https://doi.org/10.1590/S0104-66322011000300018.

Dantas, Tirzha, F Luna, I Silva, D de Azevedo, C Grande, A Rodrigues, and R Moreira. 2011. “Carbon Dioxide-Nitrogen Separation through Adsorption on Activated Carbon in a Fixed Bed.” *Chemical Engineering Journal* 169 (1–3): 11–19. https://doi.org/10.1016/j.cej.2010.08.026.

Darabkhani, Hamidreza G., Nelia Jurado, George Prpich, John E. Oakey, Stuart T. Wagland, and Edward J. Anthony. 2018. “Design, Process Simulation and Construction of a 100 KW Pilot-Scale CO2 Membrane Rig: Improving in Situ CO2 Capture Using Selective Exhaust Gas Recirculation (S-EGR).” *Journal of Natural Gas Science and Engineering* 50 (April 2017): 128–38. https://doi.org/10.1016/j.jngse.2017.09.012.

Datta, Amitava, Supravat Mondalz, and Subhas Dutta Gupta. 2008. “Perspectives for the Direct Firing of Biomass as a Supplementary Fuel in Combined Cycle Power Plants.” *International Journal of Energy Research* 32. https://doi.org/10.1002/er.

DECC. 2015. “Amber Rudd’s Speech on a New Direction for UK Energy Policy.”

Department of Energy and Climate Change and The Rt Hon Amber Rudd MP. 2015. https://www.gov.uk/government/speeches/amber-rudds-speech-on-a-new-direction-foruk-%0Aenergy-policy%0A.

Delorme, Marc, Reinhard Six, Daniel Mugnier, Jean-Yves Quinette, Nadja Richler, Frank Heunemann, Edo Wiemken, et al. 2004. “Climasol: Solar Air Conditioning Guide.” 2004. http://www.cres.gr/climasol/index_files/pdf/climasol.pdf.

Diego, M. E., J. M. Bellas, and M. Pourkashanian. 2018. “Techno-Economic Analysis of a Hybrid CO2 Capture System for Natural Gas Combined Cycles with Selective Exhaust Gas Recirculation.” *Applied Energy* 215 (February): 778–91. https://doi.org/10.1016/j.apenergy.2018.02.066.

Diego, Maria Elena, Jean Michel Bellas, and Mohamed Pourkashanian. 2017. “Process Analysis of Selective Exhaust Gas Recirculation for CO2 Capture in Natural Gas Combined Cycle Power Plants Using Amines.” *Proceedings of the ASME Turbo Expo* 3 (December): 1–10. https://doi.org/10.1115/GT2017-64387.

Ding, Junyuan, Brice Freeman, and Gary T. Rochelle. 2017. “Regeneration Design for NGCC CO2Capture with Amine-Only and Hybrid Amine/Membrane.” *Energy Procedia* 114 (November 2016): 1394–1408. https://doi.org/10.1016/j.egypro.2017.03.1264.

Ditaranto, Mario, Jørgen Hals, and Tor Bjørge. 2009. “Investigation on the In-Flame NO Reburning in Turbine Exhaust Gas.” *Proceedings of the Combustion Institute* 32 II: 2659–66. https://doi.org/10.1016/j.proci.2008.07.002.

Do, D. D., and H. D. Do. 2001. “Surface Diffusion of Hydrocarbons in Activated Carbon: Comparison between Constant Molar Flow, Differential Permeation and Differential Adsorption Bed Methods.” *Adsorption* 7 (3): 189–209. https://doi.org/10.1023/A:1012780700536.

EBTF. 2011. “Project CAESAR - European Best Practice Guidelines for Assessment of CO2 Capture Technologies.” http://caesar.ecn.nl/fileadmin/caesar/user/documents/D_4.9_best_practice_guide.pdf.

Eldrid, R., Lynda Kaufman, and Paul Marks. 2001. “GER-4194 - The 7FB: The Next

Evolution of the F Gas Turbine."

ElKady, Ahmed M., A Evulet, A Brand, TP Ursin, and A Lynghjem. 2008. "Exhaust Gas Recirculation in DLN F-Class Gas Turbines for Post-Combustion CO2 Capture." *Proceedings of the ASME Turbo Expo, 2008: Power for Land, Sea and Air* 3.

ElKady, Ahmed M., Andrei Evulet, Anthony Brand, Tord Peter Ursin, and Arne Lynghjem. 2009a. "Application of Exhaust Gas Recirculation in a DLN F-Class Combustion System for Postcombustion Carbon Capture." *Journal of Engineering for Gas Turbines and Power* 131 (3): 1–6. https://doi.org/10.1115/1.2982158.

———. 2009b. "Application of Exhaust Gas Recirculation in a DLN F-Class Combustion System for Postcombustion Carbon Capture." *Journal of Engineering for Gas Turbines and Power* 131 (3): 1–6. https://doi.org/10.1115/1.2982158.

Emirates Steel. 2019. "Abu Dhabi CCS." 2019. https://www.emiratessteel.com/index.php/en/corporate-responsibility/environmental/co2-capture-project.

Equinor. 2019. "Carbon Storage." 2019. https://www.equinor.com/en/how-and-why/climate-change/carbon-storage.html.

ETI. 2016. "Reducing the Cost of CCS Developments in Capture Plant Technology," 18.

———. 2017. "Thermal Power with CCS: Final Project Report." *Energy Technologies Institute*, 2017.

European Commission. 2019. "Paris Agreement." European Commission. 2019. http://ec.europa.eu/clima/policies/international/negotiations/paris/index_en.htm.

Evulet, Andrei T., Ahmed M. ELKady, Anthony R. Branda, and Daniel Chinn. 2009. "On the Performance and Operability of GE's Dry Low NOx Combustors Utilizing Exhaust Gas Recirculation for PostCombustion Carbon Capture." *Energy Procedia* 1 (1): 3809–16. https://doi.org/10.1016/j.egypro.2009.02.182.

Freguia, Stefano, and Gary T. Rochelle. 2003. "Modeling of CO2 Capture by Aqueous

Monoethanolamine." *AIChE Journal* 49 (7): 1676–86. https://doi.org/10.1002/aic.690490708.

Gassnova. 2019. "CO2 Capture Facility at Karsto Norway - Front End Engineering and Design (FEED) Study Report."

GCCSI. 2018. "The Global Status of CCS: 2018." *Global CCS Institute*.

General Electric Power Generation. 2016. "F-Class Power Plants." 2016. https://powergen.gepower.com/products/power-plants/f-class-power-plants.html.

Gibson, J. A.Arran, Enzo Mangano, Elenica Shiko, Alex G. Greenaway, Andrei V. Gromov, Magdalena M. Lozinska, Daniel Friedrich, Eleanor E.B. Campbell, Paul A. Wright, and Stefano Brandani. 2016. "Adsorption Materials and Processes for Carbon Capture from Gas-Fired Power Plants: AMPGas." *Industrial and Engineering Chemistry Research* 55 (13): 3840–51. https://doi.org/10.1021/acs.iecr.5b05015.

Giles, A, R Marsh, D Pugh, J Runyon, B Goktepe, A Valera-Medina, and P Bowen. 2019. "Experimental and Numerical Investigation of CO2 Dilution on CO/NOx Emissions in Premixed Swirling Flames at Pressures up to 0.55 MPa." *Combustion Science Technology*, no. under review.

Glueckauf, E., and J. I. Coates. 1947. "Theory of Chromatography - Part IV - The Influence of Incomplete Equilibrium on the Front Boundary of Chromatograms and on the Effectiveness of Separation." *Journal of the Chemical Society (Resumed)*, no. 0 (January): 1315. https://doi.org/10.1039/jr9470001315.

Gnanapragasam, Nirmal V., Bale V. Reddy, and Marc A. Rosen. 2009. "Optimum Conditions for a Natural Gas Combined Cycle Power Generation System Based on Available Oxygen When Using Biomass as Supplementary Fuel." *Energy* 34 (6): 816–26. https://doi.org/10.1016/j.energy.2009.03.006.

Goff, George S., and Gary T. Rochelle. 2004. "Monoethanolamine Degradation: O2 Mass Transfer Effects under CO2 Capture Conditions." *Industrial and Engineering Chemistry Research* 43 (20): 6400–6408. https://doi.org/10.1021/ie0400245.

González-Salazar, Miguel Angel. 2015. “Recent Developments in Carbon Dioxide Capture Technologies for Gas Turbine Power Generation.” *International Journal of Greenhouse Gas Control* 34 (x): 106–16. https://doi.org/10.1016/j.ijggc.2014.12.007.

González Díaz, Abigail. 2016. “Sequential Supplementary Firing in Natural Gas Combined Cycle Plants with Carbon Capture for Enhanced Oil Recovery.” Doctor of Philosophy Thesis, University of Edinburgh, Edinburgh. 2016.

González Díaz, Abigail, Eva Sancheza, J. M. Gonzalez Santalób, Jon Gibbinsa, and Mathieu Lucquiaud. 2014. “On the Integration of Sequential Supplementary Firing in Natural Gas Combined Cycle for CO2-Enhanced Oil Recovery: A Technoeconomic Analysis for Mexico.” *Energy Procedia* 63: 7558–67. https://doi.org/10.1016/j.egypro.2014.11.791.

Grace, J.R., Knowlton, T.M., Avidan, A.A. 1997. *Circulating Fluidized Beds*. Springer.

Grande, Carlos A., Carlos Gigola, and Alírio E. Rodrigues. 2003. “Propane-Propylene Binary Adsorption on Zeolite 4A.” *Adsorption* 9 (4): 321–29. https://doi.org/10.1023/A:1026223914143.

Grande, Carlos A., and Alírio E. Rodrigues. 2008. “Electric Swing Adsorption for CO2 Removal from Flue Gases.” *International Journal of Greenhouse Gas Control* 2 (2): 194–202. https://doi.org/10.1016/S1750-5836(07)00116-8.

Green, Andrew. 2012. “CCS Next Generation Gas Capture Technology.” 2012. https://www.eti.co.uk/programmes/carbon-capture-storage/ccs-next-generation-gas-capture-technology.

Haszeldine, R. S. 2009. “Carbon Capture and Storage: How Green Can Black Be?” *Science* 325 (September). https://doi.org/10.1017/CBO9780511635359.007.

Hellat, J., and Hoffmann J. 2016. Combined cycle power plant with flue gas recirculation. US9249689 B2, issued 2016.

Herraiz, Laura. 2016. “Selective Exhaust Gas Recirculation in Combined Cycle Gas Turbine Power Plants with Post-Combustion CO2 Capture.” *Doctor of Philosophy Thesis, University of Edinburgh, Edinburgh*, 2016.

Herraiz, Laura, Dougal Hogg, Jim Cooper, Jon Gibbins, and Mathieu Lucquiaud.

2015. “Reducing Water Usage with Rotary Regenerative Gas/Gas Heat Exchangers in Natural Gas-Fired Power Plants with Post-Combustion Carbon Capture.” *Energy* 90: 1994–2005. https://doi.org/10.1016/j.energy.2015.07.032.

Herraiz, Laura, Erika Palfi, Mathieu Lucquiaud, and Eva Sanchez_Fernandez. 2019. “Rotary Adsorption: Selective Recycling of CO2 in Combined Cycle Gas Turbine Power Plants.” *Frontiers in Energy Research*, no. under review.

Herraiz, Laura, Eva Sánchez Fernández, Erika Palfi, and Mathieu Lucquiaud. 2018. “Selective Exhaust Gas Recirculation in Combined Cycle Gas Turbine Power Plants with Post-Combustion CO2 Capture.” *International Journal of Greenhouse Gas Control* 71 (June 2017): 303–21. https://doi.org/10.1016/j.ijggc.2018.01.017.

Hogg, Dougal. 2016. “Conversation with Dougal Hogg, Chief Engineer, Heaters - Howden Fans & Heaters.”

———. 2018. “Conversation with Dougal Hogg, Chief Engineer, Heaters - Howden Fans & Heaters.”

Horlock, J. H., D. T. Watson, and T. V. Jones. 2001. “Limitations of Gas Turbine Performance Imposed by Large Turbine Cooling Flows.” *Journal of Engineering for Gas Turbines and Power* 123 (3): 487–94. https://doi.org/10.1115/1.1373398.

Howden. 2019. “Gas-Gas-Heaters.” 2019. https://www.howden.com/en-gb/products-and-services/heaters/gas-gas-heater.

Huang, Weilong, Wenying Chen, and Gabrial Anandarajah. 2017. “The Role of Technology Diffusion in a Decarbonizing World to Limit Global Warming to Well below 2 °C: An Assessment with Application of Global TIMES Model.” *Applied Energy* 208 (March): 291–301. https://doi.org/10.1016/j.apenergy.2017.10.040.

Huang, Yu, Tim C. Merkel, and Richard W. Baker. 2014. “Pressure Ratio and Its Impact on Membrane Gas Separation Processes.” *Journal of Membrane Science* 463: 33–40. https://doi.org/10.1016/j.memsci.2014.03.016.

IEA. 2016. “IEA World Energy Outlook.” 2016.

IEAGHG. 2012. “CO2 Capture at Gas Fired Power Plants.” *IEAGHG* 08.

———. 2014. “Assessment of Emerging CO2 Capture Technologies and Their Potential to Reduce Cost.”

———. 2017. “Valuing Flexibility in CCS Power Plants.”

IGSCC (2012). n.d. “Innovative Gas Separation for Carbon Capture.” EPSRC. Accessed August 23, 2019. http://gow.epsrc.ac.uk/NGBOViewGrant.aspx?GrantRef=EP/G062129/1.

Inventys Inc. 2019. “Inventys Technology.” 2019. http://inventysinc.com/technology/.

Iordanidis, A. A. 2002. *Mathematical Modeling of Catalytic Fixed Bed Reactors*. *PhD Thesis*.

IPCC. 2014. “Climate Change 2014 Mitigation of Climate Change.” *Contribution of Working Group III to the Fifth Assessment Report of the Intergovernmental Panel on Climate Change*. https://doi.org/10.1146/annurev-environ-021113-095626.

Jonshagen, K. 2011. *Modern Thermal Power Plants: Aspects on Modelling and Evaluation*.

Jonshagen, Klas, Nikolett Sipöcz, and Magnus Genrup. 2011. “A Novel Approach of Retrofitting a Combined Cycle With Post Combustion CO2 Capture.” *Journal of Engineering for Gas Turbines and Power* 133 (1).

Jonsson, Maria, and Jinyue Yan. 2005. “Humidified Gas Turbines - A Review of Proposed and Implemented Cycles.” *Energy* 30 (7): 1013–78. https://doi.org/10.1016/j.energy.2004.08.005.

Joos, P. 1999. “Dynamic Surface Phenomena.” https://books.google.co.uk/books?hl=de&lr=&id=J7ksF43dgCIC&oi=fnd&pg=PR9&dq=Dynamic+Surface+Phenomena&ots=9xvuiXo4VV&sig=trqjrUoC4FJfR9SqTyJMSIR8mbs.

Jørgensen, S.B. 1986. “Fixed Bed Reactor Dynamics and Control - A Review.” *IFAC Control of Distillation Columns and Chemical Reactors*.

https://doi.org/10.1016/s1474-6670(17)59393-3.

Joss, Lisa, Matteo Gazzani, and Marco Mazzotti. 2017. “Rational Design of Temperature Swing Adsorption Cycles for Post-Combustion CO2 Capture.” *Chemical Engineering Science* 158 (September 2016): 381–94. https://doi.org/10.1016/j.ces.2016.10.013.

Kajszika, HW. 1998. “Adsorptive Abluftreinigung Und Lösungsmittelrückgewinnung Durch Inertgasregenerierung.” https://books.google.co.uk/books?hl=de&lr=&id=hvqvkWi3ux4C&oi=fnd&pg=PA1&dq=Kajszika+1998&ots=nFKdsd5ecb&sig=qkvfOPsmNbzt8R9eOkNb40iLUI4.

Kehlhofer, Rolf, Frank Hannemann, Franz Stirnimann, and Bert Rukes. 2009. *Combined-Cycle Gas and Steam Turbine Power Plants*. 3rd ed. PennWell.

Khalighi, Mona, Shamsuzzaman Farooq, and Iftekhar A. Karimi. 2012. “Nonisothermal Pore Diffusion Model for a Kinetically Controlled Pressure Swing Adsorption Process.” *Industrial and Engineering Chemistry Research* 51 (32): 10659–70. https://doi.org/10.1021/ie3004539.

Kitto, John B., and Steven C. Stultz. 2005. *Steam - Its Generation and Use*. 41st ed. Barberton, Ohio, U.S.A.: The Babcock & Wilcox Company.

Koelbl, Barbara Sophia, Machteld A. van den Broek, André P.C. Faaij, and Detlef P. van Vuuren. 2014. “Uncertainty in Carbon Capture and Storage (CCS) Deployment Projections: A Cross-Model Comparison Exercise.” *Climatic Change* 123 (3–4): 461–76. https://doi.org/10.1007/s10584-013-1050-7.

Kolasinski, Kurt W. 2012. *Surface Science: Foundations of Catalysis and Nanoscience*. *John Wiley & Sons, Ltd*. https://doi.org/10.1002/9781119941798.ch3.

La, D., Y. J. Dai, Y. Li, R. Z. Wang, and T. S. Ge. 2010. “Technical Development of Rotary Desiccant Dehumidification and Air Conditioning: A Review.” *Renewable and Sustainable Energy Reviews* 14 (1): 130–47. https://doi.org/10.1016/j.rser.2009.07.016.

Lee, Seul Yi, and Soo Jin Park. 2015. “A Review on Solid Adsorbents for Carbon Dioxide Capture.” *Journal of Industrial and Engineering Chemistry* 23: 1–11.

https://doi.org/10.1016/j.jiec.2014.09.001.

Lepaumier, Helene, Dominique Picq, and Pierre Louis Carrette. 2009. “New Amines for CO2 Capture. II. Oxidative Degradation Mechanisms.” *Industrial and Engineering Chemistry Research* 48 (20): 9068–75. https://doi.org/10.1021/ie9004749.

Li, H., Mario Ditaranto, and David Berstad. 2011. “Technologies for Increasing CO2 Concentration in Exhaust Gas from Natural Gas-Fired Power Production with Post-Combustion, Amine-Based CO2 Capture.” *Energy* 36 (2): 1124–33. https://doi.org/10.1016/j.energy.2010.11.037.

Li, H., Mario Ditaranto, and Jinyue Yan. 2012. “Carbon Capture with Low Energy Penalty: Supplementary Fired Natural Gas Combined Cycles.” *Applied Energy* 97: 164–69. https://doi.org/10.1016/j.apenergy.2011.12.034.

Li, H., S. Flores, Y. Hu, and J. Yan. 2009. “Simulation and Optimization of Evaporative Gas Turbine with Chemical Apsorption for Carbon Dioxide Capture.” *International Journal of Green Energy* 6 (5).

Li, H., Geir Haugen, Mario Ditaranto, David Berstad, and Kristin Jordal. 2011. “Impacts of Exhaust Gas Recirculation (EGR) on the Natural Gas Combined Cycle Integrated with Chemical Absorption CO2 Capture Technology.” *Energy Procedia* 4: 1411–18. https://doi.org/10.1016/j.egypro.2011.02.006.

Li, Jian Rong, Ryan J. Kuppler, and Hong Cai Zhou. 2009. “Selective Gas Adsorption and Separation in Metal-Organic Frameworks.” *Chemical Society Reviews* 38 (5): 1477–1504. https://doi.org/10.1039/b802426j.

Lim, Jae Woo, Yunho Choi, Hee Seung Yoon, Young Kwon Park, Jin Heong Yim, and Jong Ki Jeon. 2010. “Extrusion of Honeycomb Monoliths Employed with Activated Carbon-LDPE Hybrid Materials.” *Journal of Industrial and Engineering Chemistry* 16 (1): 51–56. https://doi.org/10.1016/j.jiec.2010.01.022.

Lindquist, T. O., P. M. Rosen, and T. Torisson. 2000a. “Evaporative Gas Turbine Cycle – a Description of a Pilot Plant and Operating Experience.” *Proceedings of ASME Advanced Energy Systems Division*.

———. 2000b. “Theoretical and Experimental Evaluation of the EvGT Process.”

Proceedings of ASME Advanced Energy Systems Division.

Lindquist, Torbjorn, Marcus Thern, and Tord Torisson. 2002. “Experimental and Theoretical Results of a Humidification Tower in an Evaporative Gas Turbine Cycle Pilot Plant.” *ASME Turbo Expo 2002: Power for Land, Sea, and Air* 2.

Lowell, S, JE Shields, MA Thomas, and M Thommes. 2012. “Characterization of Porous Solids and Powders: Surface Area, Pore Size and Density.” https://books.google.co.uk/books?hl=de&lr=&id=IwvSBwAAQBAJ&oi=fnd&pg=PA1&dq=Characterization++of++Porous++Solids++and+++Powders&ots=2oeDf1S6QN&sig=Y-QxU8FcdnRyaYDKmuJhZzU3py8.

Mangano, E., S. Brandani, M. C. Ferrari, H. Ahn, D. Friedrich, M. L. Lozinska, P. A. Wright, et al. 2013. “Efficient and Rapid Screening of Novel Adsorbents for Carbon Capture in the UK IGSCC Project.” *Energy Procedia* 37 (0): 40–47. https://doi.org/10.1016/j.egypro.2013.05.083.

Marsh, R, A Giles, J Runyon, D Pugh, P Bowen, S Morris, A Valera-Medina, T Best, K Finney, and M Pourkashanian. 2016. “Selective Exhaust Gas Recycling for Carbon Capture Applications: Combustion and Operability Measurement.” *The Future of Gas Turbine Technology 8th International Gas Turbine Conference, 12-13 October, Brussels, Belgium*, no. October: 1–9.

Marx, Dorian, Lisa Joss, Max Hefti, Ronny Pini, and Marco Mazzotti. 2013. “The Role of Water in Adsorption-Based CO2 Capture Systems.” *Energy Procedia* 37: 107–14. https://doi.org/10.1016/j.egypro.2013.05.090.

Merkel, Timothy C., Xiaotong Wei, Zhenjie He, Lloyd S. White, J. G. Wijmans, and Richard W. Baker. 2013. “Selective Exhaust Gas Recycle with Membranes for CO2 Capture from Natural Gas Combined Cycle Power Plants.” *Industrial and Engineering Chemistry Research* 52 (3): 1150–59. https://doi.org/10.1021/ie302110z.

MIT. 2016. “Petra Nova W.A. Parish Fact Sheet: Carbon Dioxide Capture and Storage Project.” 2016. https://sequestration.mit.edu/tools/projects/wa_parish.html.

———. 2019. “Century Plant.” 2019. https://sequestration.mit.edu/tools/projects/century_plant.html.

Mohn, Thea Ragna. 2012. “Heat Capacity Measurements of Porous Materials at Cryogenic Temperatures,” no. June: 1–72.

Moreno-Castilla, Carlos, and Agustín F. Pérez-Cadenas. 2010. “Carbon-Based Honeycomb Monoliths for Environmental Gas-Phase Applications.” *Materials* 3 (2): 1203–27. https://doi.org/10.3390/ma3021203.

MUST. 2020. “Adsorption and Separation Lab.” 2020. http://web.mst.edu/~rezaeif/projects.html.

National Energy Technology Laboratory. 2010. “Carbon Capture Approaches for Natural Gas Combined Cycle Systems.” *U.S. Department of Energy Report No. DOE/NETL-2011/ 1470*.

———. 2013. “Current and Future Technologies for Natural Gas Combined Cycle (NGCC) Power Plants.” *U.S. Department of Energy, Office of Fossil Energy DOE/NETL-341/061013,*.

National Grid. 2019. “Future Energy Scenarios 2019.” *Future Energy Scenarios*, no. July: 162.

NRG Energy. 2019. “Petra Nova.” 2019. https://www.nrg.com/case-studies/petra-nova.html.

Oexmann, Jochen. 2011. “Post Combustion CO2 Capture: Energetic Evaluation of Chemical Absorption Processes in Coal Fired Steam Power Plants.” *Doctor of Philosophy Dissertation, Technical University of Hamburg-Harburg, Hamburg*.

Paepe, Ward De, Frank Delattin, Svend Bram, and Jacques De Ruyck. 2012. “Discussion of the Effects of Recirculating Exhaust Air on Performance and Efficiency of a Typical Microturbine.” *Proceedings of the 24th International Conference on Efficiency, Cost, Optimization, Simulation and Environmental Impact of Energy Systems, ECOS 2011* 45 (1): 745–56. https://doi.org/10.1016/j.energy.2011.11.060.

Pal, Parimal. 2017. *Industrial Water Treatment Process Technology*.

Pavri, R., and G.D. Moore. 2001. “Gas Turbine Emissions and Control.” *GE Power Systems*.

Plaza, M. G., S. García, F. Rubiera, J. J. Pis, and C. Pevida. 2010. “Post-Combustion

CO2 Capture with a Commercial Activated Carbon: Comparison of Different Regeneration Strategies." *Chemical Engineering Journal* 163 (1–2): 41–47. https://doi.org/10.1016/j.cej.2010.07.030.

Plaza, Marta G., Fernando Rubiera, and Covadonga Pevida. 2017. "Evaluating the Feasibility of a TSA Process Based on Steam Stripping in Combination with Structured Carbon Adsorbents to Capture CO2 from a Coal Power Plant." *Energy and Fuels* 31 (9): 9760–75. https://doi.org/10.1021/acs.energyfuels.7b01508.

Poullikkas, Andreas. 2005. "An Overview of Current and Future Sustainable Gas Turbine Technologies." *Renewable and Sustainable Energy Reviews* 9 (5): 409–43. https://doi.org/10.1016/j.rser.2004.05.009.

PSE Enterprise. 2016a. "GCCS V1.1.0 / Windows." 2016. https://www.psenterprise.com/products/.

———. 2016b. "GPROMS ModelBuilder V4.1.0 / Windows." 2016. https://www.psenterprise.com/products/gproms.

———. 2016c. "GSAFT - Advanced Thermodynamics." 2016. https://www.psenterprise.com/products/gsaft.

Querejeta, N., M. G. Plaza, F. Rubiera, C. Pevida, T. Avery, and S. R. Tennisson. 2017. "Carbon Monoliths in Adsorption-Based Post-Combustion CO2 Capture." *Energy Procedia* 114 (November 2016): 2341–52. https://doi.org/10.1016/j.egypro.2017.03.1366.

Rao, Ashok. 2015. "Evaporative Gas Turbine (EvGT)/Humid Air Turbine (HAT) Cycles." *Handbook of Clean Energy Systems*, 1–18. https://doi.org/10.1002/9781118991978.hces141.

Rezaei, F., and P. Webley. 2010. "Structured Adsorbents in Gas Separation Processes." *Separation and Purification Technology* 70 (3): 243–56. https://doi.org/10.1016/j.seppur.2009.10.004.

Rezaei, Fateme. 2011. *Optimization of Structured Adsorbents for Gas Separation Processes*.

Rezaei, Fateme, and Paul Webley. 2009. "Optimum Structured Adsorbents for Gas

Separation Processes." *Chemical Engineering Science* 64 (24): 5182–91. https://doi.org/10.1016/j.ces.2009.08.029.

Ribeiro, Rui P., Ticiane P. Sauer, Filipe V. Lopes, Regina F. Moreira, Carlos A. Grande, and Alírio E. Rodrigues. 2008. "Adsorption of CO2, CH4, and N2 in Activated Carbon Honeycomb Monolith." *Journal of Chemical & Engineering Data* 53 (10): 2311–17. https://doi.org/10.1021/je800161m.

Rodrigues, A. E., and Grande C. A. 2005. "Propane / Propylene Separation by Pressure Swing Adsorption Using Zeolite 4A." *Industrial and Engineering Chemistry Research* 44 (23): 8815–29.

Røkke, Petter E., and Johan E. Hustad. 2005. "Exhaust Gas Recirculation in Gas Turbines for Reduction of CO2 Emissions. Combustion Testing with Focus on Stability and Emissions." *ECOS 2005 - Proceedings of the 18th International Conference on Efficiency, Cost, Optimization, Simulation, and Environmental Impact of Energy Systems* 8 (4): 1427–34.

Russo, Giuseppe, George Prpich, Edward J. Anthony, Fabio Montagnaro, Neila Jurado, Giuseppina Di Lorenzo, and Hamidreza G. Darabkhani. 2018. "Selective-Exhaust Gas Recirculation for CO 2 Capture Using Membrane Technology." *Journal of Membrane Science* 549 (November 2017): 649–59. https://doi.org/10.1016/j.memsci.2017.10.052.

Ruthven, D. M., and C. Thaeron. 1996. "Performance of a Parallel Passage Adsorbent Contactor." *Separation and Purification Technology* 12 (1): 43–60. https://doi.org/10.1016/S1383-5866(97)00016-6.

Ruthven, Douglas M. 1984. *Principles of Adsorbtion and Adsorbtion Processes*. John Wiley & Sons.

Samanta, Arunkumar, An Zhao, George K H Shimizu, Partha Sarkar, and Rajender Gupta. 2012. "Post-Combustion CO2 Capture Using Solid Sorbents: A Review." *Industrial and Engineering Chemistry Research* 51 (4): 1438–63. https://doi.org/10.1021/ie200686q.

Sanchez Fernandez, E., M. Sanchez del Rio, H. Chalmers, P. Khakharia, E. L.V. Goetheer, J. Gibbins, and M. Lucquiaud. 2016. "Operational Flexibility Options

in Power Plants with Integrated Post-Combustion Capture." *International Journal of Greenhouse Gas Control* 48: 275–89. https://doi.org/10.1016/j.ijggc.2016.01.027.

Sander, Frank, Richard Carroni, Stefan Rofka, and Eribert Benz. 2011. "Flue Gas Recirculation in a Gas Turbine: Impact on Performance and Operational Behavior." *ASME 2011 Turbo Expo: Turbine Technical Conference and Exposition* 4.

SaskPower. 2019. "Boundary Dam Power Station." 2019. https://www.saskpower.com/our-power-future/our-electricity/electrical-system/system-map/boundary-dam-power-station.

SELECT. 2014. "Selective Exhaust Gas Recirculation for Carbon Capture with Gas Turbines: Integration, Intensification, Scale-up and Optimisation." 2014. http://gow.epsrc.ac.uk/NGBOViewGrant.aspx?GrantRef=EP/M001482/1.

Sexton, Andrew J., and Gary T. Rochelle. 2011. "Reaction Products from the Oxidative Degradation of Monoethanolamine." *Industrial and Engineering Chemistry Research* 50 (2): 667–73. https://doi.org/10.1021/ie901053s.

Shahkarami, Sepideh. 2017. "CO2 CAPTURE FROM GASES USING ACTIVATED CARBON."

Shahkarami, Sepideh, Ramin Azargohar, Ajay K. Dalai, and Jafar Soltan. 2015. "Breakthrough CO2 Adsorption in Bio-Based Activated Carbons." *Journal of Environmental Sciences (China)* 34: 68–76. https://doi.org/10.1016/j.jes.2015.03.008.

Shahkarami, Sepideh, Ajay K. Dalai, Jafar Soltan, Yongfeng Hu, and Dongniu Wang. 2015. "Selective CO2 Capture by Activated Carbons: Evaluation of the Effects of Precursors and Pyrolysis Process." *Energy and Fuels* 29 (11): 7433–40. https://doi.org/10.1021/acs.energyfuels.5b00470.

Sharifzadeh, Mahdi, and Nilay Shah. 2015. "Comparative Studies of CO2 Capture Solvents for Gas-Fired Power Plants: Integrated Modelling and Pilot Plant Assessments." *International Journal of Greenhouse Gas Control* 43: 124–32. https://doi.org/10.1016/j.ijggc.2015.10.009.

Sing, K.S.W. 1985. “Reporting Physisorption Data for Gas / Solid Systems with Special Reference to the Determination of Surface Area and Porosity.” *Pure & Applied Chemistry* 57 (11): 603–19.

Singh, Ajay, and Karl Stéphenne. 2014. “Shell Cansolv CO2 Capture Technology: Achievement from First Commercial Plant.” *Energy Procedia* 63: 1678–85. https://doi.org/10.1016/j.egypro.2014.11.177.

Stec, Marcin, Adam Tatarczuk, Lucyna Więcław-Solny, Aleksander Krótki, Tomasz Spietz, Andrzej Wilk, and Dariusz Ścpiewak. 2016. “Demonstration of a Post-Combustion Carbon Capture Pilot Plant Using Amine-Based Solvents at the Łaziska Power Plant in Poland.” *Clean Technologies and Environmental Policy* 18 (1): 151–60. https://doi.org/10.1007/s10098-015-1001-2.

Sulzer Chemtech. 2016. “Structured Packings for Distillation , Absorption and Reactive Distillation.”

Swisher, Joseph A., and Abhoyjit S. Bhown. 2014. “Analysis and Optimal Design of Membrane-Based CO2 Capture Processes for Coal and Natural Gas-Derived Flue Gas.” *Energy Procedia* 63: 225–34. https://doi.org/10.1016/j.egypro.2014.11.024.

Takahashi, Toru, Yoshinobu Nakao, and Eiichi Koda. 2007. *Analysis and Evaluation about Advanced Humid Air Turbine System*.

Thakkar, Harshul, Stephen Eastman, Amit Hajari, Ali A. Rownaghi, James C. Knox, and Fateme Rezaei. 2016. “3D-Printed Zeolite Monoliths for CO2 Removal from Enclosed Environments.” *ACS Applied Materials and Interfaces* 8 (41): 27753–61. https://doi.org/10.1021/acsami.6b09647.

Treybal, Robert. 1980. *Mass - Transfer Operations*.

Turi, Davide, Minh Ho, Maria-Chiara Ferrari, Paolo Chiesa, D. E. Wiley, and Matteo C. Romano. 2018. “CO2 Capture from Natural Gas Combined Cycles by CO2 Selective Membranes.” *International Journal of Greenhouse Gas Control* 61.

UNFCCC. 2017. “United Nations Framework Convention on Climate Change. The Paris Agreement.” 2017. http://unfccc.int/paris_agreement/items/9485.php.

United States Environmental Protection Agency - Office of Air Quality Planning and

Standards. 2002. *EPA Air Pollution Control Cost Manual*. https://doi.org/10.1126/science.203.4380.500.

Vargas, Diana P., Liliana Giraldo, and Juan C. Moreno-Piraján. 2012. "CO2 Adsorption on Activated Carbon Honeycomb-Monoliths: A Comparison of Langmuir and Tóth Models." *International Journal of Molecular Sciences* 13 (7): 8388–97. https://doi.org/10.3390/ijms13078388.

Voleno, Alberto, Matteo C. Romano, Davide M. Turi, Paolo Chiesa, Minh T. Ho, and Dianne E. Wiley. 2014. "Post-Combustion CO2 Capture from Natural Gas Combined Cycles by Solvent Supported Membranes." *Energy Procedia* 63: 7389–97. https://doi.org/10.1016/j.egypro.2014.11.775.

Walsh, P.P., and P. Fletcher. 2004. *Gas Turbine Performance*.

Wang, M., A. Lawal, P. Stephenson, J. Sidders, and C. Ramshaw. 2011. "Post-Combustion CO2 Capture with Chemical Absorption: A State-of-the-Art Review." *Chemical Engineering Research and Design* 89 (9): 1609–24. https://doi.org/10.1016/j.cherd.2010.11.005.

Wang, Qiang, Jizhong Luo, Ziyi Zhong, and Armando Borgna. 2011. "CO2 Capture by Solid Adsorbents and Their Applications: Current Status and New Trends." *Energy and Environmental Science* 4 (1): 42–55. https://doi.org/10.1039/c0ee00064g.

Webley, Paul A. 2014. "Adsorption Technology for CO2 Separation and Capture: A Perspective." *Adsorption* 20 (2–3): 225–31. https://doi.org/10.1007/s10450-014-9603-2.

Wijmans, J.G., T.C. Merkel, and R.W. Baker. 2011. Process for separating Carbon Dioxide from flue gas using parallel carbon dioxide capture and sweep-based membrane separation steps. US Patent 8177885B2, issued 2011.

———. 2012a. Gas separation process using membranes with permeate sweep to remove CO2 from gaseous fuel combustion exhaust. 8177885-B2, issued 2012.

———. 2012b. Power Generation process with partial recycle of carbon dioxide. US Patent 8220248-B2, issued 2012.

Wilcox, J. 2012. *Carbon Capture*. https://doi.org/10.1360/zd-2013-43-6-1064.

Wilcox, Jennifer, Reza Haghpanah, Erik C. Rupp, Jiajun He, and Kyoungjin Lee. 2014. "Advancing Adsorption and Membrane Separation Processes for the Gigaton Carbon Capture Challenge." *Annual Review of Chemical and Biomolecular Engineering* 5 (1): 479–505. https://doi.org/10.1146/annurev-chembioeng-060713-040100.

Xu, Dong, Penny Xiao, Jun Zhang, Gang Li, Gongkui Xiao, Paul A. Webley, and Yuchun Zhai. 2013. "Effects of Water Vapour on CO2 Capture with Vacuum Swing Adsorption Using Activated Carbon." *Chemical Engineering Journal* 230: 64–72. https://doi.org/10.1016/j.cej.2013.06.080.

Yamauchi, Hisashi, Akio Kodama, Tsutomu Hirose, Hiroshi Okano, and Ken Ichiro Yamada. 2007. "Performance of VOC Abatement by Thermal Swing Honeycomb Rotor Adsorbers." *Industrial and Engineering Chemistry Research* 46 (12): 4316–22. https://doi.org/10.1021/ie061184e.

Yang, R.T. 1986. "Gas Separation by Adsorption Processes." https://books.google.co.uk/books?hl=de&lr=&id=Ygb-BAAAQBAJ&oi=fnd&pg=PP1&dq=Gas+Separation+by+Adsorption+Processes&ots=b66h5WsP02&sig=pE1h-eOKye9qmKjzpZRVm0qH-4A.

Zeng, Tao, Hongyu Huang, Noriyuki Kobayashi, and Jun Li. 2017. "Performance of an Activated Carbon-Ammonia Adsorption Refrigeration System." *Natural Resources* 8 (10): 611–31. https://doi.org/10.4236/nr.2017.810039.

Zhang, Yingying, Yujiao Xie, Yudan Zhu, Xiaohua Lu, and Xiaoyan Ji. 2014. "Energy Consumption Analysis for CO2 Separation from Gas Mixtures with Liquid Absorbents." *Energy Procedia* 61: 2695–98. https://doi.org/10.1016/j.egypro.2014.12.280.

Zhang, Yue, Brice Freeman, Pingjiao Hao, and Gary T. Rochelle. 2016. "Absorber Modeling for NGCC Carbon Capture with Aqueous Piperazine." *Faraday Discussions* 192: 459–77. https://doi.org/10.1039/c6fd00030d.

Appendix

Appendix A Calibration Curves of the Mass Flow Controller and Measurement Accuracies

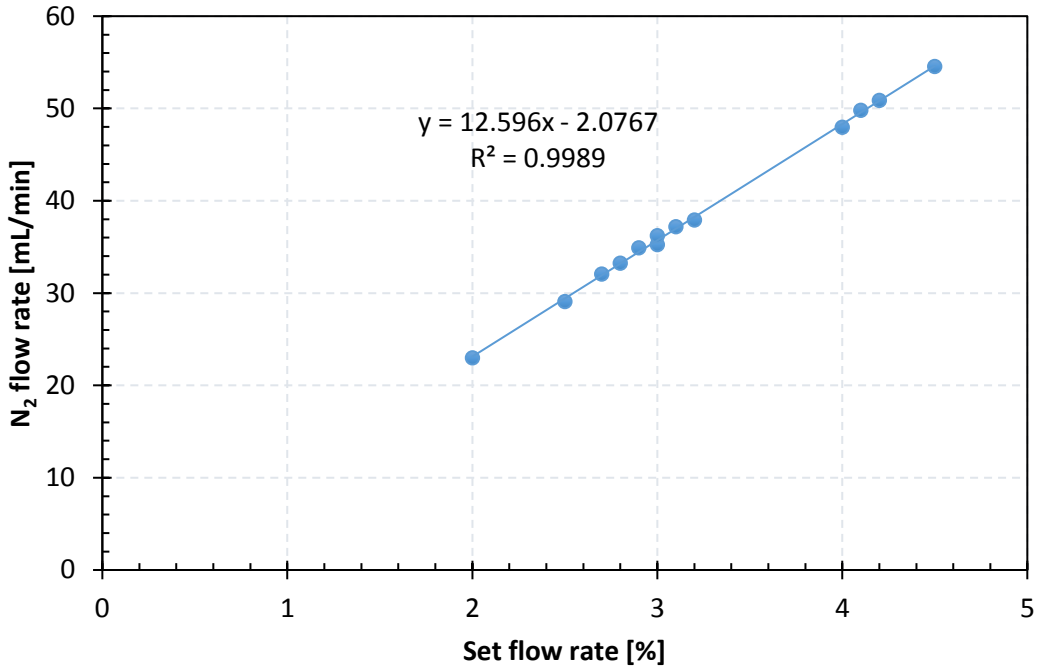

Figure A-1: **Calibration data for N_2 mass flow controller used in the adsorption experiments with the KOH activated carbon at 80 psi**

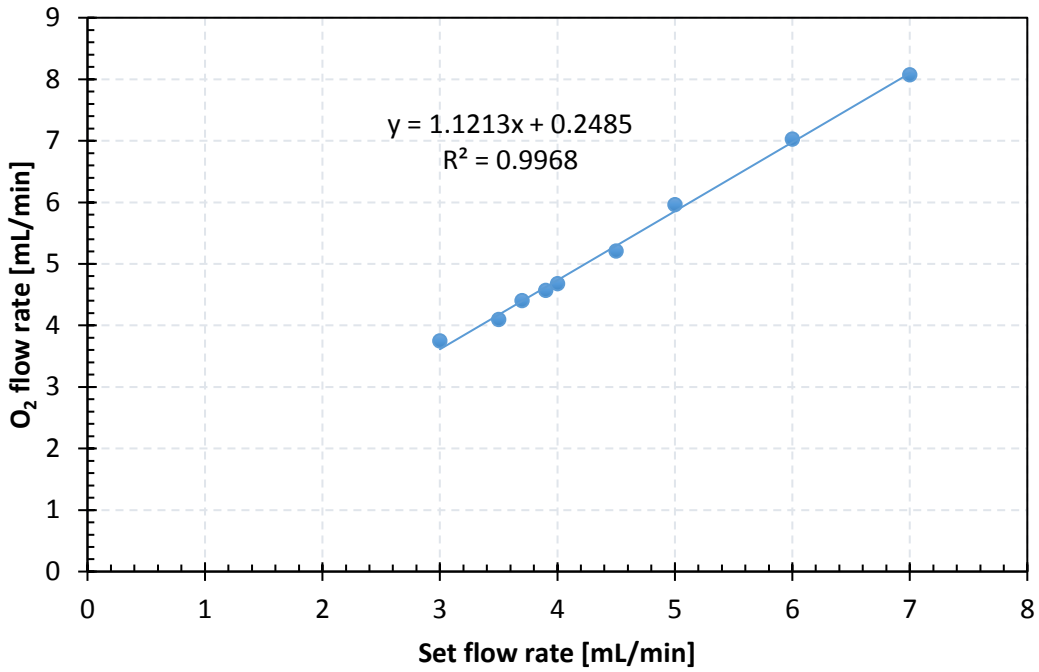

Figure A-2: **Calibration data for O_2 mass flow controller used in the adsorption experiments with the KOH activated carbon at 80 psi**

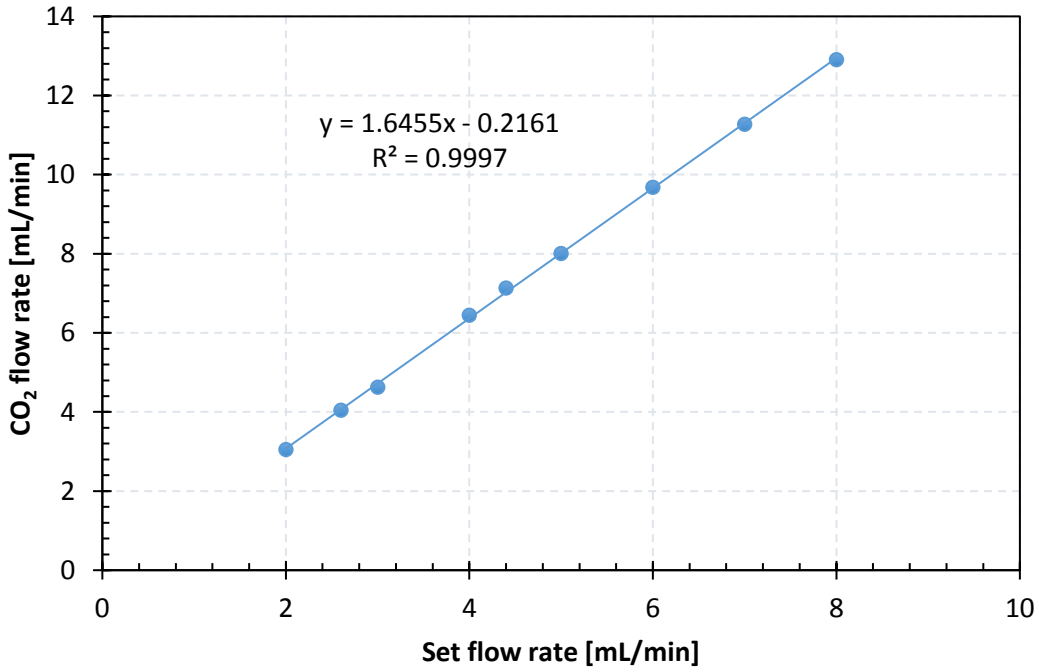

Figure A-3: **Calibration data for CO_2 mass flow controller used in the adsorption experiments with the KOH activated carbon at 80 psi**

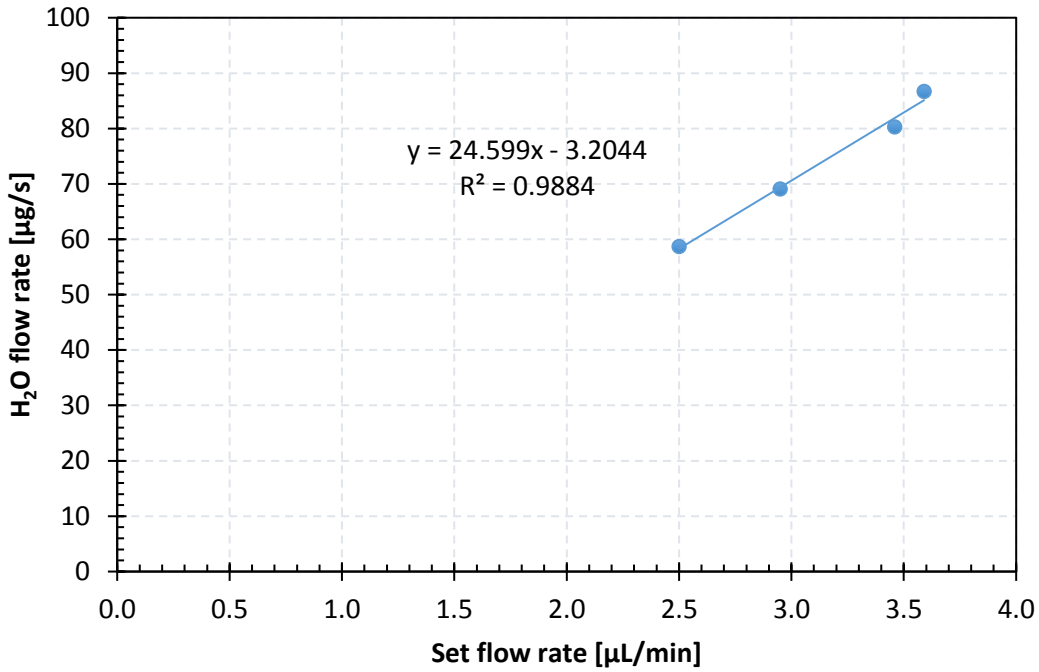

Figure A-4: Calibration data for H_2O mass flow controller used in the adsorption experiments with the KOH activated carbon

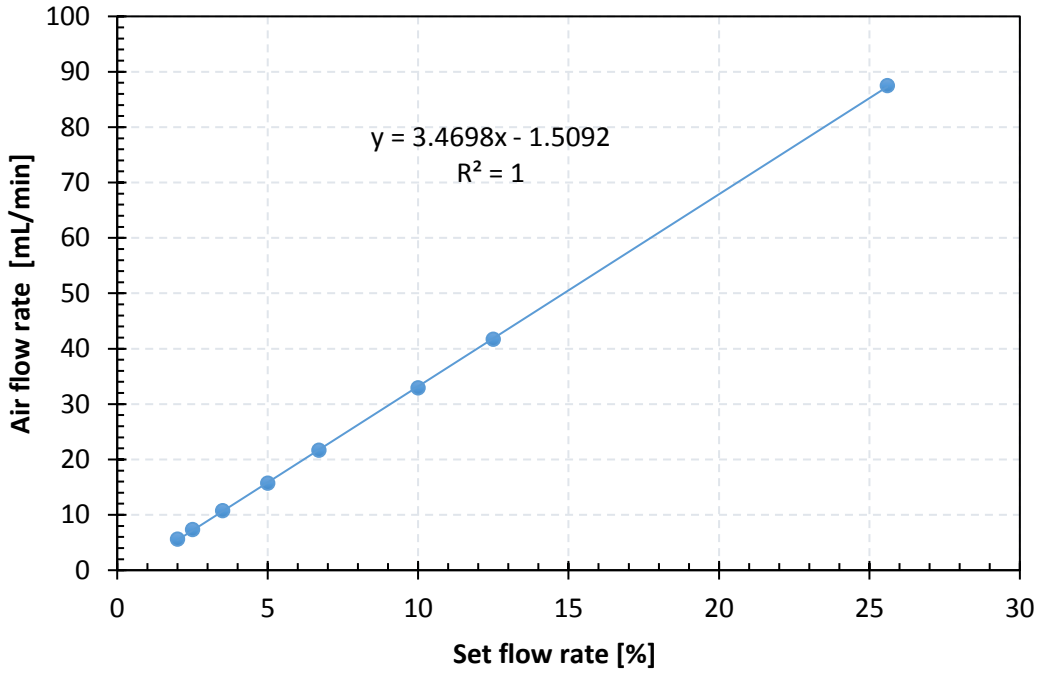

Figure A-5: Calibration data for Air mass flow controller used in the adsorption experiments with the KOH activated carbon at 52 psi

Appendix B Measurement Accuracies and Uncertainties

Variables (a, b, c, …) have an uncertainty (σ_a, σ_b, σ_c, …) based on the equipment used. The error is given by the standard deviation (σ_x) of a measurement. When a calculation requires more than one variable to solve (equation (B.1)), a propagation of error is necessary to determine the uncertainty (equation (B.1)). This propagation of error is performed on the adsorption capacity calculation as described in Section 3.1.4 and reported in Section 4.1. The uncertainties of the measurement equipment is provided in Table B-1.

$$x = f(a, b, c, \dots) \tag{B.1}$$

$$\sigma_x^2 = \left(\frac{\delta x}{\delta a}\right)^2 \cdot \sigma_a^2 + \left(\frac{\delta x}{\delta b}\right)^2 \cdot \sigma_b^2 + \left(\frac{\delta x}{\delta c}\right)^2 \cdot \sigma_c^2 \dots \tag{B.2}$$

Table B-1: Accuracy of the measurement equipment

Measurement equipment	Accuracy
490 micro-GC, Agilent Technologies Inc., USA	0.5 ppm ± 0.5 %
MFC 5850E A/B, Brooks Instrument, USA	ml/min ± 2%
2416, Eurotherm, USA	1◦C ± 0.2%

Appendix C Operational Profiles of the Equilibrium Model

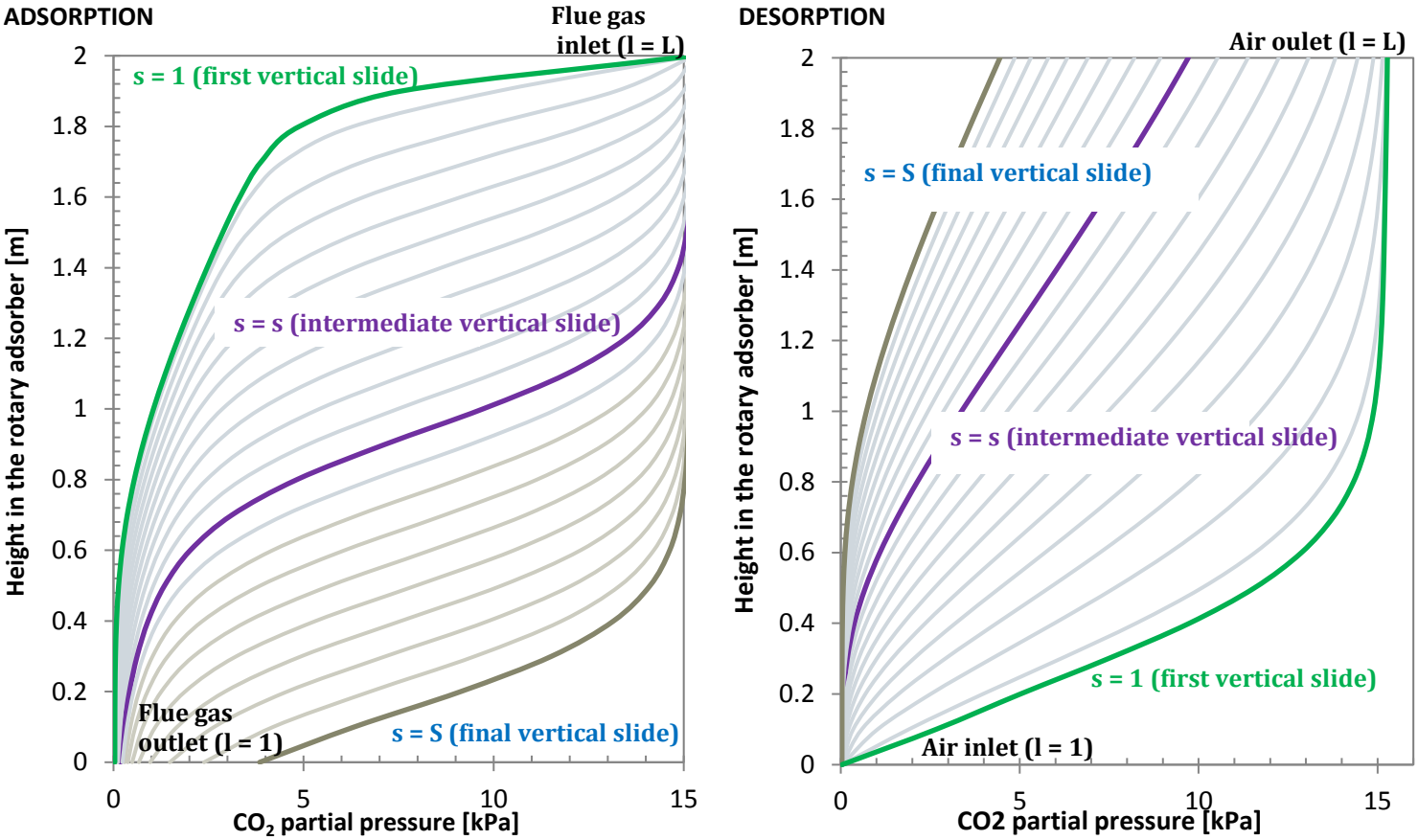

Figure C-1: **CO2 partial pressure profiles of (a) the flue gas (adsorption) and (b) the air (desorption) in height direction for each vertical section. SEGR parallel configuration (97/96), Adsorbent: KOH activated carbon, Equilibrium model**

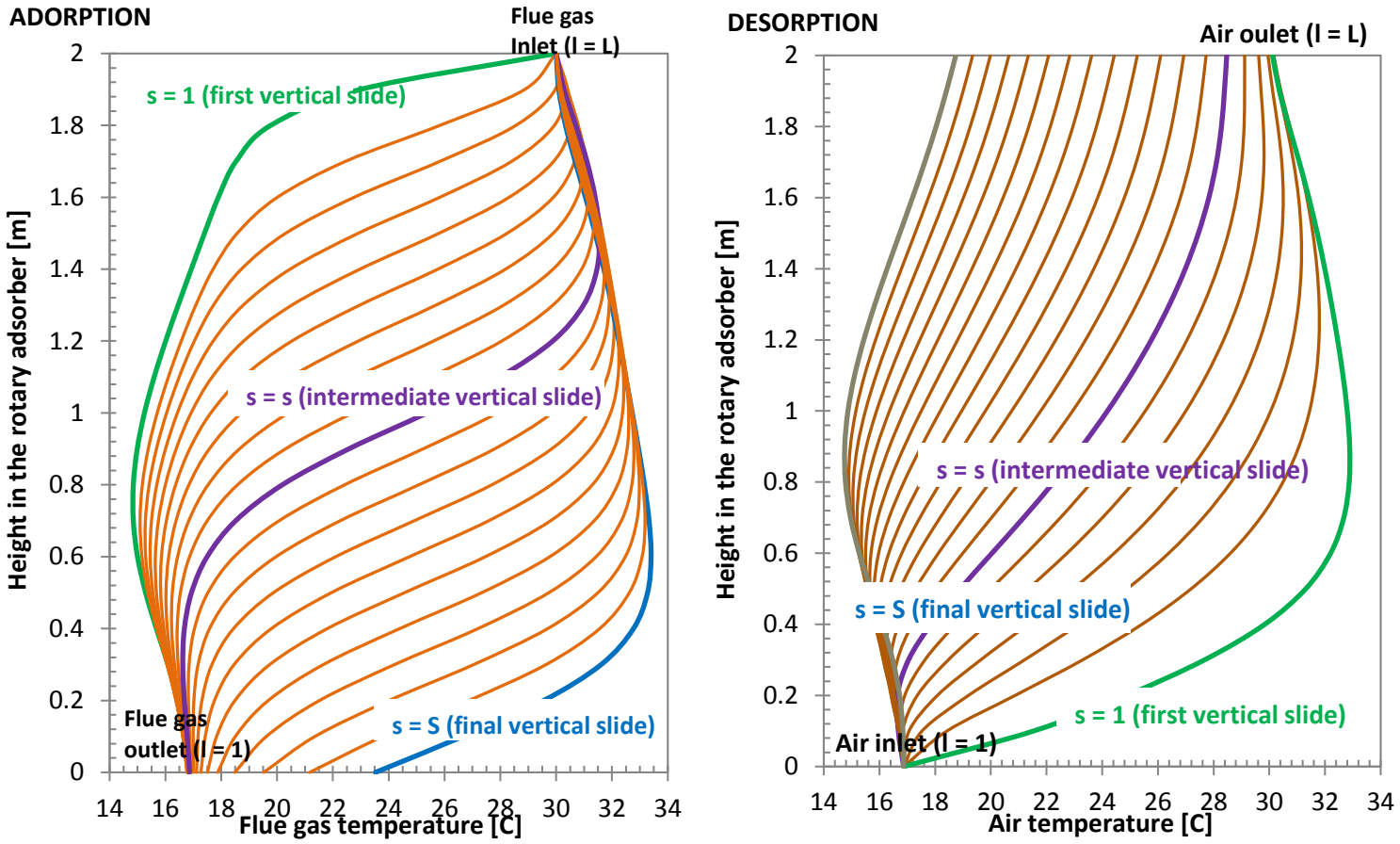

Figure C-2: **Temperature profiles of (a) the flue gas (adsorption) and (b) the air (desorption) in height direction for each vertical section. SEGR parallel configuration (97/96), Adsorbent: KOH activated carbon, Equilibrium model**

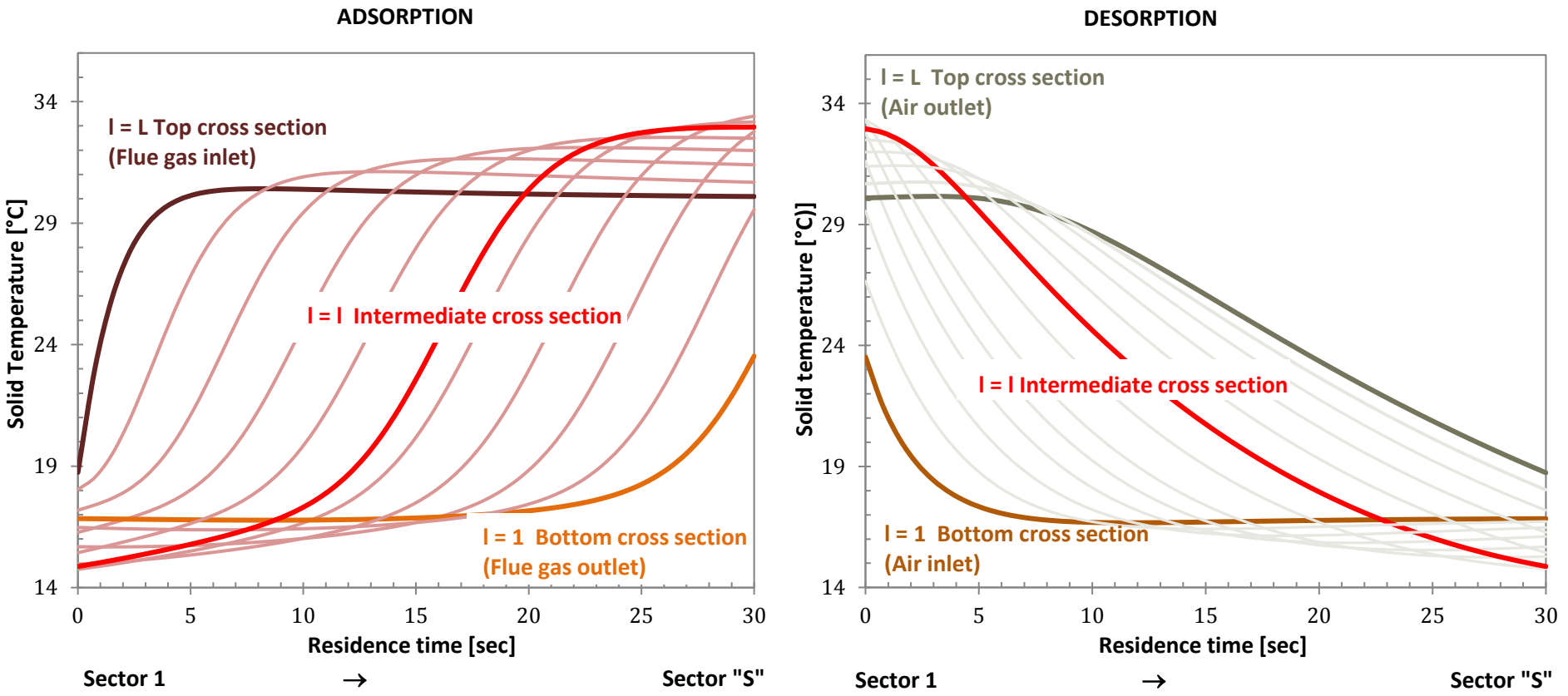

Figure C-3: **CO2 adsorption profile for adsorption (a) and desorption (b) in rotational direction for each horizontal section. SEGR parallel configuration (97/96), Adsorbent: KOH activated carbon, Equilibrium model**

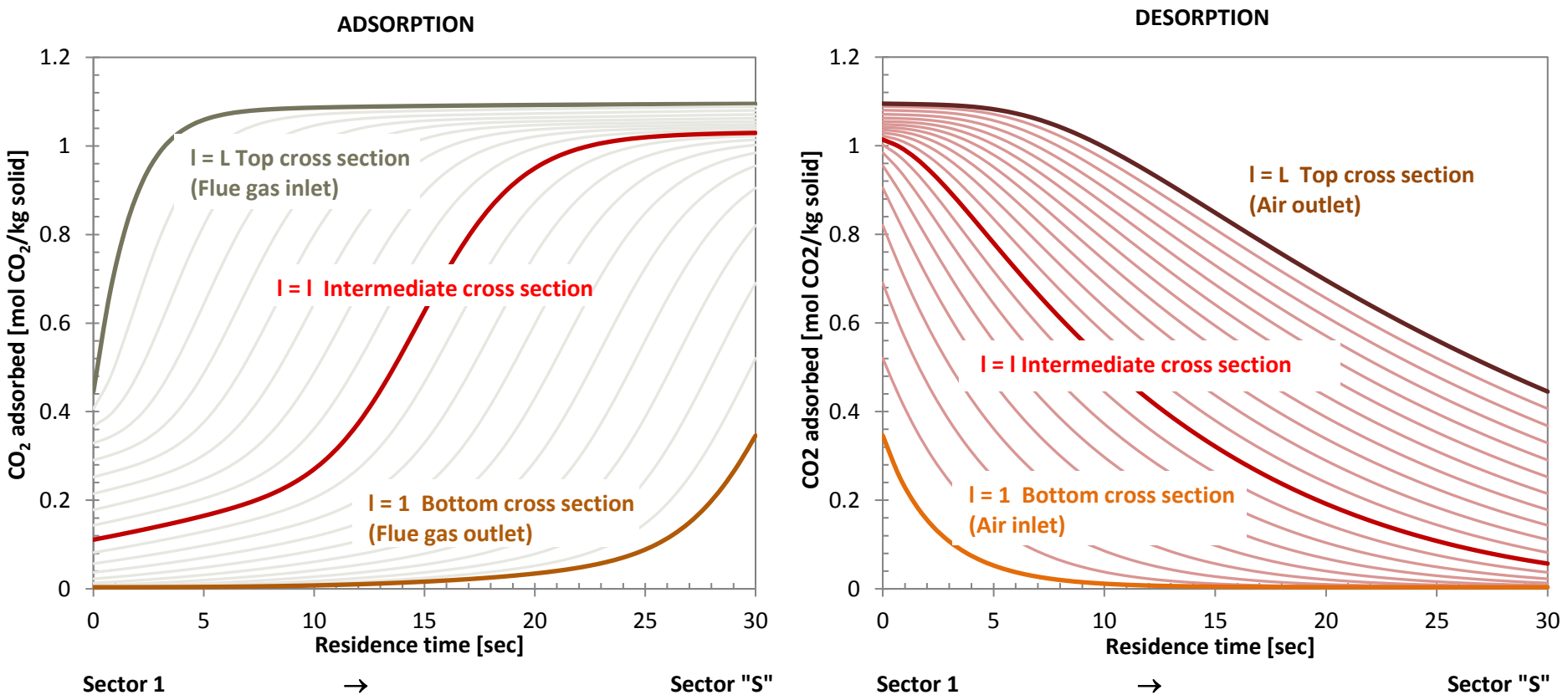

Figure C-4: **Temperature profiles of the solid (a) in the adsorption section and (b) in the desorption section in rotational direction for each horizontal section. SEGR parallel configuration (97/96), Adsorbent: KOH activated carbon, Equilibrium model**

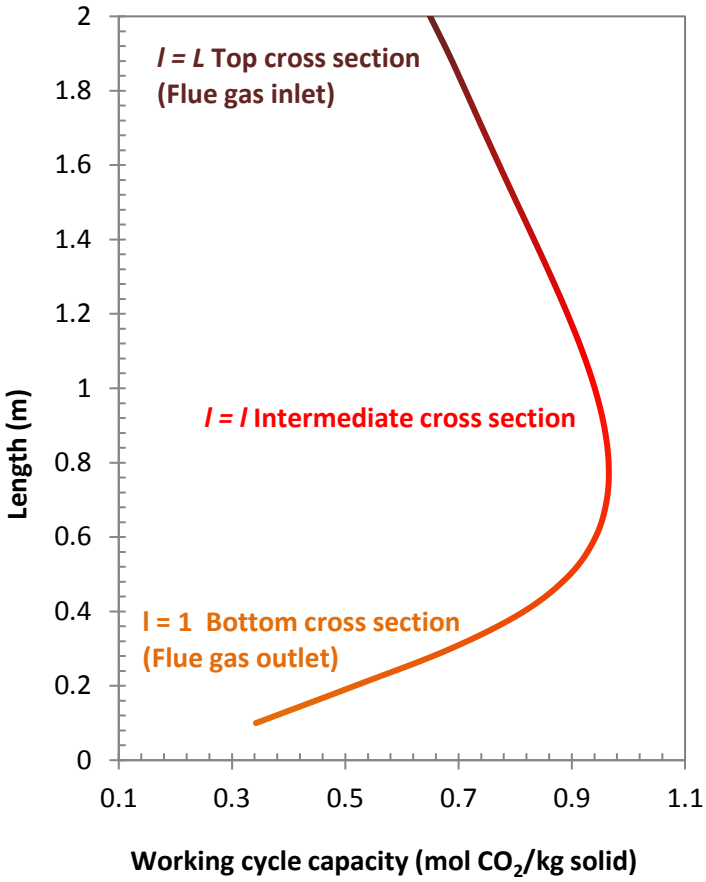

Figure C-5: **Working cycle capacity of the adsorbent along the height of the rotary wheel in height direction. SEGR parallel configuration (97/96), Adsorbent: KOH activated carbon, Equilibrium model**

Appendix D Technical Data of the Reference Power Plant

D.1 Ambient Air Conditions

Table D-1: Ambient air conditions

Pressure (ISO)	kPa	101.325
Temperature (ISO)	°C	15
Relative humidity, Φ	%	60
Composition, dry molar fraction (%)		
N_2	%vol	78.08
CO_2	%vol	0.03
H_2O	%vol	0.00
Ar	%vol	0.94
O_2	%vol	20.95
Molar Mass	g/mol	28.86

D.2 Natural Gas

Table D-2: Natural gas supply specifications

Fuel type	Natural Gas	
Supply temperature	°C	10
Supply pressure	MPa	7
Composition, dry molar fraction (%)		
CH_4	%vol	89
C_2H_6	%vol	7
C_3H_8	%vol	1
C_4H_{10}	%vol	0.11
N_2	%vol	0.89
CO_2	%vol	2
S	ppm	<5
Molar mass	g/mol	17.84
CO_2 emissions	g/kWh (LHV)	208.00
Heating values		
Low heat value (LHV) @ 25°C	MJ/kg	46.94
High heat value (HHV) @ 25°C	MJ/kg	51.58

D.3 Technical Parameters for the Combined Cycle Gas Turbine Power Plant

Table D-3: Technical parameters for the steam cycle of the CCGT plant

Heat recovery steam generator parameters		
HRSG efficiency	%	99.7
Temperature differences		
ΔT approach main steam	°C	42
ΔT approach hot reheated steam	°C	34
ΔT pinch gas boiling - liquid in evaporator	°C	10
ΔT subcooling economiser	°C	3
Pressure losses		
ΔP gas side	kPa	2.6
ΔP HP SH	%	3.5
ΔP HP ECO	%	2.6
ΔP IP RH	%	3
ΔP IP SH	%	2
ΔP IP ECO	%	3
ΔP LP SH	%	2
ΔP LP ECO	%	1.3
ΔP system - LIVE STEAM	%	9
ΔP system - COLD RH	%	7
ΔP system - HOT RH	%	9
ΔP system - LP STEAM	%	9
Temperature losses		
From superheater / reheater to turbine (approximately 0.5 K)	kJ/kg	1

Table C-3: Technical parameters for the steam cycle of the CCGT plant (continued)

Condenser		
P condenser	kPa	4.814
Saturation temperature	°C	32.2
Temperature pinch	°C	3.2
Feed water temperature (after feed water pump)	°C	32.2
Cooling water supply (CWS) temperature	°C	18
Cooling water return (CWR) temperature	°C	29
Condenser duty	MW	224.3
Power to thermal duty (Electric consumption for heat rejection of rejected thermal power)	%	0.8
Feed water pumps		
Pump efficiency	%	70
Generator efficiency	%	98.5
Steam turbines		
HP Steam turbine		
Pressure inlet	bar	170
Inlet temperature	°C	600
Isentropic efficiency	%	88.15
IP Steam turbine		
Pressure inlet	bar	40
Inlet temperature	°C	600
Isentropic efficiency	%	92.40
LP Steam turbine		
Pressure inlet	bar	3.75
Inlet temperature	°C	266.93
Isentropic efficiency	%	88.00
Fuel heater		
Fuel Inlet Temperature	°C	9.00
Fuel Outlet Temperature	°C	117.00
IP water inlet temperature	°C	252.85
Temperature pinch	°C	26.98
Efficiency calculations		
Mechanical efficiency	%	99.6
Generator efficiency	%	98.5

Appendix E Data Summary for Simulations

Table E-1: Ambient air condition for sizing the SEGR regenerative rotary CO2 transfer device for the retrofit cases

Ambient air		
Temperature	◦C	15
Pressure	bar	1.033
Humidity	%	60
Mass flow rate	kg/s	562.2
Molar flow rate	mol/s	19482.4
Fan		
Efficiency	%	85
Pressure difference	bar	0.02

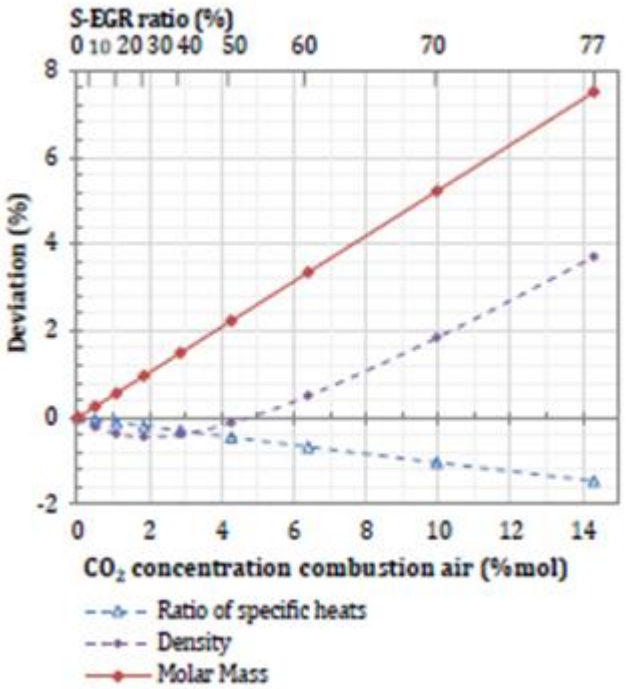

Figure E-1: Sensitivity of the deviation of the working fluid properties from the reference configuration with air combustion at ISO conditions as a function of the working fluid CO2 concentration at the compressor inlet. Configuration CCGT with PCC and SEGR in parallel (Herraiz 2016)

Appendix F Sensitivity to SEGR Ratio

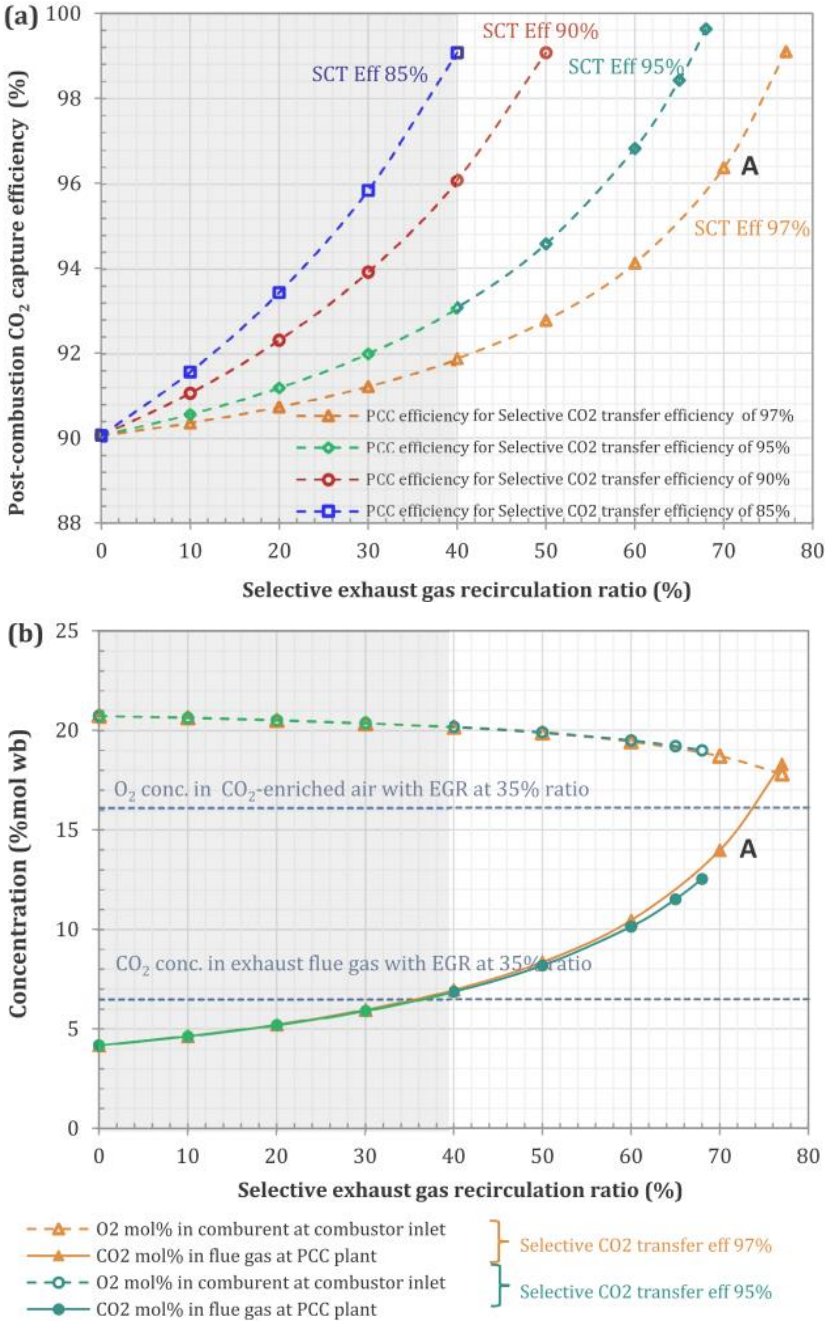

Figure F-1: **(a) Sensitivity of the post-combustion CO2 capture rate and (b) Sensitivity of CO2 concentration in the flue gas at the inlet of the post-combustion capture system and O2 concentration in the CO2-enriched combustion air to the selective exhaust gas recirculation ratio, for a range of selective CO2 transfer rates; SEGR in parallel for 90% overall CO2 capture level** (Herraiz et al. 2018)

Appendix G Block Flow Diagrams

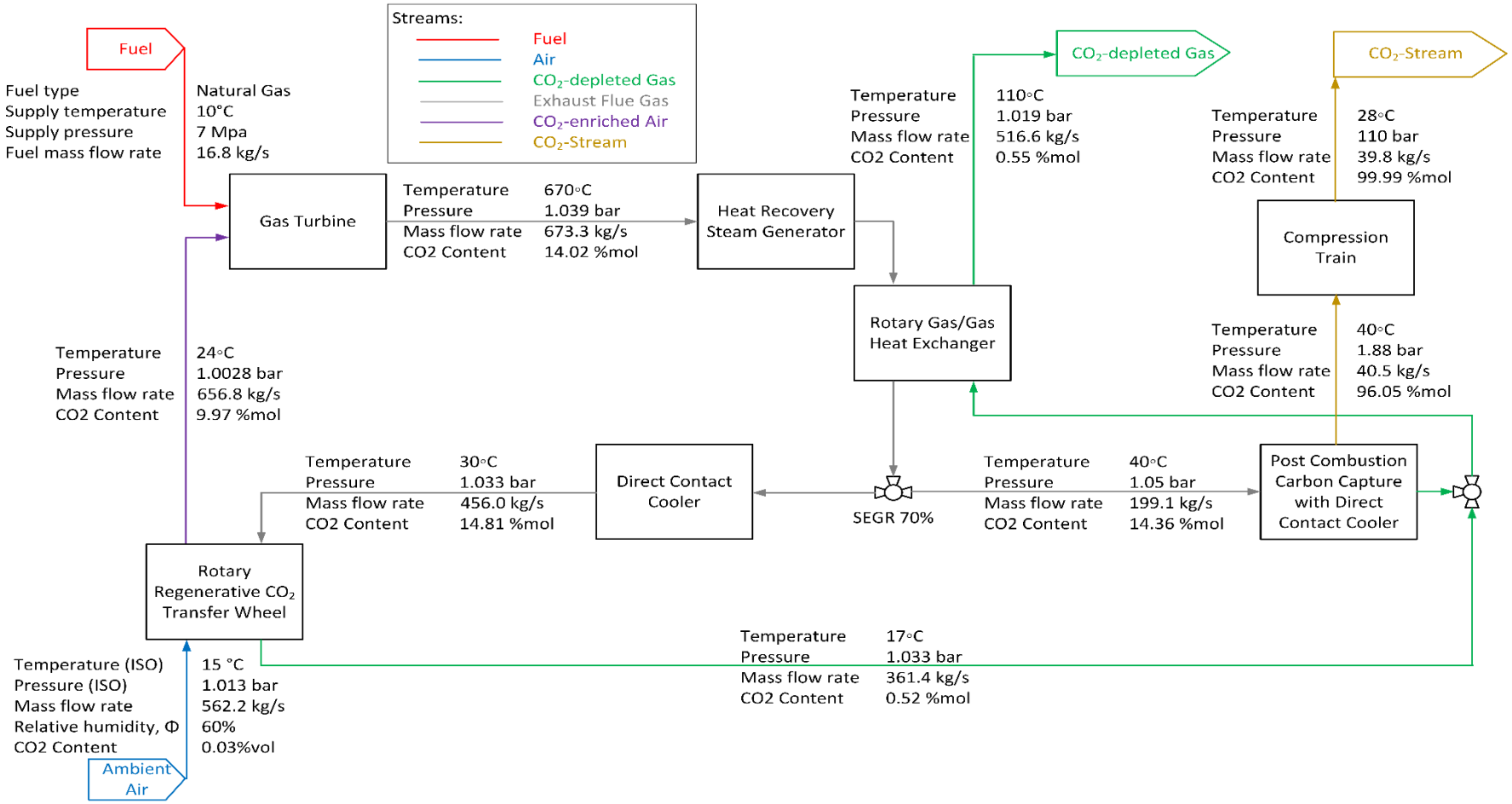

Figure G-1: Block flow diagram configuration New Built; CCTG with PCC and SEGR, SEGR ratio 70%

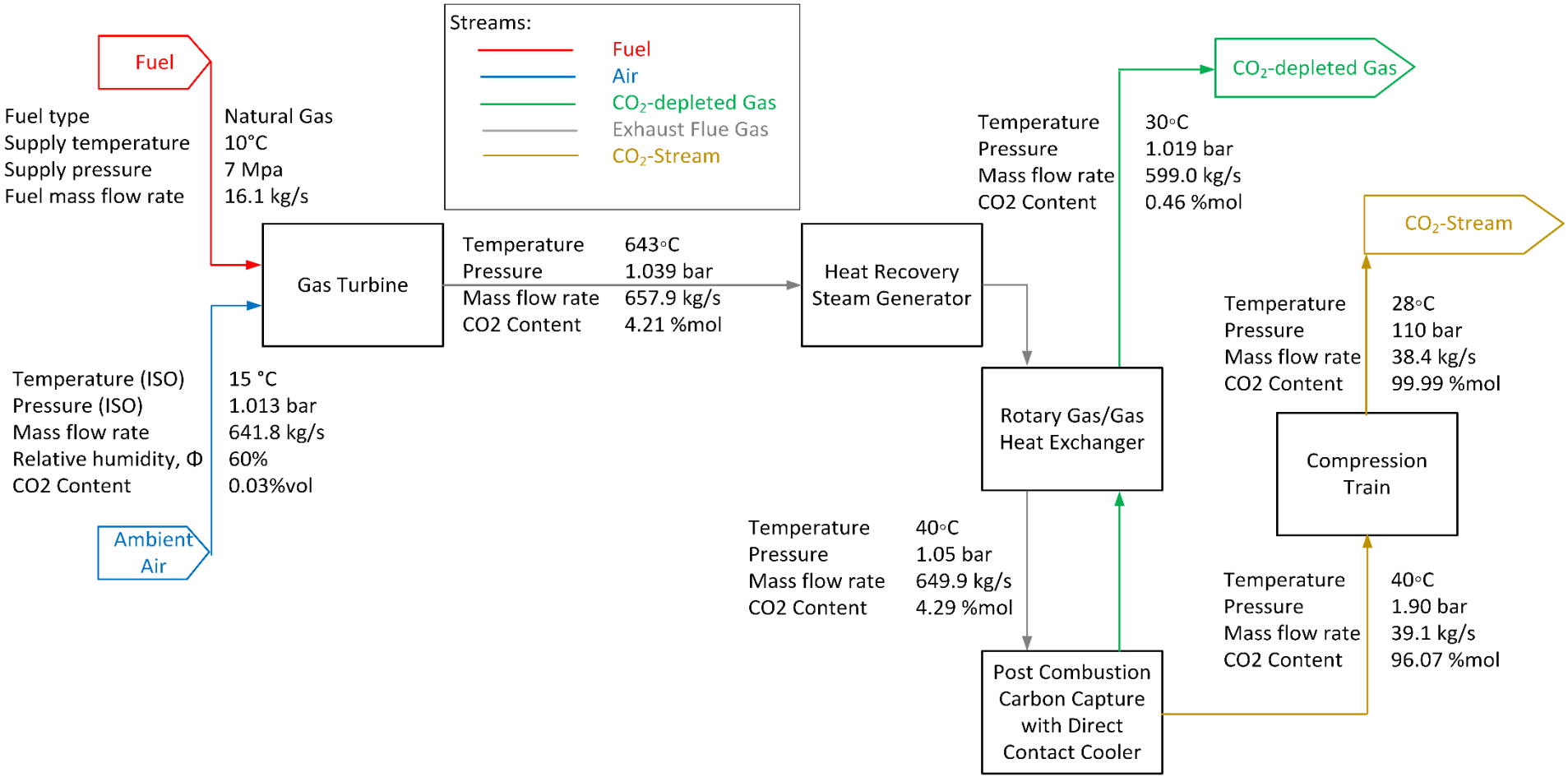

Figure G-2: Block flow diagram configuration Full Scale CP; CCTG with PCC